APPENDIX C

IDENTIFICATION OF FACTORS CONTROLLING THE DEVELOPMENT OF SUBSIDENCE IMPACTS FORECASTING METHODOLOGY TO THE I-70 ALIGNMENT OVER LONGWALL MINING OF THE TUNNEL RIDGE MINE, WASHINGTON COUNTY, PA

Task #3: Post-Undermining Activities
Submitted 3 October 2020; Revised 18 January 2020

The University of Pittsburgh Master Agreement
Contract No. 4400018535

Project Team

Anthony Iannacchione, Associate Professor, Principal Investigator*
Luis Vallejo, Professor, Co-Principal Investigator
Julie Vandenbossche, Professor
Mingzhou Li, Graduate Research Student
Emily Adelsohn, Graduate Research Student
Robert Winn, Graduate Research Student
** - Email ati2@pitt.edu, Phone: 412-624-8289*

Task 3 Report Outline

SECTION I – INTRODUCTION

Subsection Ia – Project Scope

1.0 Background

Over 800 longwall coal mining panels have been extracted in Washington and Greene Counties, Pennsylvania since the late 1960's. Of this total, twenty-six panels have undermined parts of two interstate highways, I-70 and I-79 by five longwall mines: Gateway, Eight-Four, Cumberland, Emerald, and Tunnel Ridge. This last mine, Tunnel Ridge, extracted its first longwall panel under an interstate highway in 2019 (Panel 15). This same mine controls a large unmined reserve of the Pittsburgh Coalbed in Washington County, Pennsylvania. This reserve is of sufficient quality and quantity to be profitably mined using the longwall mining method. This large coal reserve is transected by I-70 for ~4.6-miles of its length.

Over the last five decades, there has been a great deal of effort to understand how a longwall subsidence basin formation impacts surface features, such as buildings, water supplies, streams and wetlands. In particular, the University of Pittsburgh has provided important assessments of these impacts for the Pennsylvania Department of Environmental Protection (Iannacchione, et al., 2011; Tonsor, et al., 2014; and Bain, et al., 2019). Less is known as to how subsidence can impact interstate highways, and even less is known about the impact to embankments and cuts that carry these highway alignments. In some areas, careful monitoring of conditions and asphalt re-surfacing can effectively repair the subsidence damage with only minimal impact to highway traffic. In other cases, overpass structures carrying I-79 have been replaced (Iannacchione, et al., 2011). Traffic delays occurred that were associated with reducing the highway capacity down to a single-lane of travel prior to the undermining, while asphalt relief sections and the asphalt overlay were constructed, and during panel extraction. These delays were most noticeable during the maintenance milling disruptions performed as surface defects developed as a result of the undermining. The University is not aware of any subsidence impacts causing an accident or injuring the traveling public.

This project has two distinct study areas. The first has to do with detailed monitoring of the I-70 highway alignment during the undermining by longwall Panel 15 of the Tunnel Ridge Mine. The results of this monitoring effort are presented in the University's Task 2 Report (Iannacchione, et al., 2020). It should be noted that monitoring stopped a few months after Panel 15 passed under the study area. No attempt was made to monitor the I-70 study area conditions when the adjacent Panel 16 was extracted in the fall of 2019.

2.0 Contract

The University of Pittsburgh (herein referred to as 'the University' submitted a proposal to PennDOT in May 2018. This proposal required the University to study and analyze data collected by the University, PennDOT, and its contractors associated with the undermining of Panel 15 at the Tunnel Ridge Mine. It also requires the University to assess the risk to other areas along Pennsylvania interstate alignments that might be impacted by longwall subsidence in the future.

The University received a notice to proceed with this effort on 3 October 2018. The contract was to end, no later than, 4 January 2021 at a cost of $516,348.30. The project is administered by Shelley Scott and technical advisor Roy Painter. Communication and reporting on contract activities occurred through regularly scheduled monthly meetings and through required reporting activities. This report is an example of a required reporting task.

The five major reporting tasks are listed below. Three have now been completed:

- Task 1: Pre-Undermining Activities - A report containing a summary of the pre-undermining activities, along with a PowerPoint presentation of research findings by 5 August 2019, COMPLETED 14 July 2019 (Iannacchione, et al., 2019)
- Task 2: Undermining Activities - A report containing a summary of the undermining activities, along with a PowerPoint presentation of research findings by 3 April 2020, COMPLETED 17 DECEMBER 2019 (Iannacchione, et al., 2020)
- Task 3: Post-Undermining Activities - A report of the Subsidence Forecasting, along with a PowerPoint presentation of research findings by 3 October 2020, PRESENTATION DELIVERED ON 21 SEPTEMBER (virtual), DRAFT REPORT 3 OCTOBER 2020
- Task 4: Draft Final Report by 17 November 2020
- Task 5: Final Report by 19 December 2020

The Final Report will summarize the most important information contained in Tasks Reports 1, 2 and 3 and provide recommendations for future study. This report, referred to as the Task 3 Report, focuses on post-undermining activities performed by the University and future longwall mining of the Tunnel Ridge Mine under I-70 in Washington County, PA.

Subsection Ib – Objective

Alliance Coal plans to continue to mine the Tunnel Ridge Mine with the longwall mining method in both Pennsylvania and West Virginia over the next two decades. This will result in the undermining of I-70. One of their panels, Panel 15, undermined I-70 early in 2019 and more are planned in the future. The broad objectives of this research are to:

1) Investigate the influence of longwall mining on highway alignments and associated slopes and embankments,
2) Evaluate how the highway deforms during undermining with a focus on determining its transient and long term characteristics as well as the permanent deformation,
3) Utilize models and field measurements to better understand subsidence impacts to the highway alignment, and
4) Determine how other future highway alignments could be impacted as a result of undermining.

Subsection Ic – Overview

The Task 3 Report focuses on three topics. The first is to conduct additional analysis of data obtained during the mining of Panel 15 under I-70 during the winter of 2019. In particular, the project team combined observations from both the University and PennDOT, expanding the inventory of identified subsidence impacts. It also became apparent that the roadway pavement, especially after the longwall face passed under Embankment #1, behaved in an unexpected manner. This led to additional characterization of the vertical subsidence, horizontal deformation, and horizontal strain along the roadway at distinct time periods as the undermining was occurring. This more careful analysis helped to better identify the onset of highway impacts and the causes of the unexpected behavior. See Section II for this discussion.

The second major topic is to assess the risk to I-70 from longwall mining subsidence within the extended study area. This area encompasses the Tunnel Ridge reserves of the Pittsburgh Coalbed in western Pennsylvania (see Section IIIa). A portion of these reserves has the potential to be mined beginning in 2024. In this report, the University is using the knowledge gained during the undermining of Panel 15, to evaluate potential longwall mining subsidence impacts within the extended study area along I-70. To accomplish this task, the University had to first propose a likely plan for longwall mining. Once that was accomplished, highway assets were located and characterized. Next, the SDPS model was used to predict potential surface subsidence along I-70 from the West Alexander to the Claysville interchange. These steps allowed the University the opportunity to evaluate how the 28 significant assets located within the extended study area, might react to these potential subsidence events. See Section III for this discussion.

The third major topic was to perform a detailed analysis of the embankments carrying I-70 within the extended study area. The University constructed detailed models of the study area embankments and subjected them to a simulated, dynamically formed, subsidence basin to define the resulting effects using the Finite Element Method. The Shear Strength Reduction Method was used to evaluate the stability conditions of embankments under different material property values. This evaluation found that the potential for instabilities along the highway surface increased with decreasing overburden. It was also found that excessive deformations increased as the orientation of the highway approached 90-deg to the direction of longwall panel advance. See Section IV for this discussion.

SECTION II - FINAL ANALYSIS OF I-70 UNDERMINING BY PANEL 15

The Task 2 Report provides a record of observations and monitoring data collected during the undermining of I-70 by Panel 15 of the Tunnel Ridge longwall coal mine. While considerable analyses were performed on these data, additional research has led to several new lines of investigation. For example, Section IIa compares SDPS subsidence prediction profiles with highway alignment surveys. This comparison more clearly revealed the interaction between ground movements, pavement deformation, and observed impacts. Dr Vandenbossche joined the project and was able to help the University's efforts to characterize the behavior of the pavement.

Subsection IIa – SDPS Comparison with Survey Data and Observed Features

The inconsistencies between the predicted SDPS surface movements and the actual survey data collected along the highway shoulder led the University to ask the question

> *"What explanation can be formulated for why the movement along the highway's shoulder showed a strong correlation on the eastern portion of the study area but deviated significantly from predicted horizontal movement in the western portion of the study area?"*

In general, there was excellent agreement between the predicted SDPS vertical subsidence and that measured along the highway shoulder. Differences were found to be associated with Embankment #1. The Task 2 Report stated that Embankment #1 experienced additional consolidation and associated lateral spreading as a result of subsidence. During the initial undermining of I-70 by Panel 15, the horizontal movements both parallel and perpendicular to the highway showed good agreement with those predicted by SDPS. Significant differences between measured and predicted occurred after 5 February 2019.

The first step in this analysis, required the data from both the SDPS model and the surveys be transformed to the direction of the roadway (parallel and perpendicular). This was made easier by the fact that the road was straight, allowing it to be manipulated consistently throughout the alignment. In this section, four longwall face positions are discussed in detail (Figure IIa.1). These face positions were selected because observations and survey measurements were collected either on those dates or within one day of the date.

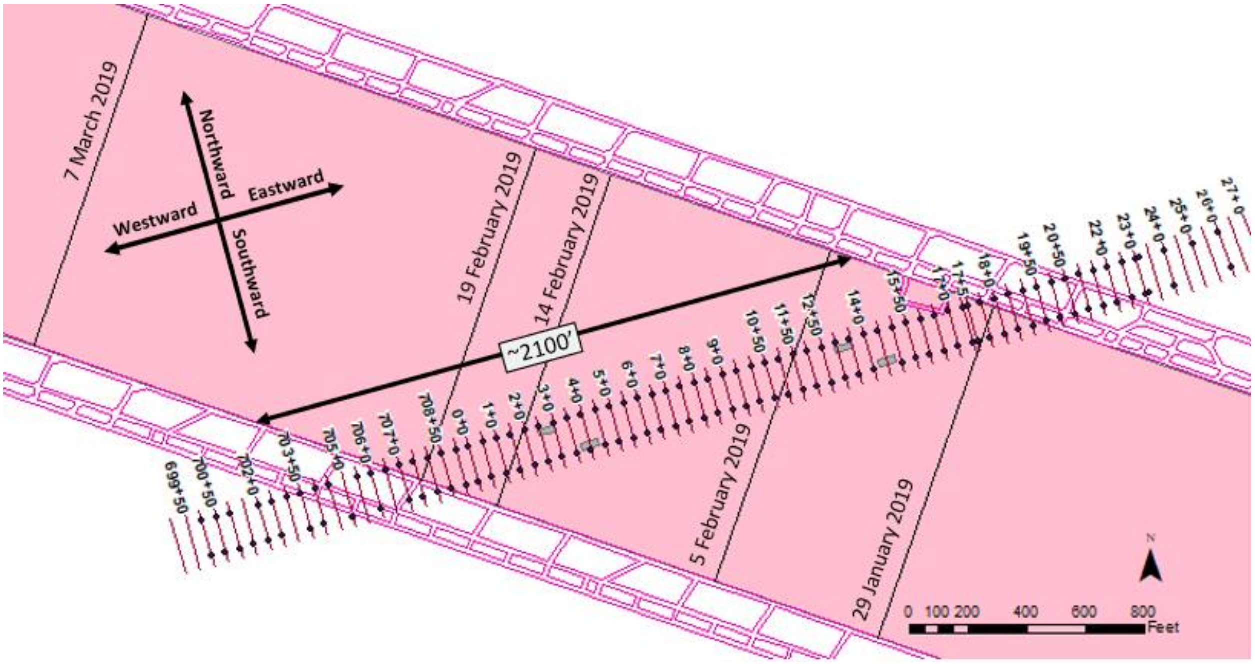

Figure IIa.1 - Panel 15 showing the location of the longwall face positions and highway alignment surveys discussed in this section. The 7 March 2019 longwall face position is beyond the map boundaries

1.0 Final Subsidence

The analysis began by comparing the predicted final subsidence basin to that observed during the undermining of I-70 within the initial study area. The final permanent vertical subsidence basin predictions were made in SDPS using a 3D grid model that is interpolated along the highway alignment after the panel is completely mined out (Figure IIa.2). These predictions were compared with the highway alignment surveys recorded on 26 March 2019 and a select number of observations collected throughout the study. When examining this figure, several comments can be made:

- The impact of Embankment #1 is clear, the measured highway alignment surveys show enhanced subsidence under its extent. Prior to the commencement of the mining, the University's latest SDPS topography simulation predicted the maximum vertical subsidence to be ~4.3-ft. There was over 5-ft of vertical subsidence measured at a location on the surface of Embankment #1 where the fill is the thickest (~75-ft). The additional subsidence is caused by the settlement of the fill comprising Embankment #1. It should be noted that the SDPS model cannot account for features like embankments.
- Minor heave was measured along the shoulder of the westbound lanes directly over the gate road entries for Panel 15.
- The western slopes of the vertical subsidence basin are similar for both the highway alignment surveys and the SDPS model.

- The eastern slopes of the vertical subsidence basin are also similar until the highway travels over the embankment. The additional vertical subsidence over the embankment is the cause.

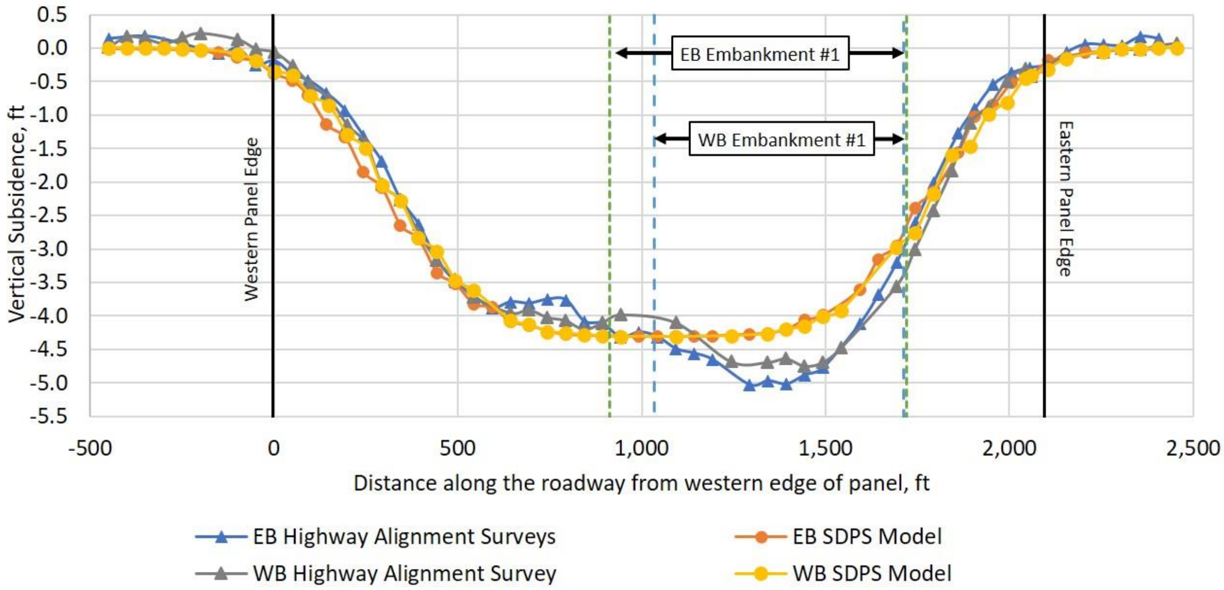

Figure IIa.2 – Final vertical subsidence associated with the extraction of Panel 15 along I-70 showing both highway alignment surveys and SDPS model results for both the westbound (WB) and eastbound (EB) travel lanes

As can be seen in the Figure IIa.3 for the eastbound lanes, both the horizontal movements parallel and perpendicular to the roadway experienced some deviations from the SDPS prediction, especially in the western portion of the study area. What is more striking is the effect some of the asphalt relief sections (ARS) have on altering horizontal movement parallel and perpendicular to the roadway. Please note that the ARS are located within the travel lanes and highway alignment surveys are performed outside of the travel lane on the adjacent shoulder.

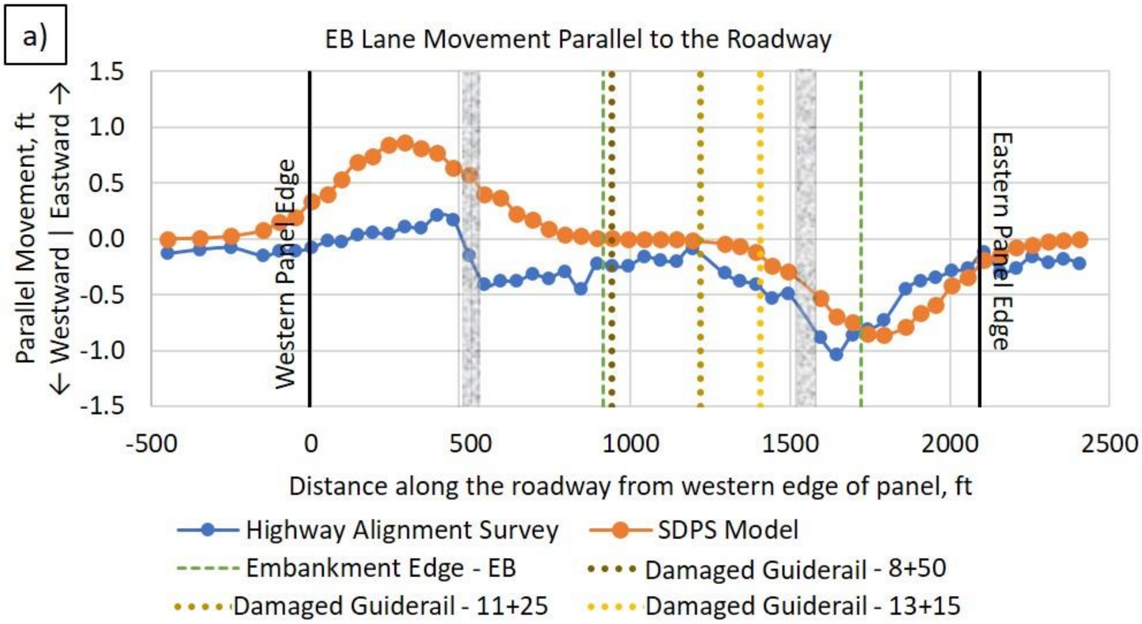

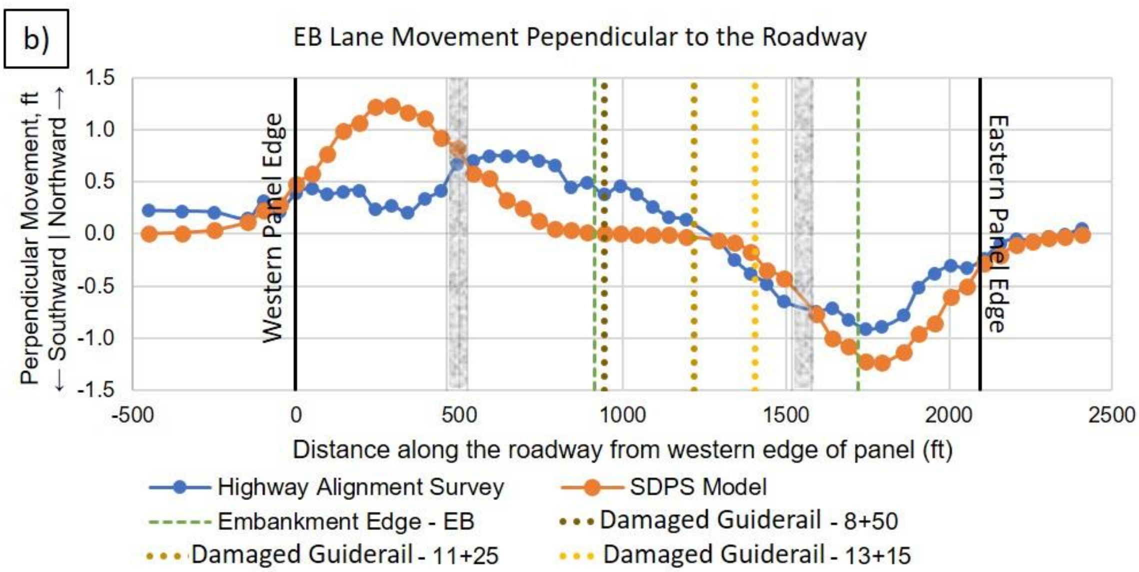

Figure IIa.3 - Comparison of horizontal movement a) parallel and b) perpendicular to the roadway with observed features on the eastbound lanes. The gray stripes indicate the location of the eastern and western asphalt relief sections. Please note that each lane and direction of movement is compared separately as longwall face positions resulted in different characteristics to the developing subsidence basin

Similar trends in parallel and perpendicular movement are shown for the westbound lanes (Figure IIa.4) where the eastern portion of the roadway experiences a significant movement to the west/south but the western portion does not show the expected movement back to the east/north. This is true for both parallel and perpendicular movement. Also, the damaged guiderail along the westbound outside shoulder at stationing 13+50 (Figure IIa.4a) is associated with relatively large parallel movements that can result in rail buckling. In addition, at stationing 9+50 (Figure IIa.4b) relatively large perpendicular movement would be more likely to shear the rails from the post.

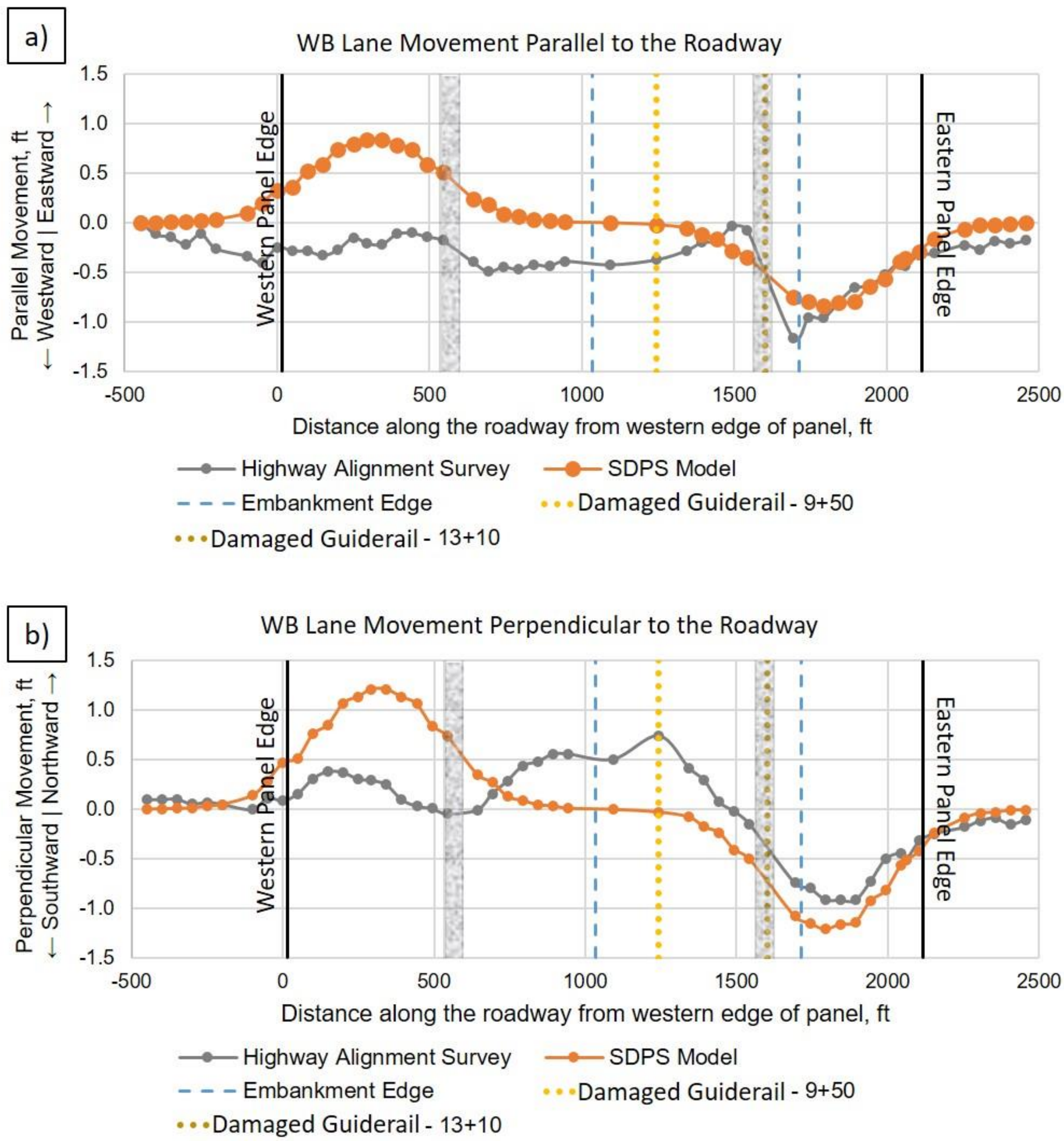

Figure IIa.4 – Comparison of horizontal movement parallel and perpendicular to the roadway with observed features on the westbound lanes

Through a review of this data, the influence of the asphalt relief sections on the permanent deformation of the continuous pavement structure is evident. These features are able to absorb some of the compressive forces in a manner that cannot be accommodated through the more rigid Portland cement concrete, causing different horizontal movements to occur. These concepts will be further explored in Section IIb.

2.0 Dynamic Subsidence

Next, the movement obtained from the SDPS models and survey observations collected during the undermining event were compared. Each set of predictions is generated in SDPS using a 3D grid model that was interpolated along the highway alignment; however, unlike the final predictions in the previous analysis, these incremental analyses are made assuming that only the area of coal behind the longwall face on a given date had been extracted. These predictions are compared with the survey measurements recorded on the respective dates and some of the more important visual observations made throughout the undermining. It is important to note that this section will make reference to some of the deformation features observed near these dates, but a more detailed analysis is discussed in Section IIb.

2.1 Subsidence on 5 February 2019

On 5 February 2019, the longwall face was beneath the center of Embankment #1 (Figure IIa.1). For both the westbound and eastbound lanes, the measured vertical subsidence closely matched the SDPS predicted values (Figure IIa.5). It is worth noting that on this date, the eastbound lanes experienced significantly more subsidence than the westbound lanes, based on their relative distance from the longwall face.

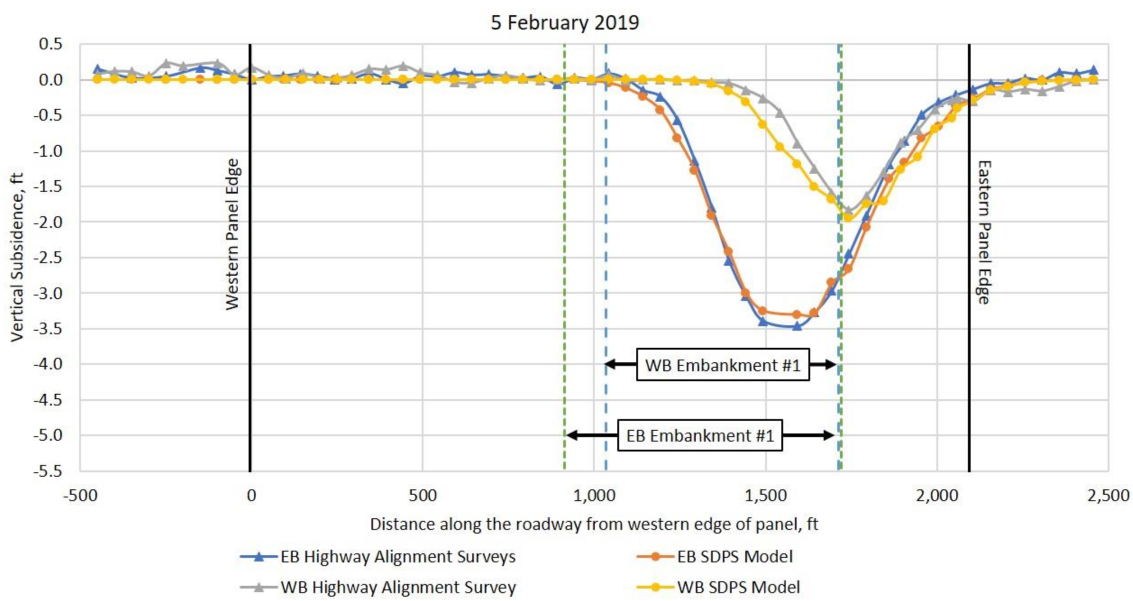

Figure IIa.5 – Comparison of vertical subsidence from survey data and SDPS model for 5 February 2019

When considering the horizontal movements (Figure IIa.6 & 7) for 5 February 2019, only minor variations are observed between the SDPS predictions and the measured survey data. As can be seen in the Figure IIa.6 for the eastbound lanes, agreement between the predicted and measured occurs in the directions both parallel and perpendicular to the roadway. Of particular note is the rapid change in the direction of movement parallel to the roadway on each side of the eastern asphalt relief section. The movement perpendicular to the roadway reveals how the eastern most section is being pulled into the developing subsidence basin.

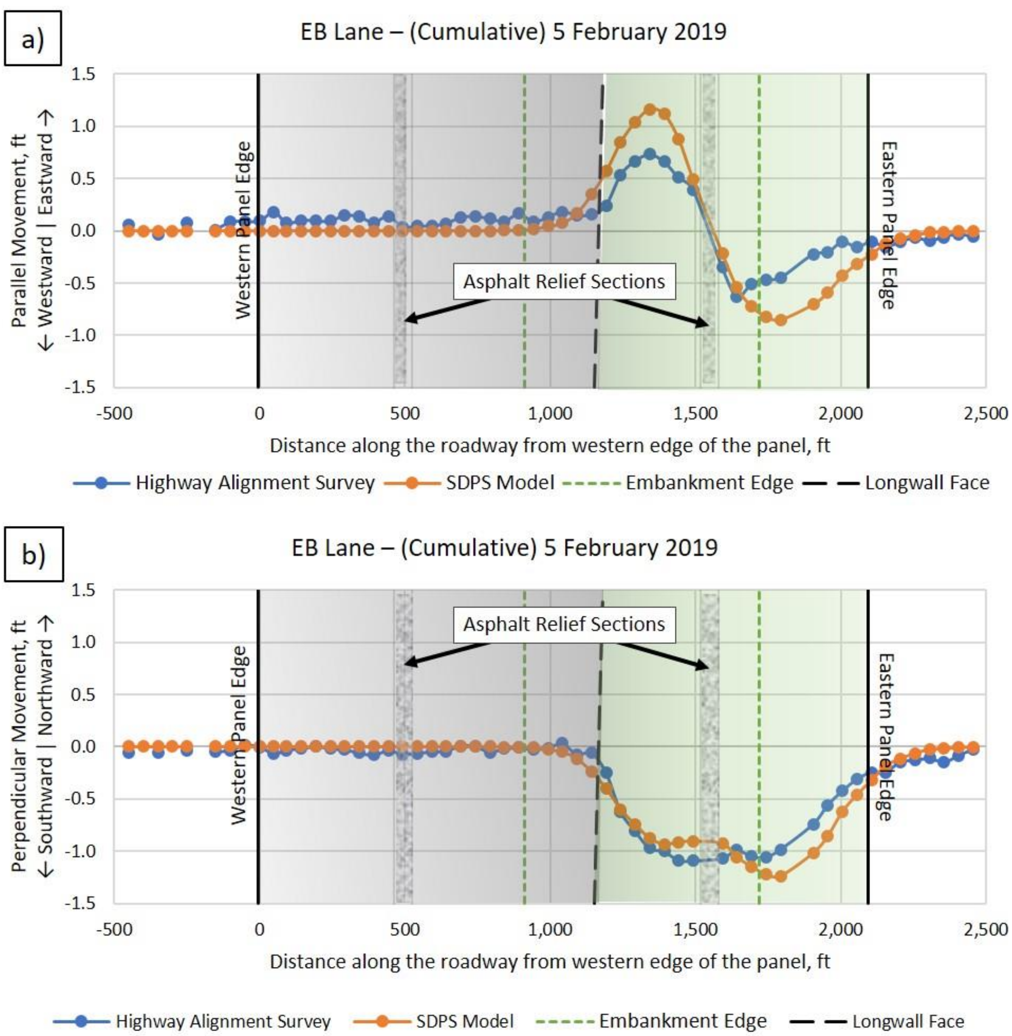

Figure IIa.6 – Comparison of the cumulative horizontal movement from eastbound highway alignment surveys and SDPS models a) parallel and b) perpendicular to the roadway, 5 February 2019

For the westbound lanes (Figure IIa.7), less movement was observed in both the parallel and perpendicular orientations than was predicted by SDPS. The rapid change in horizontal movement parallel to the direction of travel on the westbound lanes is associated with the eastern asphalt relief section.

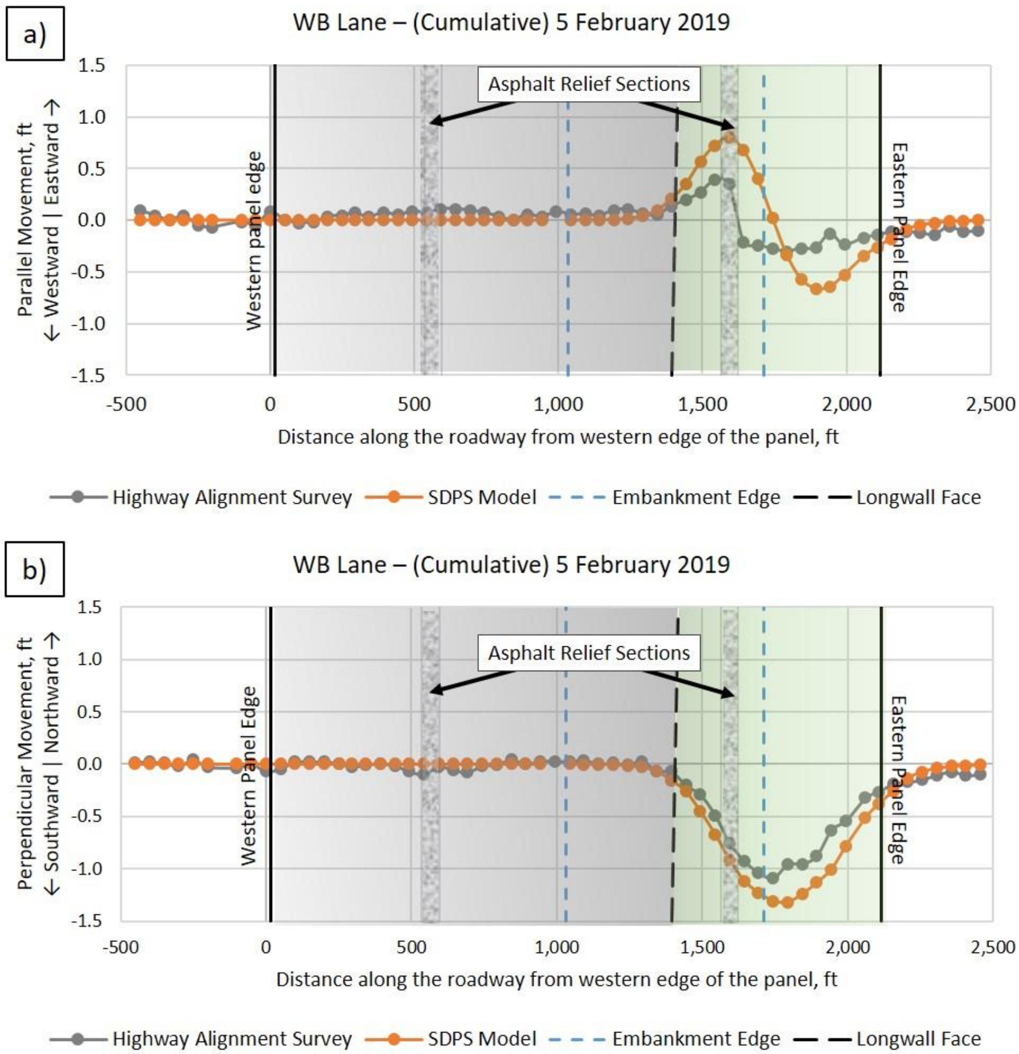

Figure IIa.7 – Comparison of the cumulative horizontal movement from westbound highway alignment surveys and SDPS models a) parallel and b) perpendicular to the roadway, 5 February 2019

Several major roadway distress features occurred between 29 January and 5 February 2019 (Appendix I). Perhaps the most significant for this discussion occurred within and adjacent to the eastern asphalt relief sections in both the eastbound and westbound lanes. Here compression bumps within asphalt relief sections (travel and passing lanes) and blowups in the pavement shoulder were first formed (Appendix I). Embankment #1 did not have any noticeable effect on horizontal movements at this point in time.

2.2 Subsidence on 14 February 2019

On 14 February 2019, the longwall face was beneath the western cut slopes in the study area. As can be seen in Figure IIa.8, the observed subsidence and predicted vertical subsidence match well on the eastern side of the study area. Beyond the embankment on the western side of the study area, the predicted verses measured vertical subsidence have similar slopes. The size of the subsidence basin is larger for the eastbound lanes because it spans a larger portion of Panel 15. The slight difference between the predicted and measured vertical subsidence for both east and westbound lanes was not expected and cannot be explained at this point without additional study.

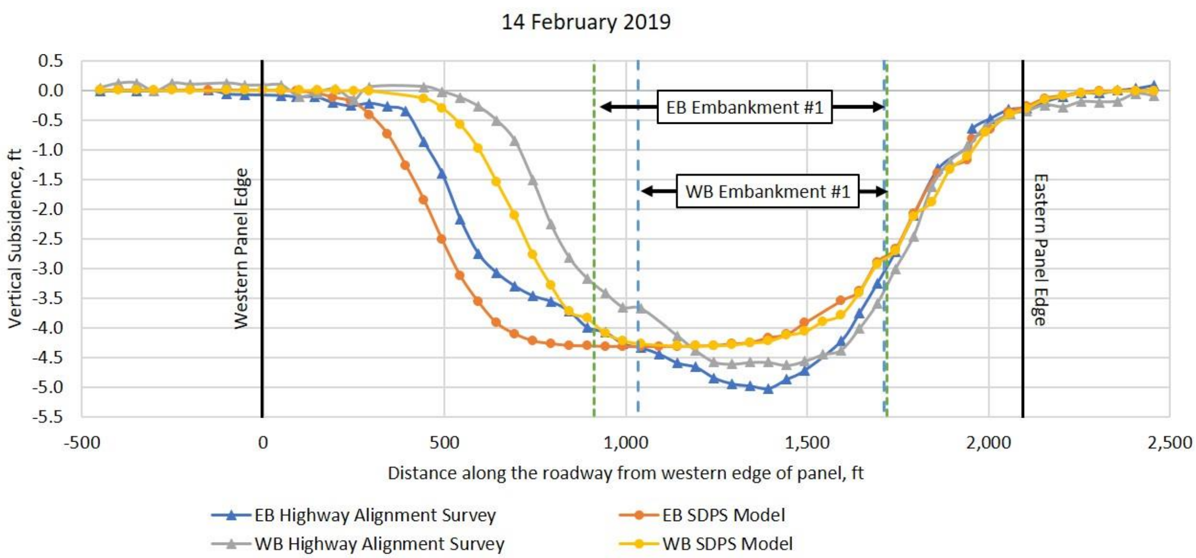

Figure IIa.8 – Cumulative vertical subsidence as of 14 February 2019 for the highway alignment surveys and SDPS model. Also showing the panel edges and location of Embankment #1

Both predicted and measured horizontal movements parallel and perpendicular to the roadway showed reasonably good comparison. Figure IIa.9 shows the survey horizontal movements in the eastbound lanes and compares the observations to SDPS predictions. The overall trends in the parallel movements show the overall movement into and toward the center of the basin (Figure IIa.9a). This profile also shows a termination in eastwardly movement of the pavement on the east side of the western asphalt relief section. On the eastern side of the study area, the measured values were close to that predicted, with slightly less movement observed east of the edge of the embankment and slightly more movement observed within the central region of the embankment. On the western side of the study area, the measured values were consistently less than that predicted. Based on this data, it appears that the asphalt relief sections and the central region of the embankment corresponded most with the variations in the horizontal movement of the roadway.

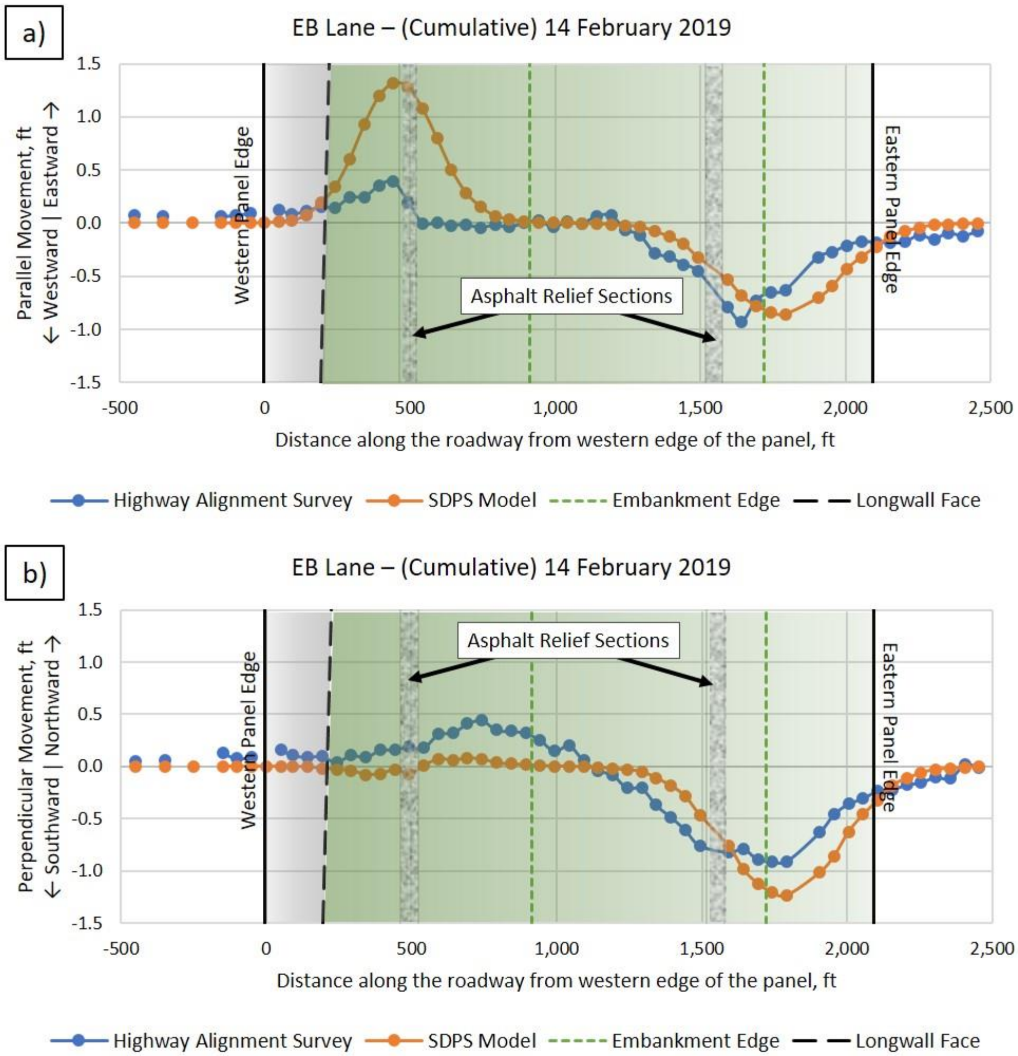

Figure IIa.9 – Comparison of the cumulative horizontal movement from the eastbound highway alignment surveys and SDPS models a) parallel and b) perpendicular to the roadway, 14 February 2019

As can be seen in Figure IIa.10 for the westbound lanes, the measured movements both parallel and perpendicular to the roadway deviated from that predicted west of Embankment #1 (Figure IIa.10a). Parallel to the roadway, a large change in the direction of horizontal movement was observed at the eastern asphalt relief section. In addition, very little movement was measured in western half of the study area. Perpendicular to the roadway, the deviations from the predicted values are more consistent throughout the study area, with the exception of the area over Embankment #1 (Figure IIa.10b). Here the shoulder moves unexpectedly to the northwest, away from the developing subsidence basin.

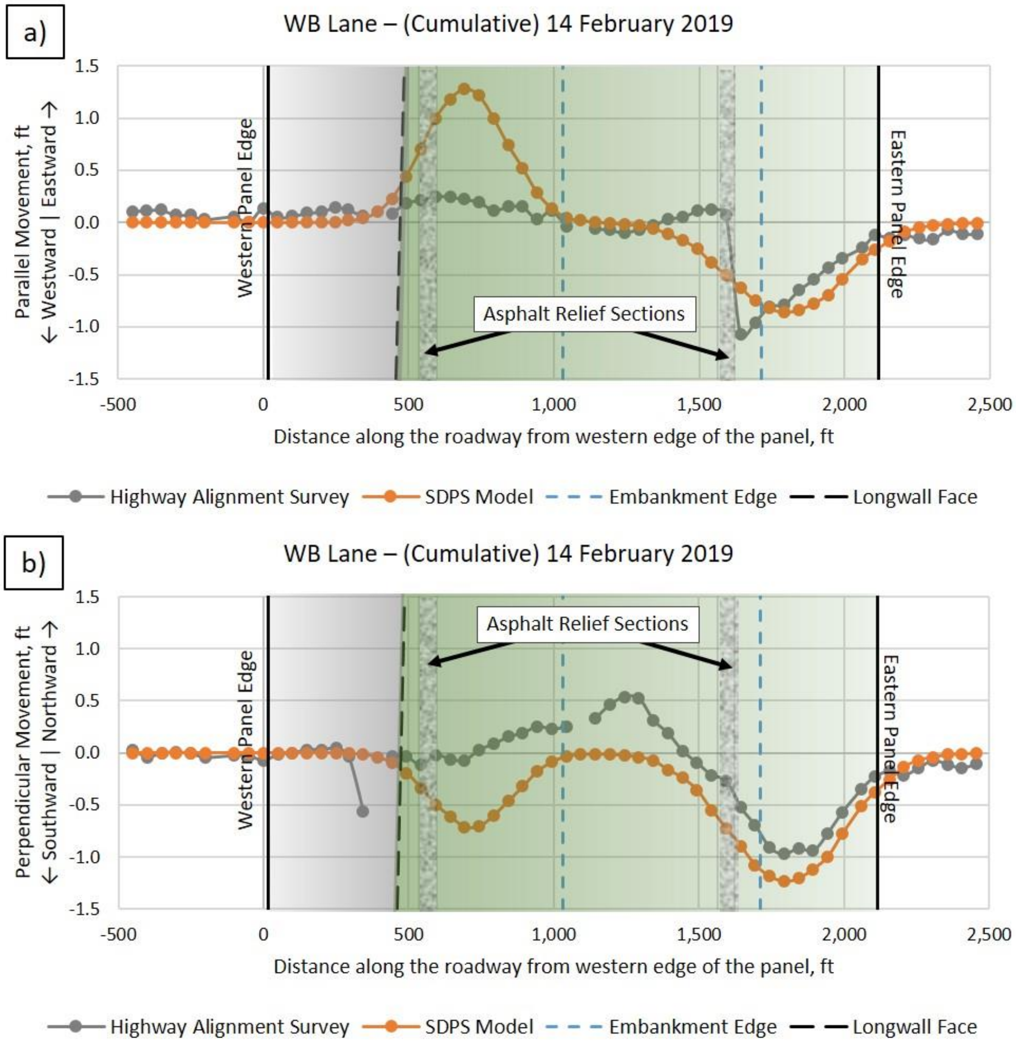

Figure IIa.10 – Comparison of the cumulative horizontal movement from the westbound highway alignment surveys and SDPS models a) parallel and b) perpendicular to the roadway, 14 February 2019

Significant changes in horizontal movement parallel to the roadway occurred between 5 to 14 February 2019 in association with the western asphalt relief section in the eastbound lanes (Figure IIa.9a) and the eastern asphalt relief section in the westbound lands (Figure IIa.10a). Here no new compression bumps were formed within asphalt relief sections (travel and passing lanes); however, a blowup in the pavement shoulder did occur several hundred feet from either asphalt relief section (Appendix I). In this same general area, several major expansion joints were observed to first open and then close over the western portion of Embankment #1 (Appendix I). Embankment #1 may have influenced movement perpendicular to the roadway for the westbound lanes.

2.3 Subsidence on 19 February 2019

On 19 February 2019, the longwall face was near the western edge of the study area. As can be seen in Figure IIa.11, the predicted and measured vertical subsidence matched well on this date, again except over Embankment #1. Like the final subsidence model, significantly more subsidence was observed on the section of highway over the central portion of the embankment than was predicted with the SDPS model. Additionally, slightly less subsidence was observed on the western side of the study area than was predicted.

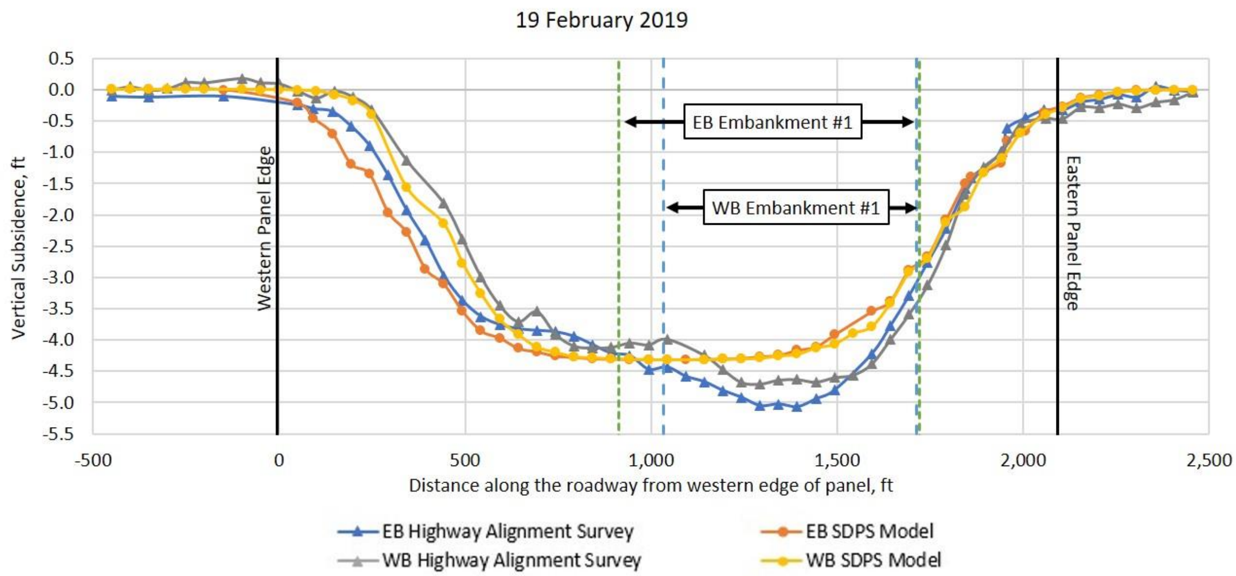

Figure IIa.11 – Cumulative vertical subsidence as of 19 February 2019 for the highway alignment surveys and SDPS model. Also showing the panel edges and location of Embankment #1

On 19 February 2019, the eastbound lanes showed reasonably good agreement between the predicted and measured horizontal movement both parallel and perpendicular to the roadway (Figure IIa.12). For the eastbound lanes, the longwall face had completely passed under the highway. The movement parallel to the roadway showed significant changes through both the eastern and western asphalt relief sections. However, the movement perpendicular to the roadway was close to zero in the portion of the road between the western asphalt relief section and the western panel edge (Figure IIa.12b).

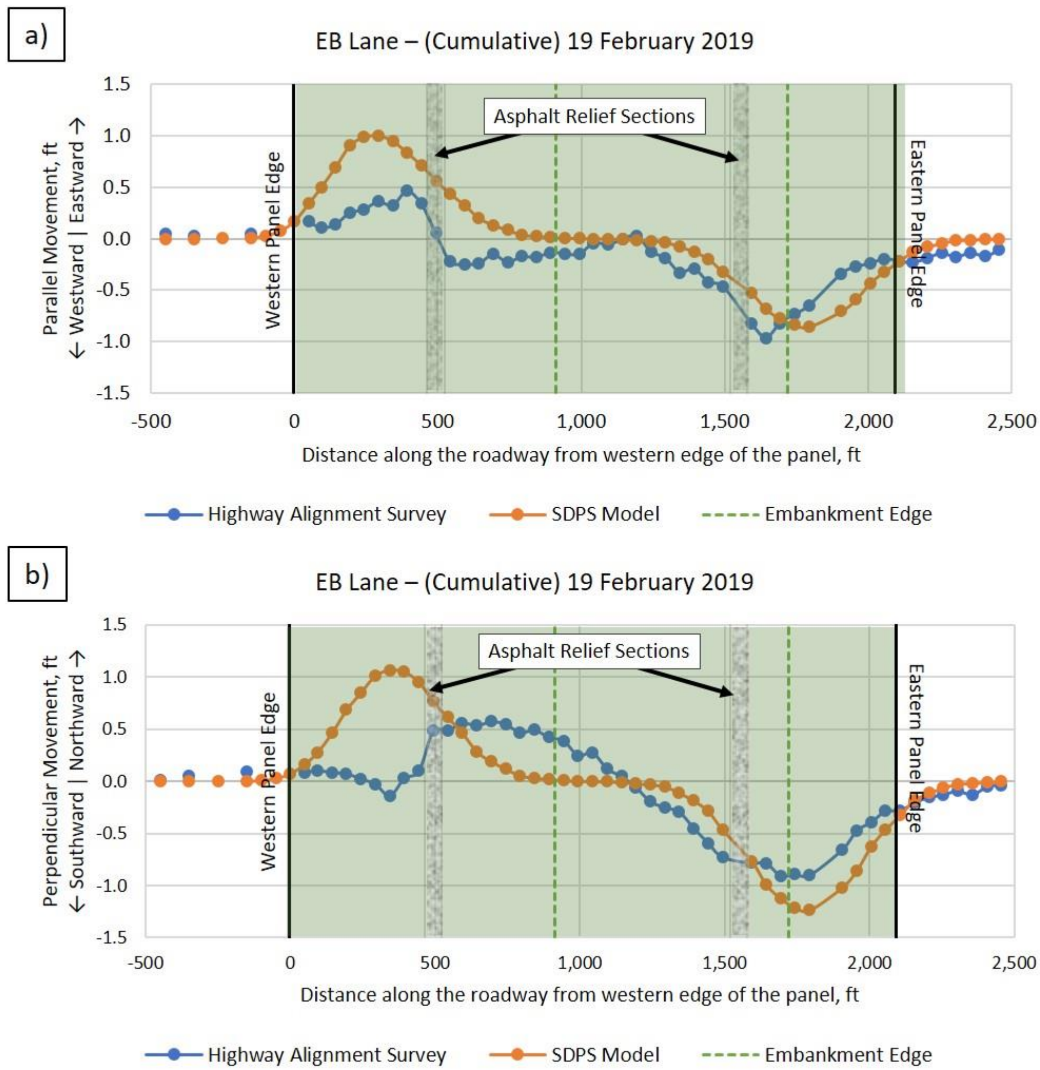

Figure IIa.12 – Comparison of the cumulative horizontal movement from the eastbound highway alignment surveys and SDPS models a) parallel and b) perpendicular to the roadway, 19 February 2019

For the westbound lanes, the horizontal movement parallel to the roadway again experienced significant changes through both the eastern and western asphalt relief sections (Figure IIa.13a). In the eastbound lanes west of Embankment #1, the movement perpendicular to the roadway is consistently to the northwest. The lack of movement between the western asphalt relief section and the western panel edge deviates significantly from the predicted movement (Figure IIa.13b). These data demonstrate the most significant deviation between predicted and measured horizontal movement in the western portion of the study area.

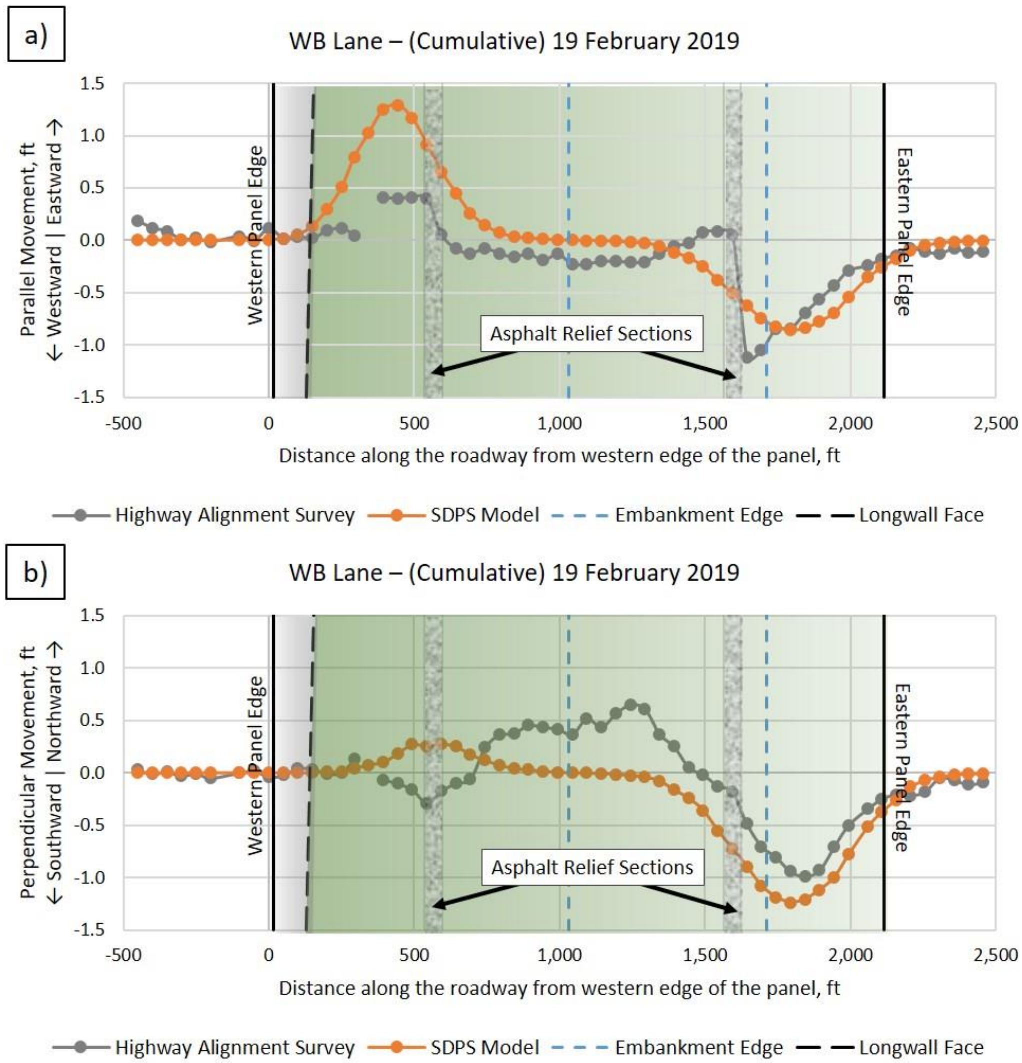

Figure IIa.13 – Comparison of the cumulative horizontal movement from the westbound highway alignment surveys and SDPS models a) parallel and b) perpendicular to the roadway, 19 February 2019

The major distress features observed between 14 and 19 February 2019 is the compression bump that extended across both lanes along the edge of the western asphalt relief sections. In addition, many transverse cracks are present between the western asphalt relief section and the western panel edge. Most of these cracks are associated with the expansion joints that showed signs of widening during this period (Appendix I).

2.4 Subsidence on 7 March 2019

By 7 March 2019, the longwall face moved sufficiently far from the highway so as to greatly reduce the potential for additional subsidence. The surface is now considered to be almost in its final position (compare Figure IIa.2 with Figure IIa.14). There are two interesting observations associated with the vertical subsidence over the gate road entries. The westbound lanes over the eastern gate road entries showed ~0.3-ft of measured vertical subsidence. This did not mirror predictions. Also, the eastbound lanes over the western gate road entries showed ~0.2-ft of vertical heave.

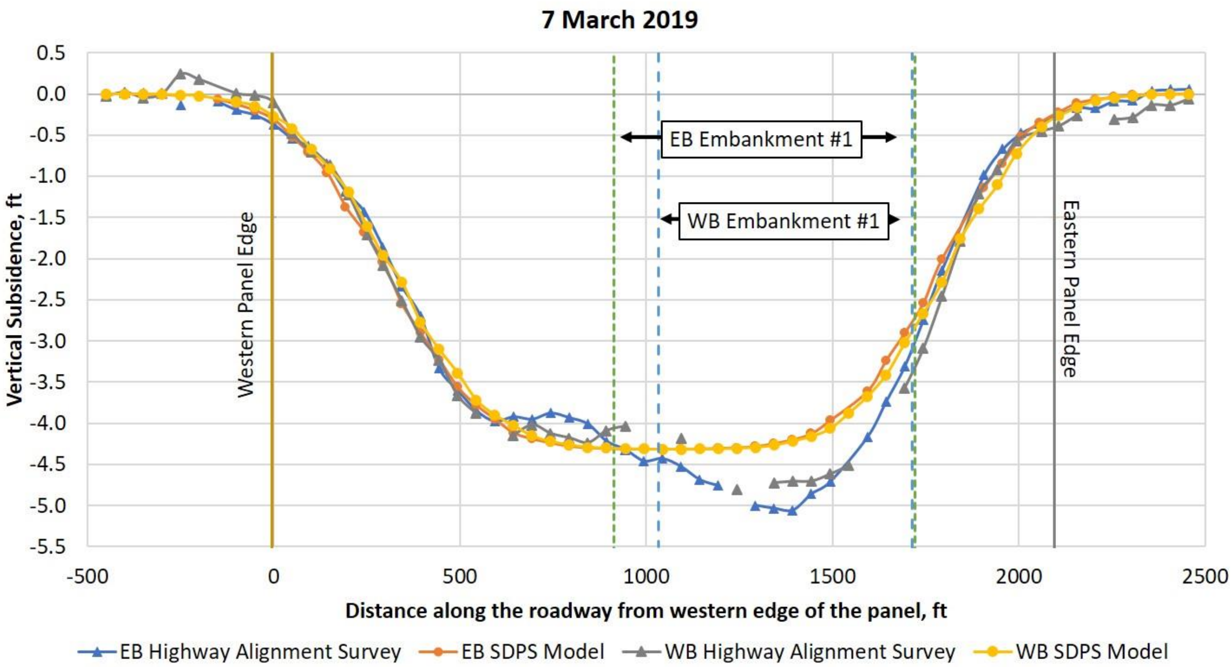

Figure 14 - Cumulative vertical subsidence as of 7 March 2019 for the highway alignment surveys and SDPS model. Also showing the panel edges and location of Embankment #1

The horizontal movements parallel and perpendicular to the roadway for both the eastbound and westbound lanes showed similar trends as those provided for 19 February 2019. In addition, no new pavement distress features were observed from 19 February to 7 March 2019.

2.5 Incremental Changes in Horizontal Movement

The data presented so far in this section represents cumulative plots of vertical subsidence and horizontal movement both parallel and perpendicular to the roadway. Cumulative plots help to evaluate the general development of the subsidence basin at different points in time. It is important to compare measured verses predicted subsidence through time so that expected (normal) and unexpected (abnormal) conditions can be recognized. However, cumulative subsidence values do not capture the characteristics of the dynamic subsidence wave. This is significant since the passage of the dynamic wave can result in dramatically different patterns of movement. It is important to recognize that many of the most significant impacts occur during discrete time periods. When subsidence conditions are grouped in segments of time, a comparison between subsidence characteristics and roadway impacts can be better accomplished.

To help overcome this issue, changes in subsidence conditions were analyzed for distinct increments of time. Figure IIa.15a shows the measured movement parallel to the roadway at four different times (29 January to 5 February 2019; 5 to 14 February 2019; 14 to 19 February 2019; and 19 February to 7 March 2019). When these eastbound lane measured profiles at different increments in time are compared to those predicted (Figure IIa.15b), the following observations are made:

- From 29 January to 5 February 2019 – measured and predicted horizontal movements show similar trends.
- From 5 to 14 February 2019 - measured and predicted horizontal movements show similar trends for the eastern portion but different for the western portion of the study area.
- From 14 to 19 February 2019 - measured and predicted horizontal movements show different trends.
- From 19 February to 7 March 2019 – unable to determine trends based on the existing data.

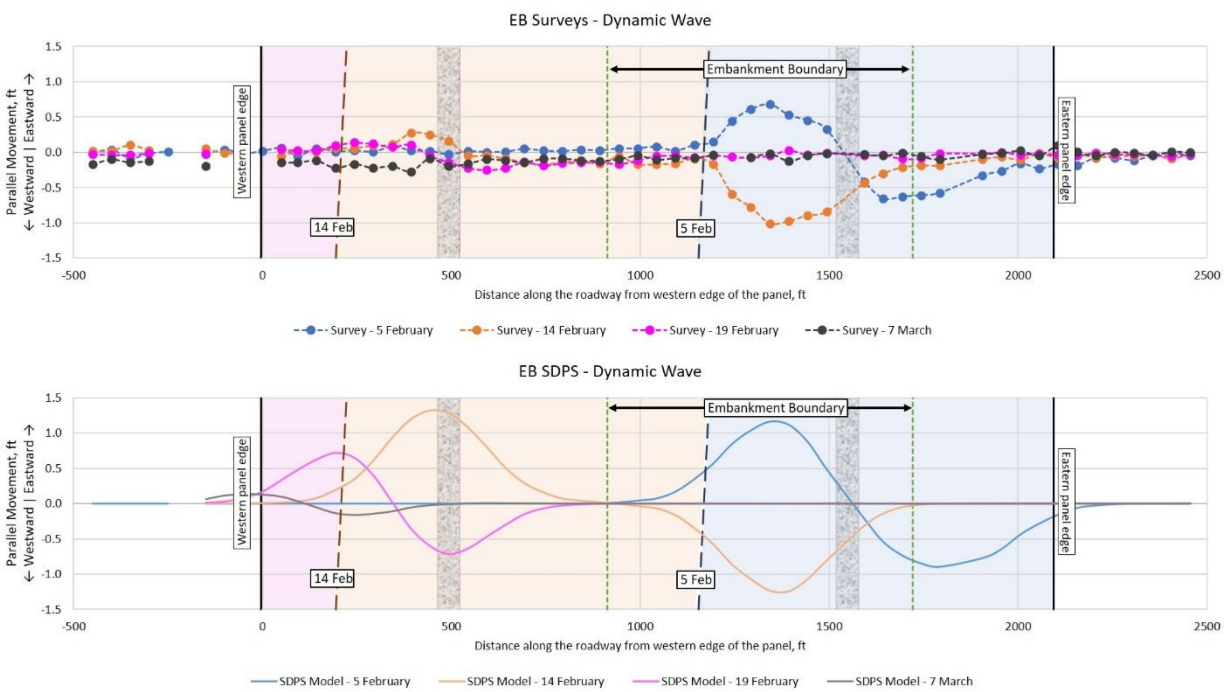

Figure IIa.15 – The dynamic nature of the developing subsidence basin is illustrated by superimposing the incremental changes in horizontal movement of the eastbound lanes at four dates; a) measured values along the highway shoulder, and b) predicted values along the surface

The westbound lanes provide another opportunity to analyze the dynamic subsidence wave (Figure IIa.16). The westbound lanes are closer to the longwall face then similar profiles from the eastbound lanes (Figure IIa.15). In addition, on 19 February 2019, the longwall face had not yet undermined the final ~100-ft of the westbound lanes. When analyzing the measured profiles along the westbound lane at different increments in time (Figure IIa.16a) with those predicted (Figure IIa.16b), the following observations are made:

- From 29 January to 5 February 2019 – measured and predicted horizontal movements show similar trends, although the magnitude of the measured values are less.
- From 5 to 14 February 2019 - measured and predicted horizontal movements show similar trends for the eastern portion but different for the western portion of the study area.
- From 14 to 19 February 2019 - measured and predicted horizontal movements show similar trends for the eastern portion of the study area, although the magnitude of the measured values are less than those predicted. The measured values for the western portion of the study area are inconclusive since crucial survey points are not available.
- From 19 February to 7 March 2019 – measure horizontal movements are not matching the predicted values in the western portion of the study area.

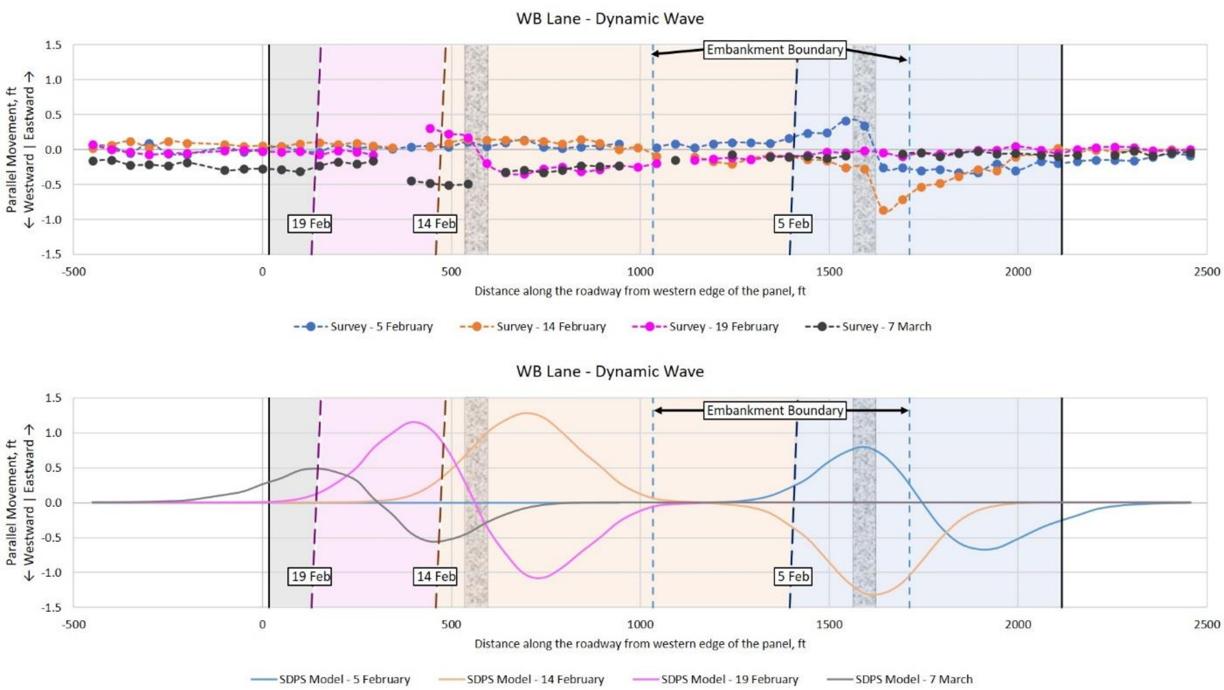

Figure IIa.16 - The dynamic nature of the developing subsidence basin is illustrated by superimposing the incremental changes in horizontal movement of the westbound lanes at four dates; a) measured values along the highway shoulder, and b) predicted values along the surface

3.0 Discussion

Overall, the University determined that inconsistencies between the measured and predicted vertical subsidence of the highway are likely due to the influence of Embankment #1 and its effect on additional vertical subsidence. The SDPS model cannot account for fill settlement behavior. There were also minor differences in the size of the subsidence basin during 14 February 2019 and the occurrence of both measureable vertical subsidence and heave over the gate road entries on 7 March 2019. In general, the SDPS predictions of vertical subsidence were very similar to those measured along the highway shoulder.

In terms of horizontal deformation, the structural design features of the pavement and the asphalt relief sections on both the eastern and western side of the study area are shown to significantly alter horizontal movements along the continuous pavement structure. Throughout the subsidence event, horizontal movement occurring parallel to the roadway dissipated mainly within the asphalt relief sections. These relief sections performed as intended and were effective in minimizing maintenance interventions to the highway pavement. The connectivity of the pavement provided by the tied concrete shoulders and the dowel bars extended across the subsidence basin and restrained the horizontal movement, as indicated by the survey data exhibiting smaller movements than the results from the SDPS model.

Analysis of the horizontal movements parallel and perpendicular to I-70 in the study area show that the highway, defined by the continuous characteristics of the pavement structure, begin to behave differently than predicted after 5 February 2019. This is the approximate time when the longwall face moves under and away from Embankment #1. At this point, the ground surface begins to be pulled into the developing subsidence basin (Figure IIa.17a). At the same time, the measured survey points along the highway shoulder show the highway to be dragged toward the area of greatest vertical subsidence (Figure IIa.17b). In some areas close to the longwall face, the highway is moving in a different direction than the predicted surface on which it rest. It is thought that the highway began to twist at this point affecting how its western portion responded to the developing subsidence basin. The distress that developed in the pavement surface supports this theory, and will be discussed further in Section IIb. It is possible that this twisting is associated with a critical angle between the highway and the direction of longwall mining. The 35-deg angle found in the initial study area, as demonstrated above, can influence the potential for twisting. It is also likely that angles closer to zero or 90-deg are less likely to induce highway twisting.

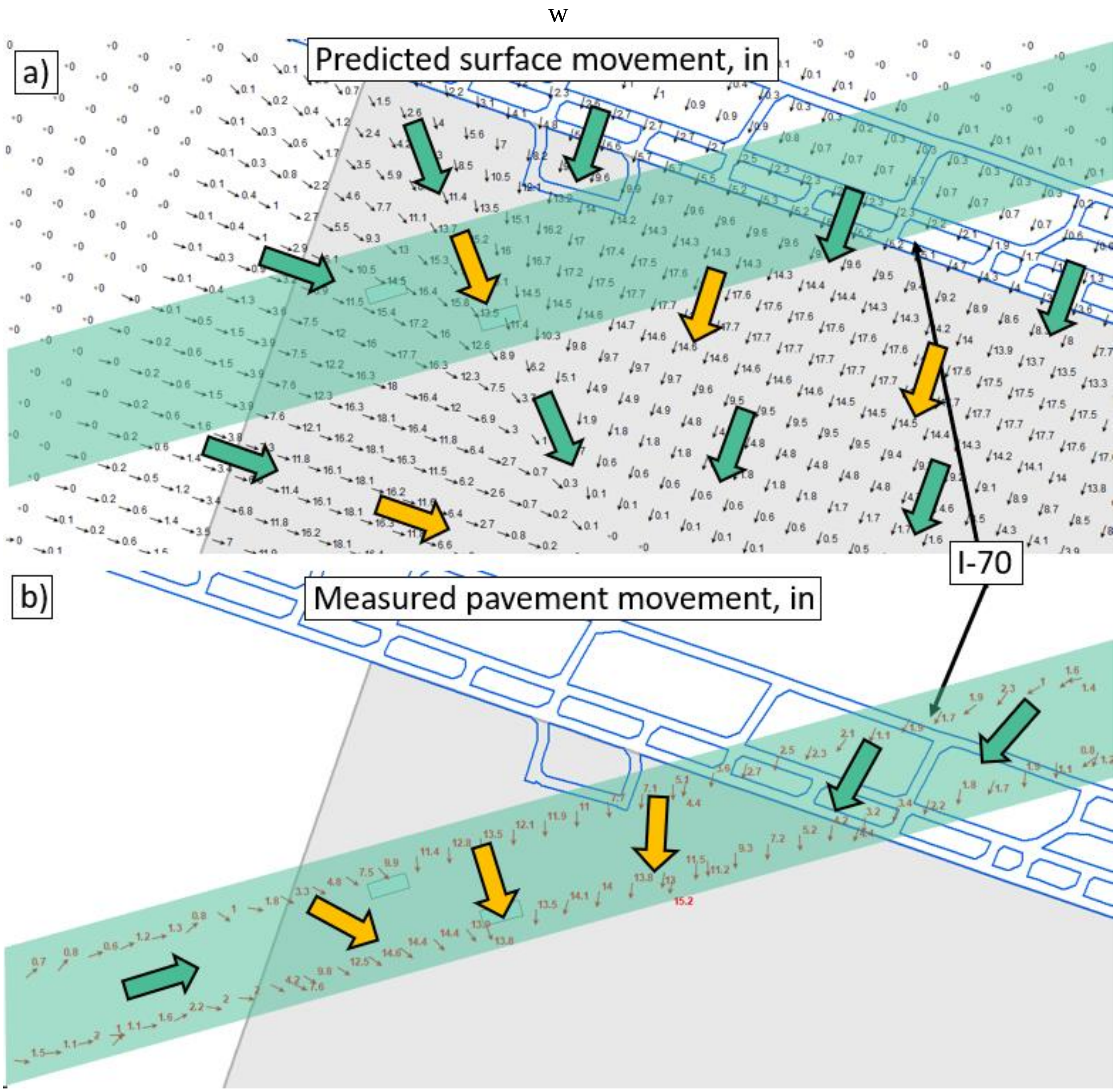

Figure IIa.17 – a) horizontal deformation as predicted by the SDPS model showing the movement of the surface into the developing subsidence basin on 5 February 2019; b) measured pavement movement along the highway shoulder on 5 February 2019

The relationship between horizontal movement and some of the other types of pavement damage observed is less constant throughout the subsidence event. Some of the compression bumps, blowups, and damaged guiderails seem to correspond with areas of significant movement either parallel or perpendicular to the roadway, but this was not always the case. The relationship between the horizontal movements and the pavement deformations is central to the discussion that follows in Section IIb.

Subsection IIb – Pavement Analysis

1.0 Pavement Structure

I-70 is a four-lane divided highway originally constructed in 1968. The topography in this region is hilly so large cut sections and embankments exist within the West Virginia and Western Pennsylvania region. This section of I-70 was reconstructed in 1989. A cross section of the reconstructed highway is provided in Figure IIb.1. It consists of a 13-in jointed plain concrete pavement (JPCP) with two 12-ft lanes per direction. This was placed on an open graded subbase that is 8-in thick in areas of cut and 10-in thick in areas of fill. The skewed (1:6) transverse joints are 20-ft apart and contain 1.5–in diameter dowels that are 18-in long. The pavement has 4-ft inside and a 10-ft outside tied concrete shoulders that are 8-in thick adjacent to the lanes and tapered down 6-in at the outside edge. The tied shoulders contain #5 bars spaced 30-in on center and the transverse joints has 1.5-in diameter dowel bars. This section of roadway was eventually overlaid with 4 to 5-in of asphalt.

The travel lanes were constructed with a typical 2-pct cross slope, which sloped towards the outside shoulder. Both shoulders were constructed with a typical 4-pct cross slope, which sloped towards the outside shoulder. The westbound and eastbound travel lanes are separated with a grass median that varies between 30 and 70-ft in width.

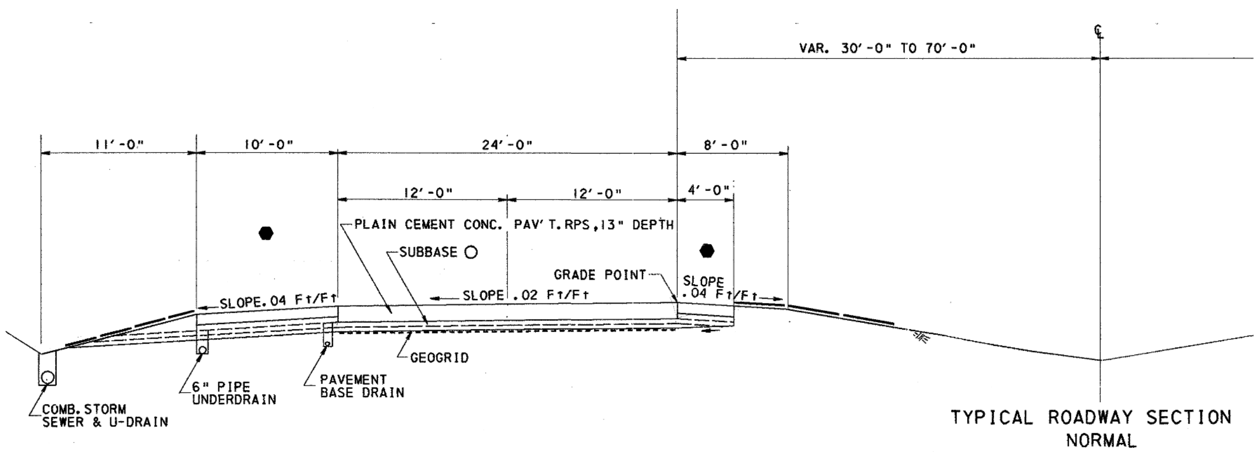

Figure IIb.1 – Typical cross section of I-70 from plans of 1980s highway reconstruction

2.0 Pre-Mining Mitigation Activities

Prior to the undermining of this section of I-70, the pavement was modified to better accommodate the large stresses and strains expected during undermining.

2.1 Asphalt Relief Sections (ARS)

Four asphalt relief sections were constructed in the portion of I-70 undermined by Panel 15. Construction of the relief sections consist of removing 60-ft sections of the JPCP and the asphalt overlay and replacing it with an asphalt pavement. They were constructed in areas where the highest compressive strains were expected to occur from the subsidence. The asphalt relief section is designed to absorb large compressive strains. In some cases, these strains are great enough to form compression bumps in the asphalt. If these compressive bumps develop, they can be quickly milled to restore the roadway profile while limiting disruption to traffic. On the other hand, significant compression strains in the JPCP portions of the highway can form 'blowups'. Photos and detailed descriptions of these distresses can be found in Appendix I. When a blowup develops in a concrete pavement, it cannot be repaired as quickly. Special attention was paid to the performance of these asphalt relief sections throughout the duration of the undermining. The location of these relief sections can be seen in Figure IIb.2. They were constructed approximately 300-ft from the edge of the gate roads of the longwall mine, which is approximately the predicted location of maximum compressive strain.

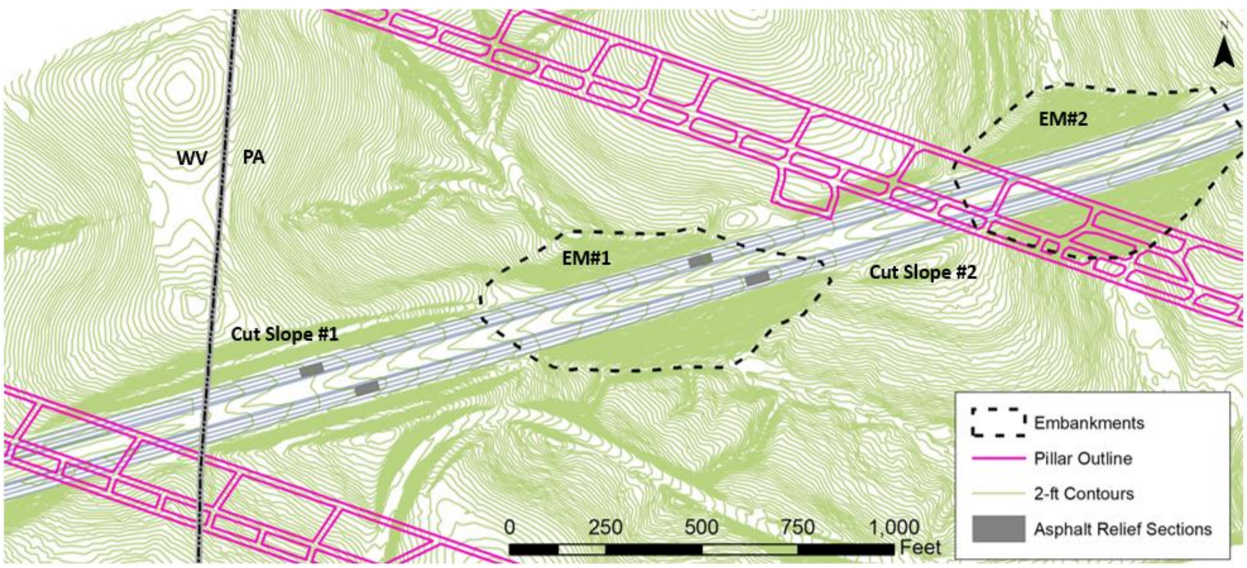

Figure IIb.2 – Location of asphalt relief sections within initial I-70 study area

Asphalt relief sections, such as these have been used by PennDOT during previous undermining operations. An example of this application was provided by PennDOT (Painter, 2011) when the B5 panel of the Emerald mine undermined I-79 in August of 2007 (Figure IIb.3). In this case, the asphalt relief sections were 250 to 300-ft from the panel edge. As was done previously, these asphalt relief sections were only constructed in the travel lanes and the concrete shoulder adjacent to these asphalt relief section remained in place. This allowed the concrete shoulder to provide connectivity between the adjacent overlaid JPCP across these asphalt relief sections.

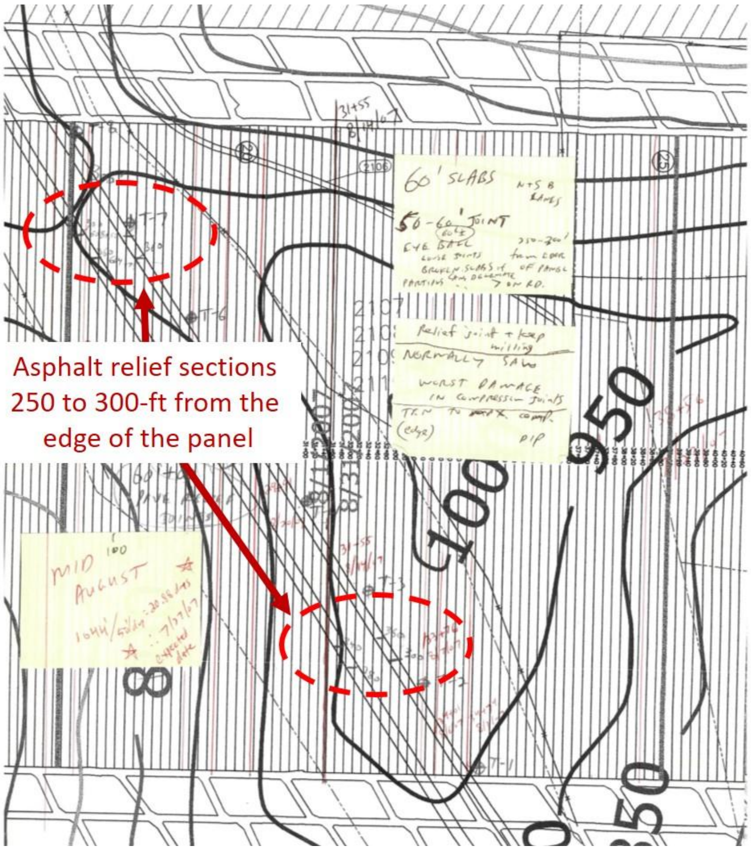

Figure IIb.3 – 2007 map of the Emerald Mine B3 panel Mine showing the location of the asphalt relief sections (Painter, 2011)

2.2 Asphalt Overlay

Approximately six months prior to the undermining of this section of I-70, a mill and fill was performed. This consisted of milling 2-in of the existing asphalt overlay and replacing that with 2-in of new asphalt. The new overlay provided a non-distressed surface, so that the damage directly associated with the undermining can more easily be observed. Joints were sawed into the asphalt overlay directly above the transverse joints in the underlying jointed plain concrete pavement. It was observed that there was difficulty in matching the underlying joints in the JPCP when sawing them into the asphalt overlay. Joints sawed into the asphalt overlay did not exhibit the consistent 1:6 skew that is in the underlying JPCP. The transverse joints sawed into the asphalt were sealed.

2.3 Pavement Cores

Ten cores were taken from the pavement structure after the undermining was completed, but prior to performing the post-mining rehab activities on the roadway. As such, these cores represent the pavement structure after the subsidence basin had fully developed. The location where each core was pulled and the respective core label are provided in Figure IIb.4. The cores were taken from the driving lane, shoulder, and asphalt relief section. All cores were taken from the either the driving (outside) lane or the outside shoulder.

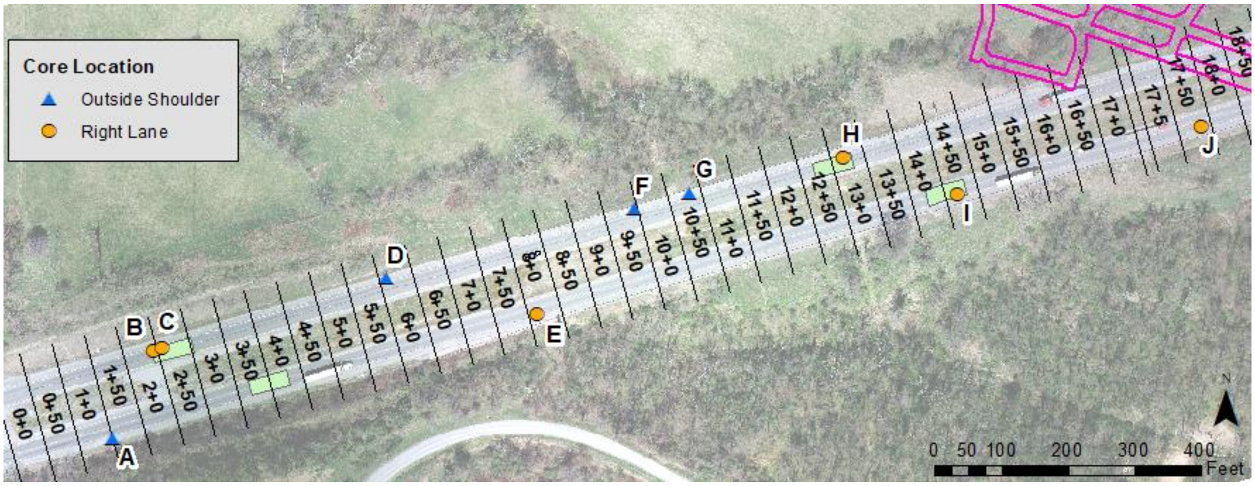

Figure IIb.4 – Location of pavement cores collected in the initial study area

Two cores were taken throughout the study area in the driving lanes. Images of the samples collected from these cores can be seen in Table IIb.1. As displayed in the table, the driving lane consisted of 14-in concrete pavement and a 5-in asphalt overlay at these two locations.

Four cores were pulled from the outside shoulder. Images of the samples collected from these cores are provided in Table IIb.1. Three of the four cores taken from the outside shoulder consisted of 9-in of concrete with 5-in of asphalt and the fourth core was 13-in of asphalt and no concrete. It appears that the full-depth asphalt shoulder was limited to this panel location (Sta. 6+11, and in the outer shoulder of the westbound lane). The remaining of portions of the shoulder consist of JPCP under an asphalt overlay.

Three cores were taken in the asphalt relief sections with images of the samples shown in Table IIb.1. The asphalt relief sections consisted of approximately 20-in of full depth asphalt.

Table IIb.1 – Summary of pavement core information

ID	Location	Category	Asphalt Layer (in)	Concrete Layer (in)	Picture
A	1+50 EB	Outside Shoulder	5	9	
B	2+42 WB	ARS, Driving Lane	21	0	
C	2+56 WB	ARS, NA Lane	20	0	
D	6+11 WB	Outside Shoulder	13	0	
E	8+16 EB	Driving Lane	5	14	
F	9+96 WB	Outside Shoulder	5	9	
G	10+81.5 WB	Outside Shoulder	5	9	
H	13+18 WB	ARS, Driving Lane	18	0	
I	14+68 EB	ARS, Driving Lane	18	0	
J	17+86 EB	Driving Lane	5	14	

WB-Westbound lanes; EB-Eastbound lanes; ARS-Asphalt relief section; NA-Not available

3.0 Global Movement of Highway during Undermining

Regular surveys were conducted throughout the undermining process. A total of 147 points along the highway surface were surveyed by PennDOT's surveyors 11 times during the undermining event. These points were based on the center highway alignment and were offset 62-ft to be located in the shoulder of the highway. These surveys have a horizontal precision of 0.24-in and a vertical precision of 0.6 to 1.2-in, but the accuracy of the surveys is likely higher. Based on the data, the horizontal accuracy of these surveys is likely around 1-in, which would suggest the vertical accuracy is approximately 2-in. An additional 590 points located on the embankment and cut slopes were surveyed by SPK Engineering to characterize the movement of the slopes. The SPK surveys have a reported accuracy of 0.36 to 0.48-in in both the horizontal and vertical planes.

Additionally, LiDAR scans were completed during the undermining event using a mobile LiDAR unit, collecting the positions of millions of points along the road surface. These scans have a precision of 0.2 to 0.4-in in the horizontal plane and 0.016-ft (5-mm) in the vertical plane. However, post processing of the LiDAR data decreased the accuracy of the scans to approximately 1-in in both the horizontal and vertical planes.

3.1 Final Subsidence Basin Movement

Traditionally, a supercritical longwall subsidence basin is trough shaped. The panel subsides symmetrically along the long and short axis. The ground surface at the center of the panel drops by the maximum vertical subsidence and then slopes upwards at its edges to the original ground elevation beyond the longwall panel. As a result of this extension and bending of the ground surface, the points on the surface move on the horizontal plane at different rates towards the center of the longwall panel.

A discussion on the overall length change of the pavement is presented first, followed by a discussion on the effects of more localized regions of the pavement placed into tension and compression.

3.1.1 *Vertical Subsidence Effects on Pavement*

Survey data was compiled and analyzed to determine the location of highway surface and the adjacent slopes after the final subsidence. Figure IIb.5 shows the vertical displacement of the highway after final subsidence. The majority of the subsidence on the highway surface occurs in the center of the panel.

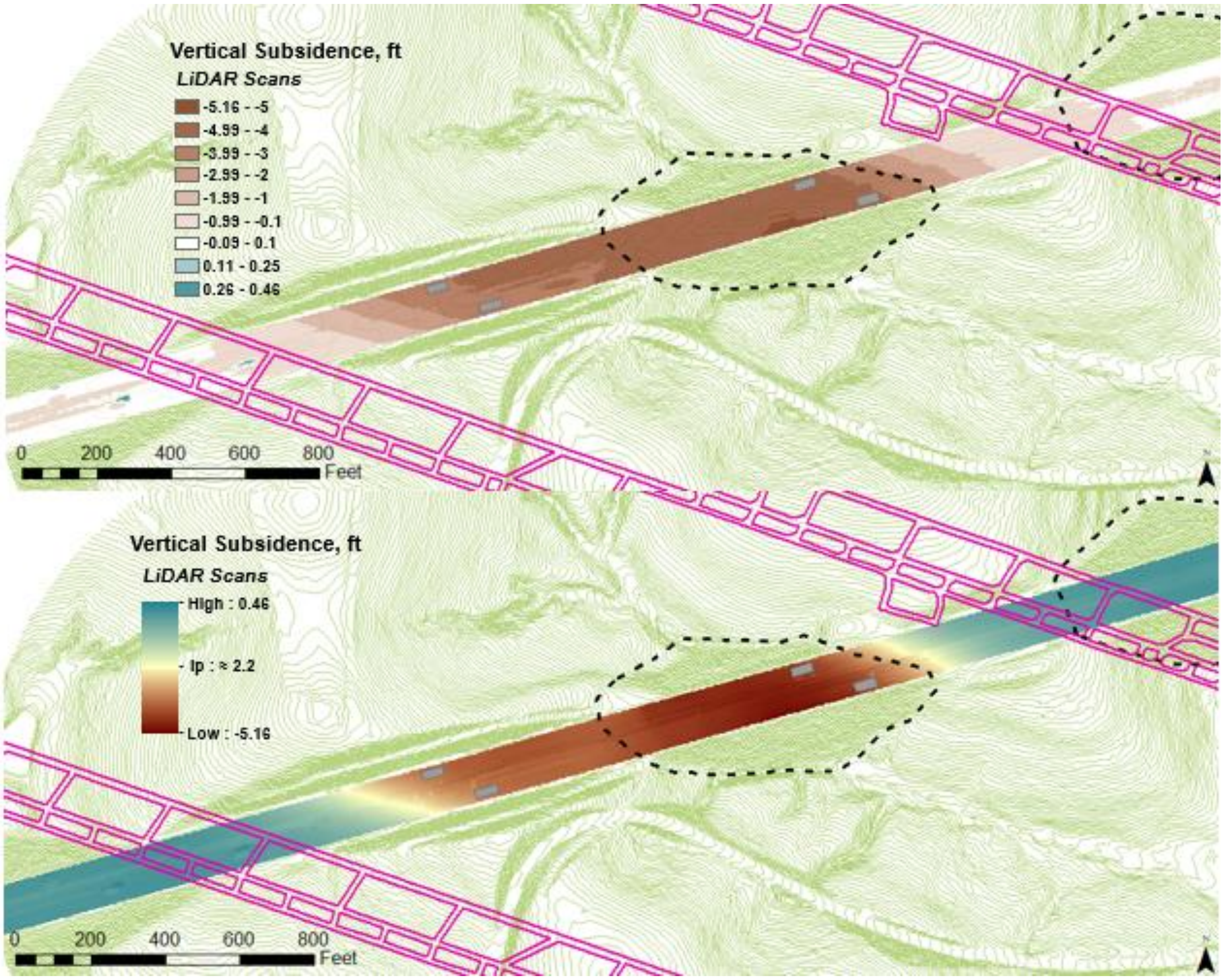

Figure IIb.5 – Final vertical subsidence of I-70 caused by the mining of Panel 15 (March 2019)

The length of the surface, and hence potentially the length of the pavement, can increase or decrease depending on the topography prior to the undermining. To show how the length of the pavement surface changes, the University conducted an analysis to characterize the amount a surface profile would change in length based on the topography (shape of the profile) prior to the subsidence. Three surface profiles were examined (Figure IIb.6). The first profile is a flat surface, the second consists of a hill in the center of the panel to be mined, and the third consists of a valley in the center of the panel. All profiles are symmetrical with each profile terminating at the ends of the panel and central portion of the profile spanning across the panel. The hill (and the valley) profile has a linear increase (decrease) in elevation, which peaks at a 100-ft difference in elevation at the center of the panel.

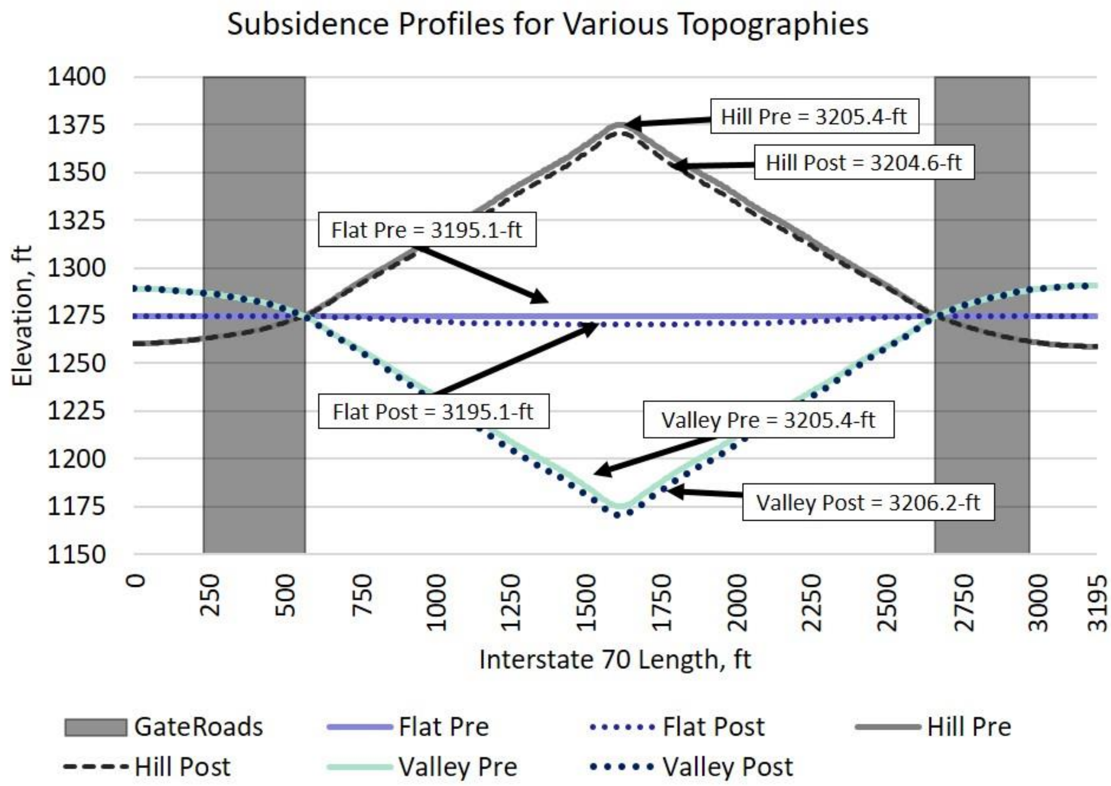

Figure IIb.6 – Effects of three general surface topographic features on the extension / compression of the overlaying pavement

Each model was predicted to experience 4.3-ft of vertical subsidence. It is logical to assume that as the ground subsides downward, a topographically flat surface would result in a depression and could potentially extend the overall length of the effected pavement. It is also assumed that a highway spanning a valley would also experience an increase in overall pavement length. Conversely, a highway spanning a hill would subside slightly downward, resulting in a decrease in the length of the pavement after the subsidence.

Decreasing the length can result in the development of transverse joint spalling, blowups and compression bumps immediately as well as over time. As the transverse joint width (spacing between the slabs) is reduced with a reduction in the length of the pavement, the space available to accommodate thermal expansion of the slab during the summer months is reduced. This can lead to the development of transverse joint spalling, blowups and compression heaves when the pavement temperatures are higher. Increasing the length of the surface, and hence the length of the pavement will allow these joints to open. This is very problematic if there are not shear transfer devices (dowel bars) along the transverse joints, as very small opening (> 30 mils) can lead to a loss of contact between the slab faces and load is not transferred from one side of the joint to the other. Dowel bars are able to provide load transfer across this joint as the joint widens, although degradation can potentially occur at a greater rate as the joint width becomes increasingly wide and remains that way for the remaining service life of the pavement. Ideally, the joint is located at the center of the dowel bar with ~9-in of the dowel bar embedded into each slab but rarely do actual construction expansion joints actually are positioned at the exact central point of the bar. If at any time the joint width widens to the point where the bar becomes dislodged from either of the adjacent slabs, load transfer will be lost and subsequent thermal expansions of the slab could be problematic if misalignment occurs between the bar and the point where it was embedded into the slab.

Figure IIb.7 shows the highway elevation profile before and after undermining of I-70. The elevations are provided by the LiDAR surveys conducted along the roadway. It was determined that the highway did not increase in length after this vertical drop. The length of the highway surface before and after the subsidence was also estimated using ArcGIS. The "Add Surface Information" tool in ArcGIS was used, which measures the length of a surface along a specified line. A line was projected across the eastbound lane and it was again determined that the length of the highways surface did not increase. It can be seen from the previous analysis how the topography can affect the change in length of the surface profile. The culmination of the effects of the topography along I-70 resulted in the length of the pavement surface to be similar to that prior to the subsidence. The fact that the widths of the expansion joints before and after the subsidence were similar is an indication that this indeed the case.

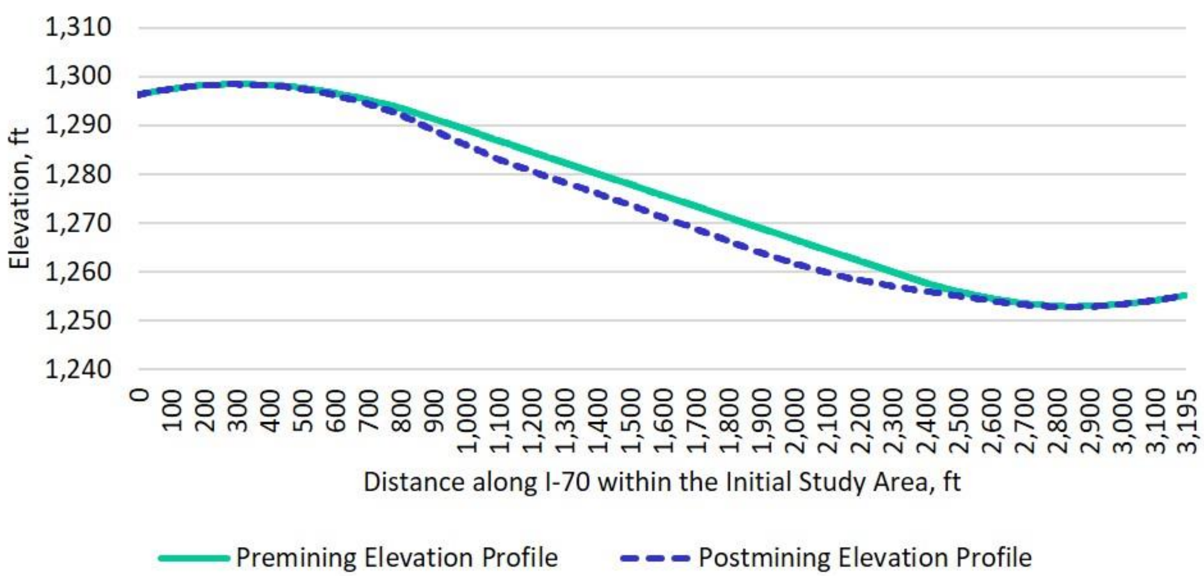

Figure IIb.7 – Highway profile before and after undermining

3.1.2 *Horizontal Deformation and Translational Movement*

The highway alignment survey points are used to provide the actual horizontal deformation (Figure IIb.8). This figure shows the magnitude and direction of horizontal deformation of the points surveyed during the undermining. The maximum horizontal movement was observed east of the asphalt relief sections above Embankment #1.

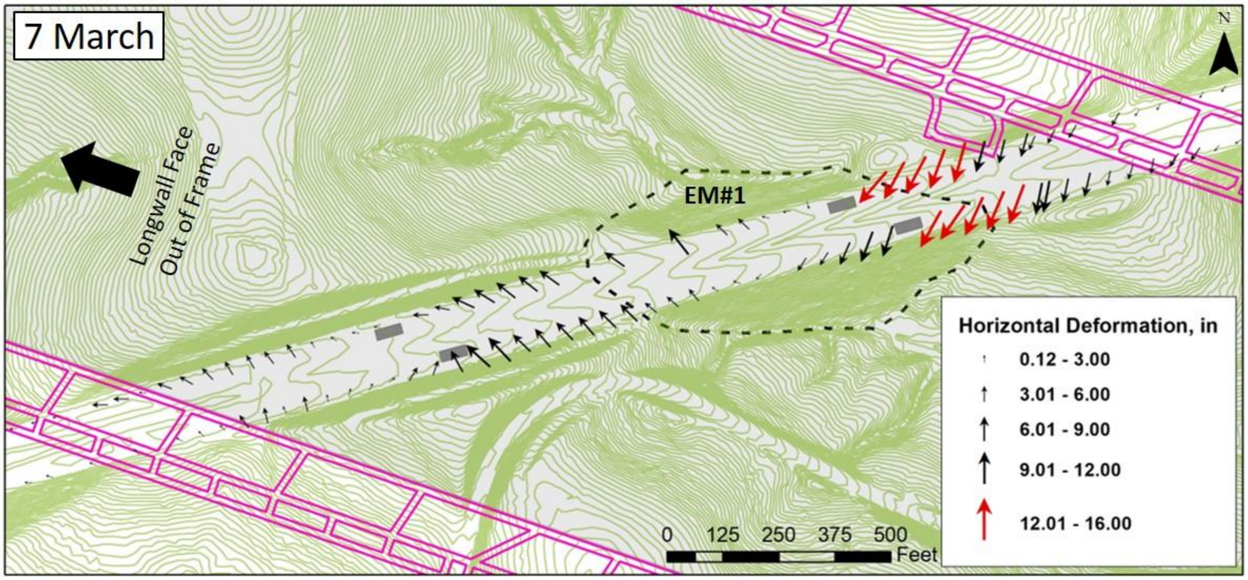

Figure IIb.8 – Final horizontal movement on the surface of I-70 caused by the mining of Panel 15

The highway surface experienced a maximum horizontal movement of approximately 1.5-ft near the eastern side of the study area. This movement was oriented primarily towards the center of the subsidence basin, which is typical of a traditional subsidence basin. This movement dissipated at the eastern asphalt relief sections near the edge of Embankment #1. The highway surface adjacent to Cut Slope #1 to the east of the western asphalt relief sections also experienced significant movement. These points moved primarily in a north-west orientation at a magnitude of between 0.5 and 1-ft. The western asphalt relief sections also dissipated the horizontal movement, causing minimal movement at the western most edge of the study area.

The direction of the movement of the highway surface on the western side of the study area is not typical for subsidence basins. When looking at the magnitudes and directions of the movement of the highway surface above the mined region (Figure IIb.8), it appears that the pavement structure is twisting throughout the study area. Rather than both extents of the highway moving towards the center of the longwall panel, the eastern side of the highway moved towards the center of the basin and the western side of the highway moved parallel to the gate roads towards the longwall face. The pavement connectivity allows it to twist and the location of the embankment defines the point at which it twists around. The pivot point appears to be over the central embankment, indicating that the granular fill material may have dissipated movement and facilitated the twisting.

3.2 Dynamic Subsidence Ground Movement

As longwall mining progresses, the subsidence basin forms gradually in a dynamic wave. This dynamic wave results in a gradual change in the magnitude and location of the horizontal stresses and strains in the surface until the ground eventually becomes stationary and what remains is the final (permanent) subsidence.

Panel 15 was mined at an average rate of 115-ft/day and was beneath the highway for approximately a month. The longwall operated only on the weekdays and there was one unscheduled shutdown day when the panel was underneath I-70.

3.2.1 *Temporal Vertical Subsidence*

As the longwall face progressed westward, the ground surface subsided vertically as the longwall basin formed. Figure IIb.9 shows the vertical subsidence measured on 5 February 2019 when the longwall face was below Embankment #1. This shows a maximum subsidence of about 3.75-ft developed on the highway surface adjacent to the top of the south slope of Embankment #1, occurring about 300-ft behind the longwall face. No point in the study area had reached the maximum predicted subsidence of 4.3-ft at this point in time. This is due to the fact that the points far enough behind the longwall face to drop to the maximum allowable subsidence are too close to the gate road entry to experience this maximum drop in surface elevation.

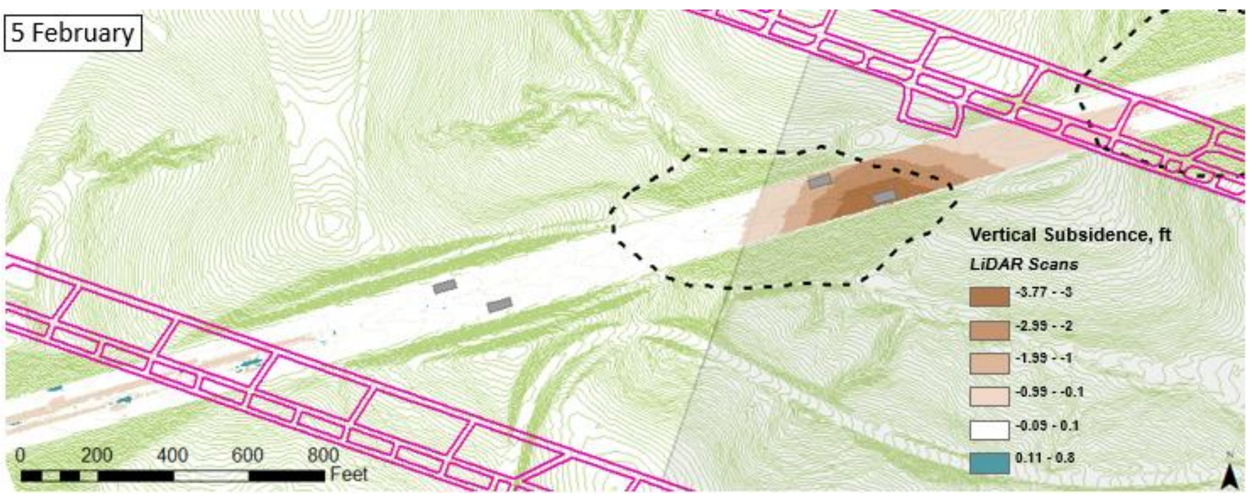

Figure IIb.9 – Cumulative Vertical subsidence on 5 February 2019. The source of data is LiDAR

Figure IIb.10 shows the vertical subsidence on 10 February 2019 when the longwall face was approaching the western asphalt relief sections. At this point in time, a maximum subsidence of more than 5.4-ft was observed on the highway surface over the center of the embankment, which was approximately 450-ft behind the longwall face on 10 February 2019. This number seems erroneous because each other scan from this date forward have a maximum vertical subsidence at approximately 5.1-ft. Notice also the regions on the interstate just ahead of the longwall face that indicate up 2-ft of vertical subsidence. This type of movement before the longwall face pass underneath these areas would certainly be unexplainable, leading the University to put the accuracy of the 10 February 2019 LiDAR scan in question. The university reported on the accuracy of the LiDAR scans in Subsection IIIg of the Task 2 Report, in which it pointed out the 10 February 2019 scan as having a lower vertical accuracy than each other scan. The University believes that could be the reason for these unexpected results in Figure IIb.10.

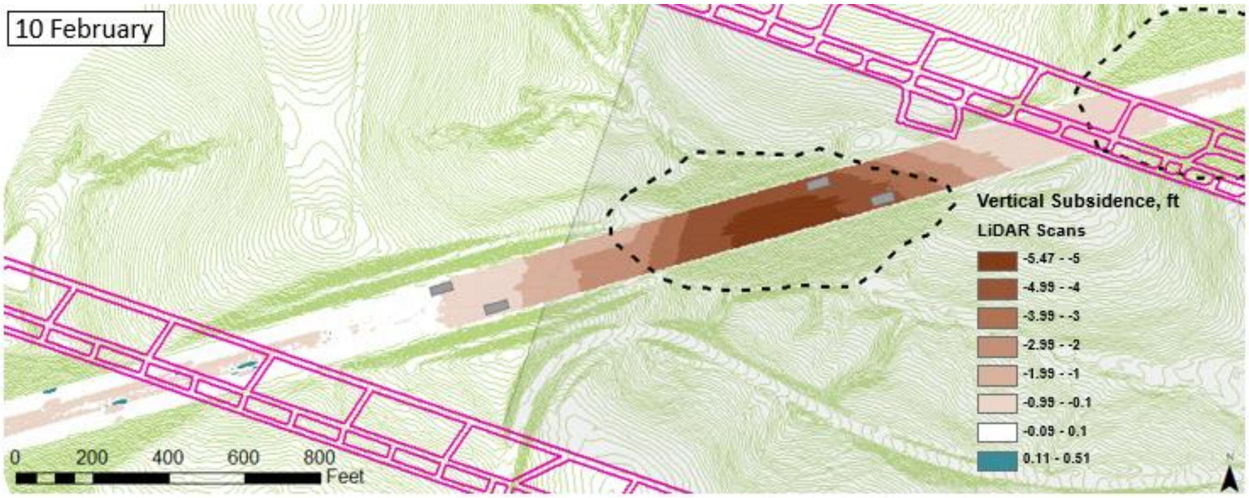

Figure IIb.10 – Vertical subsidence on 10 February 2019

Figure IIb.11 shows the vertical subsidence on 18 February 2019 when the longwall face was at the end of the highway section. This shows an area of maximum subsidence of just over 5-ft on the highway adjacent to the top of the south slope of Embankment #1, occurring about 1,090-ft behind the longwall face. By this point in time, the subsidence basin slope on the western side of the study area is approaching full development, depicting the symmetrical shape typical of that seen in a final subsidence basin. It is also worth noting that small amounts of surface heave were observed along the highway over the gate road entries and in-front of the longwall face.

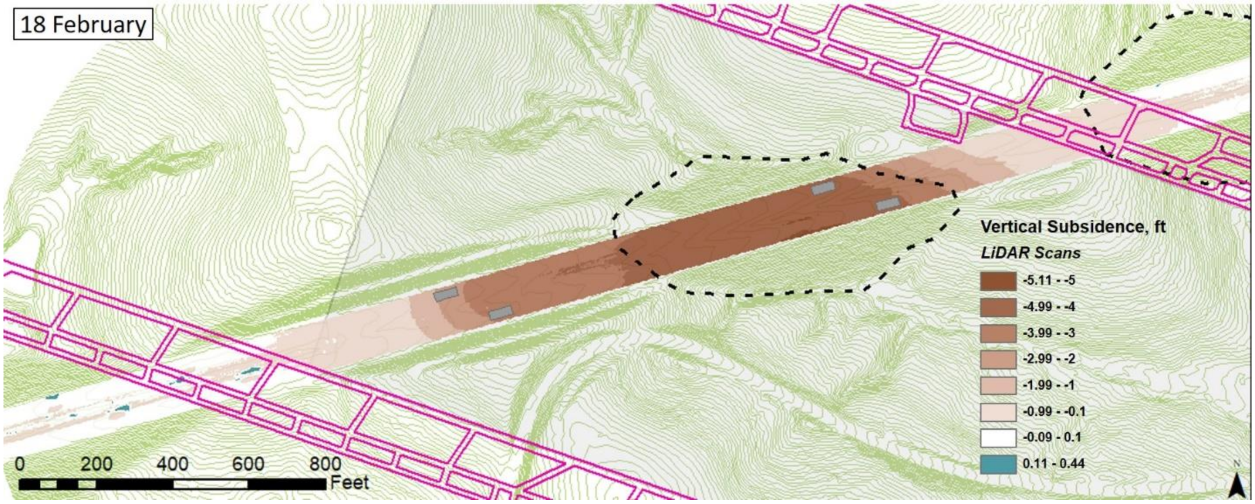

Figure IIb.11 – Vertical subsidence on 18 February 2019

3.2.2 *Temporal Horizontal Movement*

The weekly highway alignment surveys performed show the progression of the horizontal deformation of the subsidence basin as the longwall mining progressed. Figure IIb.12 shows the cumulative horizontal movement of the ground surface on 5 February 2019, when the longwall face was beneath the central portion of Embankment #1. This section of highway experienced significant horizontal movement, with magnitudes around 1.5-ft, oriented towards the center of the longwall panel. The movement of the highway surface is partially dissipated by the asphalt relief sections.

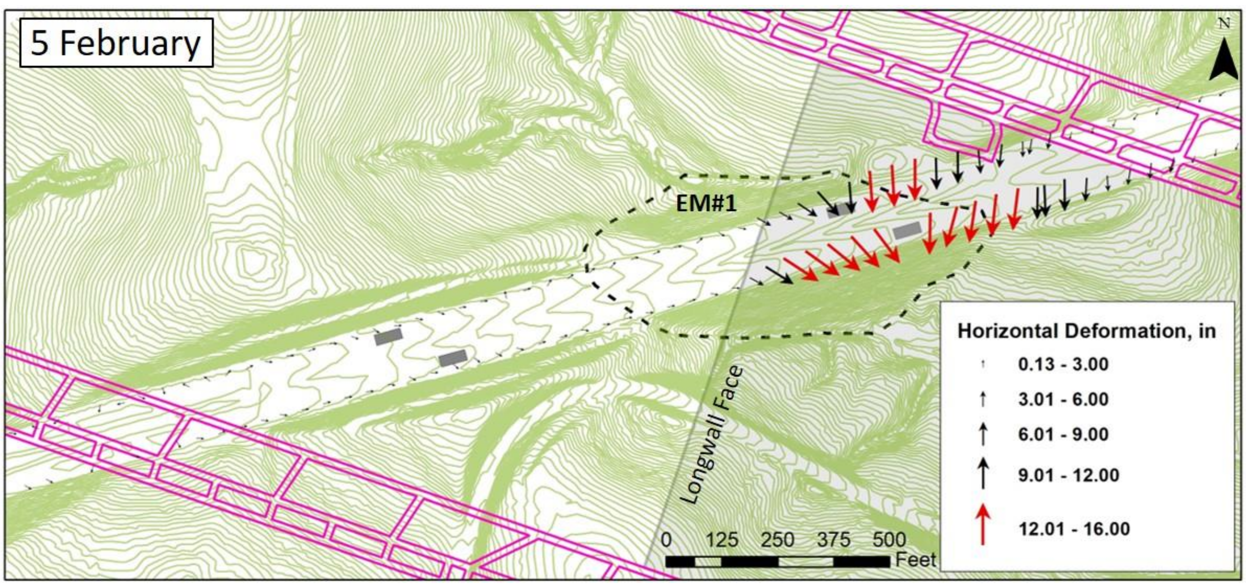

Figure IIb.12 – Cumulative horizontal movement on 5 February 2019. The source of data is the highway alignment surveys

Figure IIb.13 shows the cumulative horizontal movement of the ground surface on 14 February 2019, when the longwall face was just past the western asphalt relief sections. Like on 5 February 2019, the eastern side of the highway surface experienced horizontal movements with magnitudes around 1.5-ft that are oriented towards the center of the longwall panel. These movements are dissipated at the asphalt relief sections, causing there to be very minimal movement west of these relief sections. The movement on the west end of the study was greatly reduced as a result of the twisting action that occurred and the connectivity of the highway.

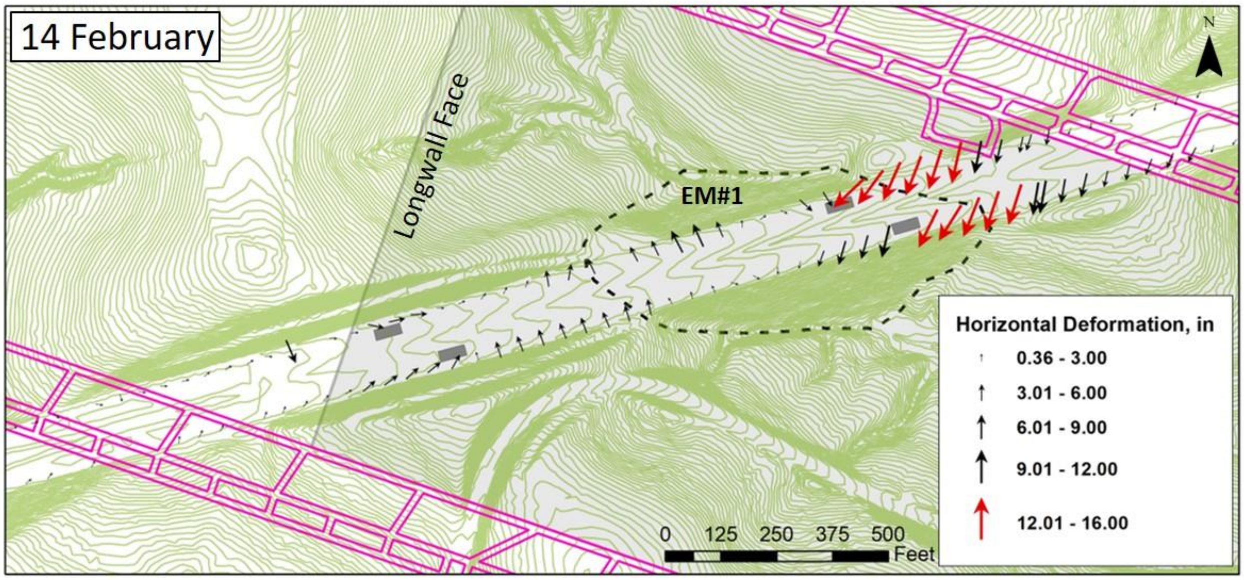

Figure IIb.13 – Cumulative horizontal movement on 14 February 2019. The source of the data is the highway alignment surveys

Figure IIb.14 shows the cumulative horizontal movement within the study area on 19 February 2019 when the longwall face was at the end of the area of highway influence. The movement observed on the highway surface had magnitudes of up to 1.5-ft on the eastern side of the study area oriented towards the center of the basin and up to 1-ft on the western side of the study area oriented towards the longwall face. These movements were dissipated at the asphalt relief sections, causing the areas just west of the asphalt relief sections to experience minimal horizontal deformation.

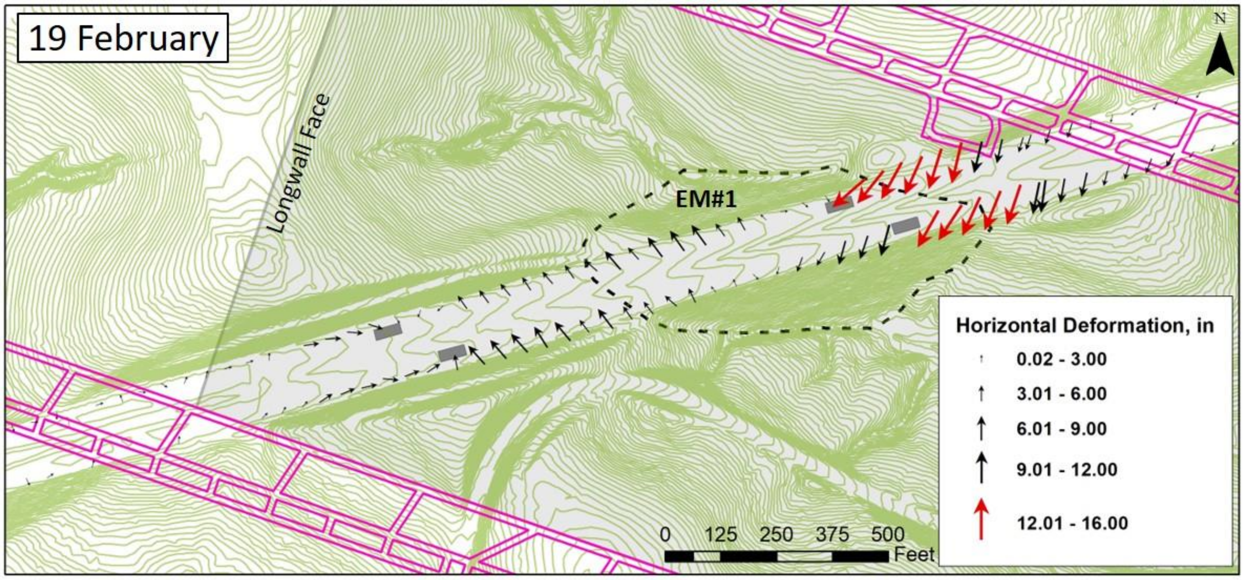

Figure IIb.14 – Cumulative horizontal movement on 19 February 2019

The horizontal movements can also be examined incrementally between surveys. The incremental movements can be seen in Figure IIb.15a. The eastern side of the highway surface experienced a lateral shift towards the center of the developing subsidence basin. The magnitude of the shift was related to the areas where the largest surface slope changes are predicted (Section IIIa.3). The incremental movement of the longwall face from position 5 February to 14 February demonstrated the strong influence of Embankment #1. The movements along the eastbound lanes to the west are in direct response to the initial easterly tilt of the surface as the longwall past under the embankment (Figure IIb.15b). The horizontal movements along the westbound lanes are directed mainly down the dip of the embankment slope. The incremental movement of the highway over the embankment was only marginally affected by longwall mining after 14 February (Figure IIb.15c).

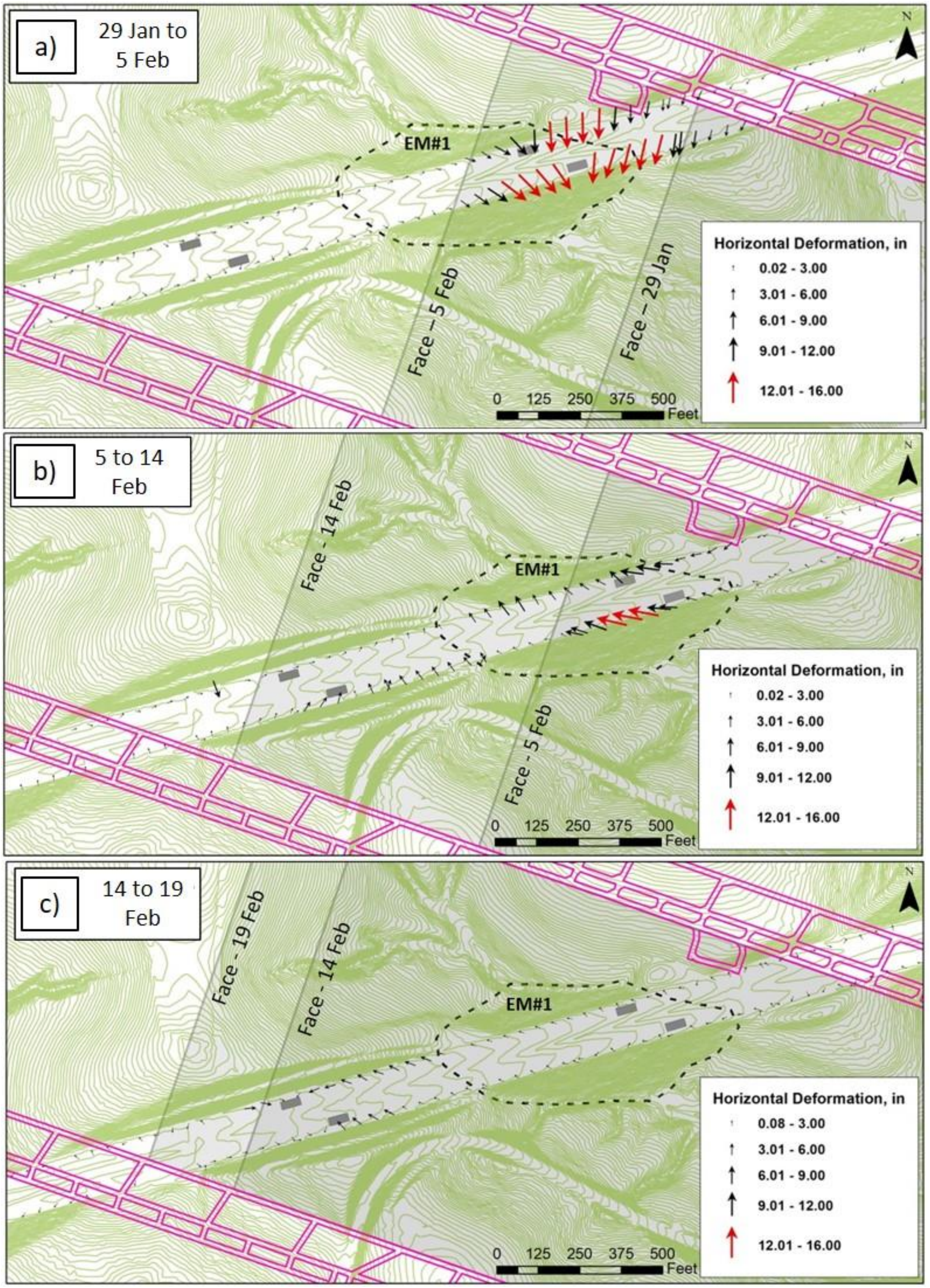

Figure IIb.15 – Incremental horizontal movement influenced by undermining as measured by the highway alignment surveys throughout the study area: a) 29 January to 5 February 2019; b) 5 to 14 February 2019; and c) 14 to 19 February 2019.

3.3 Assessing Damage to Pavement

As described previously, the highway surface experienced significant deformation as a result of the undermining event. The deformations occurred in both the vertical and horizontal planes with as much as 5-ft of vertical elevation drop in the center of the panel and as much as 2-ft of horizontal movement along the pavement surface. This segmented pavement structure deformed in a complex manner during undermining. The pavement was successively pulled then compressed and translationally shifted at different rates that contributed to the development of distress within the pavement surface. There appears to be a pivot point located in the central portion of the embankment (Figure IIb.8). The eastern side of the highway moved towards the center of the panel, while the western side of the highway moved parallel towards the gate road entries in the direction of the longwall face. This twisting was likely influenced by the structural system of connected concrete slabs subjected to a developing subsidence basin.

The movement of the road surface was likely further influenced by the material properties of the embankment and the pavement subbase. As the embankment appeared to act as a pivot point for the system, the granular fill material in the embankment may have absorbed movement and promoted rotation. Additionally, the pavement subbase consisted of an open graded granular material, which likely allowed the pavement surface to slide, in a manner analogous to a plate resting on a bed of marbles, and act independently from the material below. The presence of an open graded granular base was also beneficial in reducing stress build-up within the surface layer as it was able to act as a slip plane between the highly mobilized support layers and the pavement surface. This combination of material properties could have encouraged movement, and when combined with the structural design of the pavement, help to explain the mechanism for the observed twisting.

As discussed above, the subsidence induces vertical and horizontal deformation and there is a direct relationship between these movements and damage observed in the highway pavement. However, it is perhaps more instructive to examine how horizontal strains impact the characteristics and magnitudes of this damage, along with the horizontal movements. For example, horizontal deformations are needed to produce strain in the pavement but it is the excessive levels of deformation that results in localized strain causing the pavement to crack and separate in tension or crush, heave, or shear in compression. The relationship between horizontal strain, movement and pavement damage (distress) are examined in the following sections.

4.0 Analysis of Observed Pavement Distresses

Throughout the undermining of I-70 by Panel 15, the University visited the site weekly to observe the condition of the pavement surface. These observations were supplemented by the observations made by the PennDOT maintenance staff, who remained on site throughout the undermining event. The pavement distress observed was recorded in the field and then digitized in ArcGIS. It is worth noting that the pavement surface in Pennsylvania was overlaid with asphalt shortly before the mining occurred, so it was devoid of any surface distresses prior to the undermining.

4.1 Vertical Movement

Vertical ground movement can affect the pavement structure in primarily two ways (see Section IIa for a discussion of vertical subsidence and horizontal deformation during undermining). First, if the ground beneath the pavement subsides downward, gaps can develop between the bottom of the slab and the supporting soil. The pavement is designed to carry the expected traffic loads while under a fully supported condition. The pavement is not sufficiently thick to bridge across these gaps in support and cracking can develop as vehicle loads are accumulated. A non-uniform upward movement can also cause differential support beneath the slab, which could create localized stress concentrations.

Looking at the difference between the predicted vertical subsidence (which provides an estimate of the profile of the supporting layers beneath the slab) and the survey elevations measured on the slab surface might provide some insight on if gaps might exist between the slab and the support layers. It should be remembered that there are significant limitations to this approach in that the model can only provide an estimate of the subsidence surface and cannot account for the presence of the pavement. Therefore, this analysis is speculative and can only be verified through a forensic investigation of the pavement

4.2 Translational Movement

As previously described, the subsidence event caused the pavement surface to deform laterally as much as 2-ft along the alignment. This movement caused distress on the pavement surface. The pavement distresses were analyzed relative to the movement recorded on the pavement surface. The overall movement was deconstructed into the components of movement parallel and perpendicular to the orientation of the highway (see Section IIa).

4.3 Types of Distress in Pavement and Associated Structures

There are seven types of distresses that developed on the highway surface as a result of ground movement in the direction parallel to the highway alignment. They include the following:
Pavement:

- Transverse crack – crack that predominately propagates perpendicular to the pavement centerline (tend to occur above the transverse joint) (*see Photo #7 in Figure IIb.16)*

- Widened contraction joints –opening of the transverse contraction joints (*see Photo #1 in Figure IIb.16)*
- Longitudinal shear crack – crack that propagates along the lane-shoulder longitudinal joint when shear forces generated when the mainline expands/contracts at a different rate than the shoulder (*see Photo #6 in Figure IIb.16)*
- Diagonal shear crack –tears in the asphalt matt predominately on a diagonal across the pavement as the as the roadway is pulled into the subsidence basin (*see Photo #2 in Figure IIb.16)*
- Blowup – localized upward movement (buckling) of the concrete caused by large in-plane pressure buildup in the concrete slab (*see Photo #2 in Figure IIb.17)*
- Compression bump – large transverse bump created by localized, high in-plane pressure build-up in regions with full-depth asphalt (*see Photo #5 in Figure IIb.16)*

Guiderail:

- Guiderail displacement –buckling of the guiderail due to movement of the ground in the region of the guiderail support posts (*see Photo #4 in Figure IIb.18)*

There were two types of distress damage observed on the highway surface caused by movement perpendicular to the direction of travel. The following types of failures occurred on the pavement surface caused by perpendicular movement:

Pavement:

- Longitudinal crack – crack that predominately propagates parallel to the pavement centerline (tend to occur above the lane-shoulder longitudinal joint) (*see Photo #2 in Figure IIb.16)*
- Shoulder/edge separation – a gap that develops along the outside edge of the shoulder as the soil/backfill material adjacent to the shoulder pulls/or drops away from the pavement (*see Photo #4 in Figure IIb.17)*

Guardrail:

- Guiderail displacement – misalignment of the guiderail due to movement of the ground in the region of the guiderail support posts (*none)*

Additional photos of these distresses have been provided in Appendix I.

5.0 Comparison between Horizontal Strain and Highway Distress

The effect of the dynamic subsidence on the development of distress in the highway was investigated as the mining progressed beneath I-70. The visual distress observed was first examined with respect to the horizontal strain (strain along the axis of the highway alignment). All distress surveys were taken from the outside shoulder and the presence of live traffic in the inside lane made observations of distresses in the inside lane and inside shoulder more difficult. Therefore, the distress maps might not reflect all distresses that developed in the inside lane or inside shoulder. Horizontal strain is quantified based on two separate methods. The first method was using survey measurements made along the outside longitudinal lane/shoulder joint at the location of the highway alignment pins. The location of the highway alignment pins are depicted using blue circles in the distress maps provided in Figures IIb.16-21. The second method consists of using the SDPS software to quantify the horizontal strain. It should be noted that the first method of using the alignment pins provides an estimate of the strain in the pavement surface, while the SDPS software provides the surface strain of the granular material below the pavement and neglects the presence of the highway above it.

As previously stated, the University project team made three site visits, while the undermining of I-70 was being performed. The section below provides a discussion on the horizontal strain that was estimated to have developed on each observation date and the pavement distress that was first observed on that corresponding day. It should be mentioned that this incremental approach with discrete analysis times provides a snapshot of the horizontal strain and distress development. In reality, the strains, and resulting distresses, are changing between these periods of times due to the continuous mining process and the resulting dynamic subsidence effect. Therefore, not all of the distress first observed on the specific observation dates can be attributed to the strains estimated for that day but instead would be the result of the dynamic subsidence that occurred in days just prior.

5.1 5 February 2019 Observations

The first site visit after the commencement of mining under I-70 took place on 5 February 2019. On this day, the longwall face was approximately 1200-ft from the western panel edge in the EB lanes and 1400-ft in the WB lanes. Figure IIb.16, and IIb.17 show the strains and resulting distress observed for the EB and WB lanes of the highway, respectively.

A significant amount of distress developed in the EB lanes prior to this visit, with eight different types of distresses being observed. The two methods shown in Figure IIb.16 (highway alignment surveys and SDPS predictions) depict different strain profiles along the roadway; however, both methods show approximately the first 300-ft from the eastern panel edge to be in tension and the next 500-ft in compression. It can be seen in Figure IIb.16 (Photo #4 and #5) the asphalt relief sections absorbed the compression forces and this translated into the development of compression bumps. These compressive strains resulted in the development of blowups in the concrete shoulder at the eastern end of the asphalt relief section and adjacent to the compression bump. The compressibility of the full-depth asphalt accommodated larger strains than the adjacent, more rigid concrete shoulder. This resulted in the development of longitudinal shear cracks along the lane/shoulder joint, which divides these two regions (shown in Photo #6 in Figure IIb.16), and longitudinal cracking (shown in Photo #3 in Figure IIb.16). The region directly behind the longwall face is in tension. This caused the transverse joints to open (or widen), as shown in Figure IIb.16 Photo #1. A diagonal shear crack also developed in the asphalt overlay directly behind the longwall face (shown in Photo #2 in Figure IIb.16) as the highway was being pulled into the subsidence basin. Figure IIb.15a shows large horizontal movements of the highway towards the developing subsidence basin in the area of the eastern asphalt relief section, which corresponds to the same location of this diagonal shear crack.

Less distress was observed in the WB lanes on the 5 February 2019 site visit when compared to that in the EB lanes. The tensile strains, both measured and predicted, occurred directly behind the advancing longwall face and matched the location of a widening of the transverse joints and the development of a transverse crack in the inside shoulder, as shown in Photo #1 (Figure IIb.17). Approximately 200-ft behind the longwall face, the highway alignment survey experienced significant horizontal strain (over 10×10^{-3}) parallel to the direction of travel and occurring within the EB asphalt relief section. The SDPS predictions showed this same area as experiencing only minor compressive strains, thus demonstrating the influence of the asphalt relief sections. A blowup, compression bump and longitudinal shear cracks along the outside lane/shoulder were in an area of high predicted strain (Figure IIb.17) but low measured strain. Again this difference demonstrated the effectiveness of the asphalt relief sections in absorbing horizontal movement. The nature of these distress features is shown in Photos #2, #3 and #5 (Figure IIb.17). The majority of this movement was absorbed in region of the asphalt relief section, resulting in the compression bump and the blowup at 13+28. However, some of the differential movement is being absorbed between the shoulder (in the region of the blowup) and in the travel lanes (in the adjacent compression bump), contributing to the development of the longitudinal shear cracks directly to the east of the asphalt relief section. It should be noted that even though shoulder/edge separation is depicted on these maps for completeness, it developed as a result of strains perpendicular to the pavement and not parallel to the pavement. This shoulder/edge separation is depicted in Photo #4 in Figure IIb.17

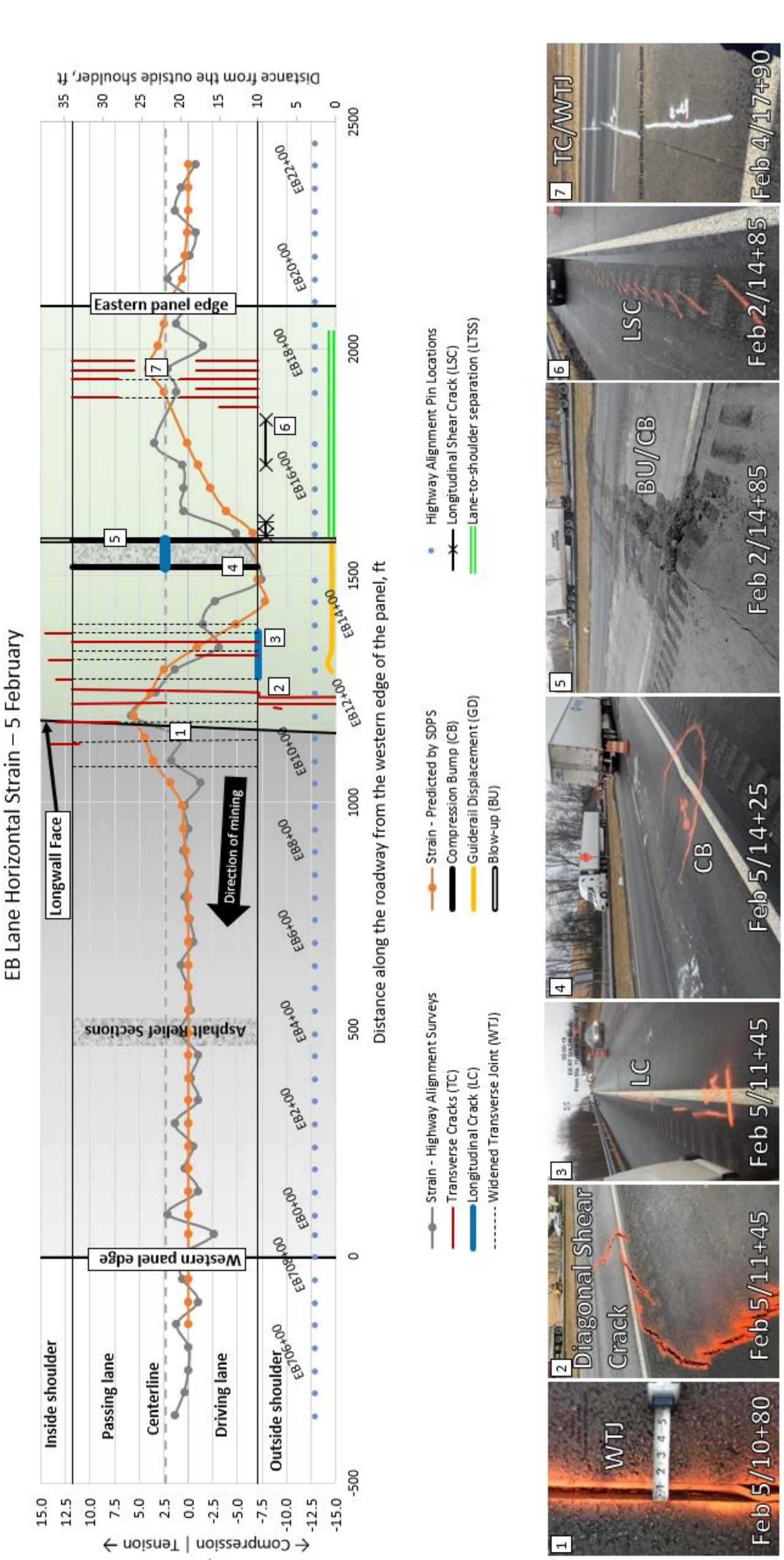

Figure IIb.16 - Horizontal strain and observed distress for EB lanes on 5 February 2019

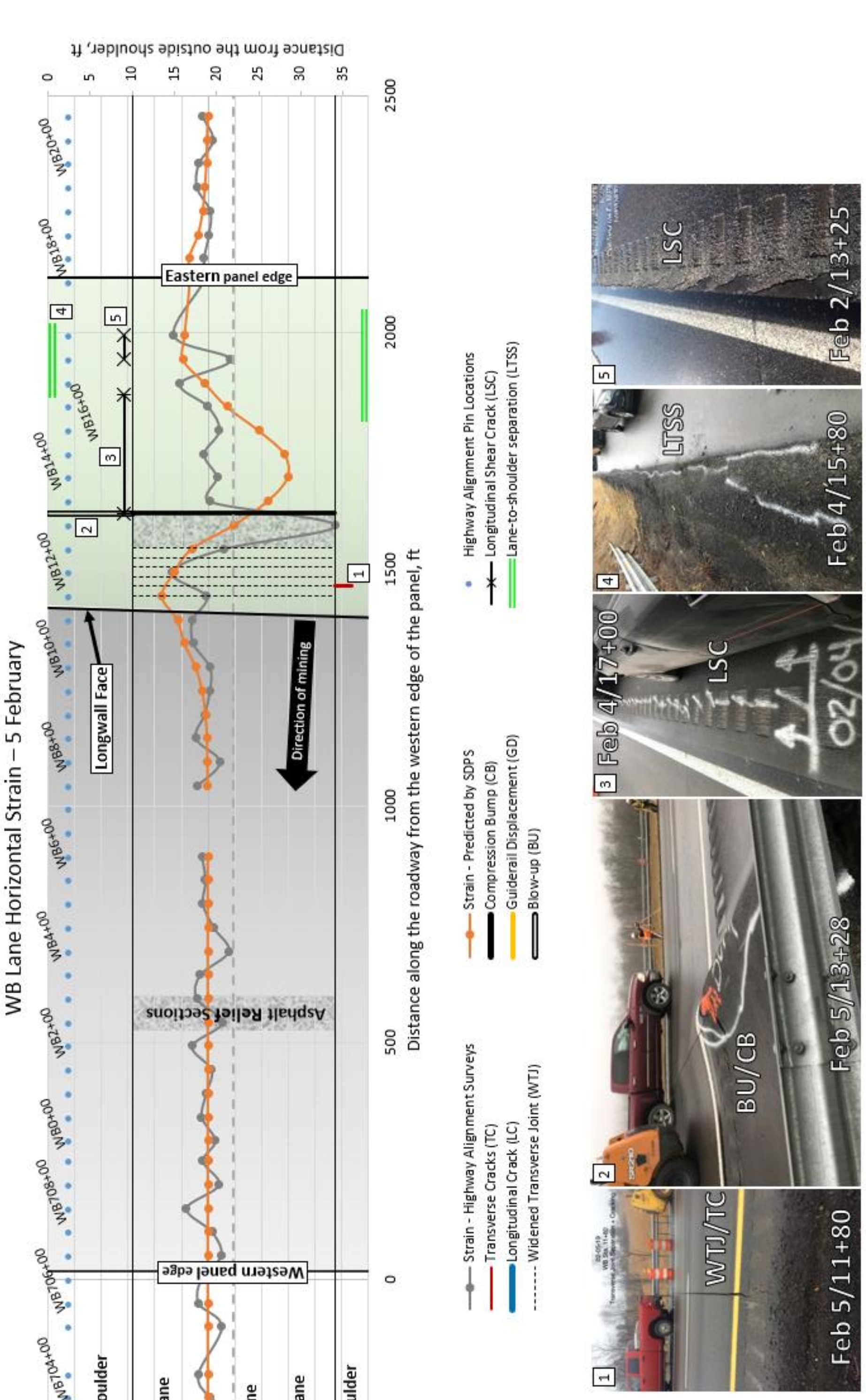

Figure IIb.17 - Horizontal strain and observed distress for WB lanes on 5 February 2019

5.2 14 February 2019 Observations

The second site visit took place on 14 February 2019, when the longwall face was nearing the western panel edge at ~200-ft away in the EB lanes and 500-ft in the WB lanes. Figure IIb.18, and IIb.19 show the horizontal strains parallel to the highway alignment and resulting distress observed in the EB and WB lanes of the highway, respectively. In the EB lanes, the predicted and measured strain profiles are similar (Figure IIb.18). This distress features near the advancing longwall face includes transverse joints that exhibited widening (at stationing 3+00 in Figure IIb.18 and Photo #1) and some transverse cracking. The transverse cracks that developed east of the region where the pavement is in no longer in tension most likely occurred a few days prior as a result of the dynamic subsidence, when the longwall face was about halfway through the panel and this portion of the highway would have been in tension.

The large opening of the joints present an opportunity for incompressibles, such as pebbles and stones, to enter. When the joints close up again, these incompressibles can cause localized tenting of the asphalt that look like localized compressive bumps. This was observed along the joint located near stationing 10+00. Regarding distresses that are attributed to compressive stress, a blowup developed in the outside shoulder approximately 750-ft and 1250-ft away from the western panel edge. The strains are low at the 750-ft location and therefore cannot be used to explain the development of the blowup. Although, Figure IIb.13 shows the whole pavement section appears to be twisting around this location as the roadway on the eastern side of the panel is being pulled toward the longwall face and the portion of the roadway on the western side is exhibiting little movement. This phenomenon could be contributing to the stresses, which resulted in this blowup. The longitudinal compression bump shown in Photo #5 of Figure IIb.18 might also be the result of this twisting and the roadway on the eastern side of the panel being pulled toward the longwall face. As the roadway shoulder mobilized, there was insufficient stiffness in the asphalt relief section to resist the deformation. Compressive strains estimated using both the SDPS and survey measurements are similar on this date near stationing 12+00, and help explain occurrence of the second blowup. The vertical plane in the pavement was already weakened at this location since the blowup occurred directly on top of the diagonal shear crack depicted in Photo #3b of Figure IIb.18. The strains are again, relatively low in this area, but there is substantial movement of the whole pavement section as it is being pulled into the direction of the mining as Embankment #1 drops vertically due to densification and spreading. The guiderail buckled in this same region, which is further evidence that this region is being compressed (Photo #4 of Figure IIb.18). The differential movements between the travel lanes and the shoulders resulting from the blowup in the shoulders contributed to the longitudinal cracking (Photo #2 of Figure IIb.18) and the longitudinal shear cracking that developed along the outside lane/shoulder joint between stationing 10+00 and 14+00.

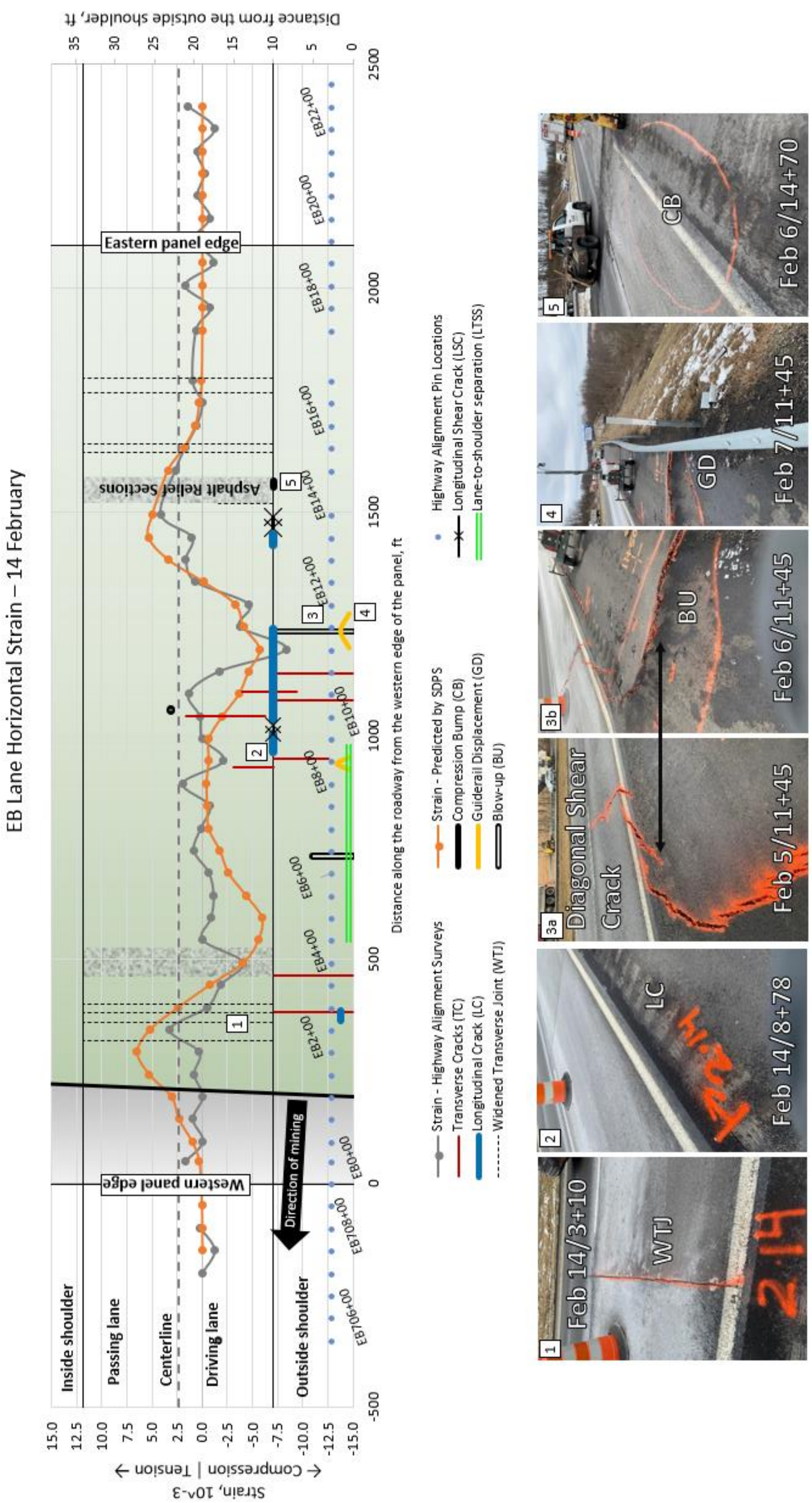

Figure IIb.18 - Horizontal strain and observed distress for EB lanes on 14 February 2019

For the WB lanes on 14 February 2019, the measured strains values are less than those predicted by the SDPS model (Figure IIb.19). The most significant differences are concentrated in the areas around the asphalt relief sections. Two blowups were observed and both were located approximately 1000 to 1250-ft from the western edge of the panel. The strains on February 14 are low in this region and cannot be used to explain the stresses necessary to generate a blowup. These stresses most likely developed between February 5 and 14 with the movement of the roadway on the eastern side of the panel shifted from a southeast direction to a northwest direction (Figure IIb.15b and c). These large movements are pivoting around the approximate location of the blowups. The dashed lines in Figure IIb.19 towards the eastern panel edge indicate transverse joints that widened as a result of the dynamic subsidence between February 5 and 14. As can be seen in the Figure IIb.19 photos, the joints were quite wide, over 2.5-in, on February 6 and 8 (Photos #1a & #2a) but eventually closed again to the original width between February 9 and 19. The location of one of the blowups is depicted in Photo #2c (Figure IIb.19). T The three photos (#2a, #2b, and #2c, Figure IIb.19) show the progressive opening and closing of the joint and the eventual blowup. The opening and closing of the joints most likely contributed to the differential movement between the traveling lanes and the shoulder that resulted in the development of the longitudinal cracks near stationing 6+00 and 9+00 and the longitudinal shear crack between 16+00 and 17+00.

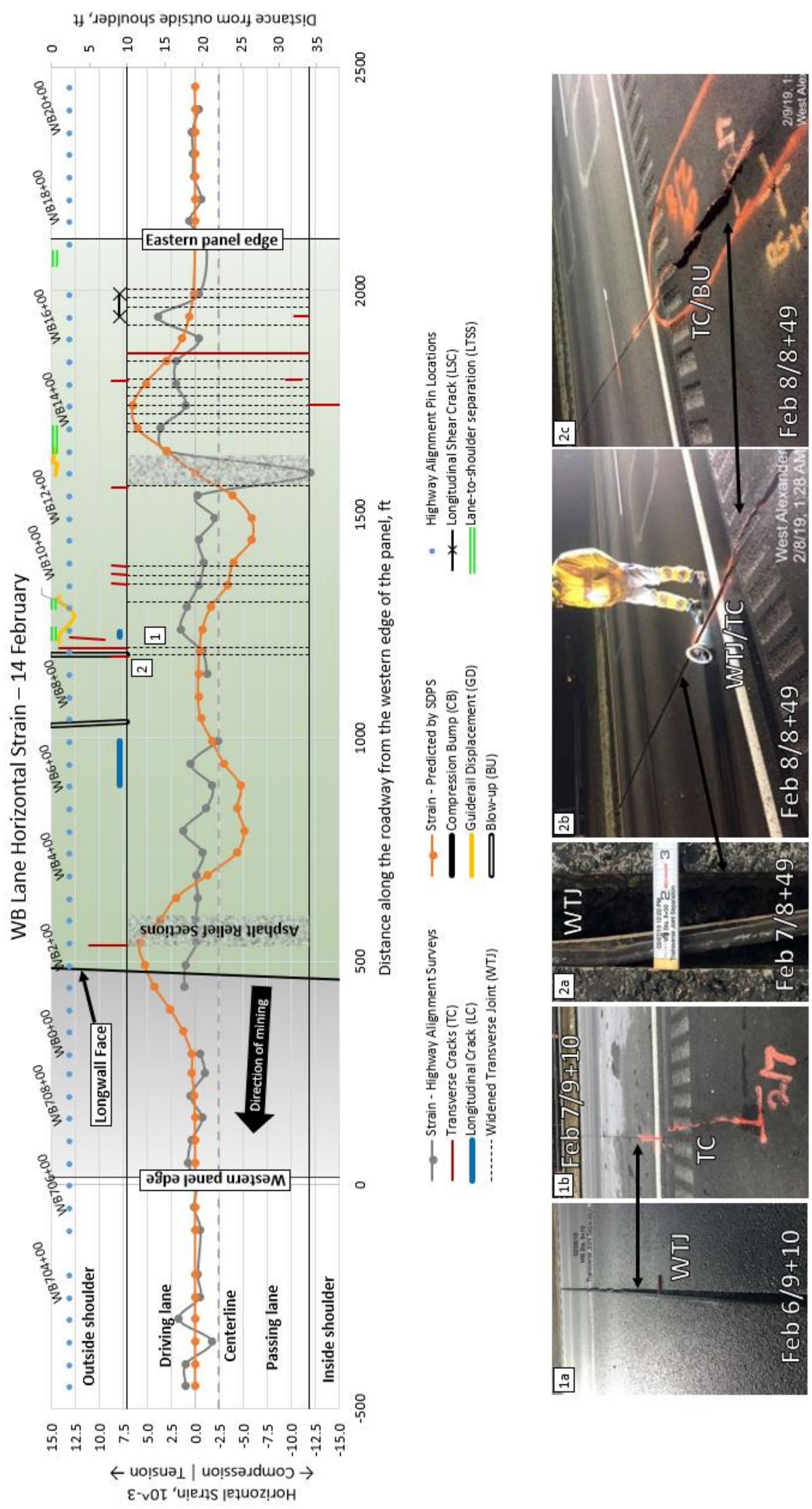

Figure IIb.19 Horizontal strain and observed distress for WB lanes on 14 February 2019.

5.3 19 February 2019 Observations

Another site visit took place on 19 February 2019. On this day, the longwall face had just past under the EB lanes of I-70 in the study area (Figure IIb.20). Transverse cracks developed and transverse joints widened along ~250-ft of roadway adjacent to the western panel edge. The Both the SDPS model and the measurements from the highway alignment surveys showed tensile strain over ~150-ft roadway (Photos #1a, #1b, and #2a, Figure IIb.20). Compression bumps also developed on each side of the western asphalt relief section ~500-ft from the western panel edge. The milled compression bump on the approach side of the asphalt relief section is shown in Photo #3 of Figure IIb.20. The compressive strains contributing to the development of these compression bumps can still be measured even on 19 February seen in Figure IIb.20 when the longwall face was ~500-ft away and the compression wave was moving to the west. At stationing 6+50 (about 750-ft east of the western panel edge) the edge of the shoulder heaved upward and is denoted as a blowup in Figure IIb.20 and Photo #4. This could have occurred as the roadway was being moved in the direction the heave developed with the granular material beneath the roadway surface migrating towards the center of the subsidence. This magnitude and direction of the movement 750-ft east of the western panel edge can be seen in Figure IIb.14. This area might have already been weakened as it is in a similar location to a blowup that had previously been observed during the 14 February site visit. It should be noted that only minor amounts of strain were measured east of the 6+50 blowups.

Figure IIb.21 shows similar distress in the same location away from the western panel edge as was seen in the EB lanes in Figure IIb.20. This included the opening (and closing) of the transverse joints and the development of transverse cracks in the region of changing tensile strain in the area from the western asphalt relief section to the advancing longwall face. There was also a compression bump on the approach side of the asphalt relief section near the western panel edge. Photo #2 in Figure IIb.21 shows this compression bump on February 16 after it was milled. The strain profiles indicate this region is in compression. The dashed line around stationing 9+00 indicates that the joint was quite wide but the transverse joint then was pushed closed. As previously stated, the large opening of the joints present an opportunity for incompressibles to enter into the joint. When the joint closes, these incompressibles can cause localized tenting of the asphalt that looks like localized compression bumps. It appears that when the widened joint near stationing 9+00 closed, incompressibles had entered the joint near the outside shoulder and created a compressive bump. This can be seen in Photo #4 in Figure IIb.21. Upward heaving of the outside edge shoulder also occurred near this location. Both the EB and WB lanes exhibited shoulder edge separation where the material adjacent to the roadway pulled away from the shoulder. This is shown in Photos #3 in Figure IIb.21.

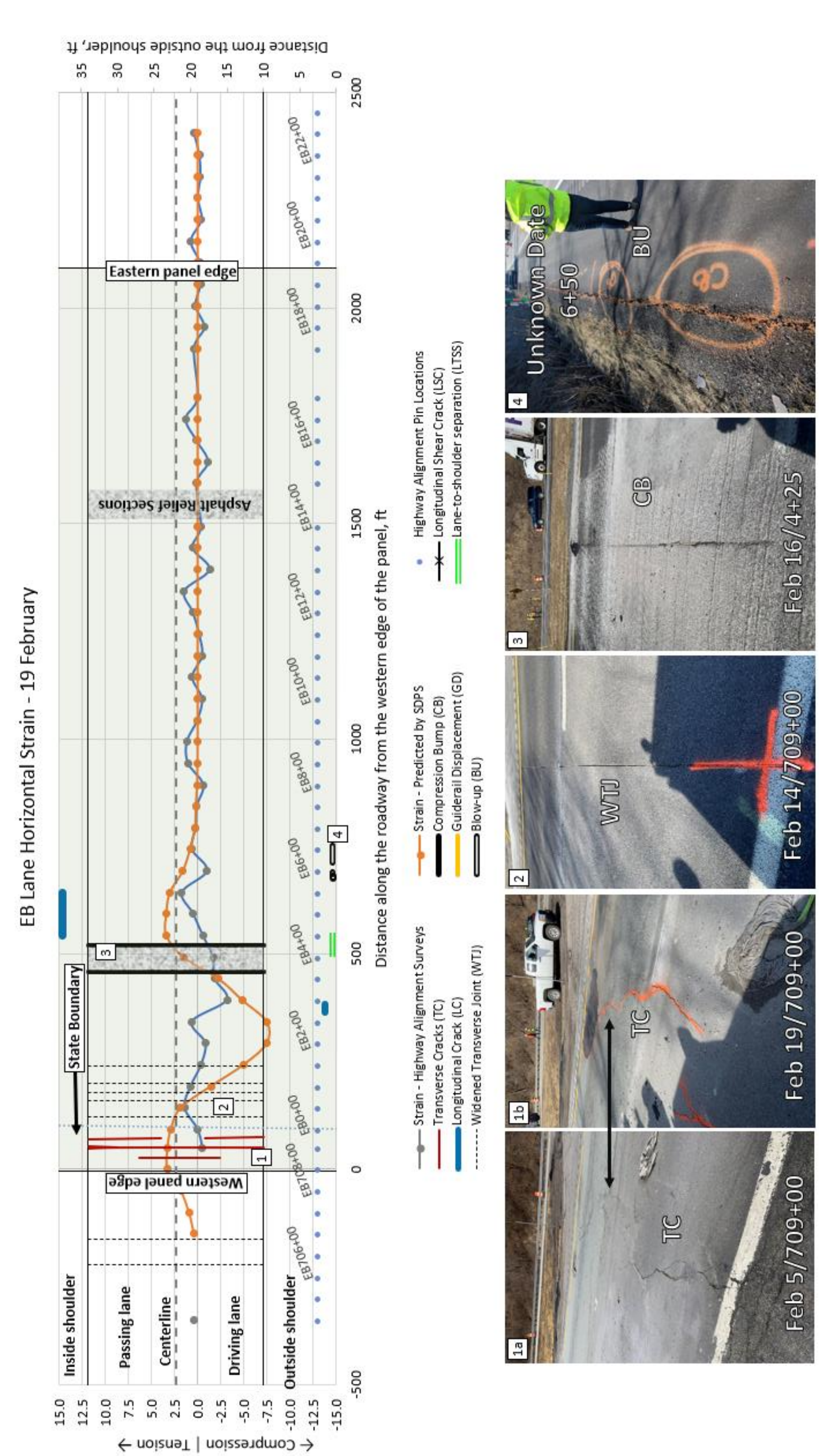

Figure IIb.20 - Horizontal strain and observed distress for EB lanes on February 19, 2019

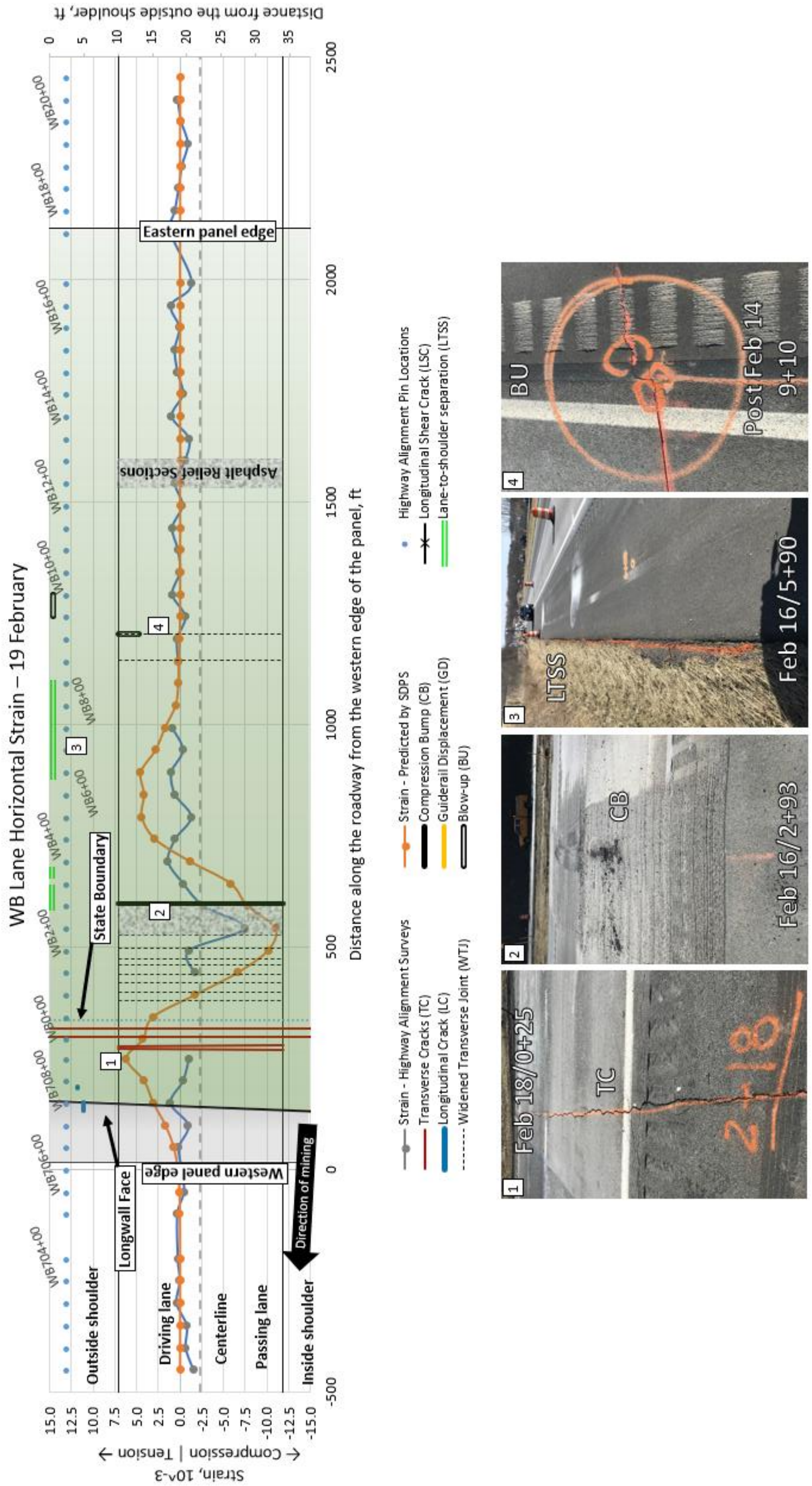

Figure IIb.21 - Horizontal strain and observed distress for WB lanes on February 19, 2019

6.0 Discussion

It has been shown that the movement, the strains, and resulting distress that developed within the pavement as a result of the subsidence was influenced by the presence of Embankment #1, the pavement design and the pre-undermining mitigation techniques (installation of asphalt relief sections and placing and overlay with sawed and sealed joints above the existing joints in the underlying JPCP). Along with the vertical drop and the associated compressive and tensile deformation that generates as a result of the highway moving towards the center of the longwall panel, the roadway appeared to twist. The eastern side of the highway moved towards the center of the basin and the western side of the highway moved parallel to the gate roads towards the longwall face. The pavement connectivity facilitates the twisting and the location of the embankment appeared to define the pivot point at which it twists around. The densification and spreading of Embankment #1 may have dissipated movement and facilitated the twisting, since the pivot point appears to be over the central portion of the embankment.

The movements observed by the survey data tended to be lower than that estimated using the SDPS software. This is attributed to the fact that the SDPS modeling neglects the presence of the pavement structure on the surface. The rigidity provided by the pavement structure restricts both the vertical and horizontal movements. Several of the design features of this particular pavement structure contributes to a higher level of restraint than might otherwise be realized. Beneath the asphalt overlay, is a jointed plain concrete pavement with tied concrete shoulders that run continuously along the edge of the pavement, even in the region adjacent to the asphalt relief section. The connectivity of the pavement provided by the tied concrete shoulders extends across the subsidence basin.

Additional connectivity along the pavement is also realized through the presence of smooth dowel bars located along the transverse joints. These dowel bars restrict vertical movements at the joints as well as horizontal movement perpendicular to the roadway. The dowel bars restricted the slabs from shifting out of alignment. While the tied shoulders, ran continuously through the asphalt relief sections in the mainline, also helped in keeping the travel lanes from migrating out of alignment. This helped resisting the twisting that developed. A single diagonal shear crack did appear to develop as a result of the twisting, although it is not clear if this distress was only in the asphalt overlay or propagated down through the JPCP. It’s possible that, although more localized, significant more damage could have developed if this connectivity in the pavement structure was not present to resist the movement. Another key benefit of the dowel bars is that they facilitated large increases in joint width without compromising joint performance. The tension and compression forces that developed during subsidence caused these joints to widen and close and the functioning dowels were able to accommodate this movement. The fact that PennDOT cut joints into the asphalt overlay directly above the transverse joints in the underlying JPCP allowed the joints to open without generating a transverse crack, although it appears one joint did not get cut and a transverse crack developed in the overlay above a transverse joint in the underlying pavement. This showed that cracks would have developed in the overlay above the joints in the underlying JPCP, if the joints were not sawed. It also appears that the location of a joint sawed in the overlay was not directly above the transverse joint in the underlying JPCP as a transverse crack developed very near to a joint sawed into the overlay. The crack developed along the same 1:6 skew as the joints in the underlying JPCP. As compared to the cracks, these sawed and sealed joints are better able to accommodate the widening that occurs when the pavement goes into tension and the subsequent closing as the pavement is compressed without getting localized tenting or compression bumps along the joint/crack due to the entering of incompressibles. The tied shoulders and functioning dowels also may have prevented some of the more catastrophic failures of the pavement surface, such as large separations of the shoulder and the lanes, transverse offsets between slabs, and vertical misalignment between slabs. These types of failures would have been far more destructive and dangerous to the traveling public but were not observed during this undermining event.

The asphalt relief sections were also very effective in absorbing the compressive stresses that built up as a result of both the dynamic and final subsidence. Six different compression bumps were documented during the undermining. All were quickly milled with minimal disturbance to the traveling public. As a result of these asphalt relief sections, there were no blowups that developed in the travel lanes. The blowups that developed in the shoulder were also milled quickly. It is possible that heaving of the shoulder did occur in one location near a prior blowup, but for the most part, milling of the blowups appeared to mitigate the damage for the remainder of the duration of the undermining. Other than this, only minor distresses developed, including longitudinal cracks and shear cracks along the longitudinal joints and separation between the granular material along the edge of the pavement and the shoulder.

The pavement was overlaid shortly after the undermining was completed. One can only speculate on the effects of the subsidence on the future performance of the pavement. For vertical subsidence, the model matches the observed trends well throughout the subsidence event, except for the section of highway immediately above Embankment #1, which experienced more subsidence than the rest of the study area. The difference between the observed vertical movement and predicted movement outside of this area could be an indicator of the gap that might be present between the top of the subsided ground and the bottom of the semi-rigid pavement structure. These gaps, if present, will result in a reduced pavement life. The assumed pavement life is estimated based on the assumption that the ground provides uniform support beneath the pavement. Pavements are not constructed sufficiently thick to “bridge” across these gaps. The asphalt overlay will allow traffic to safely traverse the roadway while any final settlement occurs. The JPCP beneath the asphalt overlay will serve as a support platform that will assist in minimizing distress from developing in the overlay as a result of the undermining. In the years to come, as this overlay is fatigued by the traffic it will carry and the ground beneath the pavement stabilizes and any final associated distress develops, the underling JPCP will serve as a solid foundation for a future unbonded JPCP overlay or a subsequent asphalt overlay.

SECTION III – ANALYSIS OF FUTURE UNDERMINING OF I-70 FROM THE WEST ALEXANDER TO CLAYSVILLE INTERCHANGES IN PENNSYLVANIA

Subsection IIIa – Extended Study Area

The extended study area encompasses the Tunnel Ridge reserves of the Pittsburgh Coalbed in western Pennsylvania (Figure IIIa.1). A portion of these reserves has the potential to be mined in the next two decades by the longwall mining method. The University is responsible for taking the knowledge gained during the undermining of Panel 15 to evaluate potential longwall mining subsidence impacts within the extended study area. The analysis that follows is meant to provide a framework for evaluating the risk potential for assets within the extended study area.

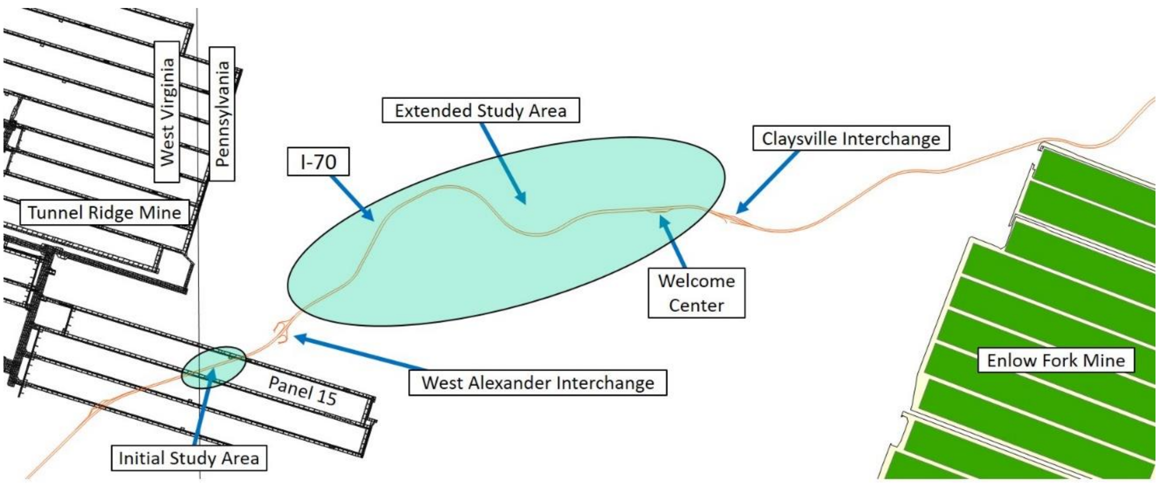

Figure IIIa.1 – Extent of I-70 overlaying unmined portion of the Tunnel Ridge Mine reserves in Washington County, Pennsylvania. Also shown are the initial and extended study areas

1.0 Predicted Longwall Panel Locations, Orientation and Width

As of the drafting of the Task 3 Report, the permit for the longwall mining district, comprising the surface area containing I-70 between the West Alexander and Claysville Interchanges, was not officially available through the PA DEP permitting process. Therefore, the University developed a potential longwall panel layout for the extended study area based on its knowledge of past and existing controlling factors. The potential longwall panel layout is used to explore risk associated with undermining within the extended study area.

1.1 <u>Panel Width</u>

Important factors in predicting longwall panel layouts are: 1) panel width, 2) panel length, 3) panel orientation, and 4) rate of face advance. The University based its logic for projecting future longwall panels in the extended study area on past experience at the Tunnel Ridge Mine and other adjacent mining operations. At the time of writing this report, the Tunnel Ridge Mine had completed the mining of 16 longwall panels (Figure IIIa.2). Individual characteristics of these panels are shown in Table IIIa.1. The average panel width is 1,080-ft with a Standard Deviation (SD) of 140-ft. Initially, panel widths were nominally 1,000-ft but increased to approximately 1,200-ft in 2015.

Table IIIa.1 – Characteristics of the 16 longwall panels at the Tunnel Ridge Mine

Panel No.	Year Complete	Width, ft	Length, ft
1	NA	1,000	7,870
2	NA	1,000	9,360
3	NA	1,000	7,510
4	NA	1,000	8,110
5	2014	990	9,090
6	2014	990	8,870
7	2015	1,010	8,750
8	2015	1,200	11,750
9	2016	1,210	15,430
10	2016	1,200	14,650
11	2017	1,210	14,570
12a	2017	1,200	11,750
12b	NA	1,200	8,010
14	NA	751	5,580
15	2019	1,190	14,444
16	2019	1,200	15,970
	Average	1,080	10,730
	SD	140	3,330
	Min	750	5,580
	Max	1,210	15,970
	Median	1,100	9,230

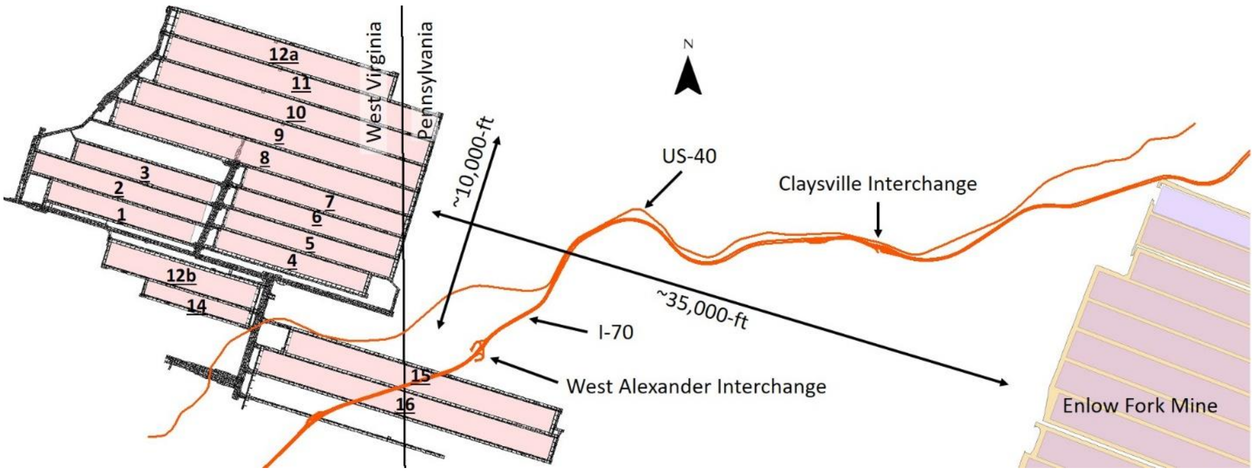

Figure IIIa.2 – Existing longwall panels at the Tunnel Ridge Mine as well as the general size of unmined reserves within the extended study area

1.2 Panel Length

The length of the longwall panels has changed considerably over time. The average panel length is 10,730-ft with an SD of 3,330-ft and ranges in length from a minimum of 5,580-ft to a maximum of 15,970-ft. It seems apparent from examining Figure IIIa.2 that typical panel length is between 15,000 and 16,000-ft.

1.3 Panel Orientation

Historical trends in longwall mining have shown that panel layouts within the Pittsburgh Coalbed longwall mines favor orientations that minimize the effects of a regional excessive horizontal stress field (Mark and Mucho, 1994). The fifteen existing longwall panels at the Tunnel Ridge Mine have an orientation of N 71° W (Figure IIIa.3). The neighboring Enlow Fork Mine has slightly similar orientations, averaging N 67° W (Figure IIIa.3). When determining the orientation of future longwall panels in the Pittsburgh Coalbed of southwestern Pennsylvania, it is logical to assume that these well-established trends will continue.

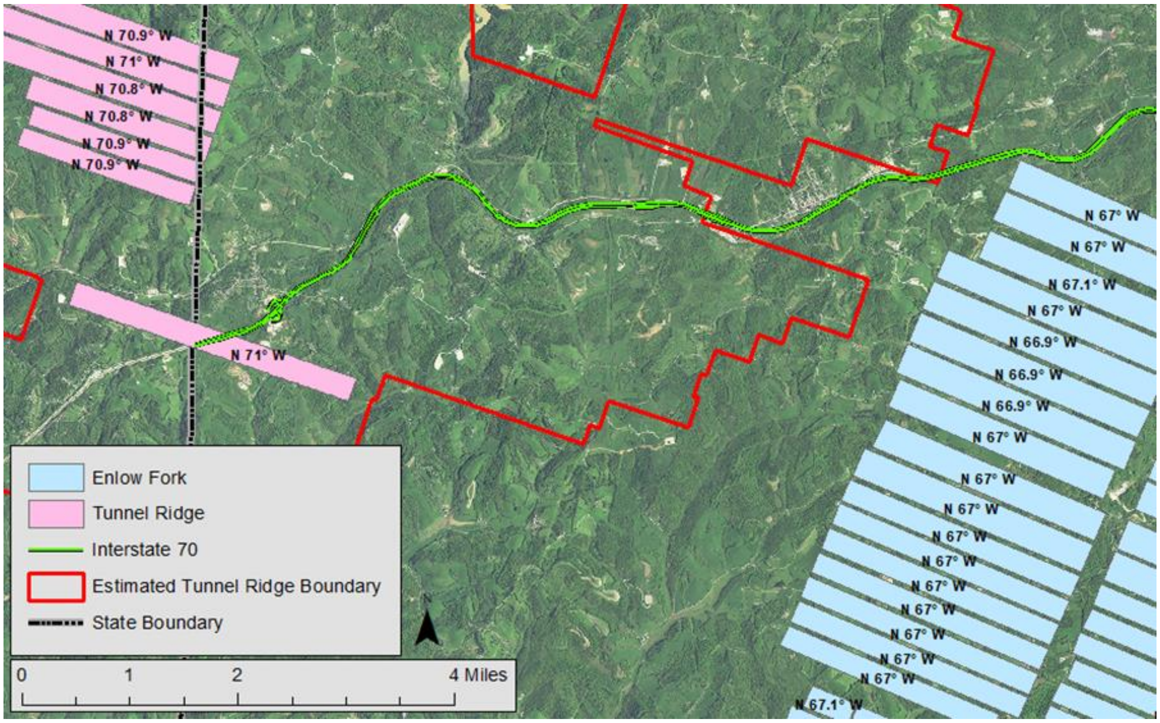

Figure IIIa.3 – Location of selected existing mined Tunnel Ridge and Enlow Fork longwall panels. The bearings show the preference for panels oriented from N 67 to 71° W within the Pittsburgh Coalbed in southwestern Pennsylvania

1.4 Panel Locations

The University projects that the extended study area will need to be split into two mining Districts separated by a main entry development. Each district will have optimum panel lengths of approximately 15,000-ft oriented N 71° W (Figure IIIa.4). The Panel 15 and 16 gate entry widths average 180-ft. These approximate dimensions are used to separate adjacent panels. The main entry developments at Tunnel Ridge are comprised of seven headings and connecting cross-cuts that average approximately 410-ft in the main's developments servicing Panel 15. The main entry system is protected from abutment loading by a combination barrier pillar / recovery entries that are approximately 530-ft for Panel 16 and 17. It should be noted that information concerning existing room-and-pillar developments, as well as extracted longwall panels, were provided to the University by the Tunnel Ridge Mining Company. It is estimated that the approximate width of the entire main entry development (headings, barriers, recovery rooms) could be 1,350-ft. The panel widths are projected to remain at their current widths (~1,200-ft) but if either technological advancements or economic conditions change, wider panels are possible in the future. The point here is that the University is not predicting panel layouts but instead projecting realistic condition to assist in the process of analyzing future risk.

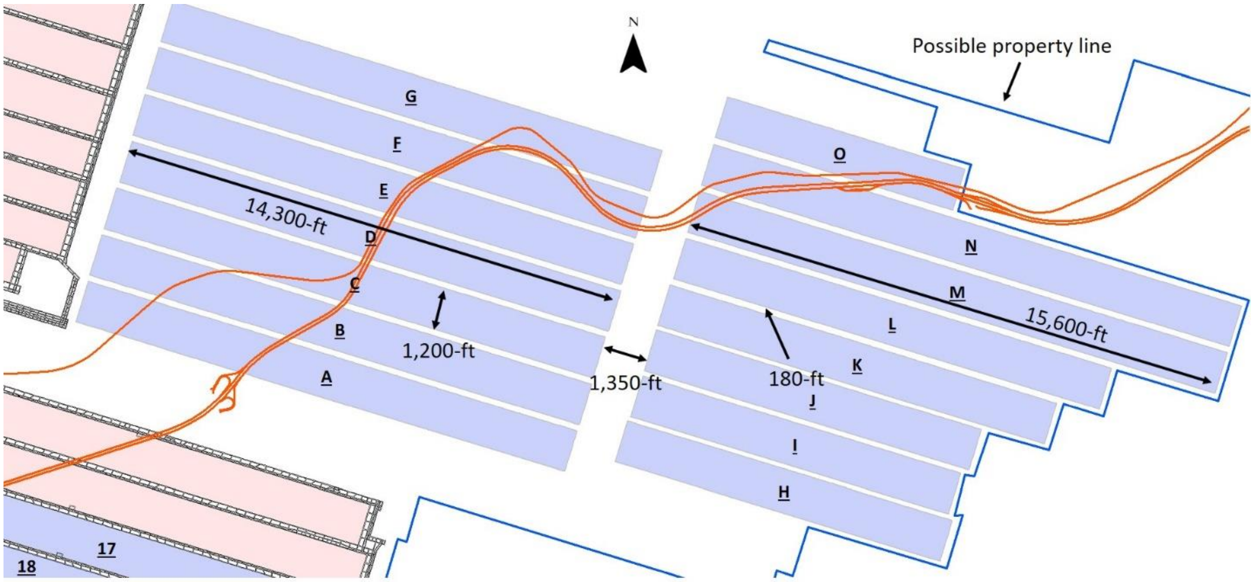

Figure IIIa.4 – Location of projected longwall panels within the extended study area

2.0 Overburden Conditions

Longwall mining in the Pittsburgh Coalbed first occurred within Pennsylvania around 1971 (Iannacchione et al., 2013). Since that time, over 600 longwall panels of various sizes, shapes, orientations and overburdens have been mined (Bain et al., 2019). The spatial reference of these panels is provided by the PADEP and available on the Pennsylvania Spatial Data Access site (PASDA, pasda.psu.edu). In addition, the elevation of the Pittsburgh Coalbed with respect to sea level and the surface topography data was also available on PASDA. Using these data, the University determined the overburden associated with the Pittsburgh Coalbed in southwestern Pennsylvania (Figure IIIa.5). The Tunnel Ridge property in Pennsylvania is in an area where overburdens range from more than 300-ft to less than 800-ft. The Tunnel Ridge Mine property outline was provided by PennDOT at the initiation of the contract. Its accuracy could not be validated.

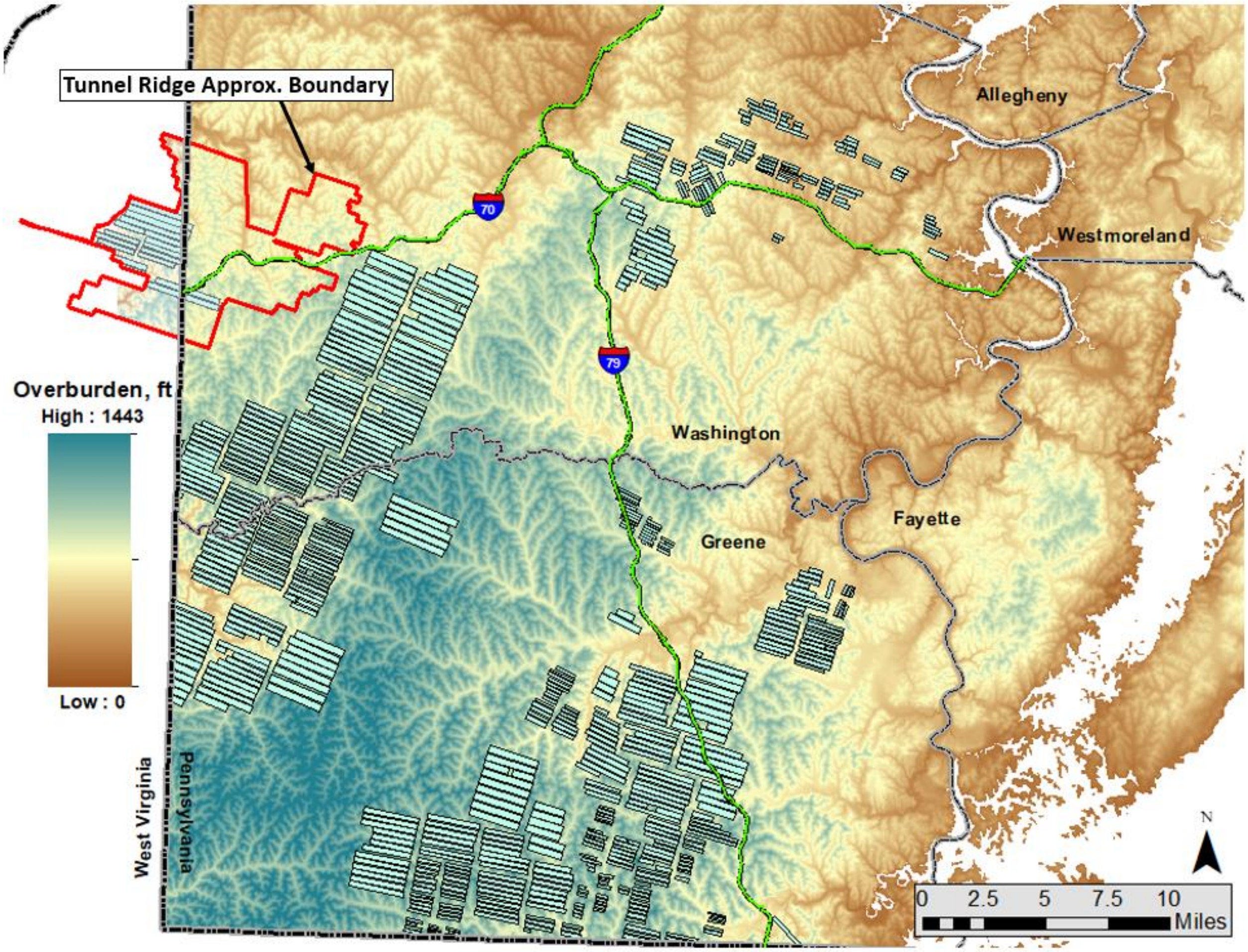

Figure IIIa.5 – Pittsburgh Coalbed overburden and the location of mined longwall panels. The potential 2018 Tunnel Ridge coal property extent is outlined in red

Overburden within a portion of the Tunnel Ridge Mine in Pennsylvania are shown in Figure IIIa.6. Also included is an outline of the Panel 15 initial study, as well as the projected longwall panels in the extended study area. The dashed line shows the extent of the portion of the extended study area within a 1,000-ft buffer of the I-70 centerline. It is this area where potential surface subsidence impacts from longwall mining are analyzed.

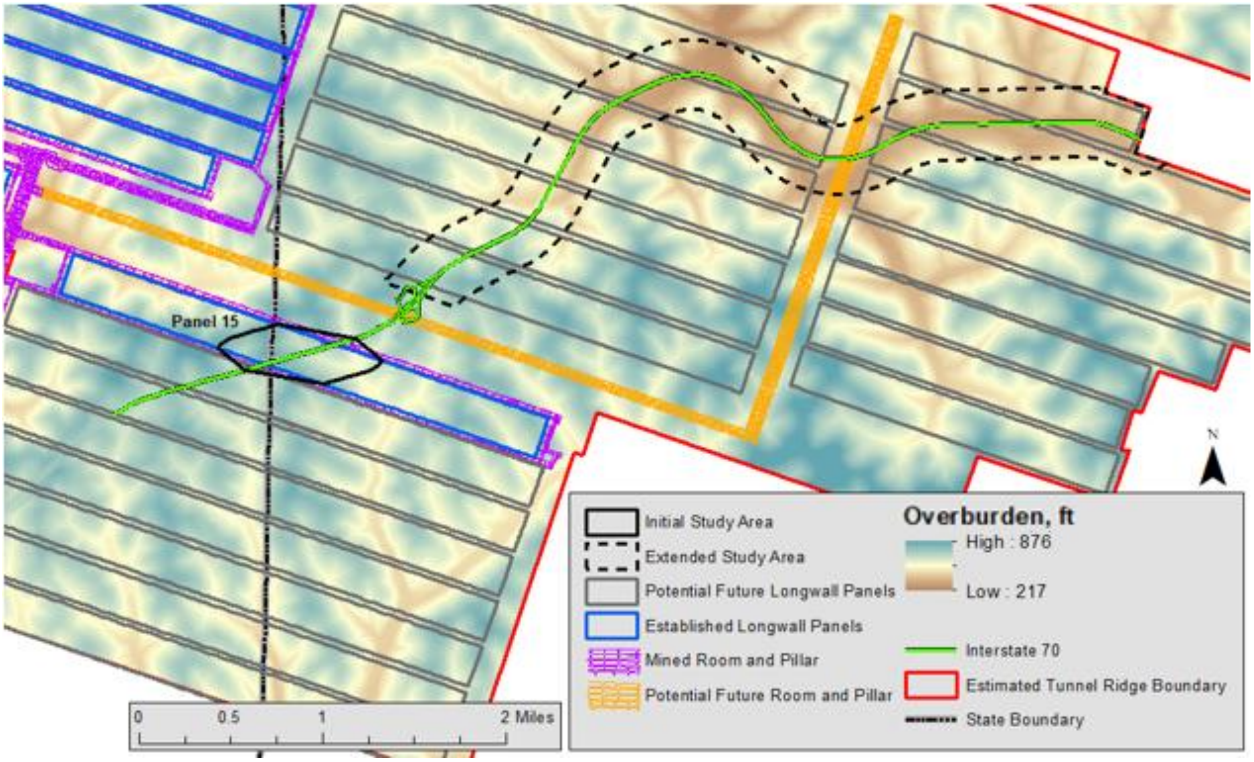

Figure IIIa.6 – Overburden map showing the location of existing and potential future longwall panels at the Tunnel Ridge Mine. Also shown are the initial and extended study areas

Overburden characteristics for both the initial and extended study areas are presented in Table IIIa.2. The average overburden within the initial study area is ~660-ft, extending 3,300-ft along I-70 (Figure IIIa.6) and spanning the subsidence basin developed by the extraction of Panel 15 (see page 3, Section I of the Task 1 Report for a description of the initial study area). In comparison, the average overburden within the extended study area is approximately 470-ft.

Table IIIa.2 – Overburden conditions within the initial and extended study areas within 1,000-ft of I-70

	Min, ft	**Max, ft**	**Range, ft**	**Mean, ft**	**Median, ft**	**STD, ft**
Initial Study Area	546	771	225	658	658	51
Extended Study Area	332	777	446	474	555	94

A graphical representation of the data provided in Table IIIa.2 is shown in Figure IIIa.7. It is obvious from this analysis that there is a significant overall reduction (~28-pct) in average overburden for panels comprising the extended study area.

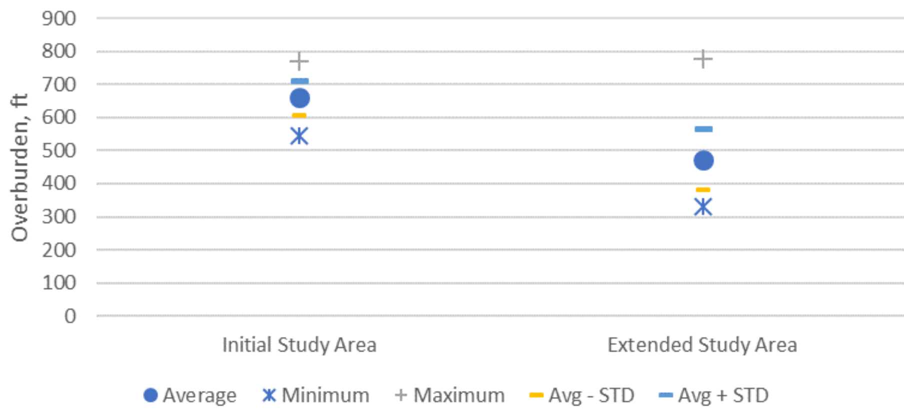

Figure IIIa.7 – Graphical representation of the overburden characteristics of the initial study area (Panel 15) and the extended study area comprising potential longwall panels under the I-70 highway alignment between the West Alexander and Claysville Interchanges

According to trends developed in the latest ACT 54 Report (Bain, et al., 2019), the overburden of longwall panels mined between 2013 and 2018 ranged from 416 to 1,293-ft. Three broad categories were identified: shallow (< 705-ft); average (705 to 907-ft); and deep (>907-ft). Overburden within the initial study area is similar to the average depth of other longwall panels mined recently in Pennsylvania. However, the University estimates that the majority of panels within the extended study area will have overburdens significantly below average and can be classified as 'shallow' for current Pennsylvania longwall mining conditions (Table IIIa.3). As discussed in several sections of this and previous reports by the University, if all other variables are left constant, less overburden will produce higher vertical subsidence and greater surface deformations and strains.

Table IIIa.3 - Overburden characteristics for the seven longwall mines operating in Pennsylvania from 2013 to 2018 (Bain, et al., 2019)

Mine	Avg., ft	SD*, ft	Min., ft	Max., ft	Category
Bailey	891	151	512	1270	Average
Cumberland	894	103	617	1192	Average
Emerald	735	80	449	895	Average
Enlow Fork	634	93	416	850	Shallow
Harvey	871	95	689	1258	Average
Monongalia County	977	124	743	1293	Deep
Tunnel Ridge**	643	61	471	723	Shallow

*SD - Standard Deviation
** - Overburden determined for the portions of Panels 8 to 11 in Pennsylvania (Figure IIIa.2)

3.0 Subsidence Basin Characteristics

For the purposes of analyzing subsidence impacts, a longwall mining panel can be thought of as containing three geometric parts: mid-panel, quarter-panels and gate road entries (Figure IIIa.8). Each part of the subsidence basin can be thought of as having distinctive features that can be used to forecast the general location and magnitude of impacts on the surface (Iannacchione, et al, 2011).

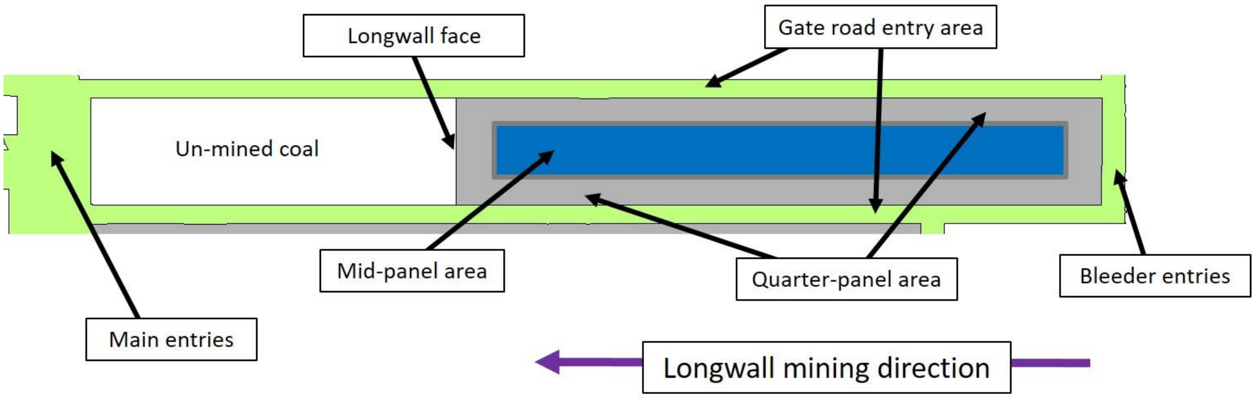

Figure IIIa.8 - Conceptual drawing shows the two geometric components of a longwall panel (mid- and quarter-panels) and the three functional components of the room-and-pillar (main, bleeder, and gate road entries) mining methods

For supercritical panels mining in the Pittsburgh Coalbed of the northern Appalachian Basin, the greatest *permanent* alteration of the surface slope and curvature should occur within the <u>quarter-panel (Qt) areas</u> (Figure IIIa.9). Examples of this permanent subsidence induced surface slope and curvature conditions are provided in Section IVb of the Task 2 Report. These data show that the quarter-panel areas are commonly the location where the highest permanent horizontal deformations and ground strains develop. The <u>middle-panel (Mid) areas</u> typically experience significant short-term *dynamic* subsidence as the longwall face passes underneath. After the passage of the longwall face and the development of the final subsidence basin, the ground surface returns approximately to its pre-mining profile (Figure IIIa.9). The <u>gate road entries (Gate) areas</u>, consisting of the room-and-pillar developments between the longwall panels, generally experience only a fraction of the subsidence found within mid-panel areas. In addition, the magnitudes of horizontal deformation and surface strain found over gate road entry areas are greatly lowered, reducing the potential for impacts to surface features.

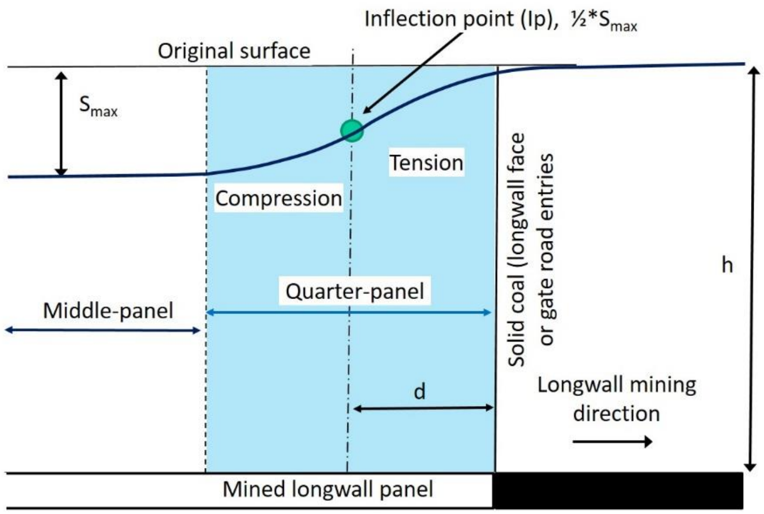

Figure IIIa.9 – Generalized surface vertical subsidence basin identifying the three generalize parts: middle-panel, quarter-panel, gate road entries.

3.1 Width of the Quarter-Panel Areas

The quarter-panel area is where most of the permanent surface change occurs. As has been explained in previous reports for this particular region, the area of permanent surface slope changes is most appropriately defined by its inflection point (Task 1 Report, Subsection IVa, pp. 51-57; Task 2 Report, Subsection IVc, p. 106). The inflection point, when applied to a subsidence basin can be thought of as a line representative of one-half of the maximum vertical subsidence (Figure IIIa.9). Conceptually, this line identifies the location of the maximum changes in surface slope and defines where the surface transitions from extensional forces to compressional forces. Empirical data for the Pittsburgh Coalbed longwall panels identifies the value '***d*** ' as the distance from the edge of the panel to the inflection point (Peng, et. al, 1995a and Peng, et al., 1995b). This value varies most significantly with overburden:

$$\boldsymbol{d} = 0.45439 * h * e^{(-0.000914*h)} \quad \text{[Eq. IIIa.1]}$$

Where: h = overburden

Previous reporting found that the most significant horizontal deformation and surface strains occur within a zone around the inflection line. In the case of Panel 15, '***d*** ' was found to be approximately 165-ft. The zone from the edge of the panel to the inflection line typically produces extension of the surface. Conversely, the most significant compression of the surface would occur up to a distance of '***d*** ' from the inflection line towards the center of the panel. At distances greater than '***d***' from the inflection line, conditions more closely aligned to the middle of the panel would apply. The University defines the width of the quarter-panel area to approximately equivalent to two times '***d***'. Using this analysis, the width of the quarter-panel area can be defined using Eq. IIIa.1 and is dependent on average local overburden conditions (Table IIIa.4).

*Table IIIa.4 – The empirical relationship for longwall panels in the Pittsburgh Coalbed where the width of the quarter-panel and middle-panel areas are based on the location of the inflection line as defined by the value of '**d**'*

Overburden	**'d'**	**Qt-panel Width, ft**	**Mid-panel Width, ft**
350	116	232	736
400	126	252	696
450	136	272	656
500	144	288	624
550	151	302	596
600	158	316	568
650	163	326	548
700	168	336	528
750	172	344	512
800	175	350	500

3.2 Profiles of Expected Vertical Subsidence

A profile function commonly used for the Pittsburgh Coalbed longwall panels demonstrates how overburden influences the Inflection Point (Ip) and changes the shape of the vertical subsidence curve and the width of the quarter-panel area (Figure IIIa.10). The use of profile functions to model the general shape of a subsidence basin has been discussed by Hood et al., 1981; Karmis et al., 1984; Peng and Cheng, 1981. This technique uses a hyperbolic tangent function to simulate the shape of a supercritical (when the panel width is greater than the overburden) subsidence basin (Eq.IIIa.2).

$$S(x) = Smax/2 * (1 - \tanh((c * x)/h)) \qquad \text{[Eq.IIIa.2]}$$

Where: c is a coefficient equal to 8.3,
x = distance from the inflection point (pointing outwards),
-x = distance from the inflection point (pointing inwards),
h = overburden, and
Smax = found from empirical relationships and is dependent on overburden and extraction thickness.

The strength of this technique is the requirement that vertical subsidence curves are symmetrical about the inflection point. Analysis of observations and monitoring data from Panel 15 (Task 2 Report) found these characteristics to be representative of the Pittsburgh Coalbed longwall mines in Pennsylvania. It should be noted that local variations, in responses to changes in mining, geology, groundwater, and topography, can cause anonymous behavior in a developing subsidence basin. Regardless, these anonymous behaviors are difficult to predict. When attempting to forecast subsidence impacts, it is appropriate to rely on models, such as the profile function technique, that track well with expected conditions.

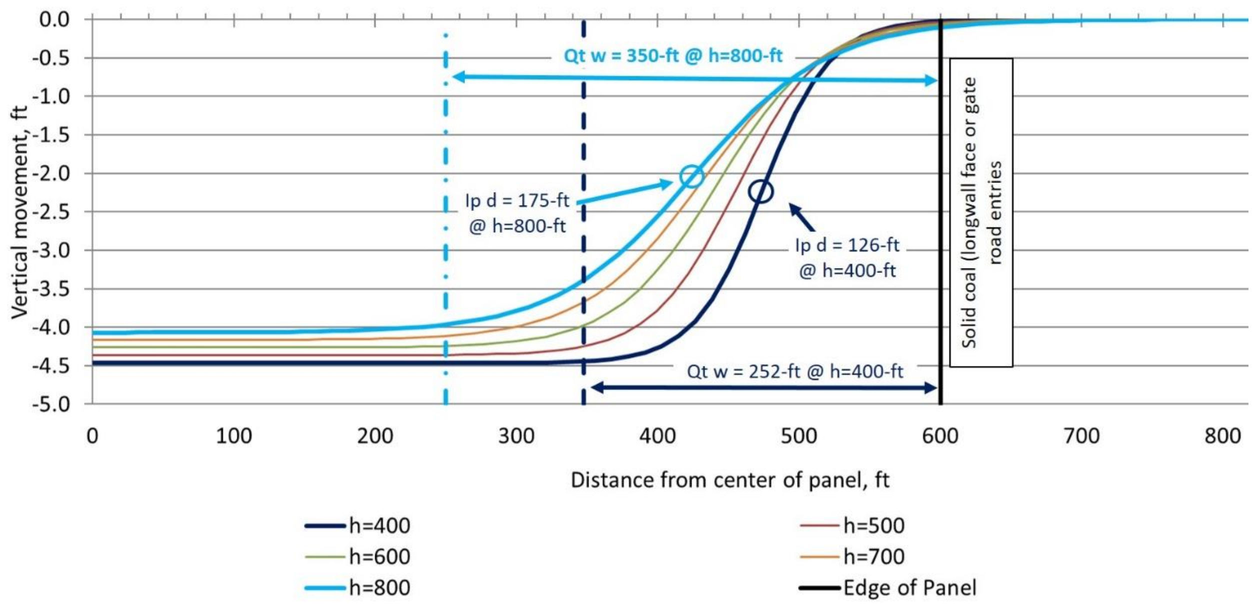

Figure IIIa.10 – Vertical subsidence profiles at overburdens ranging from 400 to 800-ft and changes to the shape of the subsidence basin and the width of the quarter-panel area

3.3 Profiles of Expected Surface Slope Changes

The profile function can also provide a general framework for understanding how structures might be impacted by either dynamic subsidence or permanent subsidence within the quarter-panel area. For flat surfaces, rigid structures are sometimes adversely affected by rapid changes in the slope of the foundation upon which they rest. Figure IIIa.11 shows how changes in slope are affected by overburden. Here again, a lower overburden produces more significant slope changes that are located closer to the panel edge. Changes in slope can be equated with horizontal movement. For example, the slope changes are expected to be greatest at the Inflection Point. At this point on the surface, the vertical settlement should be in the range of one-half the maximum subsidence. In addition, this point could also experience its maximum horizontal movement into the developing basin.

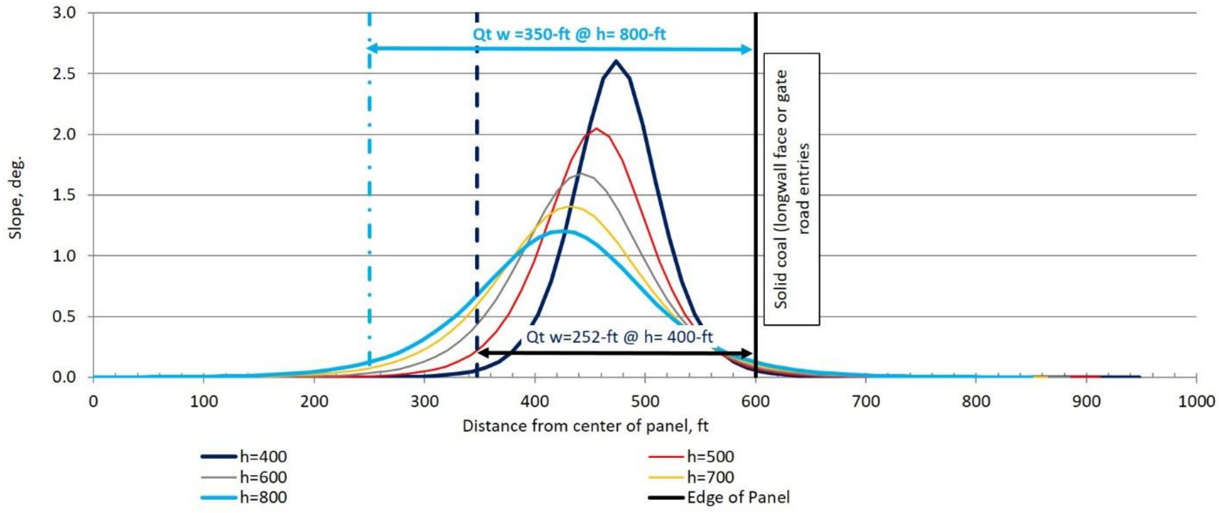

Figure IIIa.11 – Surface slope changes at overburdens ranging from 400 to 800-ft, showing how these changes are influenced by overburden

The above subsection discussion demonstrates that a longwall basin can be divided into three areas and how the sizes of these areas can be determined using empirical and analytical techniques. Each of these subsidence basin characteristics can be associated with distinctive characteristics that influence how structures are impacted on the surface. Assets within the extended study area will be placed within these categories to help understand how they will be impacted.

4.0 Tolerances for Overpasses, Retaining Walls, and Culverts

PennDOT's design standards for new or rehabilitation construction highway projects are covered in its Design Manual Part 4 (Anon, 2019) and in American Association of State Highway and Transportation Officials (AASHTO; Anon, 2004a & b). A list of design standards relevant to overpasses, conventional retaining walls, and culverts are provided in Table IIIa.5. For the purposes of this investigation, the University is most interested in applying three design specifications:

1. Overpasses, both single and continuous spans
2. Conventional retaining walls
3. Culverts (currently exploring design standards for buried structures and tunnel liners)

Table IIIa.5 - Design tolerances for overpasses, conventional retaining walls, and culverts

Structure Type	**Foundation Net Allowable Permissible Settlement**	**Permissible Differential Settlement, δ' per Span** l, **between Adjacent units (δ'/ l)** **Dimensionless Ratio**	**Permissible Differential Settlement Fraction, (δ' / l)** **Dimensionless Ratio**	**Maximum Permissible Horizontal Movement (Service / Strength); Angular Distortion between Adjacent Foundations**
Simple Span Bridge	1" (DM-4 10.5.2.2)	0.0025 (DM-4 10.5.2.2)	1/400 (DM-4 10.5.2.2)	0.5" / 1" (DM-4 11.6.2) 0.008 (AASHTO C10.6.2.2.1)
Contin-uous Span Bridge	1" (DM-4 10.5.2.2)	0.0015 (DM-4 10.5.2.2)	1/667 (DM-4 10.5.2.2)	0.5" / 1" (DM-4 11.6.2) 0.004 (AASHTO C10.6.2.2.1)
Conven-tional Retaining Walls		0.002 to 0.001 (AASHTO C11.6.2.2)	1/500 to 1/1000 (AASHTO C11.6.2.2)	
Culvert	1-deg from one side of the pipe to the other & Δ to prevent cracks in arch (AASHTO 12-27 & 12-28)	1-deg side to side & Δ for no cracking in arch (AASHTO 12-27 & 12-28); Δ = 0.01 to 0.012-pct	1-deg side to side & Δ for no cracking in arch (AASHTO 12-27 & 12-28); Δ = 0.01 to 0.012-pct	1-deg side to side & Δ for no cracking in arch (AASHTO 12-27 & 12-28); Δ = 0.01 to 0.012-pct Service Loading as per (AASHTO 12.5.2)

DM-4, PennDOT Design Manual
AASHTO LRFD Design Specification – American Association of State Highway and Transportation Officials

4.1 – Tolerances for Overpasses

The structural integrity of overpasses can be influenced by the condition of their foundations. In this study, the focus is on subsidence at the surface. Overpasses are connected to this surface through the foundation. The integrity of structures with potentially multiple foundations is dependent on stable conditions. The PennDOT Design Manual-4 states:

> *Differential settlement between substructure units results in stress redistribution in continuous beams. Large total settlements reduce vertical clearance and result in misalignment of approach roadway. The net settlement of a footing is the settlement that occurs after the supported columns or beams are set and framed.*

A key stability conditions to avoid is differential settlement between the foundations on either end of an overpass span. PennDOT and AASHTO design standards for both single and continuous span overpasses allows foundation settlement up to 1-in (Table IIIa.5). The PennDOT Design Manual-4 states:

> *The allowable settlement for shallow footings supporting bridge structures shall be based on the angular distortion (δ'/ℓ) between adjacent support units (i.e., between piers or piers and abutments) where δ' and ℓ are the differential settlement and span between adjacent units, respectively. In addition, the maximum net settlement of a footing shall not exceed 1-in. The dimensionless ratio δ'/ℓ shall be limited to 0.0025 and 0.0015 for simple and continuous span bridges, respectively.*

Eq.IIIa.3 provides a method for determining the allowable settlement:

$$\text{Allowable settlement} = \delta'/\ell \qquad \text{[Eq.IIIa.3]}$$

Where: δ' = differential settlement, in
ℓ = span between foundations, in

Because the allowable settlement is defined within existing design standards, the amount of differential settlement between the two foundations of a span can be estimated. For example, for a 35-ft simple span, the allowable settlement is 0.0025 (Table IIIa.5). This yields a permissible differential settlement of 1.05-in.

4.2 Tolerances for Conventional Retaining Walls

The PennDOT and AASHTO design manuals provide settlement requirements for conventional retaining walls. The allowable settlement is from 0.002 to 0.001 (Table IIIa.5). If Eq.IIIa.3 is used for retaining walls, the measured settlement will be along the long axis of the structure's footer. If a 35-ft long wall is considered, the allowable settlement will be between 0.42 and 0.84-in. This is significantly less for span foundations, but in the case of conventional retaining walls, the settlement will likely be spread along the length of its footer. Therefore, the different values for allowable settlement between overpasses and conventional retaining walls is justified.

Applying the tolerances provided in Table IIIa.5 to conventional retaining walls is further complicated by determining the length under which the differential settlement is measured. This complication is demonstrated in Figure IIIa.12. As the figure shows, construction joints occur at intervals ranging from approximately 10 to 20-ft and can be found within stem wall as well as the retaining wall between the stems. Unfortunately, detailed construction plans were not available during this study and field inspections were not authorized so this question could not be resolved (see Section IIIb for more discussion on this topic).

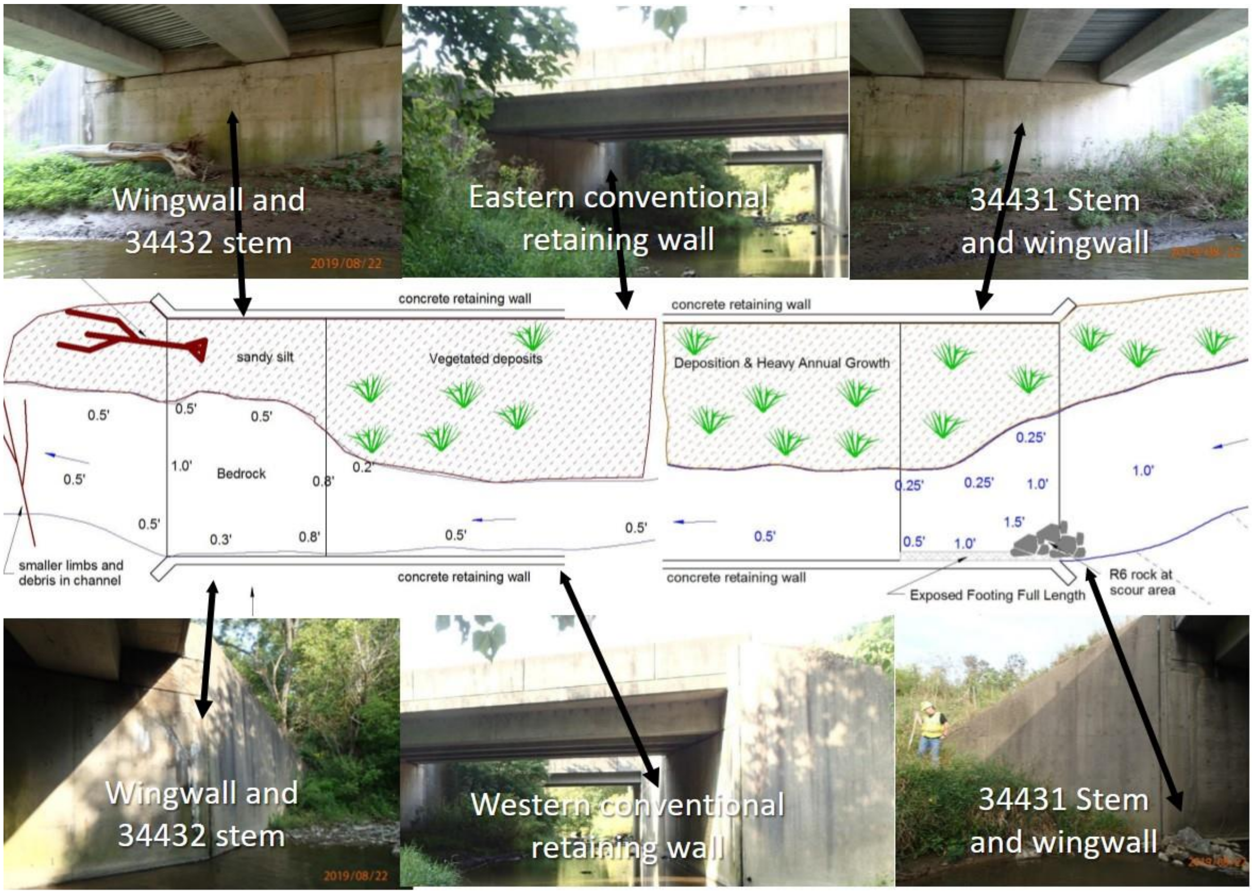

Figure IIIa.12 – Characteristics of conventional retaining walls associated with three pairs of overpasses

4.3 Tolerances for Culverts

PennDOT and AASHTO design manuals contain tolerance recommendations for culverts of the type found within the extended study area. Reinforced concrete culverts are cast-in-place and occurred either at the base of embankments or along a stream channel. In all cases, they are covered with fill ranging in thickness from 15 to 70-ft. AASHTO describes the Service Limit State (12.5.2) influenced by cracks, shear, thrust, and radial tension in reinforced concrete structures.

During construction of reinforced concrete culverts consideration is given to potential movments resulting from (AASHTO, 12.6.2.2.1):

- Longitudinal differential settlement along its length (12.6.2.2.2),
- Differential dettlement between the pipe and backfill (12.6.2.2.3), and
- Settement of fottings and unbalanced loading of skewed structure (12.6.2.2.4).

Of particular concern to this study is the potential for longitudinal differential settlement (12.6.2.2.1), occurring along the length of a culvert in response to a developing subsidence basin. Differential settlement along a culvert slope angle can cause cracks in the footing and between existing construction joints and negatively affect the flow of water within the culvert. Unfortunately, detailed construction plans were not available during this study and field inspections were not authorized so the detailed condition of these structures could not be determined.

Both the PennDOT and AASHTO design manuals provide guidelines for acceptable differential settlements across the structure taken from springline to springline, Δ (Eq.IIIa.4):

$$\Delta \leq (0.01 \text{ x } S^2) / R \qquad \text{[Eq.IIIa.4]}$$

Where:

S = span of structure between springlines of long-span plate structures (ft),
R = Rise of structure (ft), and
θ = tan^-1 (Δ/S).

The above calculation could not be applied to longitudinal differential settlement and was not determined for culverts within the extended study area.

5.0 List of Highway Assets

An inventory of assets located within the extended study area was generated and analyzed (Table IIIa.6). Assets that can be adversely impacted by surface subsidence include embankments, overpasses, culverts, pavement, guiderail, signage and a welcome center. The impact of subsidence on embankments has been a major focus of this project. For reasons that are highlighted below, Embankment #5 presents the greatest challenges to subsidence (see Section IV of this report). Significant information on the characteristics and conditions of overpasses and culverts are available through PennDOT structure safety inspection reports; however, detailed design/construction reports on overpasses, retaining walls, and culverts were not provided. Field visits were not authorized so no information was available beyond the official inspection reports for specific assets. The assets that were not evaluated include smaller diameter corrugated metal culvert, guiderail and signage. Lastly, potentially undermining the Welcome Center near the Claysville Interchange will require best-practice engineering controls capable of preventing loss of structural integrity or, at a minimum, implement recovery measures to minimize subsidence impact.

Table IIIa.6 – Characteristics of the 28 embankment, overpass, and culvert highway assets

#	SI No. / ID	BR Key	Road	Type	Feature
1	EM#4	NA	I-70, BD	Embankment	Un-named stream
2	NA	NA	I-70, BD	CMC, base of EM#4	Un-named stream
3	62-0070-0015-0860	34426	I-70, WB	MSO	Abandoned railroad
4	62-0070-0014-0987	34424	I-70, EB	MSO	Abandoned railroad
5	EM#5	NA	I-70, BD	Embankment	Trib 32857 to Dutch Fork
6	62-0070-0014-1245	34425	I-70, BD	RCC, base of EM#5	Trib 32857 to Dutch Fork
7	EM#6	NA	I-70, BD	Embankment	Trib 32862 to Dutch Fork
8	62-0040-0030-1990	34373	US-40	RCC, base of EM#6	Trib 32862 to Dutch Fork
9	62-0070-0020-0824	34427	I-70, BD		Trib 32862 to Dutch Fork
10	62-0040-0050-0000	34374	US-40	RCC	Trib 32859 Dutch Fork
11	62-0070-0020-2249	34428	I-70, BD	RCC	Trib 32859 Dutch Fork
12	62-0070-0025-2254	34430	I-70, WB	SSO with CRW	Trib 32857 to Dutch Fork
13	62-0070-0024-2105	34429	I-70, EB	SSO with CRW	Trib 32857 to Dutch Fork
14	62-0040-0070-0075	34375	US-40	SSO	Dutch Fork
15	62-0070-0035-0495	34432	I-70, WB	SSO with CRW	Dutch Fork
16	62-0070-0034-0557	34431	I-70, EB	SSO with CRW	Dutch Fork
17	62-0070-0040-0655	34433	I-70, WB	SSO	Dutch Fork
18	62-0070-0041-0735	34434	I-70, EB	SSO	Dutch Fork
19	NA	NA	US-40	RCC	Trib 32870 to Dutch Fork
20	62-0040-0100-2290	34376	US-40	RCC	Trib 32871 to Dutch Fork
21	62-0070-0045-1290	34437	I-70, WB	SSO with CRW	Dutch Fork
22	62-0070-0044-1355	34435	I-70, EB	SSO with CRW	Dutch Fork
23	62-0070-0044-1935	34436	I-70, BD	RCC	Trib 32872 to Dutch Fork
24	NA	NA	US-40	Culvert, UK	Trib 32872 to Dutch Fork
25	Welcome Center	NA	I-70	NA	Dutch Fork flood plain
26	62-0070-0050-2105	34438	I-70, BD	RCC	Trib 32874 to Dutch Fork
27	NA	NA	US-40	Culvert, UK	Trib 32874 to Dutch Fork
28	62-0040-0110-1935	34377	I-70 & US-40	RCC	Trib 32875 to Dutch Fork

NA – Not available
UK – Unknown characteristics
WB – West bound lanes
EB – East bound lanes
BD – Both east and west lanes
SSO – Single-span overpass
MSO – Multiple-span overpass
CMC – Corrugated metal culvert
RCC – Reinforced concrete culvert
CRW – Conventional retaining wall

Twenty-eight assets were identified that fell into one of four categories: embankments, overpasses, conventional retaining walls, and culvert. Table IIIa.5 list assets from west (West Alexander Interchange) to east (Claysville Interchange). The location of each of the 28 assets is shown in Figure IIIa.13.

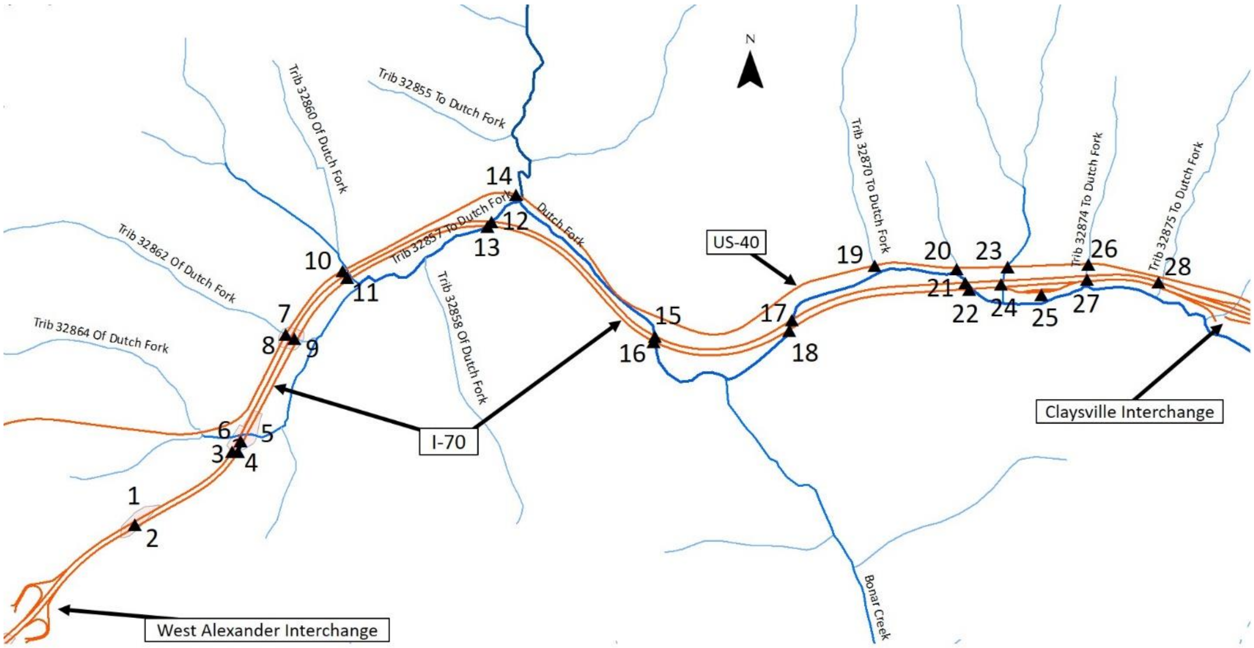

Figure IIIa.13 – Location of the 28 identified embankment, overpass, and culvert highway assets

Much of the I-70 extended study area, along with US-40, occupies the valleys associated with the Dutch Fork and its tributaries streams (Figure IIIa.14). This figure clearly shows the relationship between the I-70 alignment, the Dutch Fork and the tributaries with the assets. All but two of the assets are crossing over a stream within the Dutch Fork watershed.

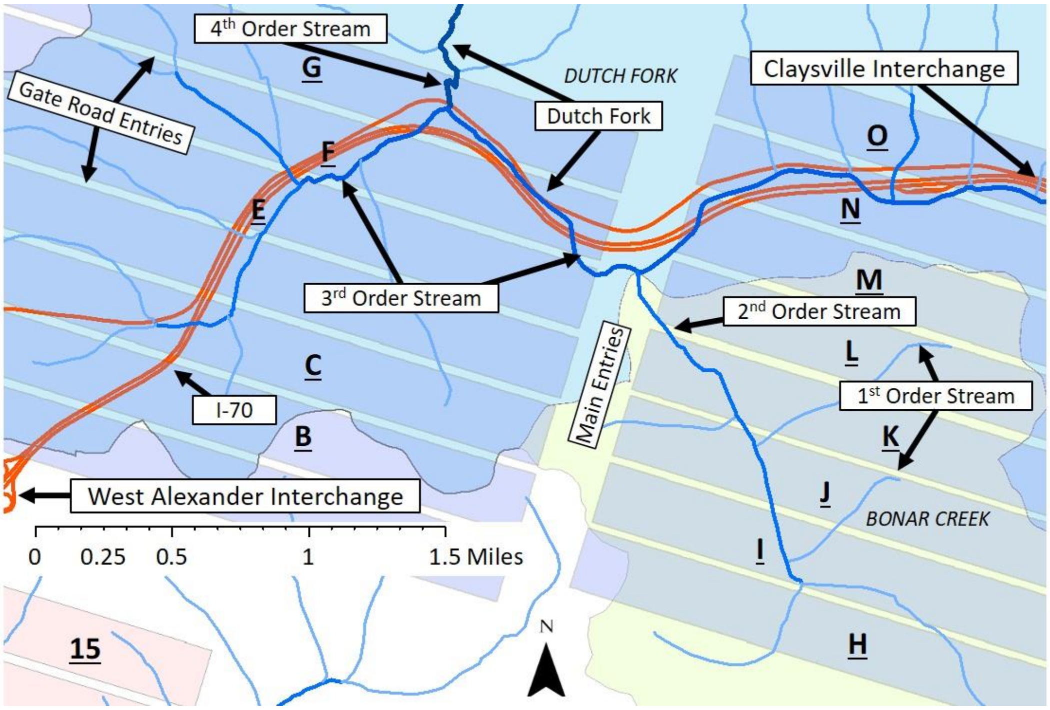

Figure IIIa.14 – The connection between the I-70 alignment and Dutch Fork and its tributaries. Many of the important assets are associated with carrying I-70 over 3rd order streams

At the writing of this report, it is not possible to know precisely how overpasses and culverts will be impacted by subsidence because the exact mine plan is not known. The purpose of this section is to provide a framework that illustrates how these different structures might respond to undermining and a developing subsidence basin. Section IIIb will provides an opportunity to do a more in-depth analysis and demonstrate how structures could respond to different overburdens and positions within the subsidence basin.

5.1 Embankments

A major focus of this research study has been to understand how embankments, constructed to carry the I-70 alignment, would perform when subjected to subsidence from longwall mining. Two of these embankments (Embankments #1 and #2) are located above or adjacent to Panel 15 (Figure IIIa.15). Embankment #1 is located entirely above the middle-panel area. Whereas Embankment #2 was located either above the gate entry area or solid, unmined coal.

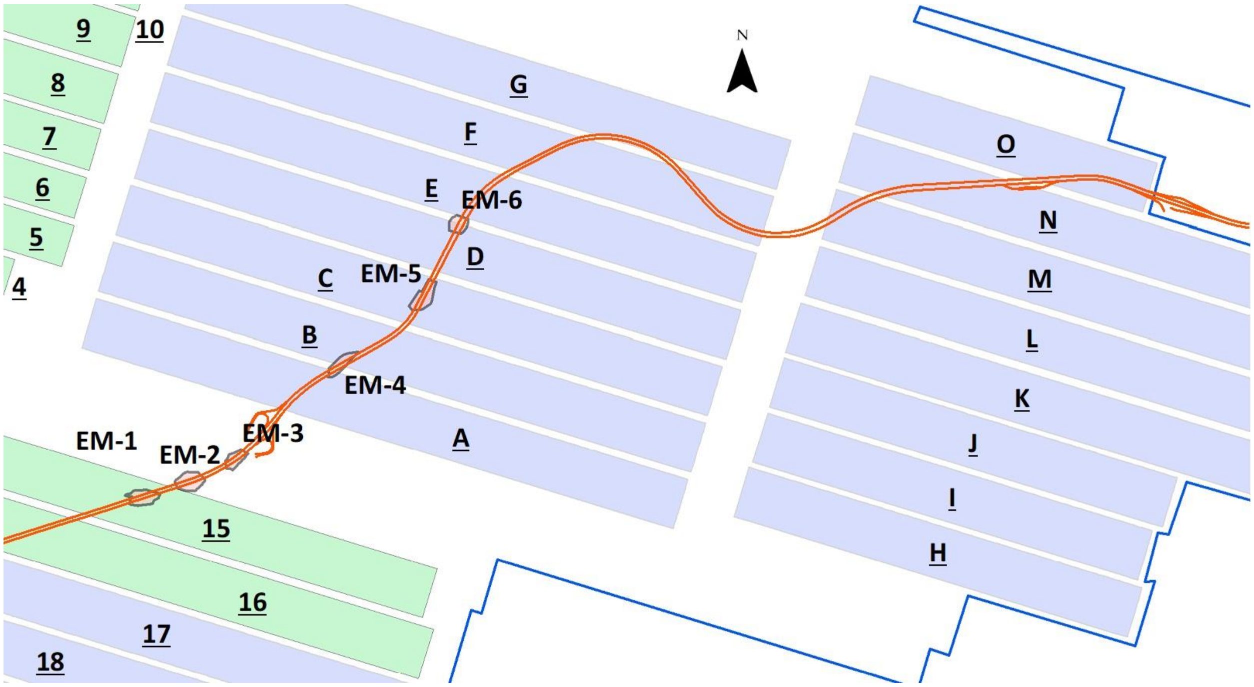

Figure IIIa.15 – Six significant embankments (EM) were constructed between the West Virginia State Line and the Claysville Interchange. Three of the embankments, #4, #5, and #6, are located within the extended study area. The green panels were extracted at the time of writing this report. The blue panel locations are projected. Actual panel locations may differ from those projected by the University

The University was provided extensive amount of field instrumentation and laboratory data that has greatly assisted in documenting and characterizing embankment performance. For example, Embankment #1 was subjected to over 4-ft of vertical subsidence at the base. Consolidation and spreading of the embankment added to this total resulting in as much as 5-ft of vertical subsidence (Section III, Task 2 Report). In addition, bands of material began to show signs of shearing near the base of the embankment, leading to the observation that the fill was starting to mobilize along this zone of deformation. Some minor slope instabilities were observed but no maintenance interventions were required. The threat of a significant instability was thought to have been overcome by the strain-hardening material properties of the embankment fill (see Section V, Task 2 Report). As a result, Embankment #1 did not fail and the uninterrupted flow of traffic along I-70 was only temporarily disrupted by pavement maintenance activities. Embankment #2 was located over the gate road entries adjacent to Panel 15 and was not adversely affected in any manner. Embankment #3 is west of the West Alexander Interchange and is not expected to be undermined by longwall mining. Three other embankments (#4, #5, and #6) occur within the extended study area (Table IIIa.7).

Table IIIa.7 – General characteristics of the three embankments within the extended study area

Embankment	Panel ID & Panel Area	Avg. Overburden, ft	Max. Length of Highway Carried by Embankment, ft	Orientation of Highway to LW Mining Direction, deg	Max. Fill Thickness, ft
#4	A-Qt & Gate, B-Qt	598	~685	42	52
#5	C-Mid & Qt	514	~785	79	70
#6	D-Qt & Gate	492	~380	79	54

Panel area: Mid = Middle-panel area, Qt = Quarter-panel area, Gate = Gate road entries area

5.1.1 *Embankment #4*

Longwall mining will occur from 540 to 620-ft below the surface of Embankment #4 for an average overburden of 580-ft (Figure IIIa.16). The angle of the I-70 highway alignment with the projected direction of mining will be approximately 42-deg. This embankment carries the highway for approximately 610-ft, where the fill achieves a maximum thickness of 52-ft. Embankment #4 is projected to span parts of Panel A & B. In this mining scenario, the smaller southwestern portion of the embankment would be pulled into the Panel A subsidence basin while its larger northeastern portion would be pulled in the opposite direction. For the larger northeastern portion of Embankment #4, both permanent extension in the southern portions and compression at the northern end are predicted. The potential for large deformations during the undermining of Embankment #4, with this panel configuration, highway orientation, and overburden, is not expected to produce significant risk to the highway.

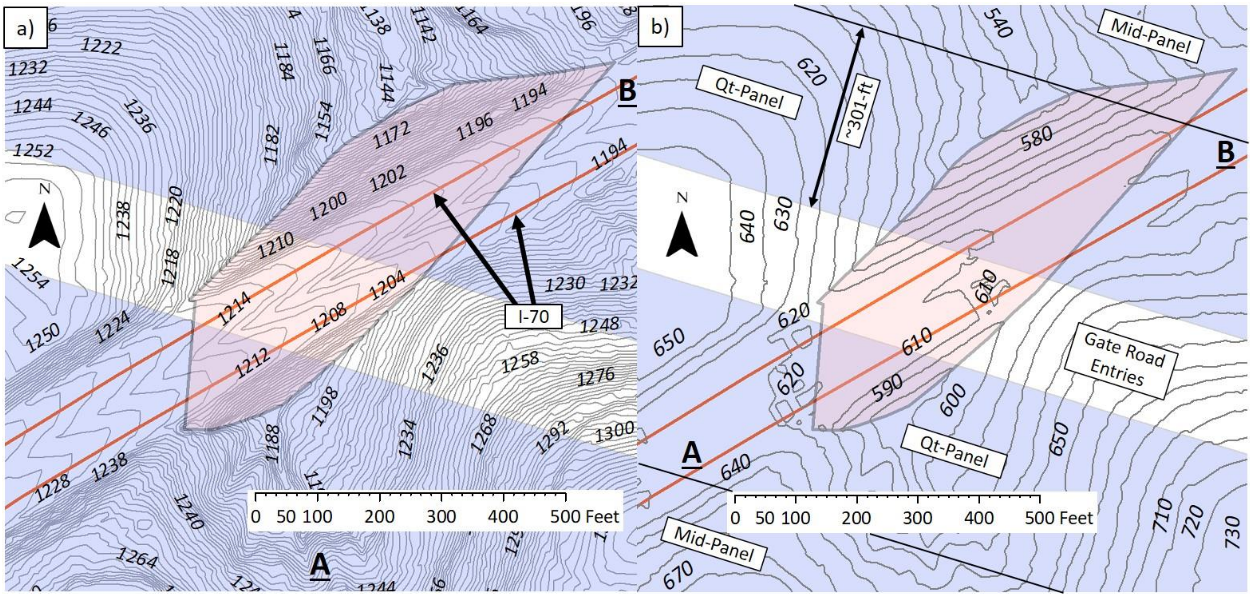

Figure IIIa.16 - a) surface topography associated with Embankment #4; b) thickness of the strata (overburden) between the extracted longwall panel and I-70

5.1.2 *Embankment #5*

Embankment #5 carries I-70 for approximately 720-ft with a maximum fill thickness of 70-ft (Figure IIIa.17). The overburden associated with this embankment ranges from 460 to 540-ft with an average of 500-ft. The angle of the I-70 highway alignment with the projected mining direction is approximately 79-deg. The greatest volume of Embankment #5 is within the middle-panel area (Figure IIIa.17b). In this scenario, the embankment will spread most significantly towards the retreating longwall face as it moves under and away from the embankment.

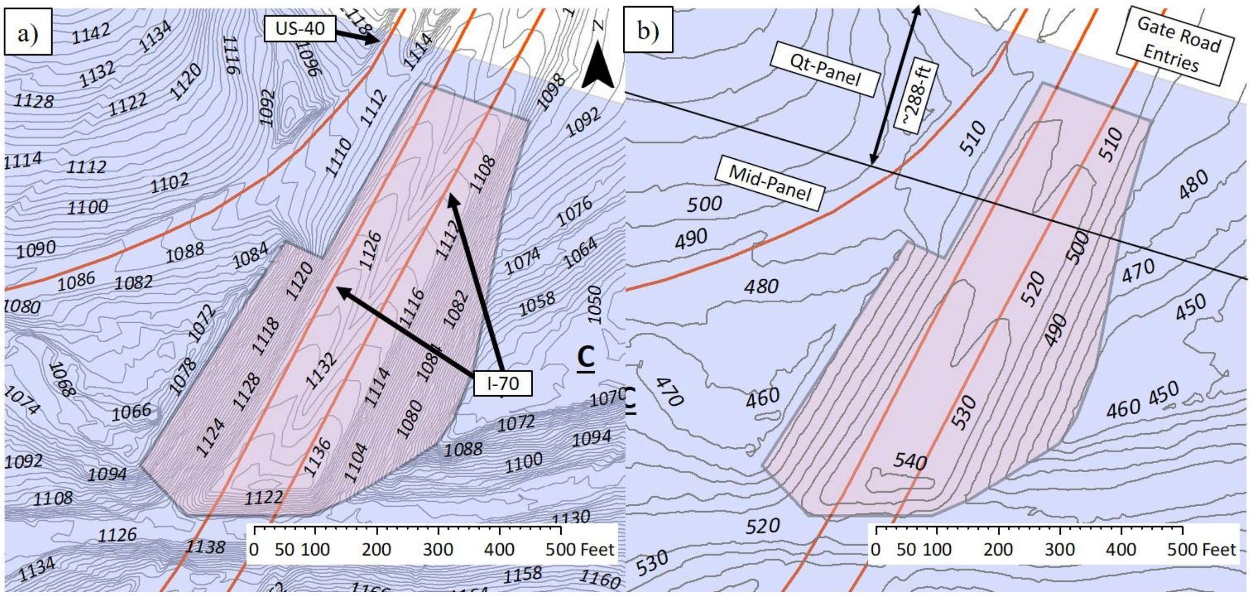

Figure IIIa.17 - a) surface topography associated with Embankment #5; b) thickness of the strata (overburden) between the extracted longwall panel and I-70

An additional complication is the presence of an abandoned railroad along the side of Embankment #5. The embankment's south side normally would be resting against bedrock. To assess the complex nature of this asset, the University performed a detail stability analysis of Embankment #5 using the finite element method, see Section IV. The thickness of the fill, angle of the highway to the direction of mining, presence of the abandoned railroad, and relatively low overburden all combined to elevate the risk for large deformations during undermining.

5.1.3 *Embankment #6*

Embankment #6 carries I-70 for only approximately 380-ft with a maximum fill thickness of 54-ft (Figure IIIa.18a). Of the six embankments, it has the least overburden, ranging from 430 to 480-ft with an average of 455-ft (Figure IIIa.18b). The angle of the I-70 highway alignment with the projected face advance is ~79-deg. The thickness of the fill, close alignment with the embankment orientation and mining direction, relatively low overburden, and partial location within the quarter-panel puts this embankment at a moderate risk for damaging deformations.

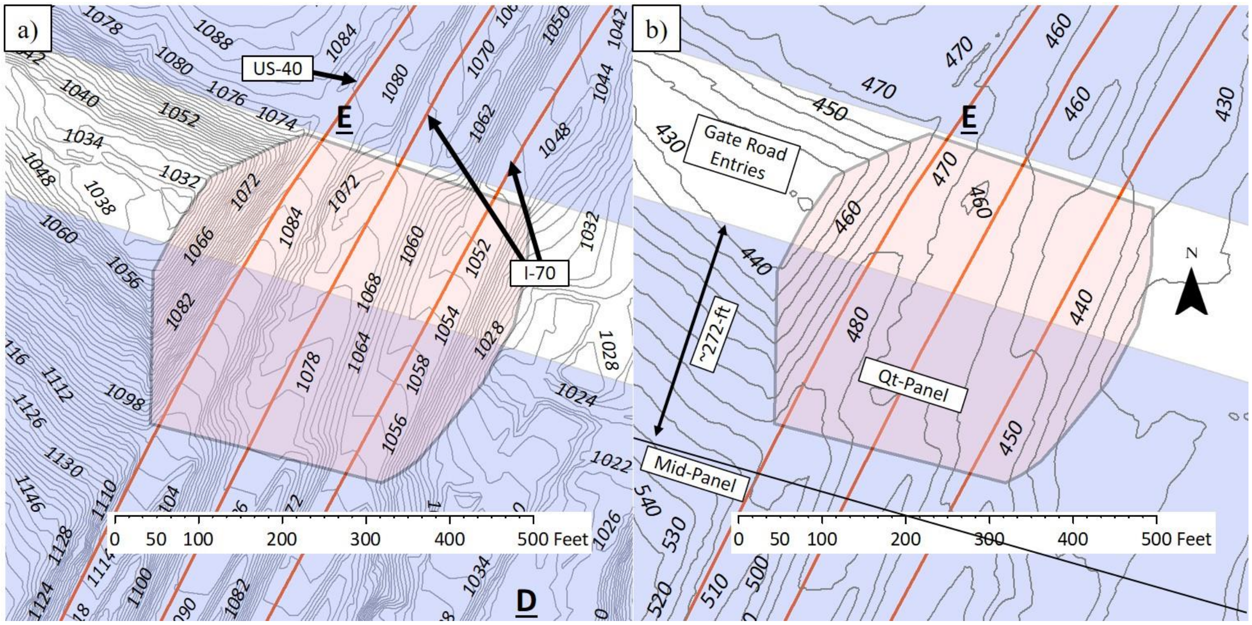

Figure IIIa.18 - a) surface topography associated with Embankment #6; b) thickness of the strata (overburden) between the extracted longwall panel and I-70

5.2 Overpasses

Driving west from the Claysville interchange, I-70 passes over the Dutch Fork three times producing six overpasses (Figure IIIa.19). Two more crossings occur along a tributary to Dutch Fork producing another four overpasses. The eleventh overpass carries US-40 over Dutch Fork as it flows north into Dutch Fork Lake and is located a little more than 500-ft from I-70.

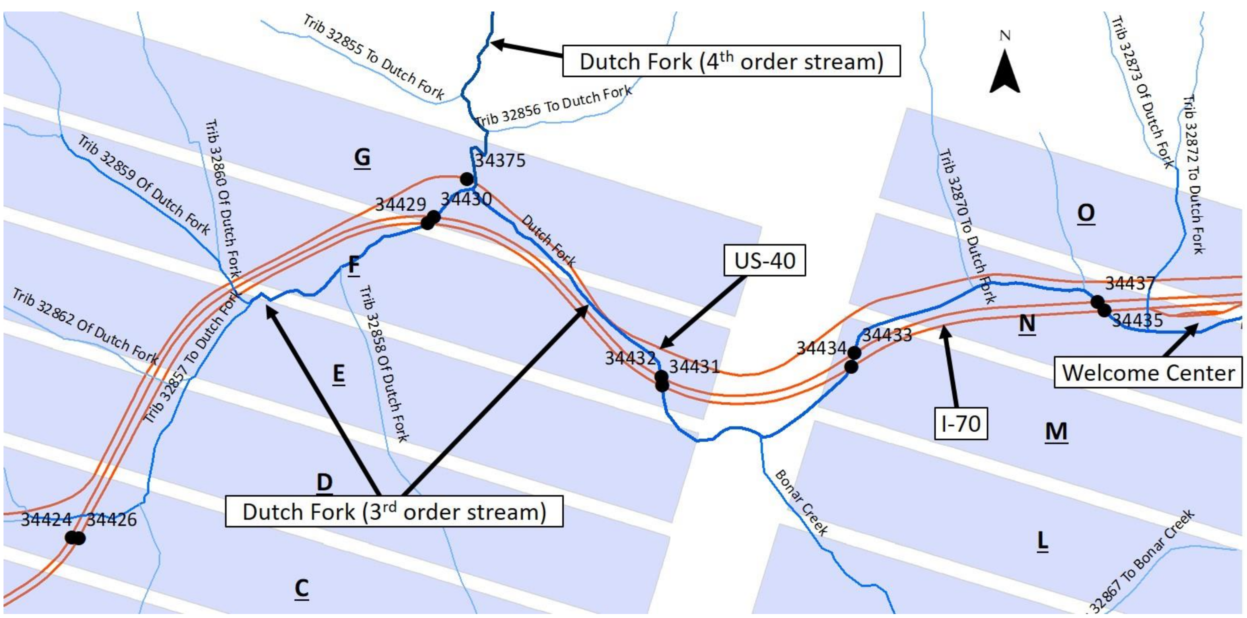

Figure IIIa.19 – Overpasses (spans) between West Alexander and Claysville Interchanges with Bridge Key numbers along I-70 and adjacent US-40. Overpass BK numbers are included.

Nine of the 11 overpasses have a simple span layout, varying mainly in length, which ranged from 30 to 52-ft (Table IIIa.8). All of the simple pans were originally constructed in 1961 but eventually reconstruction at vary times. The first reconstruction occurred in 1982 with the last in 2017. The highest concentration of these reconstructions were performed between 1989 and 1990. Eleven inspection reports, all completed in 2019, were reviewed, providing an assessment of the superstructure and substructure conditions. Structure conditions were rated from satisfactory (6) to very good (8). Two of the overpasses have multiple spans and have a structure condition rating of fair (5).

Table IIIa.8 – Characteristics of the 11 overpasses within the extended study area

BR Key / ID	Direc-tion	Panel ID - Panel area	Recon-structed	Type	Connec-ting retain-ing wall	Span length/width, ft	Sup-CR	Sub-CR	~Over-burden, ft
34426 / 62-0070-0015-0860	WB	C-Mid	1982	3 spans	N	170/55	5	5	500
34424 / 62-0070-0014-0987	EB	C-Mid	1982	3 spans	N	170/55	5	5	
34429 / 62-0070-0024-2105	EB	G-Gate/Qt	1989	Simple span	Y	30/65	6	6	350
34430 / 62-0070-0025-2254	WB	G-Qt	1990	Simple span		30/65	6	6	
34375 / 62-0040-0070-0075	US40	G-Mid	2017	Simple span	N	52/37	7	7	340
34432 / 62-0070-0035-0495	WB	F-Mid	1989	Simple span	Y	40/45	7	6	360
34431 / 62-0070-0034-0557	EB	F-Mid	1989	Simple span		40/45	8	6	
34434 / 62-0070-0041-0735	EB	M-Qt/Mid	1990	Simple span	N	45/63	7	6	370
34433 / 62-0070-0040-0655	WB	M-Qt/Mid	1989	Simple span	N	45/63	7	6	
34437/62-0070-0045-1290	WB	N-Mid	1990	Simple span	Y	34/52	7	6	380
34435 / 62-0070-0044-1355	EB	N-Mid	1995	Simple span		34/65	7	6	

WB – westbound lanes; EB – eastbound lanes
N – No; Y – Yes
Span length – parallel to highway direction
Span width – perpendicular to highway direction
Panel area: Mid = Middle-panel, Qt = Quarter-panel, Gate = Gate road entries
Superstructure (SupCR)/Substructure (SubCR) condition rating scale:

- 5 - Fair-all primary structural elements are sound but may have minor section loss, cracking spalling.
- 6 - Satisfactory-structural elements show some minor deterioration.
- 7 - Good-some minor problems
- 8 - Very good - no problems noted

5.2.1 *Three Span, Two Pier Overpasses (projected within the middle-panel area)*

The most consequential overpasses within the extended study area are twin, three-span overpasses that are ~170-ft long and have an average overburden of 500-ft (Figure IIIa.20a&b; 34424 & 34426). Both structures have two supporting piers (Figure IIIa.20c). These spans, first constructed in 1961, were last reconstructed in 1982. Both the superstructure and substructure condition ratings for these structures are rated as category 5 (Fair - all primary structural elements are sound but may have minor section loss, cracking spalling). One concern is how the existing minor section loss, cracking and spalling be further affected by subsidence. In addition, these structures are located on the side of Embankment #5 (Figure IIIa.17), potentially forming two different supporting foundation conditions under each span with one supported by fill and the other on bedrock.

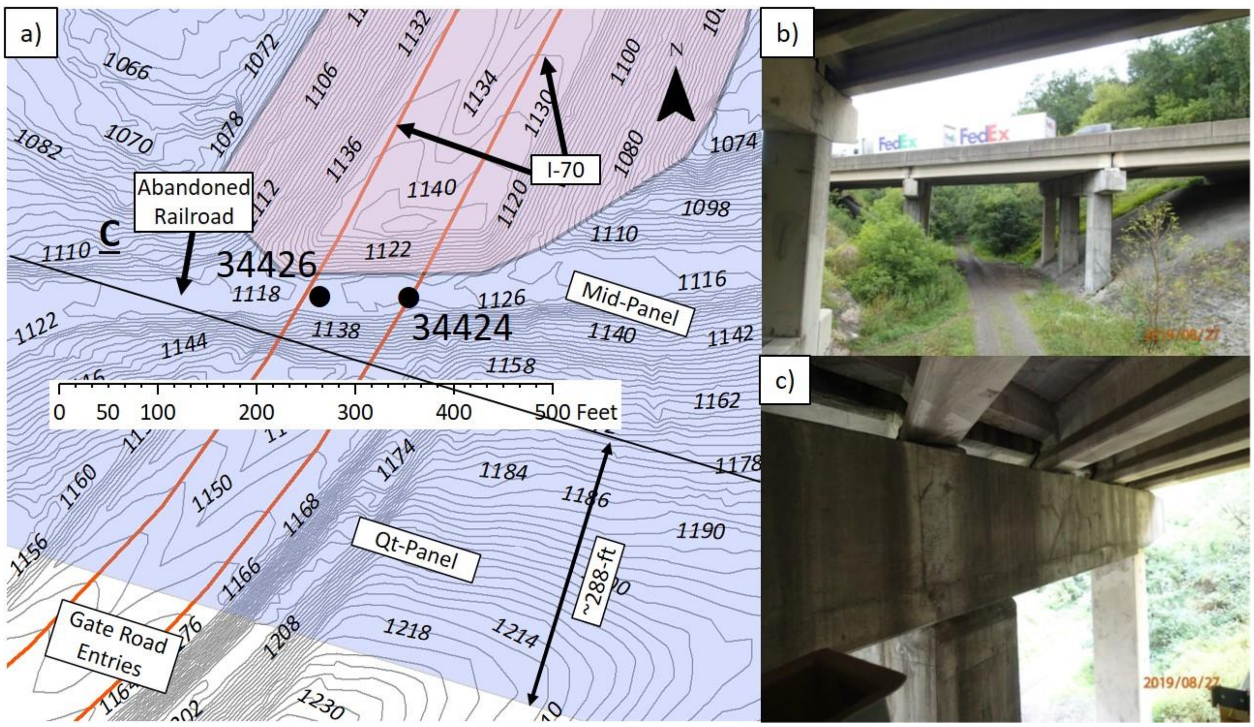

Figure IIIa.20 – a) location of Overpasses 34424 & 34426 within the middle-panel are of Panel C, b) 2019 PennDOT inspection report photograph East Bound lanes of I-70 (34424), and c) photograph near right face of pier 1

5.2.2 *Simple Span Overpass Structures*

Nine simple span overpass structures are located within the extended study area, eight along the I-70 and one along US-40 (Figure IIIa.19). Most of these structures were reconstructed in the late 1980's early 1990's and range in length from 30 to 52-ft. Both super- and sub-structure condition rating range from 6 to 8 (Table IIIa.8). The foundation of the stem walls, which in-turn supports these simple span overpasses, are critical.

5.2.2.1 Isolated Stem Walls

Three simple span overpasses have isolated stem walls, with each overpass separate and not connected in any manner with its neighbor. For example, Overpasses 34433 and 34434 (Figure IIIa.21a) rest on a stem wall flanked by wingwalls on each end (Figure IIIa.21b). The average overburden at this location is approximately 370-ft. The third isolated stem wall example is overpass 34334, which is located on US-40 close to I-70. The overburden associated with this asset is the least of any within the extended study area at approximately 340-ft.

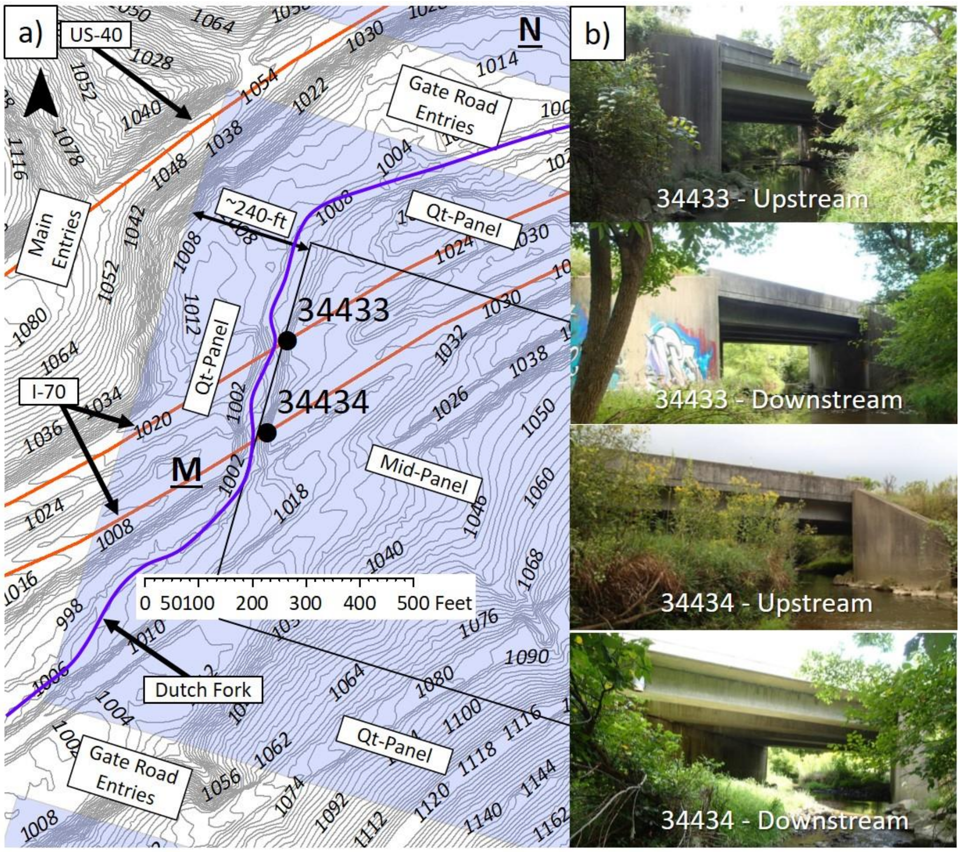

Figure IIIa.21 – Two of the three single span overpasses with isolated stem walls

5.2.2.2 Stem Walls Connected to Conventional Retaining Walls

Three pairs of overpasses are connected with conventional retaining walls. The nature of the connection could not be determined. One pair, overpasses 34431 and 34432, was previously discussed and shown in Figure IIIa.12. When compared to the two other pairs of overpasses, 34429 and 34430 (Figure IIIa.22) and 34435 and 34437 (Figure IIIa.23), the connecting conventional retaining walls average 52-ft in length and approximately 14-ft in height (Table

IIIa.9). In all cases, these retaining walls help to provide lateral support for the stem walls, prevent highway fill from entering the stream channel, and provide for stream flow under a wide range of conditions. When considering the stem and retaining walls together, the total length increases to an average of 163-ft.

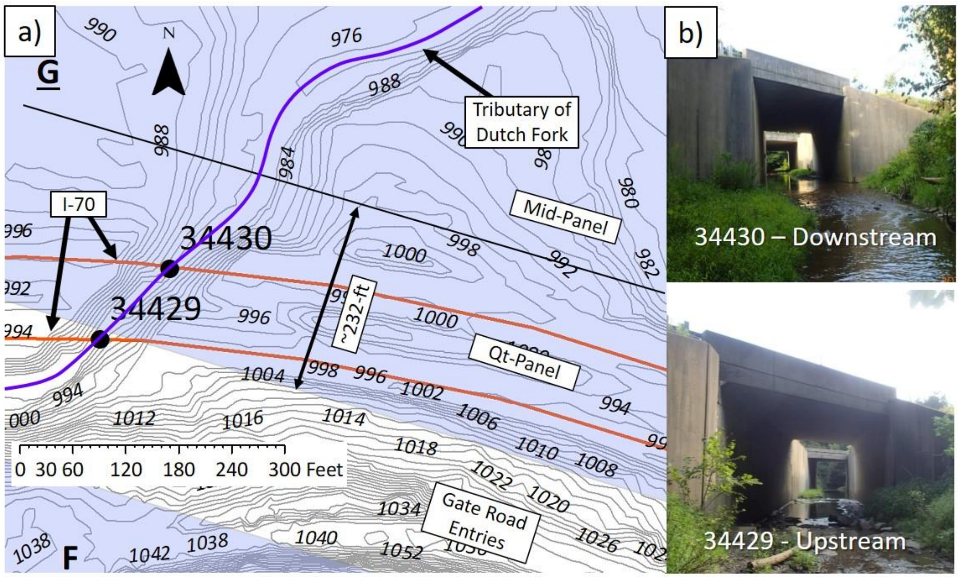

Figure IIIa.22 – Overpasses 34429 and 34430 with connecting conventional retaining wall

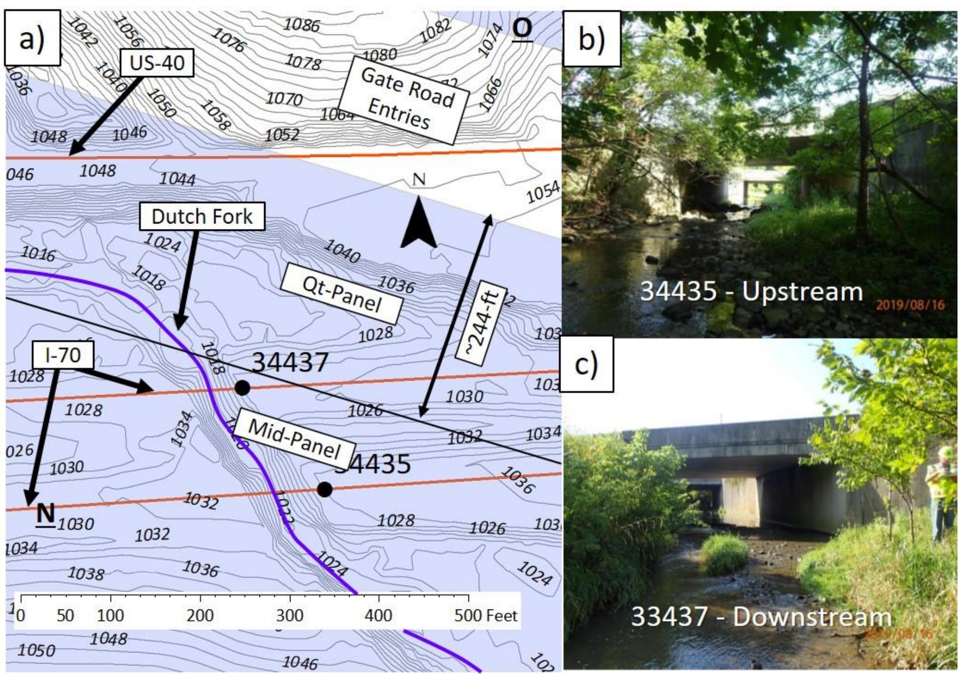

Figure IIIa.23 – a) two I-70 single span overpasses, b) upstream BK 34435 and connecting retaining wall, c) downstream BK and connecting retaining wall

Table IIIa.9 – Lengths of conventional retaining walls

BR Key (BK)	Retaining Wall Length, ft	Stem + Retaining Wall Length, ft
34435/34437	82	197
34434/34433		
34431/34432	49	143
34429/34430	57	187
34375		
34426/34424	50	160
Average	52	163
Standard Deviation	14.4	24.7

Once the location of the longwall panels are finalized, potential subsidence induced differential settlement, i.e. between opposing foundations of a given span, can be compared to design/reconstruction tolerances provided by PennDOT/AASHTO (see Section IIIa.4 of this report). The retaining walls can be examined in a similar fashion, although the allowable settlements are different for spans and walls. Examples of how this analysis can be conducted are provided in Section IIIb.

5.3 Culverts

Ten culverts are identified within the extended study area (Table IIIa.6). One relative measure of the culvert flow capacity is to examine its stream order. The stream order is a positive whole number used in geomorphology and hydrology to indicate the level of branching in a river system (Wikipedia, 2020). A 1st order stream is the uppermost or initial stream segment. When two 1st order streams meet, a 2nd order stream is the result. The nine reinforced culverts found within the extended study area carry 3rd order streams. This is an indication of the relatively significant potential flow these culverts are expected to carry.

Only one smaller diameter corrugated metal culvert was identified within the extended study area and it carries a 1st order stream (#2, Table IIIa.6). Another measure of flow significance is that regular inspections are required to track the condition of reinforced concrete culverts. As with the overpasses, inspection reports are used to assess the characteristics and conditions of the culverts. The location of the nine reinforced concrete culverts are shown in Figure IIIa.24.

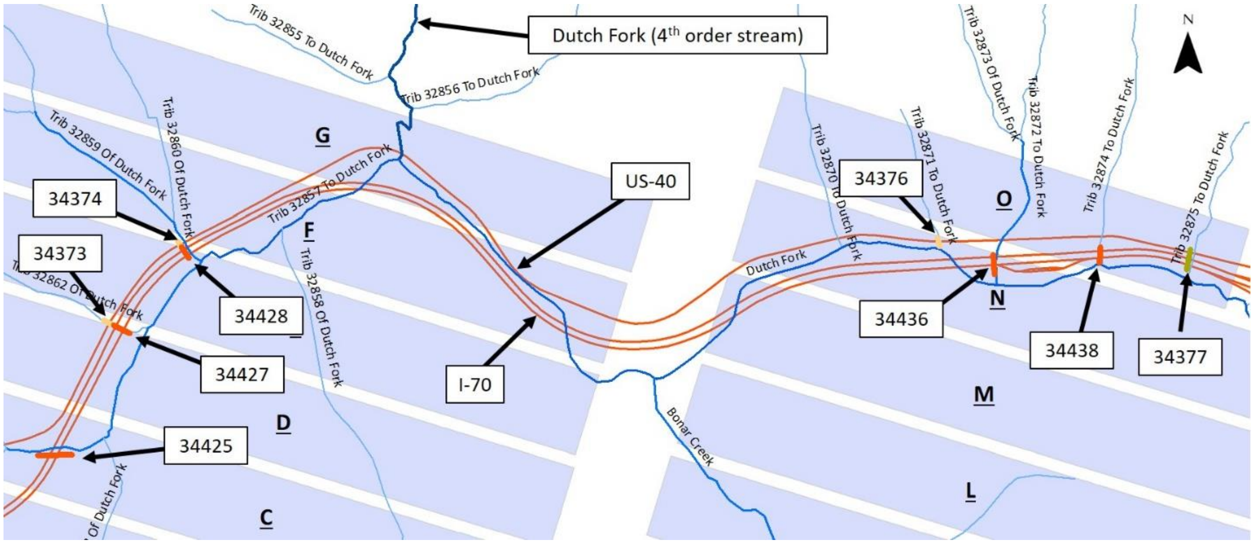

Figure IIIa.24 – Reinforced concrete culverts within the extended study area. Dutch Fork and portions of Tributary 32857 to Dutch Fork are 3rd order streams

All of the reinforced concrete culverts were constructed in 1960 or 1961 with only two reconstructed in 1995 (34436 & 34438). Six of culvert barrels have an arch shape (Table IIIa.10); three others are box shaped. The exact diameter or width of the culverts could not be determined but was sufficiently large to accommodate a 3rd order stream flow and to allow physical inspection 100-ft from the entrance. All of the culverts listed in Table IIIa.10 were inspected in 2017 or 2019. Culvert lengths ranged from 122 to 480-ft. The typical culvert contains construction joints every 10 to 20-ft within the barrel. The streams flow on concrete or bedrock floors. All culverts are under fill, ranging from 11 to 70-ft. The position or location of the culvert within the projected longwall panel is provided in Table IIIa.10.

Table IIIa.10 – Characteristics of the nine reinforced concrete culverts within the extended study area

<table>
<tr><th>BR Key (BK) / ID</th><th>R</th><th>Type</th><th colspan="2">Length, ft</th><th>CCR</th><th>Founda-tion</th><th>Max. under fill, ft</th><th>Panel ID - Panel area</th><th>Slope, ft/100-ft</th><th>Change in Slope, ft/100-ft</th></tr>
<tr><td>34425 / 62-0070-0014-1245</td><td>70</td><td>Arch</td><td>480</td><td></td><td>5</td><td>Bedrock</td><td>70</td><td>C-Mid</td><td>1.2</td><td>1.2</td></tr>
<tr><td>34373 / 62-0040-0030-1990</td><td>40</td><td rowspan="2">Arch</td><td>162</td><td rowspan="2">412</td><td>6</td><td rowspan="2">Concrete</td><td>61</td><td rowspan="2">D-Gate</td><td rowspan="2">1.9</td><td rowspan="2">2.0</td></tr>
<tr><td>34427 / 62-0070-0020-0824</td><td>70</td><td>250</td><td>6</td><td>40</td></tr>
<tr><td>34374 / 62-0040-0050-0000</td><td>40</td><td rowspan="2">Arch</td><td>94</td><td rowspan="2">280</td><td>6</td><td rowspan="2">Concrete</td><td>31</td><td>E-Gate</td><td rowspan="2">1.4</td><td rowspan="2">1.7</td></tr>
<tr><td>34428 / 62-0070-0020-2249</td><td>70</td><td>186</td><td>6</td><td>22</td><td>E-Qt</td></tr>
<tr><td>34376 / 62-0040-0100-2290</td><td>40</td><td>Arch</td><td>122</td><td></td><td>6</td><td>Bedrock</td><td>24</td><td>N-Qt</td><td>6.6</td><td>7.6</td></tr>
<tr><td>34436 / 62-0070-0044-1935</td><td>70</td><td>Box</td><td>276</td><td></td><td>7</td><td>Concrete *</td><td>11</td><td>N-Qt</td><td>0.7</td><td>2.4</td></tr>
<tr><td>34438 / 62-0070-0050-2105</td><td>70</td><td>Box</td><td>221</td><td></td><td>6</td><td>Concrete *</td><td>12</td><td>O-Qt</td><td>1.8</td><td>0.1</td></tr>
<tr><td>34377 / 62-0040-0110-1935</td><td>40 & 70</td><td>Box</td><td>287</td><td></td><td>6</td><td>Concrete</td><td>17</td><td>O-Mid</td><td>1.4</td><td>1.4</td></tr>
</table>

CCR – Culvert condition rating
R - Road
* - debris deposition
Panel: Mid = Middle-panel, Qt = Quarter-panel, Gate = Gate entries
Have not found the culvert condition rating scale:

- 5 - Fair-all primary structural elements are sound but may have minor section loss, cracking spalling.
- 6 - Satisfactory-structural elements show some minor deterioration.
- 7 - Good-some minor problems
- 8 - Very good - no problems noted

5.3.1 *Culverts Located over Middle-Panel Areas*

Culvert 34425 extends 480-ft under Embankment #5 (Figure IIIa.25). The fill reaches a maximum thickness of 70-ft under the I-70 pavement. This culvert is located over the middle of the panel approximately 600-ft from either gate entry system (Figure IIIa.25a). Because of its mid-panel position, significant deformations and both extensional and compressional strains are expected during the passage of the longwall face (dynamic subsidence). Conversely, very little permanent change to the slope of the surface (permanent subsidence) will occur. At this location with an average overburden of 500-ft, most of the permanent surface slope changes will occur within approximately 288-ft of the gate road entries.

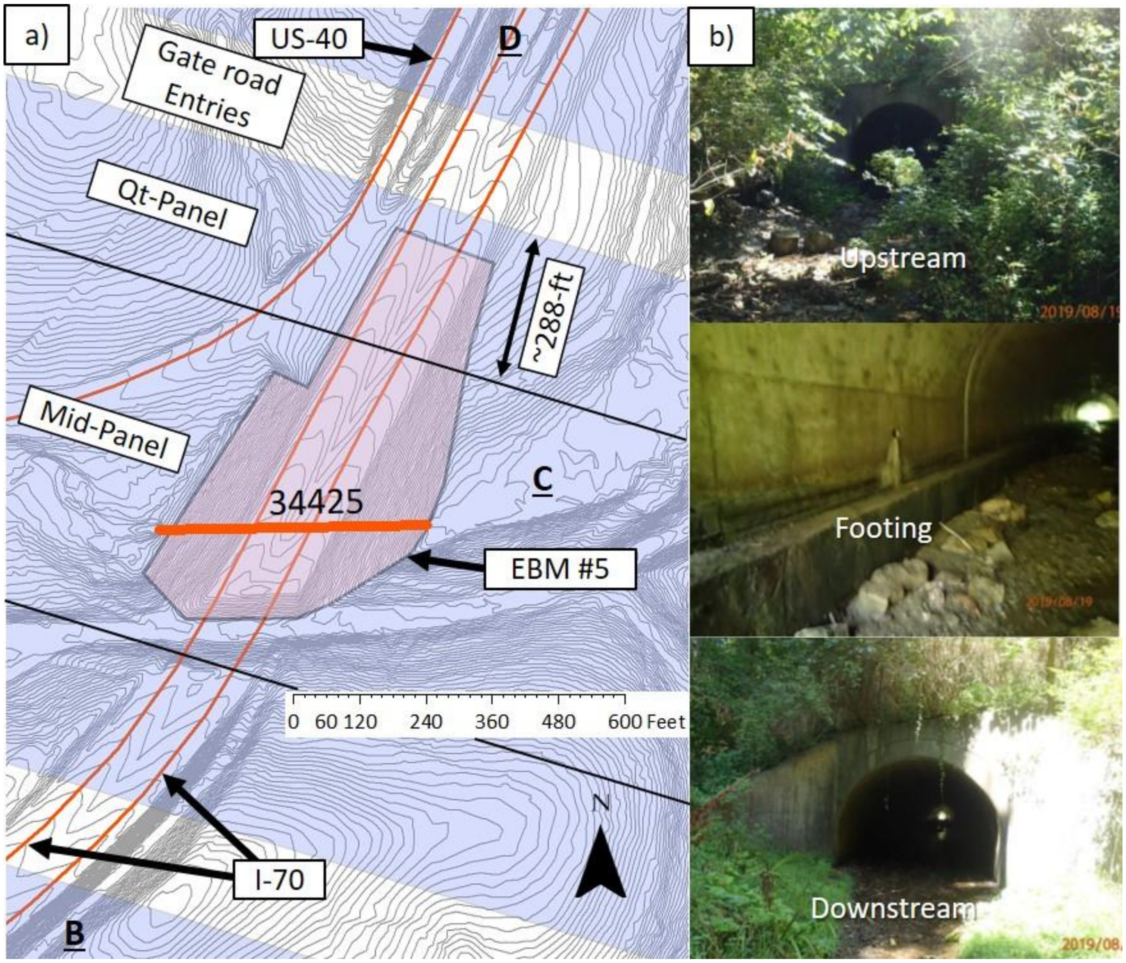

Figure IIIa.25 – a Culvert 34425 extends 480-ft under Embankment #5 and located over the middle of the panel, b) photograph of the upstream inlet wingwall, the footing within the culvert barrel, and the downstream outlet wingwall

5.3.2 *Culverts Located over Quarter-Panel Areas*

Culvert 34436 is located almost entirely within the quarter-panel area of projected Panel N. Currently, the slope of the 276-ft of culvert is only 0.7-pct. The inspection report documents the significant deposition that occurs along the culvert length. It is assumed that stream sediment deposition is related to the relative low slope of the culvert, especially in comparison to other culverts in the area (Table IIIa.10). It is possible that this culvert will see the full magnitude of the vertical subsidence change associated with a panel at approximately 400-ft of overburden or approximately 4.5-ft (Figure IIIa.10). This would have a positive impact on the current sediment deposition concerns for this culvert as its projected slope would increase to a more acceptable 2.4-deg (Table IIIa.10) after this projected undermining scenario. At this location, with an average overburden of 500-ft, most permanent surface slope changes will occur within approximately 288-ft of the gate road entries.

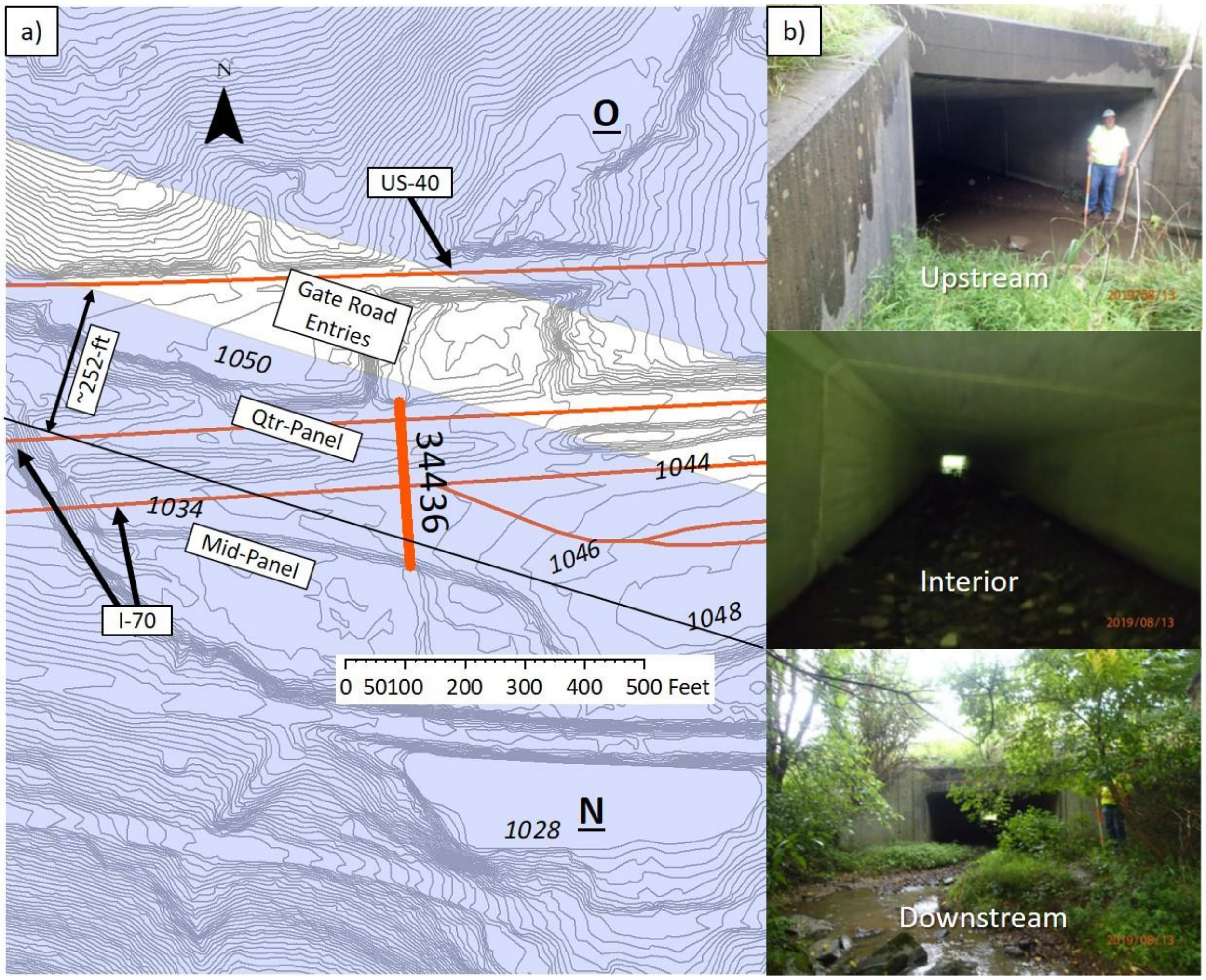

Figure IIIa.26 - Culvert 34436 extends 276-ft under I-70 and is located almost entirely within the quarter-panel area, b) photograph of the upstream box type inlet, inside length, and downstream outlet

Unfortunately the impact of this significant differential settlement along the length of the culvert could negatively impact the stability of this structure. This is especially concerning since the fill cover is relatively thin with a maximum of only approximately 11-ft. The low fill thickness is thought to provide less confinement to the culvert.

5.3.3 *Culverts Located over Gate Road Entry Areas*

Two sets of culverts pass under both I-70 and US-40 (Table IIIa.10). While they are part of the same culvert system, they are treated as separate assets and inspected and reported-on independently. The combined Culvert 34373/34427 extends 410-ft under Embankment #6 (Figure IIIa.27). Based on an average overburden of 450-ft, the majority of this culvert will be over projected gate road entries and should experience significantly less deformations/strains than structures located in the adjacent quarter-panel section. This projection of conditions represents a potential lower risk of significant impact to the culvert.

Figure IIIa.27 – a) Arched culvert 412-ft in length at the base of Embankment #6, b) photograph of the Culvert 34373 inlet conditions, concrete floor, and Culvert 34427 outlet conditions

The final reinforced concrete Culvert 34374/34428 spans portions of the gate road entries and approximately half the width of the quarter-panel area (Figure IIIa.28a). Under these projections, the outlet of 34428 is located close to the inflection point, indicating that approximately one-half the maximum subsidence will develop, or approximately 2.4-ft based on the 450-ft of overburden. The position of 34428 is likely contained almost entirely within a zone of surface extension. Under projected conditions, the potential for subsidence impact on Culvert 34374/34428 could be lower than that of 34425 (Embankment #5, Figure IIIa.25) for three reasons: 1) half the total vertical subsidence is expected, 2) lower fill thickness conditions are present, i.e. a maximum of 31-ft as opposed to 70-ft, and 3) it has a higher culvert condition rating (CCR), i.e. 6 as opposed to 5. Conversely, the overburden of Culvert 34374/34438 is, on average, approximately 50-ft less than 34425 and the change in slope will be permanent as opposed to only dynamic for 34425.

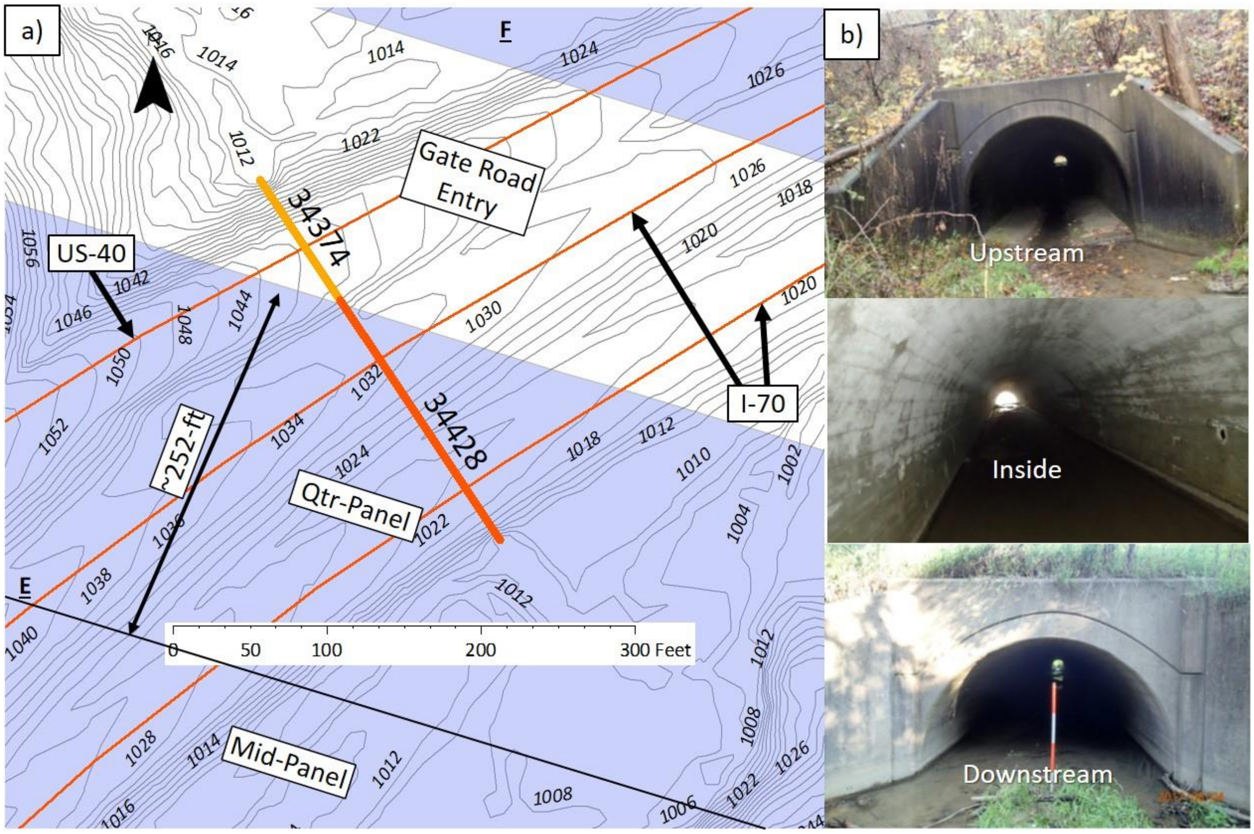

Figure IIIa.28 – a) Arched culvert 280-ft in length extending over parts of the gate road entry and quarter-panel areas of Panel E, b) photographs of the 34374 inlet, inside and 34428 outlet conditions

6.0 Selected Examples of Past Experience

The University searched the literature for examples where structures like those discussed in this section were undermined by longwall mining. Two examples were found. The first occurred at the Emerald Mine in 2006. In this case, a 170-ft twin span was undermined by Panel B4 in December of 2006 (Figure IIIa.29a). The span was located approximately 230-ft from the adjacent gate road entry areas (Figure IIIa.29b). This is in the zone where the deformations and compressive strains are at their maximum. Because this road had low vehicle demand, PennDOT decided to protect the structure by backfilling below the span with aggregate (Figure IIIa.29c). After the subsidence basin had fully formed, PennDOT removed the overpass and backfilled the area, thus eliminate this cross-over route (Figure IIIa.29d).

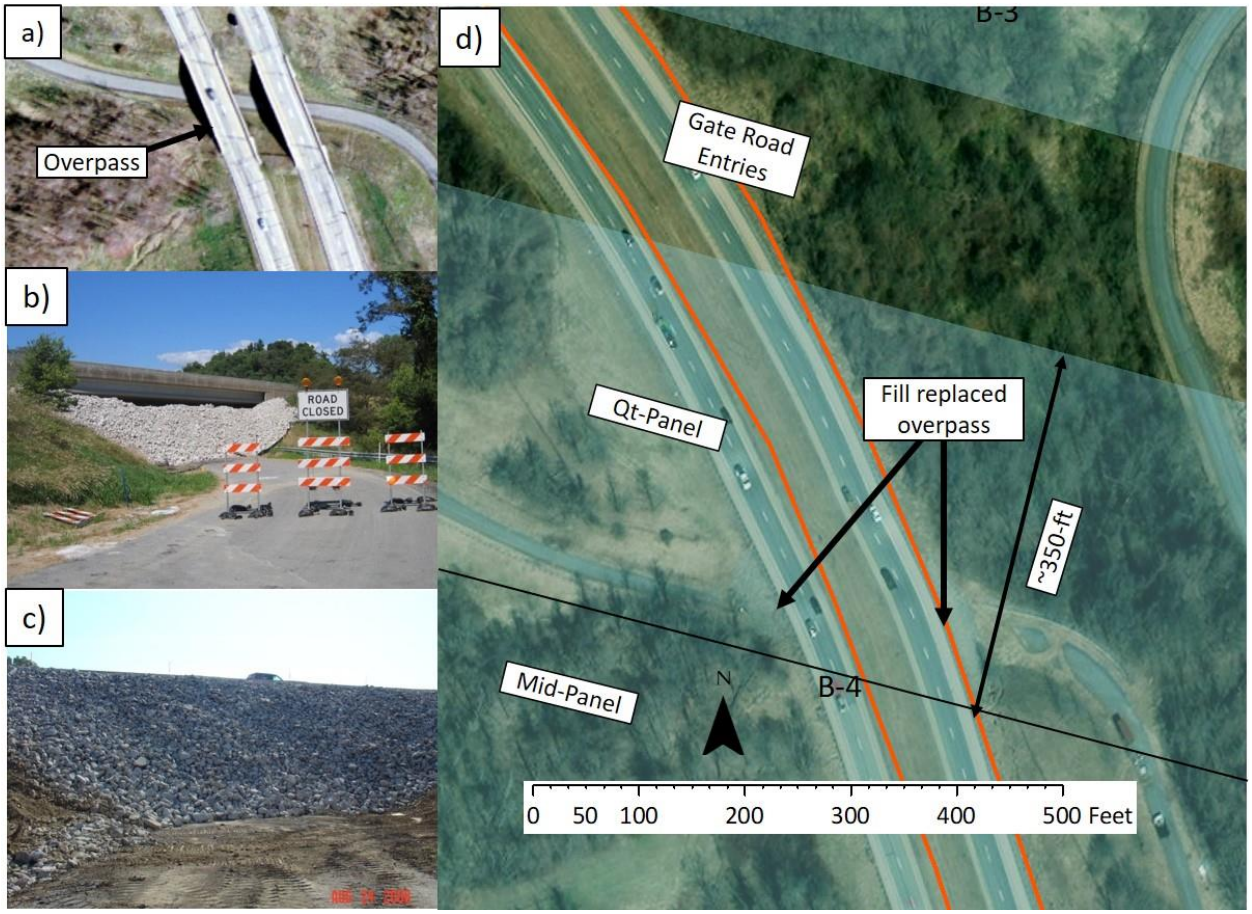

Figure IIIa.29 – a) Overpass prior to undermining in 2006; b) Post undermining photo showing the position of the longwall panel and adjacent gate road entries; c) Pre-mining support of overpass; and d) Post-undermining reconstruction of the I-79 alignment.

In 1999-2000, Mine Eighty-Four undermined I-70 east of the I-70/I-79S interchange. Longwall panels were ingeniously laid out to maximize the length of I-70 above the gate road entries between 3 South and 4 South (Figure IIIa.30). The amount of vertical subsidence above the longwall gate road entries is a fraction of that experienced over the panel. As a result, compressive and tensile strains are greatly diminished.

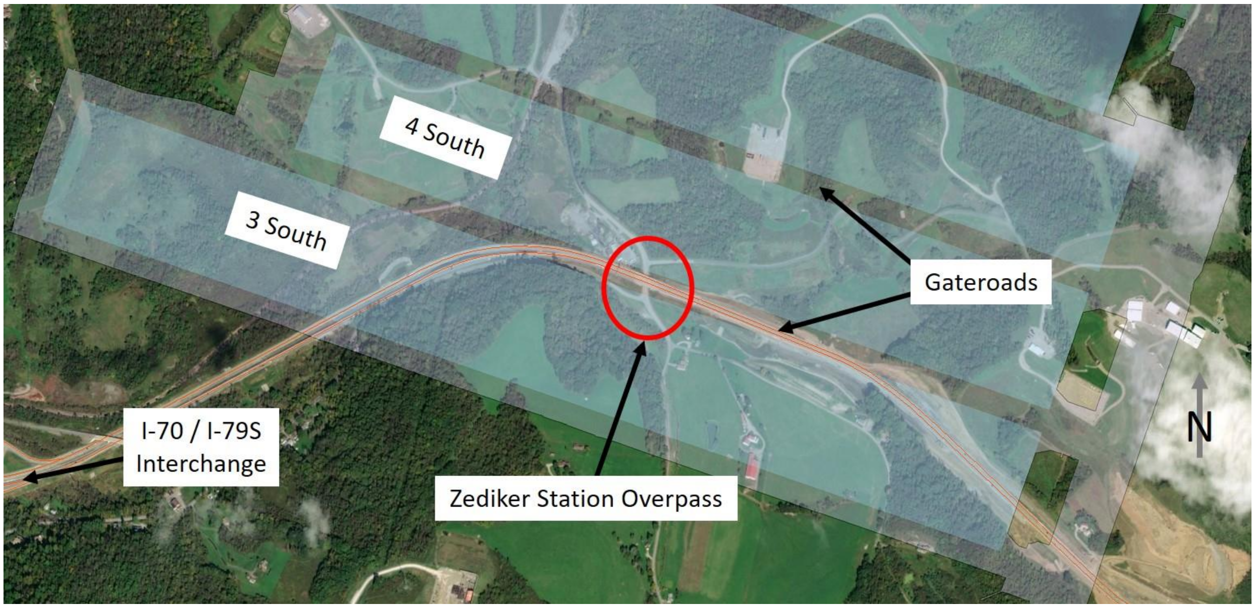

Figure IIIa.30 – Mine Eighty-Four's longwall panels underneath I-70 east of the I-70/I-79S interchange

The Zediker Station overpass is located above the gate road entries and was not expected to experience significant deformation. However, any unplanned deformation could negatively impact the stability of the overpass and compromise public safety. In response, PennDOT installed free-standing structures to provide additional vertical support to the span (Figure IIIa.31a). These structures are comprised of wood cribs set on a foundation of concrete blocks (Figure IIIa.31b). The entire structure was capped with sand bags and I-beams to gain contact with the overcast supports. PennDOT has reported that the overpassed experience no adverse reaction to undermining (Painter, 2020). Eighteen years after undermining, the Zediker Station overpass was replaced with a much larger overpass as part of the I-70 expansion and modernization program (Figure IIIa.31c).

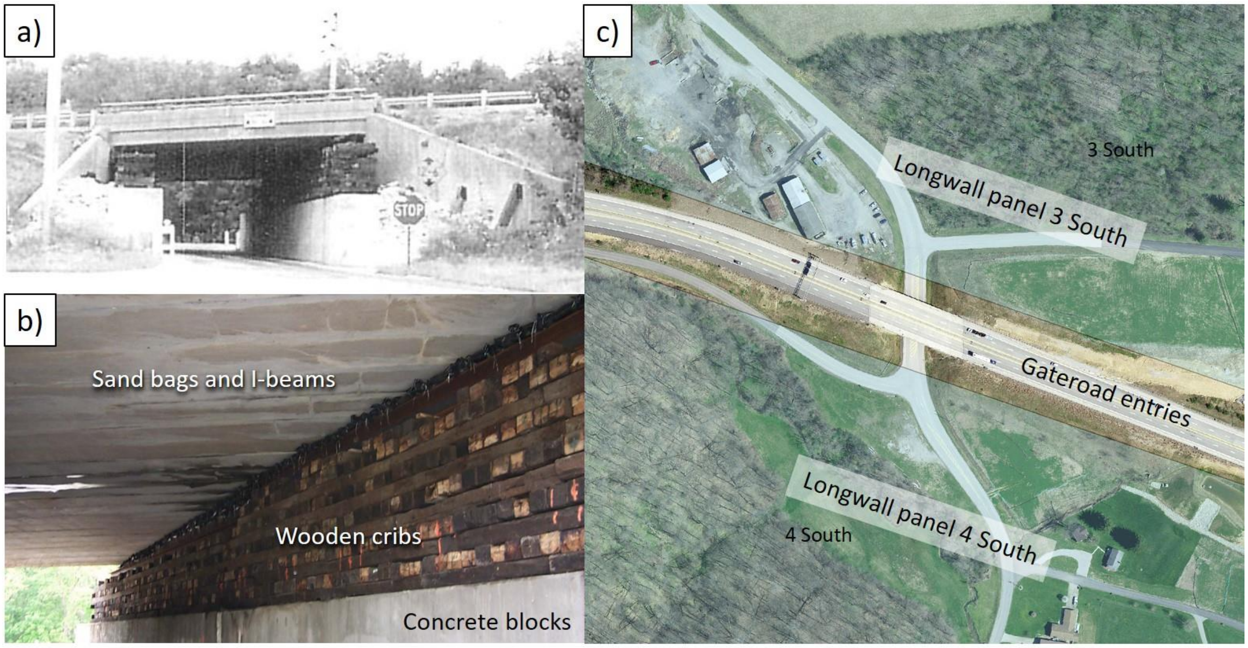

Figure IIIa.31 – a) Zediker Station overpass prior to undermining in 1999 (image from O'Connor 2001); b) additional support added to superstructure (image from O'Connor 2001); c) location of the overpass above the gate road entries between panels 3 South and 4 South (image from 2019 after the overpass had been recently reconstructed)

7.0 Discussion

The extended study area encompasses the Tunnel Ridge reserves of the Pittsburgh Coalbed in western Pennsylvania that has the potential to undermine the I-70 highway alignment. PennDOT is interested in establishing the risk from longwall mining subsidence to this alignment focusing on existing asset structures including overpasses, retaining walls, and culverts. The University is using the knowledge gained during the undermining of Panel 15 to evaluate potential longwall mining subsidence impacts. This was partially accomplished by proposing a likely panel layout for longwall mining, inventorying the major highway assets, and locating these assets within the subsidence basin. In addition, important characteristics of each asset were compiled and analyzed. The availability of established tolerances for overpasses, retaining walls, and culverts subjected to mining induced subsidence were discussed and evaluated. Once these tasks were accomplished, highway assets were located within the potential subsidence basins and their potential for being impacted by longwall mining subsidence characterized.

It should be noted that the actual panel layout for future Tunnel Ridge mining operations may be different than that proposed by the University. The operator has a legal responsibility to follow established regulatory approval guidelines and submit a proposed plan for mining this area to the Pennsylvania Department of Environmental Protection (DEP). The DEP must approve all planned subsidence prior to mining. Once the plan is approved, all of these assets should be re-evaluated. It is possible that PennDOT will provide input to this process.

Subsection IIIb – SDPS Model Surface Subsidence Prediction of Mining within the Extended Study Area

In this subsection, an overview of the SDPS model are presented and selected assets within the extended study area are subjected to detailed analysis. In Section IIIa, impacts to assets that could potentially be undermined were characterized using a combination of empirical relationships (Peng, 1992) and projections of subsidence surface profiles using the hyperbolic tangent function method. Here, nine selected assets are studied using output from the SDPS program and compared to established tolerances. This more in-depth analysis helps to establish a framework by which risk of future subsidence impacts can be assessed.

1.0 Overview of the SDPS Model

An analysis of subsidence throughout the extended study area was completed using the Surface Deformation Prediction System (SDPS) software. There is a substantial number of studies that have used either the SDPS model or some other version of the influence function method to analyze underground longwall coal mining subsidence impacts (Agioutantis, et al., 1988; Newman, et al., 2001; Karmis, et al., 2008; Aqioutantis and Karmis, 2013; and Hescock and Agioutantis, 2017).

The analysis of the extended study area was completed using the potential panel layout described previously (Section IIIa.1). These potential panels are modeled in SDPS using the overburden and topography for the study area and the standard parameters (i.e. extraction thickness, hard rock percentage, etc.) determined for Panel 15 (Section IVb, Task 2 Report). The SDPS models were calibrated to the observed and measured data points collected along the highway alignment making up the initial study area. It should be noted that the SDPS model was not calibrated for the lower overburden conditions found in the extended study area. Hence, the empirical projections of the width of the quarter-panel area are displayed on graphs showing the subsidence profiles from the SDPS model.

The following factors were used for both the initial and extended study area analysis:

- Extraction thickness is approximately 7.25-ft (typical for Pittsburgh Coalbed)
- Supercritical Subsidence Factor = variable (overburden dependent)
- Average overburden thickness is variable
- Average percentage of hard rock is approximately 30-pct
- All pillars will remain rigid, minimizing vertical subsidence over the gate roads and creating an edge effect of 175-ft
- Surface points are at pre-mining topographic elevation
- The longwall face progresses at an average rate of 115-ft/day

2.0 Predicted Final Subsidence

The analysis completed for the extended study area considered both the dynamic and permanent subsidence conditions. The analysis begins at the conclusion of the mining for all the projected longwall panels. The fifteen projected longwall panel layouts are separated into two districts separated by a set of main entries. The entire area was modeled as two separate districts, one for the panels to the west of the mains (District 1) and one for the panels to the east of the mains (District 2). The main entries contain more headings than the gate road entries adjacent to the longwall panels. The mains are designed for a functioning life span of five to twenty year. To help protect the mains from abutment loading during longwall extraction, barriers of coal are left next to the panels. This layout allows the analysis to occur in two distinct models. No significant interaction of the subsidence basins is expected between the two districts. The models were used to predict vertical subsidence, horizontal deformations, and horizontal strain due to the extraction of the 15 longwall panels within the I-70 extended study area. Prediction points throughout the study area were considered on a 50-ft grid.

2.1 Vertical Subsidence

The maximum amount of vertical subsidence that occurs on the surface due to longwall mining is indirectly proportional to the panel overburden. As such, more subsidence is predicted in areas with lower overburdens than in areas with higher overburdens. The final vertical subsidence caused by the longwall panels throughout the extended study area can be seen in Figure IIIb.1.

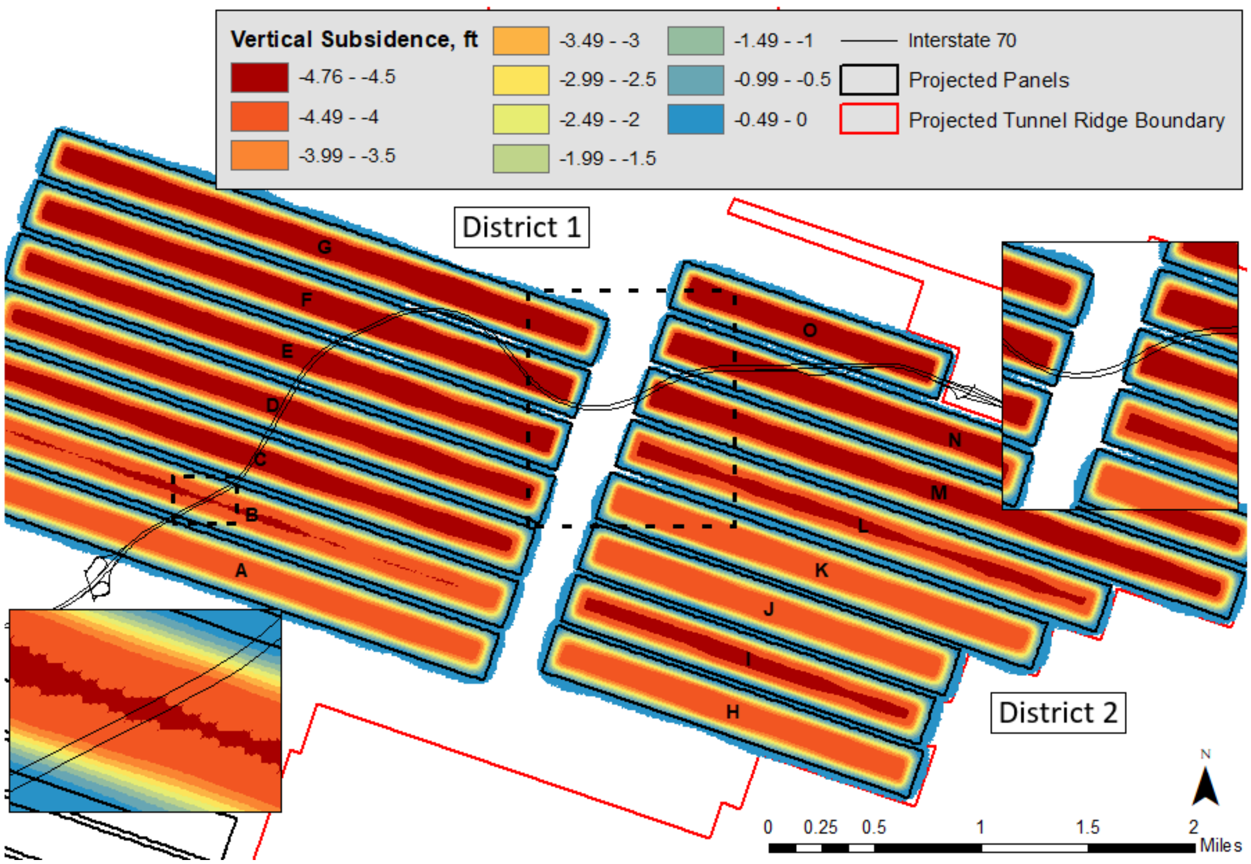

Figure IIIb.1 – Vertical subsidence caused by longwall mining throughout extended study area

For the extended study area, the panels in the northeastern along Dutch Fork are projected to have more vertical subsidence than those in the southwest (closer to the West Alexander Interchange). Variation in overburden are caused by changes in either topography or the elevation of the Pittsburgh Coalbed. For a more detailed discussion of overburden see Section IIIa.2 and Figure IIIa.6. SDPS predicts that the maximum average vertical subsidence for the 15 longwall panels will range from 4.4-ft to 4.8-ft.

2.1.1 *Vertical Subsidence in Cross-Section*

To help demonstrate changes in the shape of the subsidence basin across the extended study area, a profile was constructed from the gate road entries of Panel A and ended over the gate road entries of Panel G (Figure IIIb.2). This profile is particularly relevant as it begins at relatively high overburden and finishes at relatively low overburden.

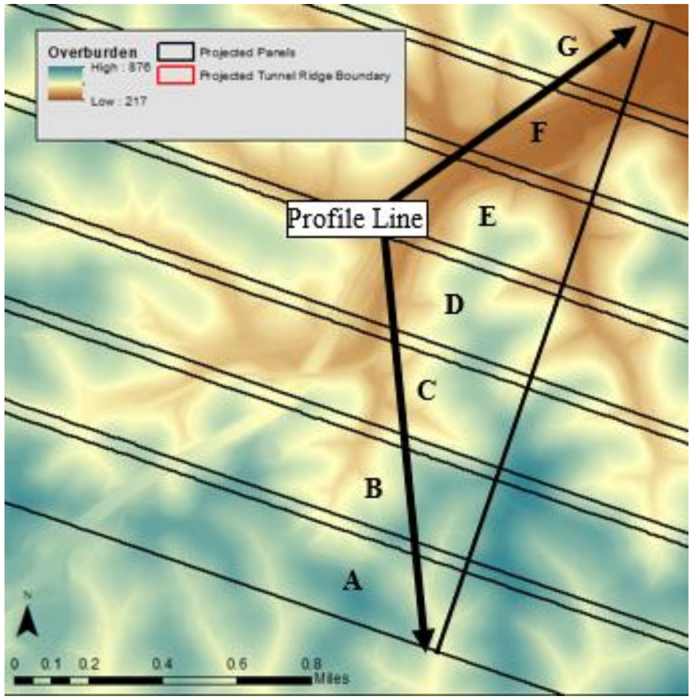

Figure IIIb.2 – Location of a profile line crossing Panels A through G showing a diverse range of overburden

The influence of overburden along the profile from Panel A to G on the maximum vertical subsidence is clearly shown in Figure IIIb.3. As overburden decreases from Panel A to G (Figure IIIb.3a), the average maximum vertical subsidence increases by almost 0.4-ft (Figure IIIb.3b). The values displayed in these graphs are derived by calculating the average overburden and maximum vertical subsidence (SDPS) value along the profile from Panel A to G (Figure IIIb.2).

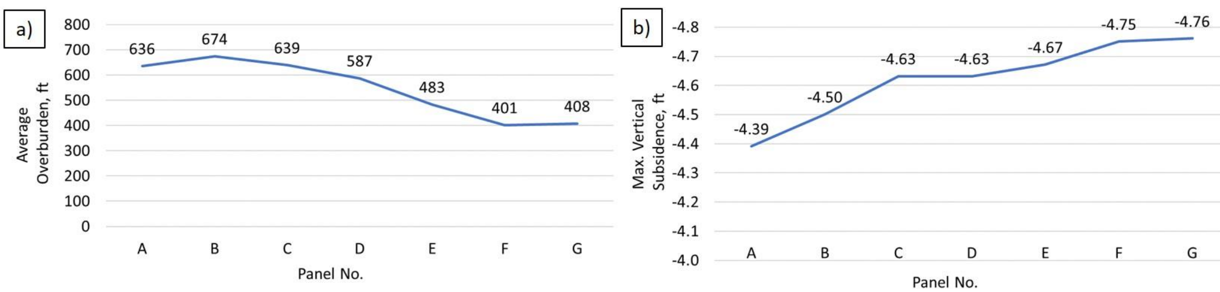

Figure IIIb.3 – Graphs of a) average overburden and b) predicted maximum vertical subsidence for Panels A to G

The change in overburden along Panel A to G profile was produced in ArcGIS using 3D Analyst (Figure IIIb.4a). For this same profile, the vertical subsidence predicted from SDPS is provided (Figure IIIb.4b). Several key relationships are confirmed related to overburden:

- The amount of maximum vertical subsidence increases as overburden decreases
- The width of the quarter-panel area decreases as overburden decreases (see Table IIIa.4)

- The shape of the vertical subsidence curve over the gate road entries changes from rounded at higher overburdens to flat at lower overburdens
- The change in the vertical subsidence profile curvature is most pronounced at the boundaries of the quarter-panel areas (increase curvature along a surface profile produces higher strains)

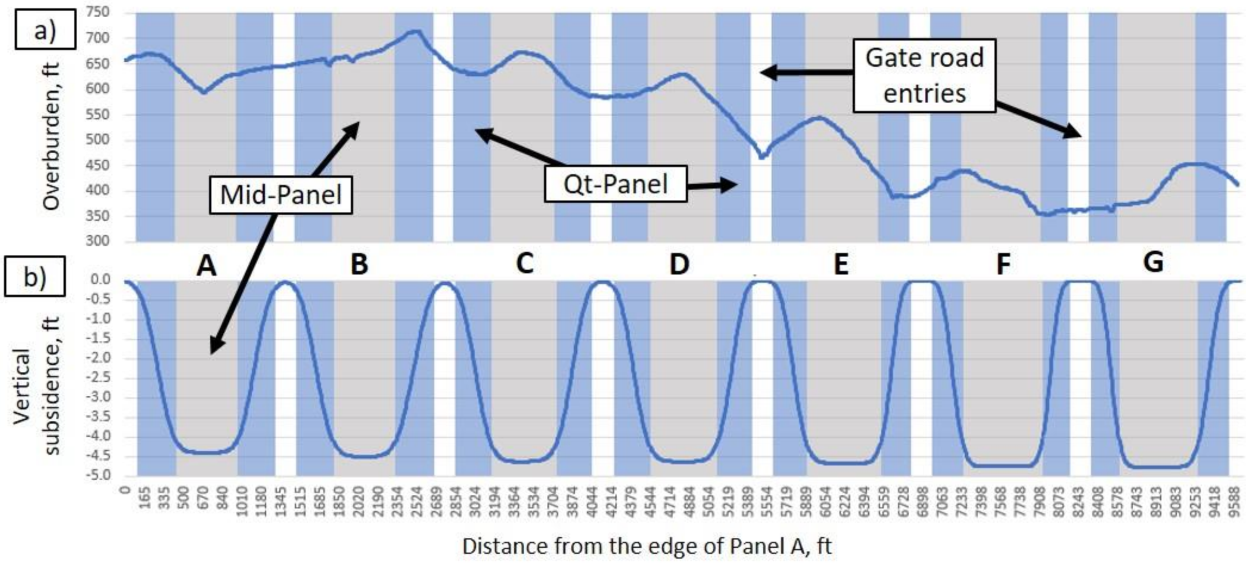

Figure IIIb.4 – Profile of a) overburden and b) vertical subsidence for Panel A to G

The influence of overburden is particularly important when examining the conditions within the quarter-panel area:

- At relatively high overburdens (Panels A to C)
  - The vertical subsidence profile within the quarter-panel area has a slightly lower overall slope

    Slope @ 650-ft of overburden = Sv (4.5-ft)/width of quarter-panel area (326-ft) = ~1.4-ft/100-ft

- At relatively low overburdens (Panels E to G)
  - The vertical subsidence profile within the quarter-panel area has a slightly higher overall slope

    Slope @ 400-ft of overburden = Sv (4.75-ft)/width of quarter-panel area (252-ft) = ~1.9-ft/100-ft

While the slope change is not large, it can have a significant influence on surface deformations and strains.

2.2 Horizontal Deformation

As with vertical subsidence, the predicted amount of surface horizontal deformations that can occur due to longwall mining is indirectly proportional to the overburden of the panel. As such, more deformations are predicted in areas with lower overburdens than in areas with higher overburdens. The final horizontal deformations caused by the extraction of the longwall panels in the extended study are can be seen in Figure IIIb.5

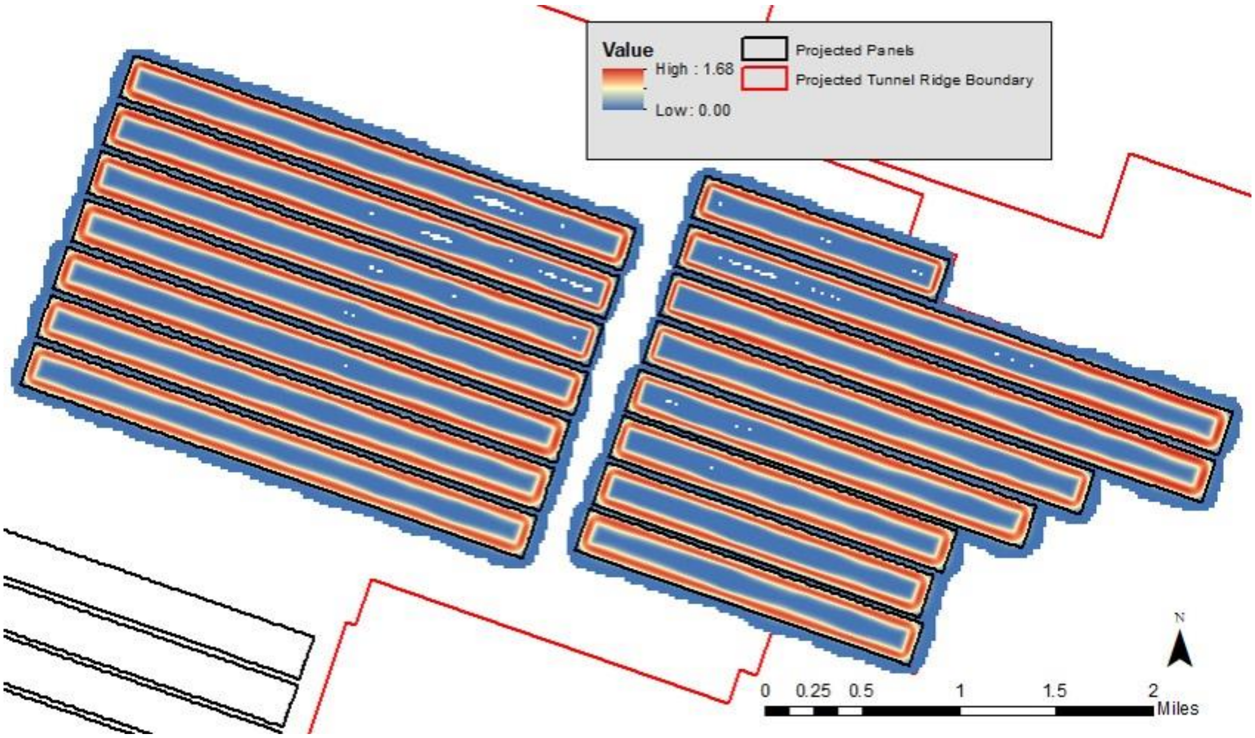

Figure IIIb.5 – Total horizontal deformation caused by longwall mining throughout the extended study area

The maximum horizontal deformation along the profile from Panel A to G ranges from 1.54-ft to 1.67-ft. The lower value represents the maximum horizontal deformation for Panel A, while the higher value represents the maximum horizontal deformation for Panel G. The increase in horizontal deformation is due to the decrease in overburden. Figure IIIb.6 shows that the average overburden for Panel A and Panel G were 636-ft and 408-ft, respectively.

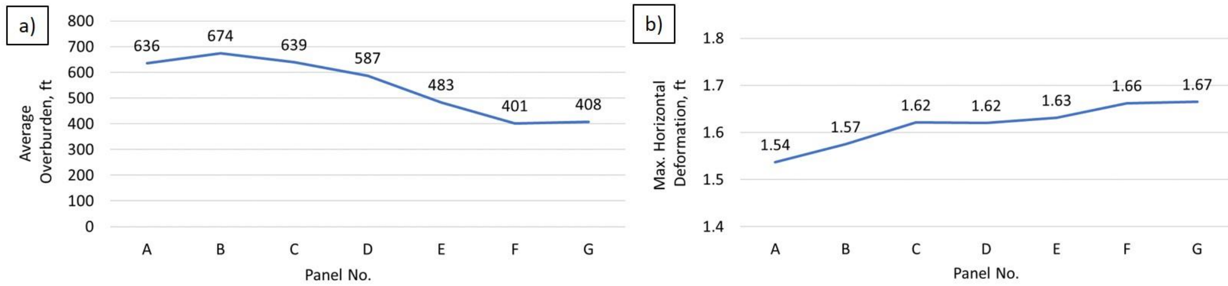

Figure IIIb.6 – Graphs of a) average overburden and b) predicted maximum horizontal deformation for Panels A to G

The change in the total horizontal deformation along the profile from Panel A to G is shown in Figure IIIb.7) with a maximum value of 1.67-ft for the extended study area. SDPS can display horizontal movement along an x and y axis. Here the horizontal deformation represents the total or the resultant of both the x and y components. Several key relationships are confirmed related to overburden:

- The amount of maximum total horizontal deformation increases slightly as overburden decreases
- The maximum total horizontal deformation occurs within the middle of the quarter-panel area and is located where the vertical subsidence profile has the greatest slope (Figure IIIb.4)
- The width of the quarter-panel areas (blue area, Figure IIIb.7) produced from empirical relationships is slightly less than the width displayed by the SDPS curves (purple line, Figure IIIb.7b)

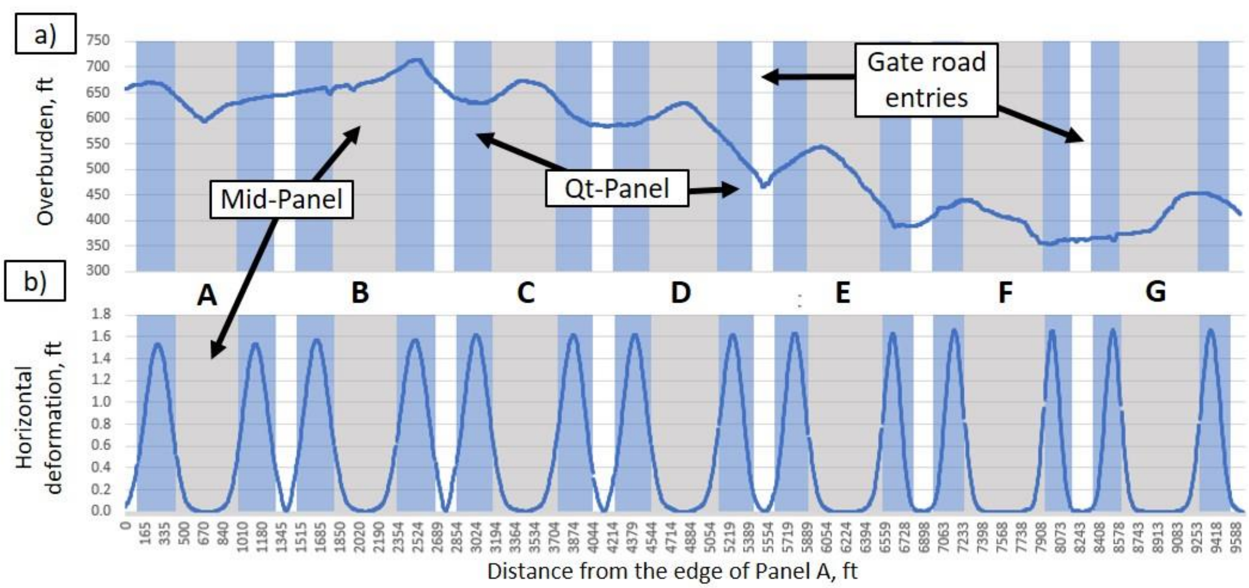

Figure IIIb.7 – Profile of a) overburden and b) predicted total horizontal deformation for Panels A to G

2.3 Surface Strain

Another important subsidence basin characteristic has to do with anticipating areas where high strain may occur on the surface due to longwall mining. A number of researchers have used horizontal strain, angular distortion, and curvature to assess surface damage from mining subsidence (Singh, 1992; Boone, 1996; Karmis, et al., 1994; Luo, et al., 2003). As previously discussed, the amount of surface strain is directly proportional to the curvature of the subsidence basin surface and indirectly proportional to the overburden of the panel. As such, more strain is predicted in areas along the margins of the subsidence basin where surface curvature is the greatest and within areas of lower overburdens. The permanent horizontal strains caused by the extraction of the longwall panels in the extended study area are shown in Figure IIIb.8. The position of high strain is easily observed where the basin surface curvature is the greatest.

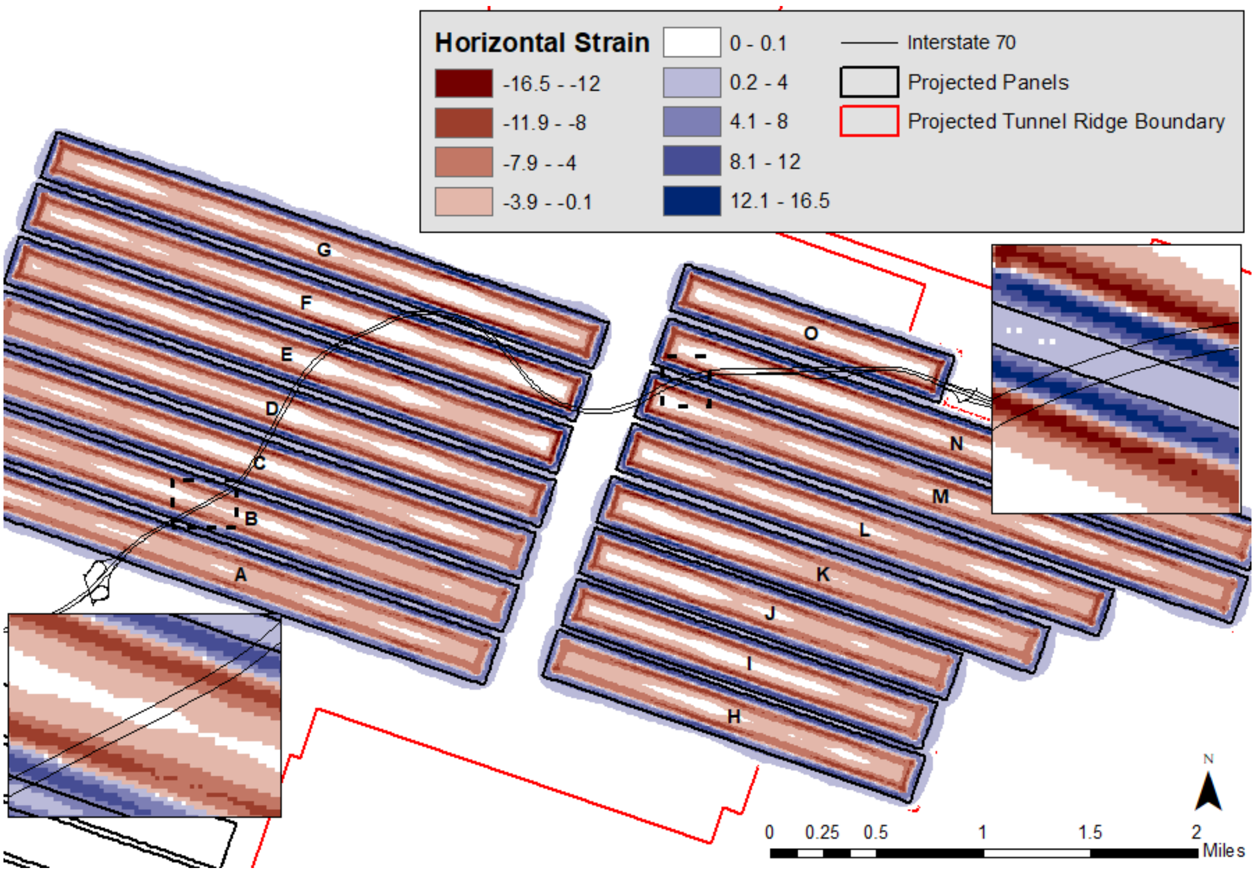

Figure IIIb.8 – Horizontal strain caused by longwall mining throughout extended study area

The influence of changing overburdens are better illustrated by analyzing the predicted maximum horizontal strains along the profile from Panels A to G (Figure IIIb.9). The maximum horizontal tensile and compressive strain predicted for these panels varies from ~9 to 16 (10^{-3})-ft/ft. The lower values were associated with Panel A and B, while the higher values were associated with Panels F and G. For this area, a decrease in the average overburden from ~700 to 400-ft could produce a 50 to 60-pct increase in the maximum horizontal strain values.

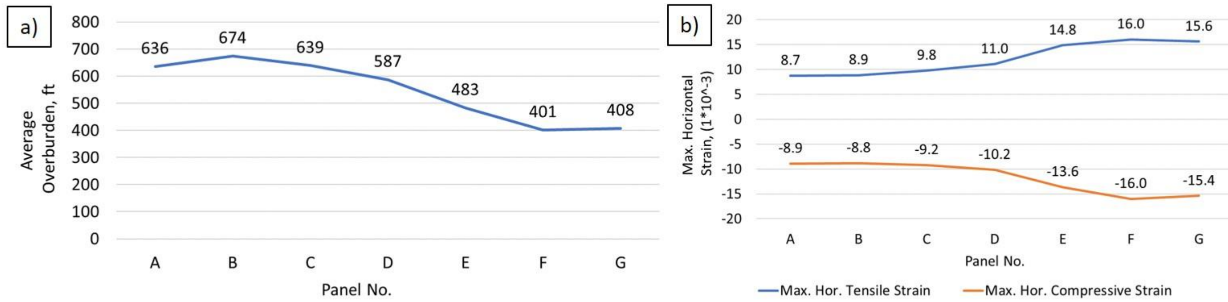

Figure IIIb.9 – Graphs of a) average overburden and b) predicted horizontal strain for Panels A to G

As stated above, it is common practice in subsidence engineering efforts to display surface strain in terms of the horizontal strain, angular distortion, and ground strain. Horizontal strain can be determined by examining the distance between two points and monitoring how that distance changes with time. If the change in horizontal length between two points increases, the surface extends (tension). If the distance decreases, the surface becomes compressed. It is worth recognizing the great work by Wardell (1957), Geddes and Cooper (1962), and Whittaker and Reddish (1989) in elevating our understanding of the role dynamic subsidence plays in this field of study. Information provided in Section II of this report, further demonstrates the importance of a propagating wave, comprised of both tensile and compressive strains, as a subsidence basin develops. Perhaps, more than any other factor, it is the excessive levels of tensile and compressive strains that damage structures. It should be noted that zones of high strain are induced by non-uniform displacements (Peng, 1992). What makes determining surface strain so important is the ability to connect measured levels with established performance standards for structures.

Several forms of surface strains are provided with the SDPS model (Agioutantis and Karmis, 2015). These forms determine strain in different ways and will often emphasize distinctive conditions. For example, ground strain takes into account variations in topography. This is especially important in areas with high relief (Peng, 1992; Karmis, et al., 1994). The topographic variations in the extended study area are moderate as I-70 follows Dutch Fork and its tributaries.

The University used the SDPS Influence Function Method option to compare differences between horizontal strain and ground strain along the profile from Panel A to G (Figure IIIb.10). The shape of the two strain curves are equivalent with peak strains occurring at similar locations. The SDPS determines horizontal strains, E(x,y), as the first derivative of the horizontal displacements with respect to x and y:

*EX = dUx/dx = -Bs * (2(PI)Smax / r^3) * (x exp [-(PI)*(x^2/r^2])* *[Eq IIIb.1]*

*EY = dUy/dy = -Bs * (2(PI)Smax / r^3) * (y exp [-(PI)*(y^2/r^2])* *[Eq IIIb.2]*

where, Smax – maximum vertical subsidence
Bs – the horizontal strain coefficient, 0.35 (customary units), Bs can be determined for local conditions as it is obvious from the above equations that as Bs increases, the magnitude of the calculated horizontal strains and displacements increases (Agioutantis and Karmis, 2015).

The SDPS program calculates eleven strain conditions but this analysis used on *EX*, *EY*, i.e., strains along the *x* and *y* axes of a horizontal plane. The larger of the two values constitutes the maximum horizontal strain (EM) at a point (either in tension or in compression). Ground strain takes into account the slope of the original surface (Agioutantis and Karmis, 2015).

> *Ground strain may be enhanced or diminished in relationship to the tensile portion depending on whether the slop is parallel to the expected through or vice versa (Agioutantis and Karmis, 2015).*

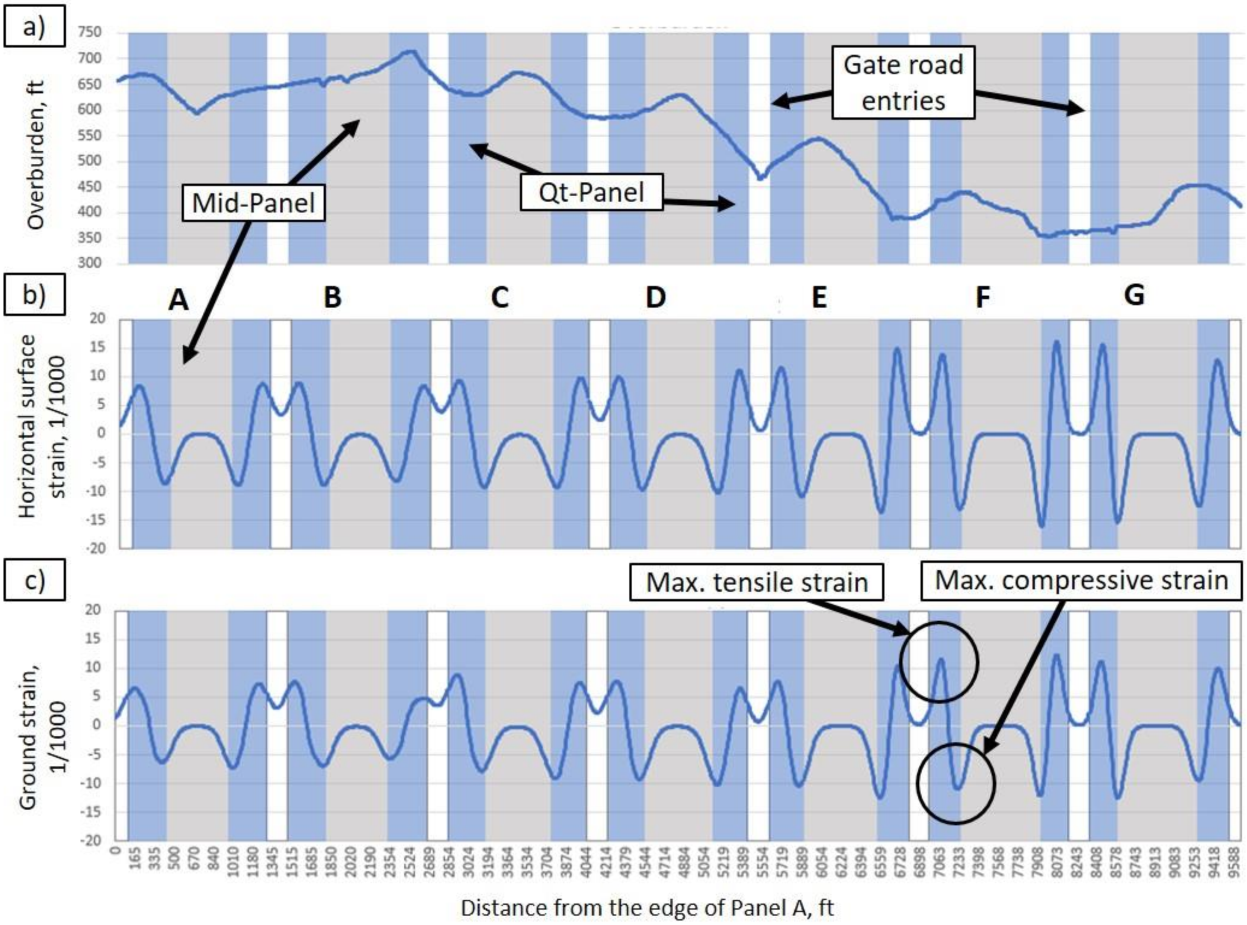

Figure IIIb.10 – Profile of overburden and predicted horizontal and ground strain for Panels A to G

Several key relationships / differences are shown between horizontal strain and ground strain in Figure IIIb.10b & c:

- In both the horizontal and ground strain profiles, the maximum tensile and compressive strain increases as overburden decreases
- In some areas, the maximum ground strain is slightly less than its horizontal counterpart
- The SDPS maximum tensile and compressive strains occur further from the gate road entries and closer to the midddle-panel area than those determined from the Profile Function and empirical relationships (Section IIIa)

2.4 Severity and Damage Assessments of Structures

Horizontal deformations are needed to produce strain, but it is the excessive levels of strain that cause structures to crack and separates in tension or crush, heave, or shear in compression. The literature contains examples of using surface strain and angular distortion measurements to assess the severity of subsidence related impacts (see references below). Several damage or severity classifications have been proposed for structures such as buildings, bridges, and reinforced retaining walls:

- Geddes and Cooper (1962) reported on data presented by Orchard that related 'percent ground strain' to class of damage (very slight up to 0.1-pct ground strain to very severe with 0.5-pct ground strain)
- The National Coal Board (Anon, 1975) presented a classification that related the 'change of length of a structure' to class of damage (very slight up to 0.003-m [0.1-ft] to very severe with more than 0.18-m [0.6-ft])
- Singh (1992) proposed damage-limit values based on angular distortion ranging from slight 1×10^{-3} to very severe $> 7 \times 10^{-3}$.
- Karmis, et al., (1994) compared and combined several damage classification schemes suggesting limits for horizontal strain (slight 0.5×10^{-3} to very severe $> 3 \times 10^{-3}$) and angular distortion (slight 1×10^{-3} to very severe $> 7 \times 10^{-3}$). Perhaps most significant is the threshold value of 1.5 to 3×10^{-3} range for horizontal strain for structures.
- A value of 1.5×10^{-3} is used as a default threshold value for the examples in the SDPS manual.

As is evident from the discussed above, horizontal strain is a commonly reported condition that is often considered as a 'damage index'. Horizontal strain is defined as the change in horizontal length between two points divided by the original horizontal distance between the two points (Figure IIIb.11a). The directional horizontal strain refers to horizontal strains along a specific direction (i.e., along a line of monitoring points or stations). For sloping surfaces, ground strain is the preferred severity assessment method. In this study, ground strain was determined from monitoring points along a particular direction, i.e. parallel and perpendicular to the highway orientation (Figure IIIb.11b). Finally, when arrays of monitoring points are considered, as in the SDPS program, a grid pattern is used to calculate ground strain at one-point based on all of its neighboring points (Figure IIIb.11c).

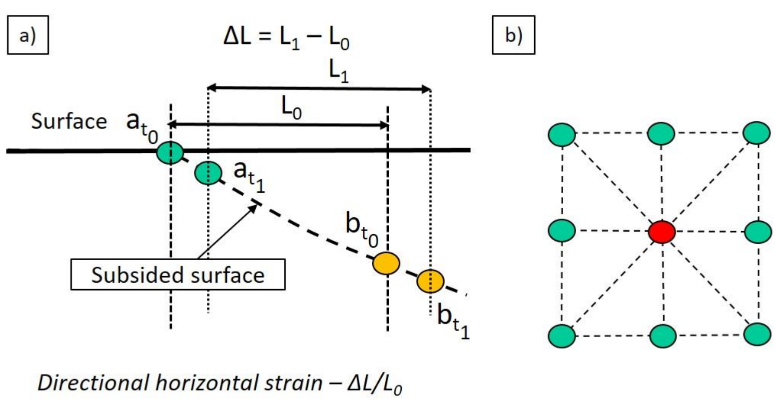

Figure IIIb.11 – a) Components of directional horizontal strain for highway alignment surveys and b) plan view of grid pattern used to calculate ground strain at one point (red) in three-dimensional space (also adapted from Andrews, 2008)

3.0 Selected Detailed Asset Analysis

Section IIIa provided a general assessment of potential subsidence impacts to assets within the extended study area. The SDPS Influence Function is used to examine potential subsidence characteristics for projected longwall panels. These more detailed SDPS models are constructed for individual panels in which multiple notable assets are projected. In each run, the subsidence basin characteristic at multiple face positions were established.

Nine assets are considered in this additional dynamic subsidence analysis. Three assets are associated with Panel C, i.e. one culvert (34425) and two overpasses (34424 and 34426). Culvert 34425 and overpasses 34424 and 34426 are located almost entirely within the mid-panel area of potential Panel C. The five other assets are found with Panel N with one culvert (34436), two overpasses (34435 and 34437) and two retaining walls. While overpasses 34435 and 34437 and their associated retaining walls are located just beyond the quarter panel boundary, culvert 34436 is located almost entirely within the quarter panel of Panel N. The location of these panels and corresponding assets can be seen in Figure IIIb.12.

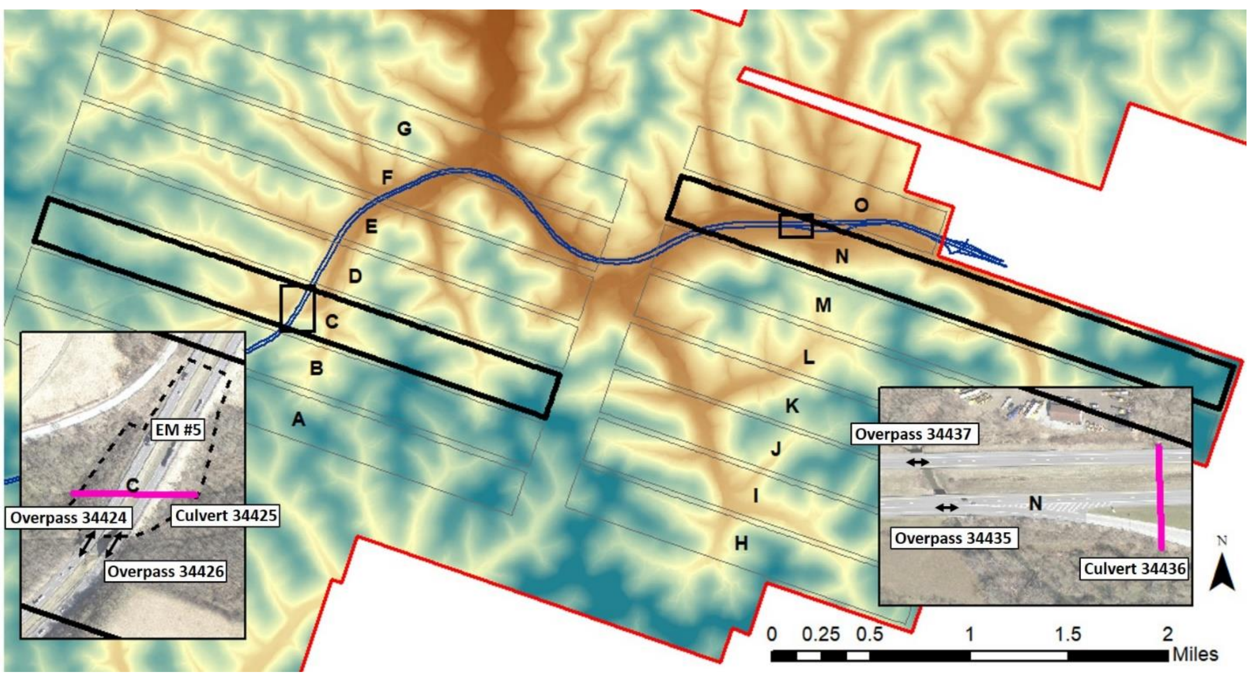

Figure IIIb.12 – Location of assets in extended study area considered for additional analysis

These models emphasize the influence of the dynamics subsidence conditions and provided an opportunity to consider different ways to assess potential damage. The permanent or final subsidence analysis allowed for the assessment of ponding or erosion conditions associated with culverts. All of these SDPS models utilized a 25-ft prediction point grid spacing. The model output predicts vertical subsidence, horizontal deformations, surface strains and angular distortions due to the extraction of the single longwall panel in the area adjacent to the I-70 alignment.

3.1 Panel C

The potential Panel C is in the center of longwall District 1, which is located on the eastern side of the projected main entries (Figure IIIa.4). The panel crosses below I-70 at approximately a 79-deg angle with an average overburden of ~500-ft. This panel was of particular interest as it contains the largest embankment in the extended study area (Embankment #5) and also contains three significant assets. The University assumes that Panel C will be mined at an average rate of 115-ft/day (similar to the advance rate observed within Panel 15). It was also assumed that the panel would be mined from west to east, towards the main entries. This area of interests contains Embankment #5, culvert 34425, and overpasses 34424 and 34426. The vertical subsidence and horizontal deformations induced on the surface by three of the face positions are provided to show how conditions change as the longwall face approached, passed underneath, and moved away from the area of interest.

Pre-undermining conditions - When the longwall face is ~550-ft from the center of the area of interest, the effects of the developing subsidence basin does not significantly impact the assets (Figure IIIb.13). Both vertical subsidence and horizontal deformation are approximately zero.

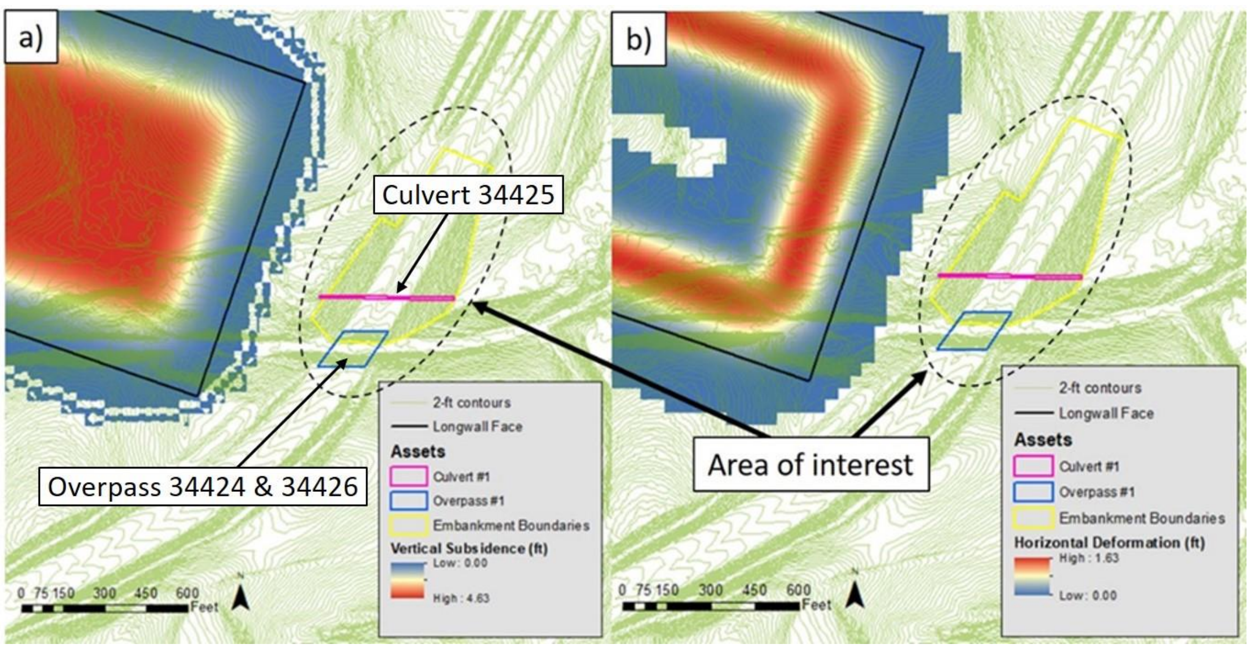

Figure IIIb.13 – a) Vertical subsidence and b) horizontal deformations predicted when the longwall face is 550-ft from the center of the area of interest containing three important highway assets

Dynamic subsidence conditions - Next, vertical subsidence and horizontal deformation conditions are shown in Figure IIIb.14 when the longwall face is just beyond the edge of area of interest. At this face position, the maximum predicted vertical subsidence is 4.6-ft with a maximum horizontal deformation of 1.6-ft towards the center of the subsidence basin. This is the approximate time when the maximum change in conditions occur for the three assets. Subsidence conditions are dynamic and can change significantly over relatively short periods of time.

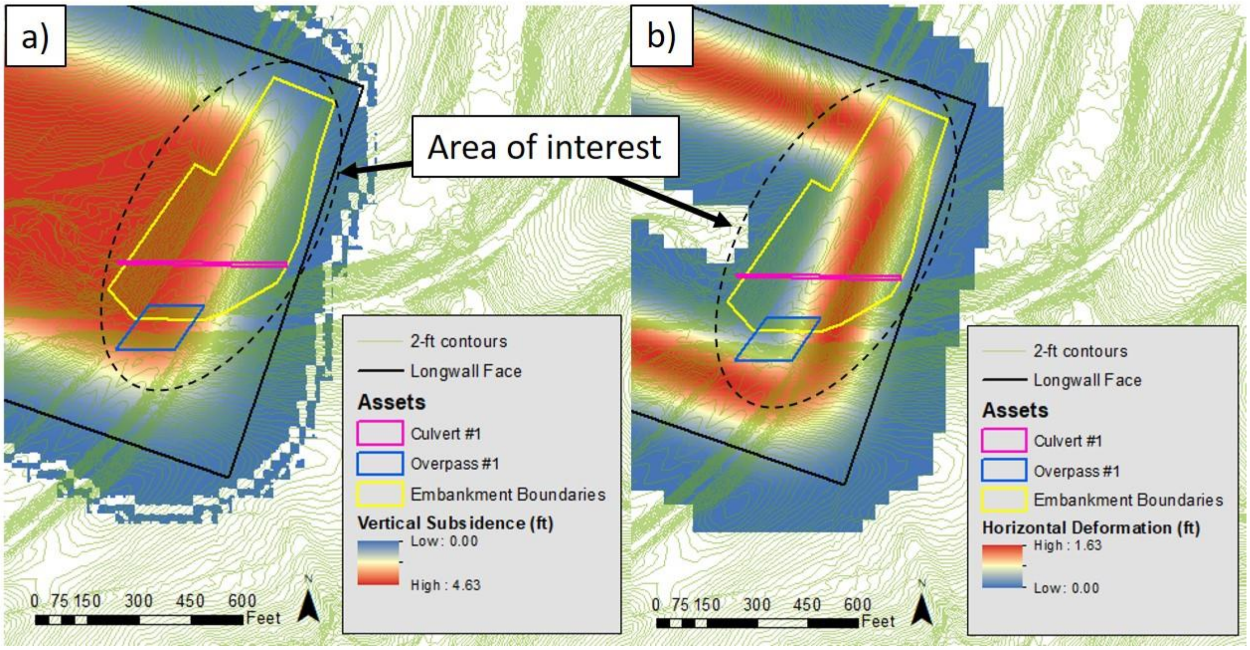

Figure IIIb.14 – a) Vertical subsidence and b) horizontal deformations predicted when the longwall face is just beyond the area of interest

Permanent subsidence conditions - Finally, the prediction of vertical subsidence and horizontal deformation conditions is provided when the longwall face is 900-ft beyond the center of the area of interest (Figure IIIb.15). At this face position, the area of interest is nearing its final mining induced subsidence conditions. Here the permanent subsidence characteristics are revealed and are identified by the long-lasting change to the slope of the surface about the quarter-panel areas.

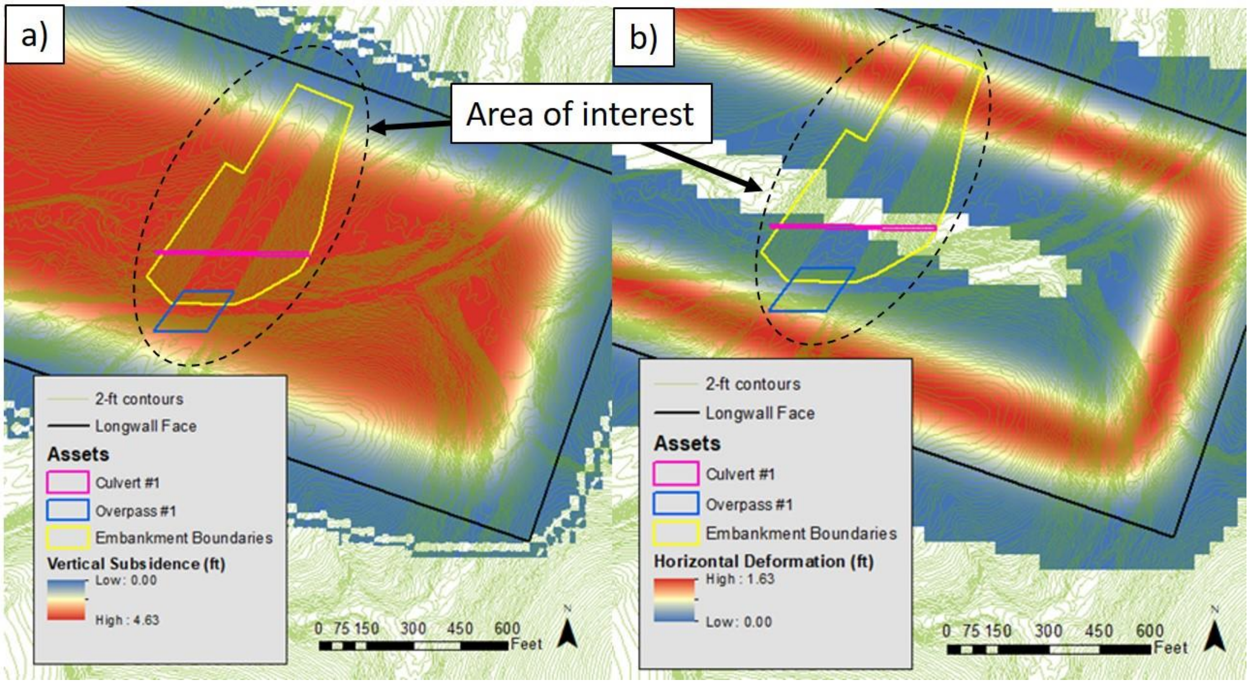

Figure IIIb.15 – a) Vertical subsidence and b) horizontal deformations predicted when the longwall face is 900-ft past the center of the area of interest

3.1.1 *Culvert 34425*

Culvert 34425 is the longest in the extended study area; is under the most fill; and has the lowest condition rating (Section IIIa.5.3). As the culvert is located in the center of potential longwall Panel C, it is expected to have experienced a similar amount of total or permanent vertical subsidence and horizontal deformation at the conclusion of the subsidence event. However, during the dynamic subsidence event associated with the passage of the longwall face, this culvert is predicted to experience significantly different deformations in both the vertical and horizontal planes. Figure IIIb.16a shows eight face positions (Face A through H) associated with the undermining of this asset. The initial face position is located just under the western end of the culvert. Eight face positions later, the longwall is over 300-ft past the eastern end of the culvert. Figure IIIb.16b shows how the surface profile above the culvert subsides. It also shows that there is no permanent change in the slope of the culvert. Figure IIIb.16c displays the change in vertical subsidence along the length of the culvert during the eight face positions. At face position D, more than 200-ft of culvert is predicted to subside at a rate of ~10-in every 50-ft. There are no design guidelines or severity indexes that would provide some indication as to how this structure will respond to these kinds of differential movements. What complicates this assessment is the role of the surrounding fill in absorbing predicted settlement rates. It should be mentioned that for a short time during the development of the subsidence basin, the inlet of the culvert has the potential to settle as much as the full 55-in more than the culvert near the outlet. Temporary ponding could result.

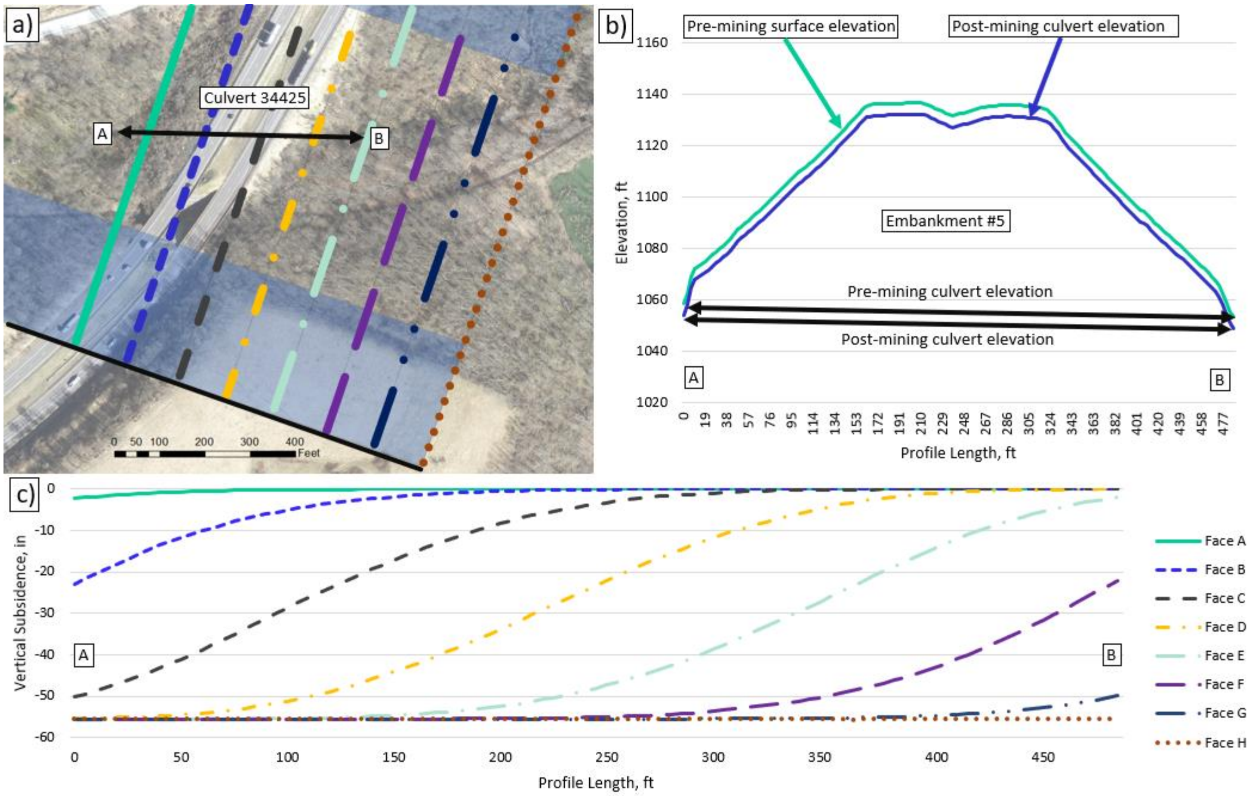

Figure IIIb.16 - Summary of predicted vertical subsidence of Culvert 34425; a) longwall face position of potential Panel C, b) pre- and post-mining surface and culvert elevations, and c) vertical subsidence at eight face positions

Culvert 34425 is expected to experience close to 20-in of differential horizontal deformation (Figure IIIb.17a). The maximum horizontal deformation occurs where the surface subsidence slope is at a maximum. This is known as the inflection point and is determined to be ~144-ft using Eq. IIIa.1 (Section IIIa.3.1). In this scenario, the maximum horizontal deformation will not occur until the longwall face is ~144-ft past the culvert inlet (Point A). From this point forward a moving wave of upwards of 20-in will propagate through the culvert (Face A to E). This wave follows the longwall face by ~144-ft. The level of horizontal deformation lessens once the longwall face is greater than 144-ft beyond the outlet (Face F). It is worth repeating that these predictions apply to surface conditions. The fill surrounding the culvert will likely alter the surface conditions in complex ways that should be evaluated further if actual conditions match these projections.

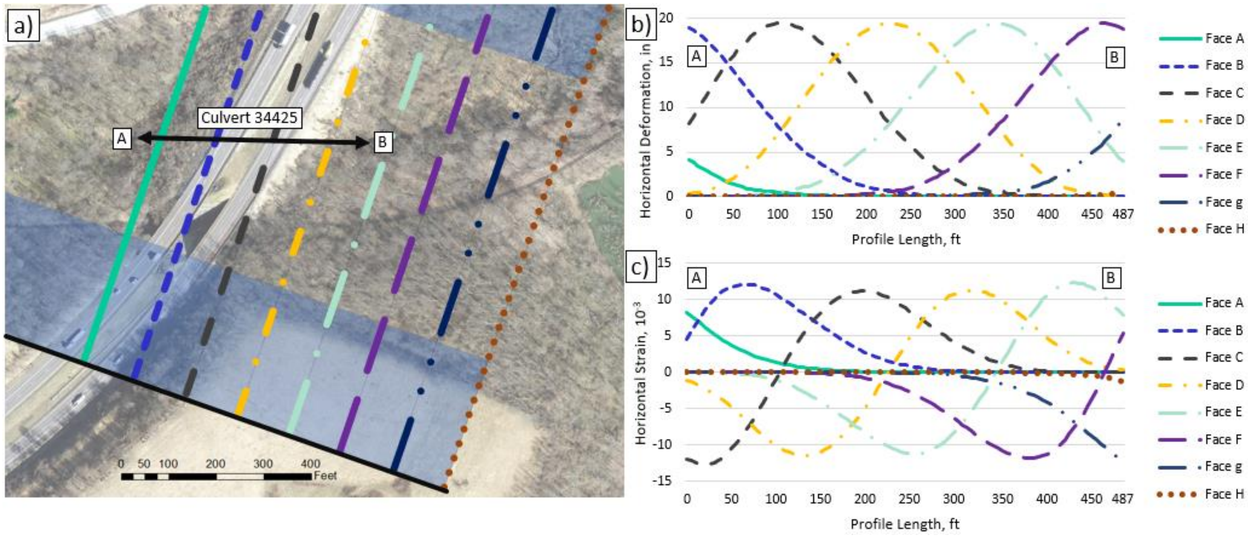

Figure IIIb.17 – a) longwall face position of potential Panel C, b) horizontal deformation, and c) horizontal strain along the length of Culvert 34425

SDPS predictions of potential horizontal strain conditions during undermining also assist in assessing damage to culverts. Figure IIIb.17c shows how the culvert first experiences tensile strain when the longwall face is at Point B (Figure IIIb.17a). When the longwall is at face Point C, the culvert could experience both a maximum horizontal tensile strain ~200-ft from the inlet, followed by a maximum compressive strain ~180-ft away. In other words, this analysis predicts that a section of pipe could experience maximum levels of tensile strain followed maximum levels of compressive strain after ~180-ft of longwall face advancement. Since the Tunnel Ridge face averages 115-ft of advance every day, every point along the culvert could experience a significant reversal in strain within 38-hr.

3.1.2 *Overpass 34424 and 34426*

Two three span overpasses, 34424 and 34426, are projected to be undermined by Panel C (Section IIIa.5.2.1). In this projection, the foundations for the northeastern abutments and both piers for each overpass will be completely within the middle-panel area. The foundations for the southwestern abutments lie within the edge of the quarter-panel area (Figure IIIb.18a). In terms of vertical subsidence, these conditions could result in a permanent ~10-in difference (~45-in at Point A and ~55-in at Point B, Face F Figure IIIb.18b) between the westbound abutment foundations of overpass 34426 and ~5-in difference (~50-in at Point C and ~55-in at Point D, Face F Figure IIIb.18c) between the eastbound abutment foundations of overpass 34424. The foundation net allowable permissible settlement (Table IIIa.5) for continuous span bridges is 1-in. In both of these overpasses, each of the three ~50-ft spans could experience greater than 1-in of settlement between vertical supports. It is also possible for excessive differential dynamic settlement to temporarily occur during longwall face advance. Dynamic subsidence could cause different spans to exceed the 1-in permissible settlement at different longwall face positions. This dynamic surface subsidence could result in repeated flexing of the structure.

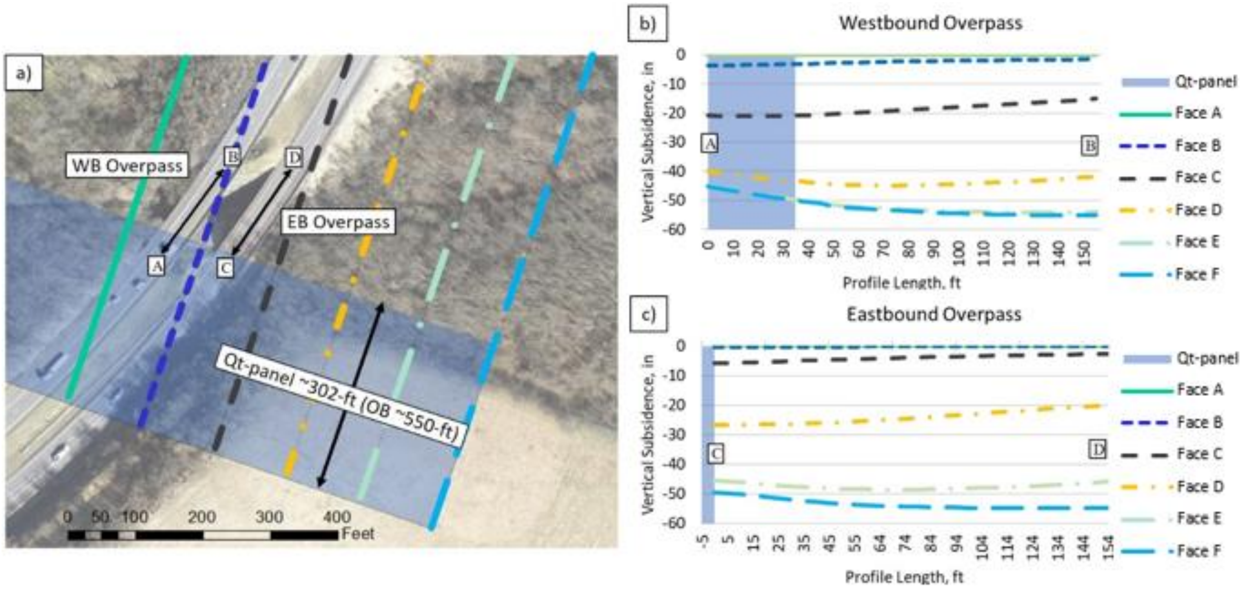

Table IIIb.18 –Predicted vertical subsidence associated with Overpasses 34424 and 34426; a) overpass and face position location; b) westbound overpass; and c) eastbound overpass

Horizontal deformations along the ground profile beneath the overpasses 34424 and 34426 are estimated to be highest when the longwall face is 100 to 300-ft past either overpass (Face C and D, Figure IIIb.19b; and Face D and E, Figure IIIb.19c). The northeastern abutments at Points B and D return to their original horizontal positions, just 55-in lower. Because the southwestern abutments at Point A is located within the quarter-panel area, Overpass 34424 abutments Points A and B are predicted to be ~13-in closer together. For this same reason, Overpass 34426 abutments Points C and D are predicted to be ~8-in nearer.

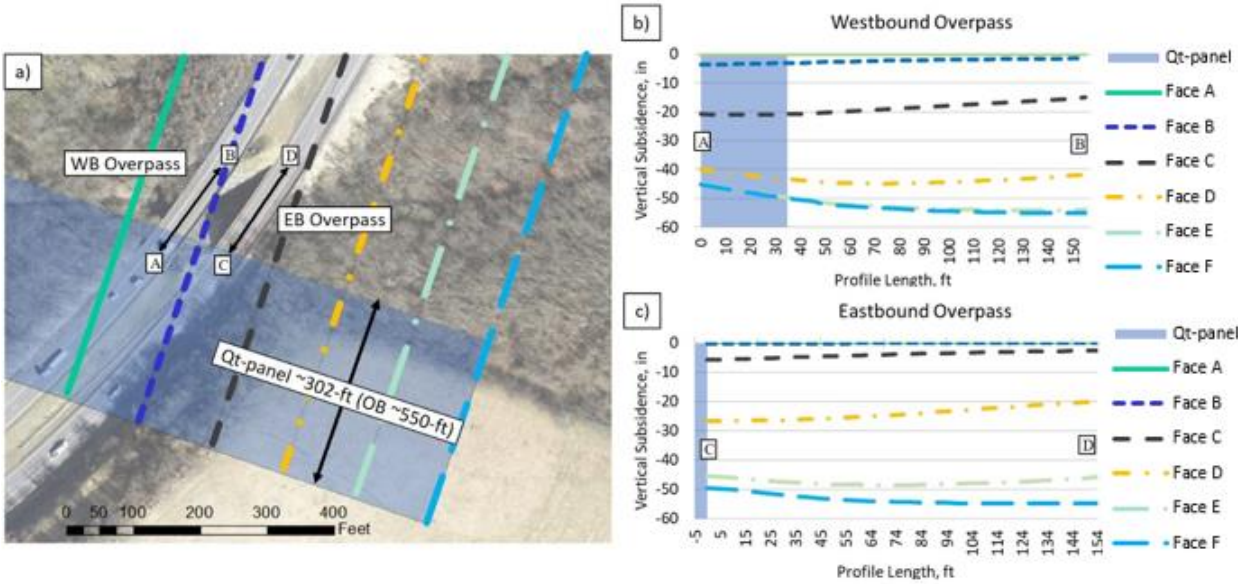

Figure IIIb.19 - Predicted horizontal deformation associated with Overpasses 34424 and 34426; a) overpass and face position location; b) westbound overpass; and c) eastbound overpass

3.2 Panel N

The potential Panel N is in the northern portion of longwall District 2. This district is located on the western side of the projected main entries (Figure IIIa.4). An area of interest within Panel N was selected to further examine the dynamic subsidence effects on select overpasses, culverts and retaining wall assets. In this area of interest, the longwall panel forms a 25-deg angle with I-70. The average overburden is ~420-ft. This area is of interest because it focuses on undermining portions of Dutch Fork where five significant assets are located, all within Panel N.

In this example, Panel N will be mined from east to west, towards the main entries. This area of interests contains Culvert 34436 under (I-70), Overpasses 34435 (EB) and 34437 (WB) carrying I-70 over Dutch Fork, and two concrete reinforce retaining walls connecting the two overpasses. The vertical subsidence and horizontal deformations induced on the surface by three longwall face positions are provided to show how conditions change as the longwall face approached, passed underneath, and moved away from the area of interest. Panel N was of particular interest to the University because it contained overpasses and retaining walls within the middle-panel area and a culvert within the quarter-panel area. These different conditions highlight the importance of performing both a dynamic, as well as a permanent, subsidence analysis.

Pre-undermining conditions - When the longwall face is ~300-ft from the center of the area of interest, the effects of the developing subsidence basin do not significantly impact the assets (Figure IIIb.20). Both vertical subsidence and horizontal deformation are approximately zero.

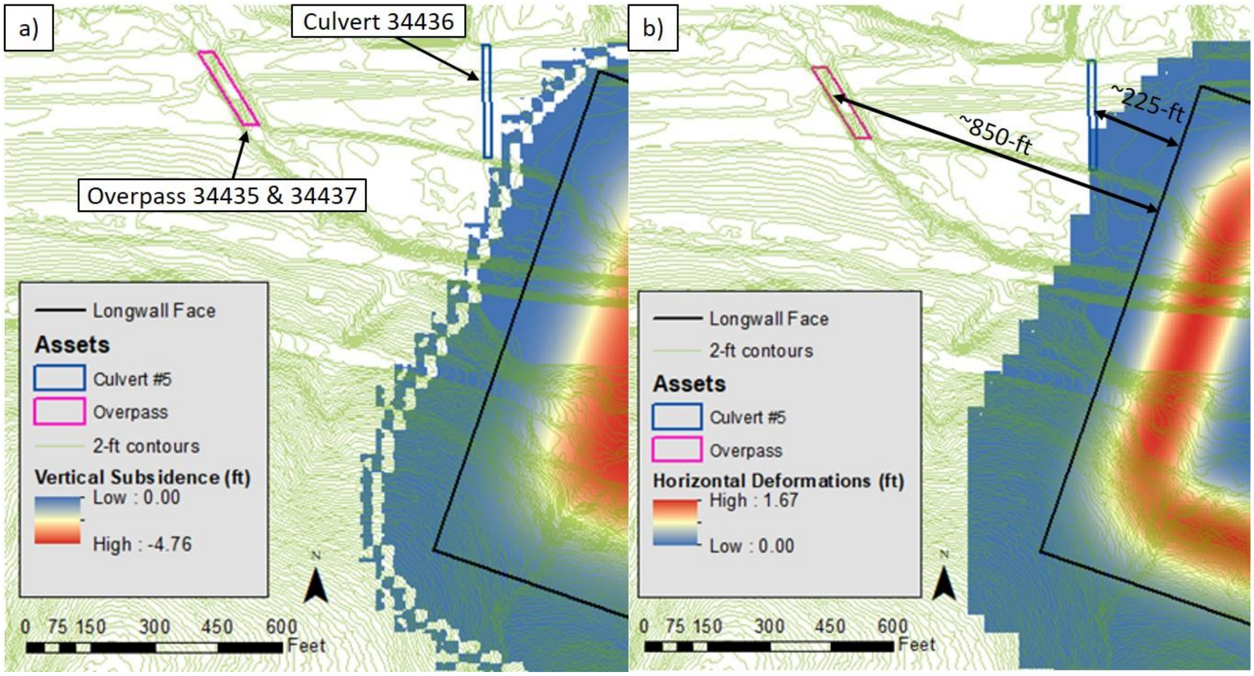

Figure IIIb.20 – a) Vertical subsidence and b) horizontal deformations predicted when the longwall face is approaching Overpasses 34435 and 34436 and Culvert 34436

<u>Dynamic subsidence conditions</u> – As the longwall face advances to a position between the five assets in the area of interest, conditions begin to change dramatically for the culvert but not at all for the overpasses and retaining walls (Figure IIIb.21). At this face position, the maximum predicted vertical subsidence of 4.76-ft with a maximum horizontal deformation of 1.67-ft is already impacting the Culvert 34436. Subsidence conditions are dynamic and can change significantly over relatively short periods of time. As the culvert asset is within the quarter-panel area, it is expected to experience less vertical subsidence and greater amounts horizontal deformation under final subsidence conditions.

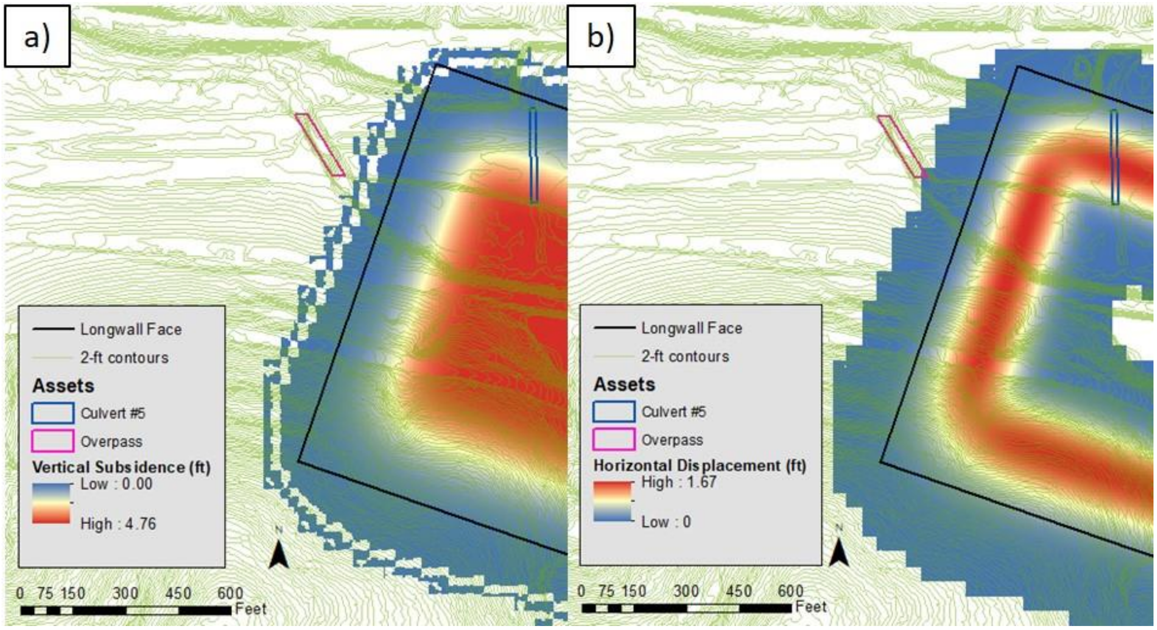

Figure IIIb.21 – a) Vertical subsidence and b) horizontal deformations predicted when the longwall face is between the overpass and culverts within the area of interest

<u>Permanent subsidence conditions</u> – The permanent predicted vertical subsidence and horizontal deformation conditions occurs when the longwall face is 450-ft beyond the Overpasses 34435 and 34437 and the associated retaining walls (Figure IIIb.22a). Here the permanent vertical subsidence characteristics associated with different portions of the subsidence basin are revealed. The overpasses and retaining walls are located within the flat portion of the subsidence basin (middle-panel area) whereas the culvert is located where permanent slope changes, and corresponding settlement, would occur (quarter-panel area).

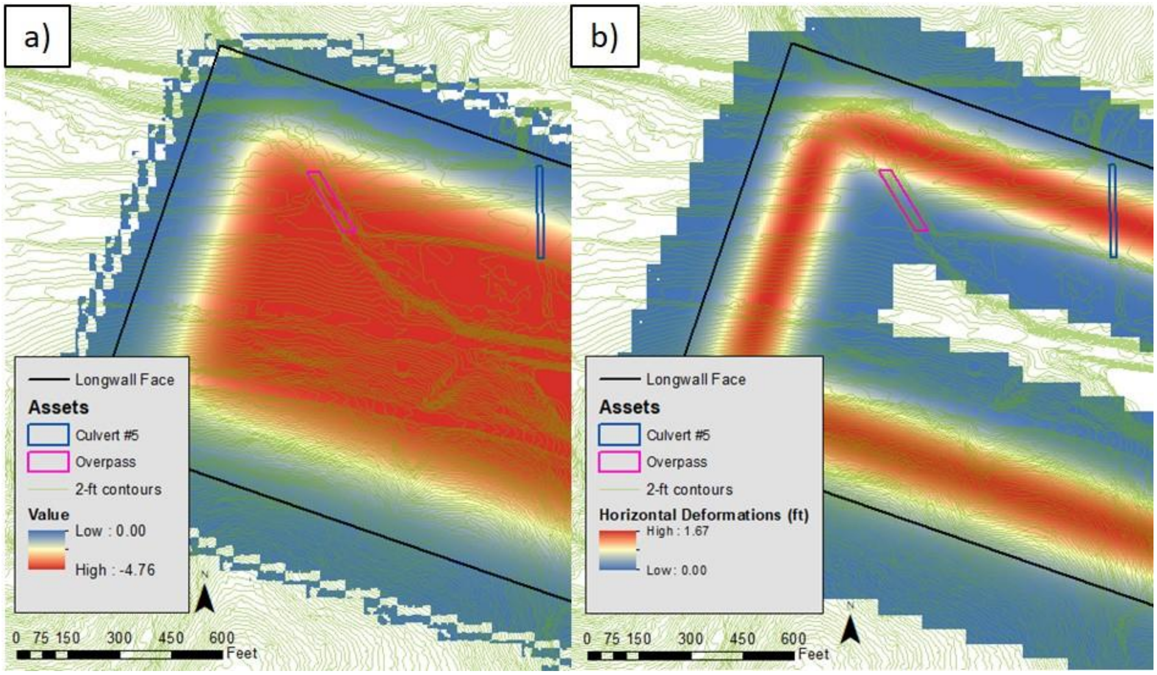

Figure IIIb.22 – a) Vertical subsidence and b) horizontal deformations predicted when the longwall face is 900-ft past the center of the area of interest

3.2.1 *Culvert 34436*

Culvert 34436 above potential Panel N will experience significant differential vertical subsidence as the longwall face approached and passed beneath it. The reason for this is associated with its location within the quarter-panel area of potential longwall Panel N (Figure IIIb.23a). This differential vertical settlement of the culvert is predicted to be permanent. Figure IIIb.23b shows the overall effect of the subsidence basin beneath Culver 34436. Vertical subsidence ranges from a few inches at the inlet to ~54-in at the outlet. This differential subsidence will result in an increase in the overall slope of the culvert from 0.7 to 2.4-deg (Table IIIa.10). While the overall gradient increases by only 1.7-deg, the last 100-ft of the culvert closest to the discharge is predicted to settle ~1.6-ft producing a 0.9-deg change in slope (Figure IIIb.23c).

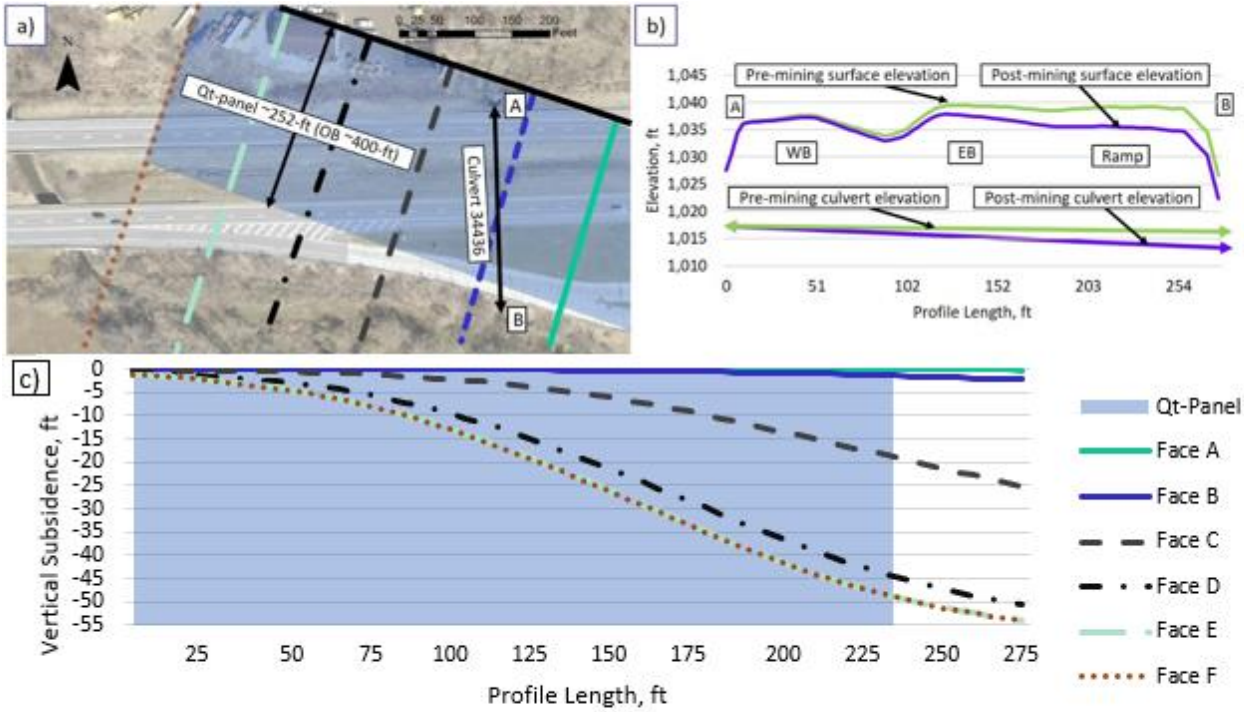

Figure IIIb.23 – Summary of predicted vertical subsidence of Culvert 34436; a) longwall face position of potential Panel N, b) pre- and post-mining surface and culvert elevations, and c) vertical subsidence at six face positions

Culvert 34436 is predicted to experience up to 20-in of horizontal deformation (Figure IIIb.24b). As discussed previously, the maximum horizontal deformation occurs where the surface subsidence slope is at a maximum. In this case, the inflection point is determined empirically to be ~126-ft using Eq. IIIa.1 (Section IIIa.3.1) at 400-ft of overburden. Using the SDPS model, the maximum horizontal deformation will not occur until the longwall face is ~150-ft (Face C, Figure IIIb.24b) past the culvert outlet at Point B. In this case, where the culvert is largely within the quarter-panel area, the point of maximum horizontal deformation will move along the culvert as shown by the horizontal deformation profiles associated with Faces C to F (Figure IIIb.24b). The final subsidence profile (Face F) produces a permanent maximum (~20-in) horizontal deformation ~150-ft from the gate road entries. As in previous examples, these predictions apply to surface conditions above the culvert, although the fill in this example is only ~11-ft at its maximum.

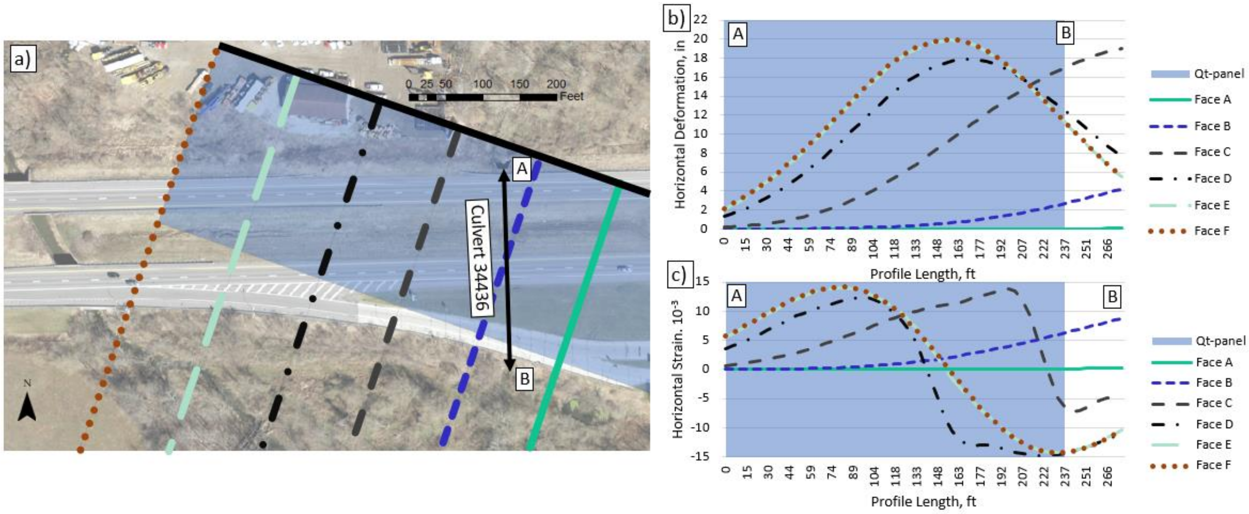

Figure IIIb.24 - Summary of predicted horizontal conditions of Culvert 34436 during undermining by Panel N; a) longwall face positions, b) horizontal deformations, and c) horizontal strains at six face positions

The horizontal strain conditions on the surface above Culvert 34436 is predicted to undergo a significant and somewhat rapid change, especially during Face D (Figure IIIb.24c). Here the horizontal strain fluctuates from +15 to -15 (10^{-3}) in ~60-ft of culvert. The impact of this dynamic change in horizontal strain to the stability of the culvert needs further study.

3.2.2 *Overpasses 34435 and 34437*

As shown in the previous sections, Overpasses 34435 and 34437 above potential Panel N will deform gradually over a several day period as the longwall face approached and passed beneath them. Conversely, because the overpasses are located within the middle-panel area of potential longwall Panel N, they are expected to experience only minor amounts of permanent differential settlement. This can be seen by comparing the vertical subsidence profiles between the foundation for Points A and B (Figure IIIb.25b) as well as Points C and D (Figure IIIb.25c). The differential settlements between these abutments at Faces F and K are predicted to be at most a few inches. A bigger risk to the structural condition of the overpasses is the dynamic differential settlement during undermining, especially when the longwall face is 200 to 300-ft past the overpasses. At Face I (Figure IIIb.26b) and Face H (Figure IIIb.25c) the foundation for the overpasses (Points A, B, C, and D) is predicted to experience as much as 10-in of differential settlement.

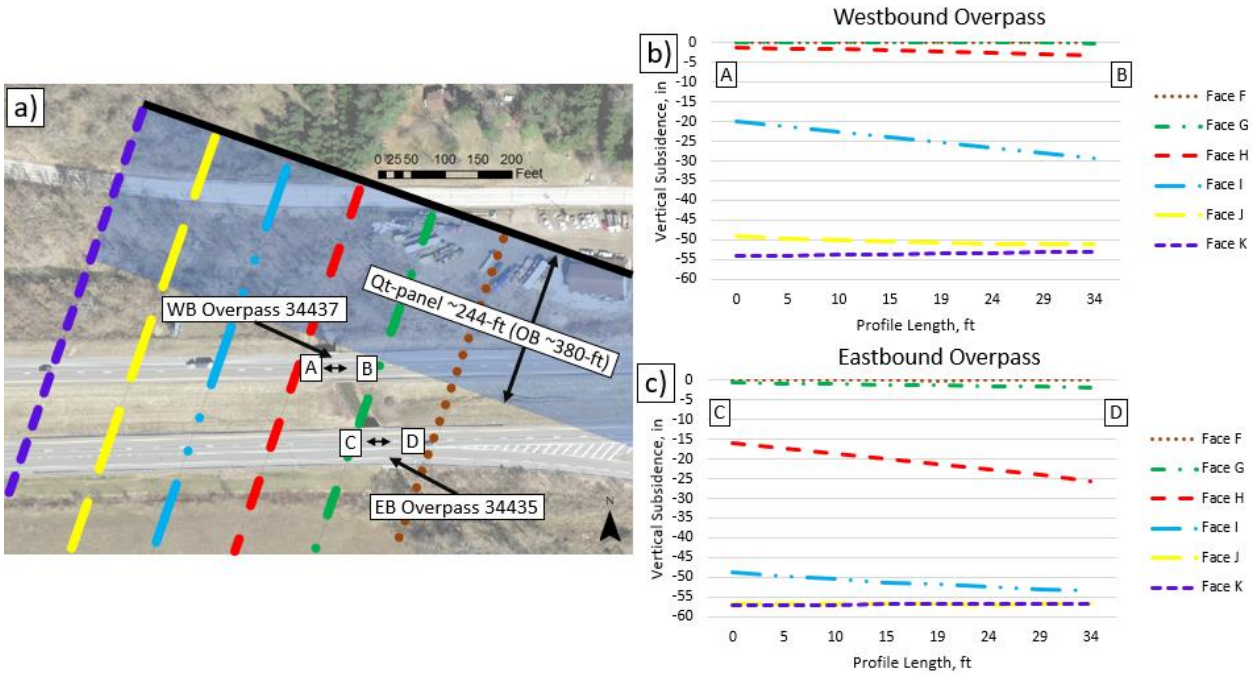

Figure IIIb.25 – Summary of predicted vertical subsidence conditions of Overpasses 34437 and 34435 during undermining by Panel N; a) longwall face positions, b) westbound overpass (A-B) vertical subsidence, and c) eastbound overpass (C-D) vertical subsidence at six face positions

The next question to consider is how predicted horizontal deformations might impact Overpasses 34435 and 34437. Differential horizontal deformations of a few inches are seen when the longwall face is underneath the overpasses (Face H, Figure IIIb.26b; and Face G, Figure IIIb.26c). Peak horizontal movement approaching 20-in are predicted when the longwall face is 200 to 300-ft past the overpass (Face I, Figure IIIb.26b; and Face H, Figure IIIb.26c). In this analysis the differential horizontal deformation is rarely more than 5-in. One exception is Face I (Figure IIIb.26b).

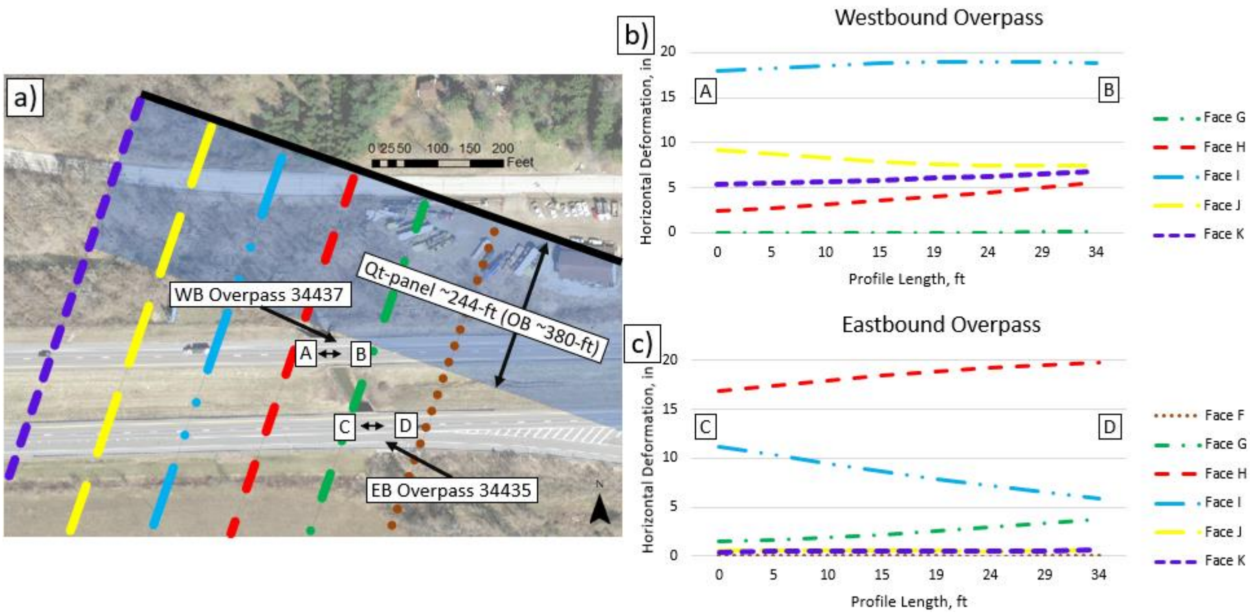

Figure IIIb.26 - Summary of predicted horizontal deformation conditions of Overpasses 34437 and 34435 during undermining by Panel N; a) longwall face positions, b) westbound overpass (A-B) horizontal deformation, and c) eastbound overpass (C-D) horizontal deformation at six face positions

3.2.3 *Reinforced Concrete Retaining Walls between Overpasses 34435 and 34437*

Six of the nine single span overpasses are connected with reinforced concrete retaining walls (Table IIIa.8). This is the case for Overpasses 34435 and 34437. In this instance, two 14-ft high by 82-ft long retaining walls located on opposite sides of the Dutch Fork channel are connected to the overpasses. The maximum differential settlement of the western retaining wall (Points A-C) is predicted to be 19-in (Face I, Figure IIIb.27b) and 16-in along the eastern retaining wall (Points B-D) (Face I, Figure IIIb.27c). Both retaining walls should drop to the southeast by less than 0.3-in per foot of wall length.

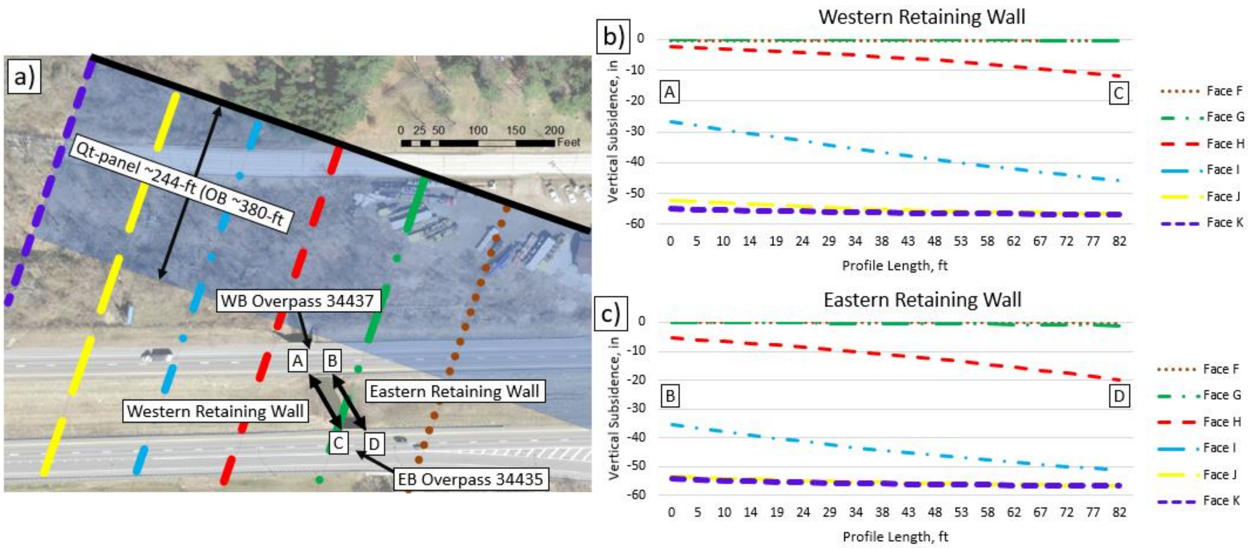

Figure IIIb.27 - Summary of predicted vertical subsidence conditions along the foundation of the retaining wall between Overpasses 34437 and 34435 during undermining by Panel N; a) longwall face positions, b) western retaining wall (Points A-C) vertical subsidence, and c) eastern retaining wall (Points B-D) vertical subsidence at six face positions

Perhaps a more important subsidence impact characteristic would be the differential movement of the retaining wall in a direction perpendicular to its length. If this differential movement is significant, it could act to twist or skew the wall. The twisting of a retaining wall will potentially have its greatest effect where it meets the stem wall beneath the overpass. It should be noted that there are no defined connections (construction joints) between the overpass stem walls and adjoining retaining walls.

In the case of the western and eastern retaining walls joining Overpasses 34435 and 34437, perpendicular movement would occur into and away from the channel for Dutch Fork. For example, the western retaining wall is predicted to move first towards the adjacent channel at Face H (Figure IIIb.28b). At the same time the eastern retaining wall will move, with the surrounding highway base, away from the channel at Face H (Figure IIIb.28c). Of course, the channel is also moving in a similar manner. However, the magnitude of the western retaining wall, the Dutch Fork channel, and the eastern retaining wall are all moving at slightly different rates along their length. This non-uniform movement is what can cause skewing or twisting of the retaining wall.

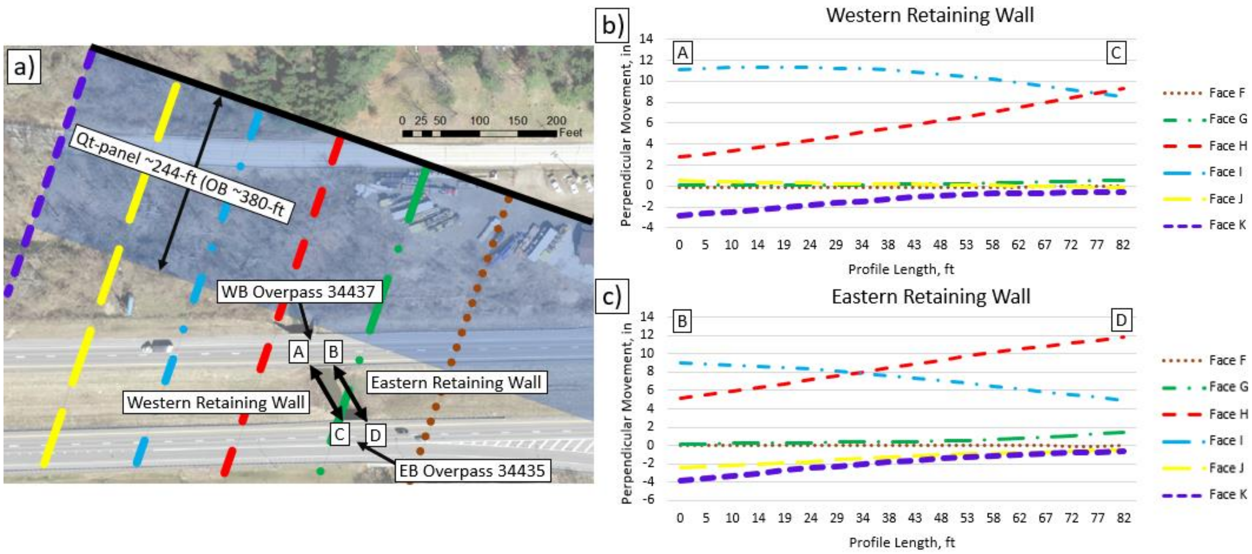

Figure IIIb.28 - Summary of predicted movement perpendicular to the foundation of the retaining wall between Overpasses 34437 and 34435 during undermining by Panel N; a) longwall face positions, b) western retaining wall (Points A-C) perpendicular movement, and c) eastern retaining wall (Points B-D) perpendicular movement at six face positions

The maximum amount of differential movement perpendicular to the channel (~6-in) is predicted to occur at Face H (Figure IIIb.28b) for the western retaining wall. What is interesting to note is what happens during Face I. Here the maximum differential movement drops to ~3-in but Point A (Figure IIIb.28b) deforms by ~ 8-in while Point C remains almost stationary. Apparently, the center of twisting occurs ~75-ft from Point C.

For the eastern retaining wall, Face H predicts a maximum of ~7-in of differential movement perpendicular to the wall (Figure IIIb.28c). When comparing Face H with Face I, the center of twisting appears to have shifted to ~30-ft from Point B.

4.0 Discussion

The SDPS model was used to predict potential surface subsidence along I-70 from the West Alexander to the Claysville interchange. This model was validated with information collected during the undermining of Panel 15 (see Section IV, Task 2 Report). It takes into account, changes in overburden and topography and is constructed to match the locations of the potential extended study area panels discussed in Section IIIa. The subsidence model also utilizes the capability of the SDPS model to perform dynamic subsidence simulations at discrete longwall face positions.

The University selected a subset of the 28 identified significant assets for further study. The aim was to illustrate how different assets, located at dissimilar positions within a subsidence basin, could react to these potential subsidence events. The impact of both permanent as well as dynamic subsidence conditions are presented. In some cases assets would see more potential impacts from permanent subsidence, i.e. culverts crossing a quarter-panel area. In other cases assets would experience impacts only during dynamic subsidence, i.e. differential settlement of overpass foundations. The SDPS model provided an opportunity to predict vertical subsidence and horizontal movements along the projection of structures. Understanding how structures deform helps to assess potential performance issues and implement the most effective engineering interventions to mitigate its impact.

SECTION IV – ORIENTATION AND OVERBURDEN INFLUENCE ON EMBANKMENTS

Subsection IVa – Behavior of Embankments Subjected to Different Highway Orientation and Overburden

The University used Finite Element Analysis (FEA) to examine the influence of highway orientation and depth of the longwall panel on embankments subjected to subsidence. For comparative purposes, modeled panels were placed within the center of a developing subsidence basin. In addition, the characteristics of Embankment #1 were used, i.e. shape, size, and material properties. The FEA focused on three different highway orientations, 0, 35, and 90-deg with respect to the direction of longwall mining. Then for the case of 0, 35, and 90-deg, four overburdens, 400-ft, 500-ft, 600-ft, and 675-ft were used to analyze these two important factors. The University found that significant deformations could occur within the modeled embankment at certain of orientations and overburdens. A chart of the factor of safety is proposed for Embankment #1 when located in the center of the panel.

1.0 Shear Strength Reduction Method (SRM)

The shear strength reduction method (SRM) has been widely utilized in slope stability analysis (Zienkiewicz et al., 1975; Matsui and San, 1992; Dawson et al,, 1999; Griffiths and Lane, 1999; Zheng et al., 2005). In SRM, in order to obtain the factor of safety equivalent to the limit equilibrium method (LEM), a strength reduction factor (SRF) is utilized. The factor is applied to reduce the original cohesion (c) and tanϕ until the slope fails. The original shear strength parameters are divided by this factor to obtain the reduced shear strength parameters c' and $tan\phi'$ as follows:

$$c' = \frac{c}{FS}\,, tan\phi' = \frac{tan\phi}{FS} \qquad \text{[Eq. IVa.1]}$$

or using the equivalent equation using the SRF,

$$c' = \frac{c}{SRF}\,, tan\phi' = \frac{tan\phi}{SRF} \qquad \text{[Eq. IVa.2]}$$

Where:

c and ϕ are the laboratory measured shear strength parameters;
SRF the shear strength reduction factor.

The critical SRF appears when the instability of the slope happens with the reduced strength parameters. The critical value of the ratio is approximately consistent with the factor of safety using Bishop's limit equilibrium method (LEM). The slipping surface can be traced from the development of the plastic shear strain.

When applying the SRM in FE analysis, the increasing SRFs are applied successively on the model to reduce the soil strength in the model until the solution runs out of convergence. In ABAQUS, the procedure is implemented by creating a field value to represent SRF applied on the FE model. The field value is set less than one before the SMR step in order to make the slope stable in the gravity and deformation steps. Then in the SMR step, the field value increases until the solution goes out of convergence. This largest SRF when failure happens is equivalent to factor of safety from LEM.

While applying SRM to practical analysis, according to the analytical test using shear strength reduction method conducted by Matsui and San (1992), the critical SRF can only be utilized as the factor of safety in analyzing an embankment slope, but not in analyzing an excavated slope. The well-defined failure shear strain zone in an embankment slope is not formed in the excavation slope due to the uncertainty of the initial shear strains before excavation and the shear strain increment is not normally distributed.

1.1 Critical Cross-Section

Centrifuge tests have indicated that the plastic shear strain zone in unstable slopes coincided with the rupture surface (Roscoe, 1970). SRF in SRM was applied to reduce the shear strength parameters until the embankment collapse. The critical regions were identified with the higher plastic strain. The critical cross section with highest plastic strain was utilized to conduct the factor of safety analysis in the next section. Figure IVa.1 indicates that the critical cross-section was located on the south facing slope in the middle of the longitudinal length of the embankment.

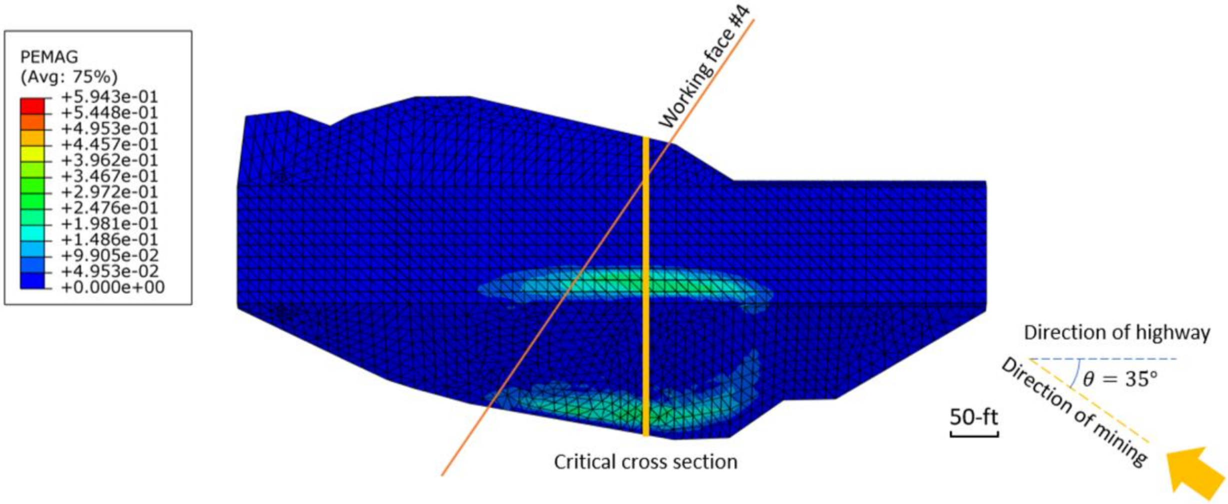

Figure IVa.1 – Critical cross-section for the factor of safety analysis taking the longwall face position #4 as an example

Other angles between the highway orientation and the direction of longwall advanced and overburdens were analyzed and summarized in Table IVa.1. The critical cross sections for these cases are found to be same as the example shown in Figure IVa.1. The factor of safety will be calculated based on this critical cross section in the following sections.

Table IVa.1 – Orientation of highway with respect to direction of mining and overburden for twelve case studies

	Highway orientation with respect to mining direction		
Overburden	**0-deg**	**35-deg**	**90-deg**
400-ft	400-ft, 0-deg	400-ft, 35-deg	500-ft, 90-deg
500-ft	500-ft, 0-deg	500-ft, 35-deg	500-ft, 90-deg
600-ft	600-ft, 0-deg	600-ft, 35-deg	600-ft, 90-deg
675-ft	675-ft, 0-deg	675-ft, 35-deg	675-ft, 00-deg

1.2 Factor of Safety using SRM and LEM

As discussed above, the factor of safety was obtained using SRM which utilizes the SRF to reduce the cohesion and $tan\phi$ until the embankment failed. Total displacement was plotted against the SRF to estimate the factor of safety. The knee point, which represented failure of the slope, was cited by Dawson (1999) as being equivalent to the factor of safety when using the LEM.

Figure IVa.3 shows the process of the determination of the factor of safety of the embankment without subsidence. The plastic strain inside the embankment at the critical cross section with

SRF equals to 3.4 is shown in Figure IVa.4. This state of plastic strain happened when the analysis reached the factor of safety knee point. For this case without subsidence, the shear band will reach the top of the embankment.

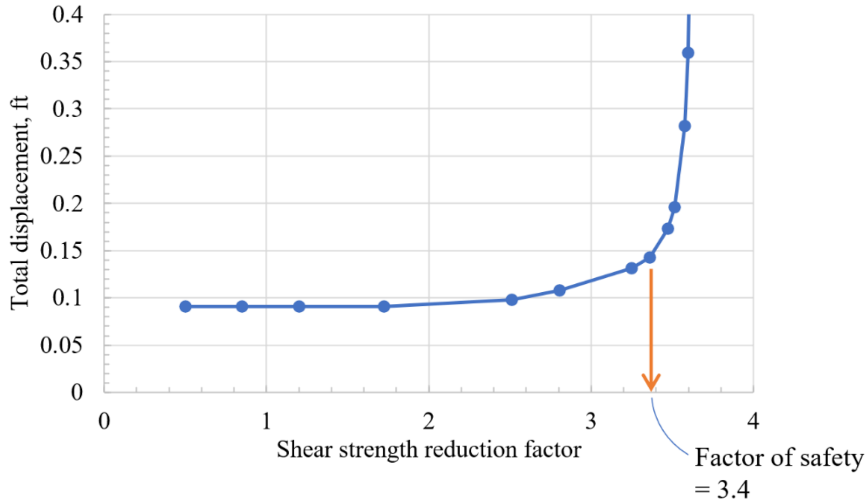

Figure IVa.3 – Total displacement at the crest of the critical cross section versus the shear strength reduction factor for the case without subsidence

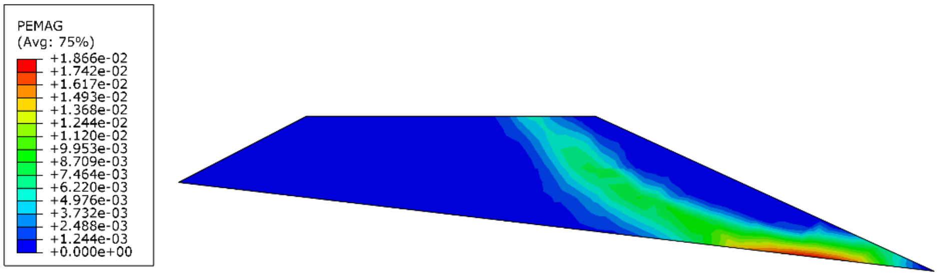

Figure IVa.4 – Shear band at the critical cross section from SRM

The SRM is validated by comparing the resulted shear band and the factor of safety obtained using SRM to those from SLIDE (slope stability software using LEM) where the LEM assumes the failure surface to be a part of circle (Figure IVa.5). The shear band in LEM has a very small thickness and will develop as soon as the equilibrium is compromised. In this case failure will occur at relatively small deformations. The factor of safety from SRM is equivalent to the LEM, i.e. 3.4. While the factor of safety calculations are similar between FEA model and the SLIDE LEM, the location and shape of the failure plane are slightly different.

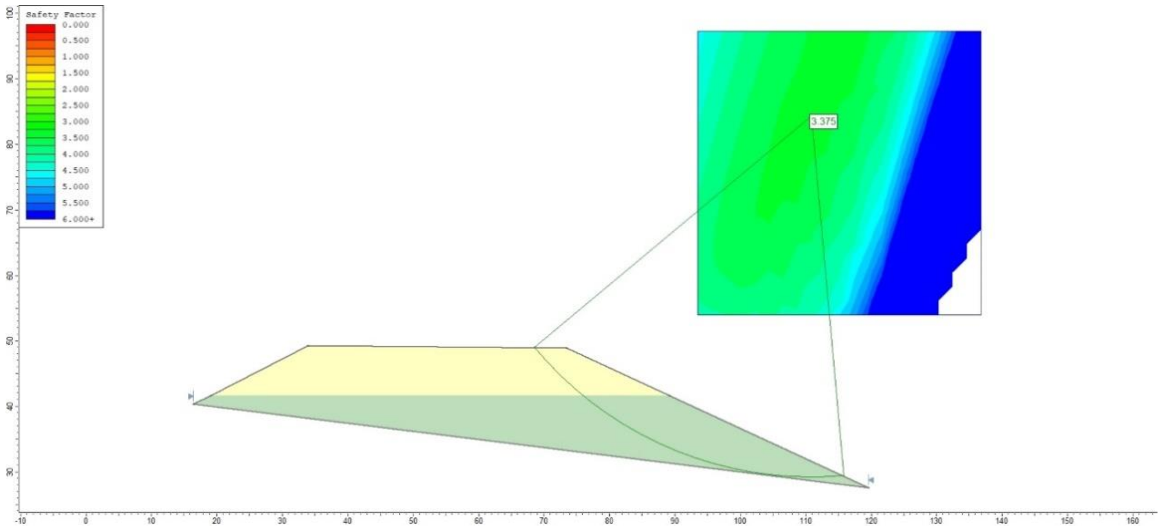

Figure IVa.5 – Failure surface and the factor of safety calculated by LEM in SLIDE using the same material properties (factor of safety=3.4 in SLIDE)

Next, the embankment was subjected to the subsidence and, as expected, more deformation was observed before the knee point. In this analysis, a lower and upper bound of the factor of safety was used to help characterize the embankment slope stability during undermining. The upper bound factor of safety is depicted when the SRM rupture surface fully develops. The lower bound factor of safety was determined when plastic deformations first localized along a band illustrating slope instability during undermining.

An example of factor of safety determination considers Embankment #1, when the longwall working face was located under the middle of the embankment (working face position #4 in Figure IVa.6). As shown in Figure IVa.7, the lower bound factor of safety was found to be 1.1. Before this point, the displacement increased at a relatively low rate. After this point, the embankment begins to noticeably deform. The upper bond factor of safety is found to be 3.4, where the total displacement starts to increase exponentially and the shear band develops at the cross section.

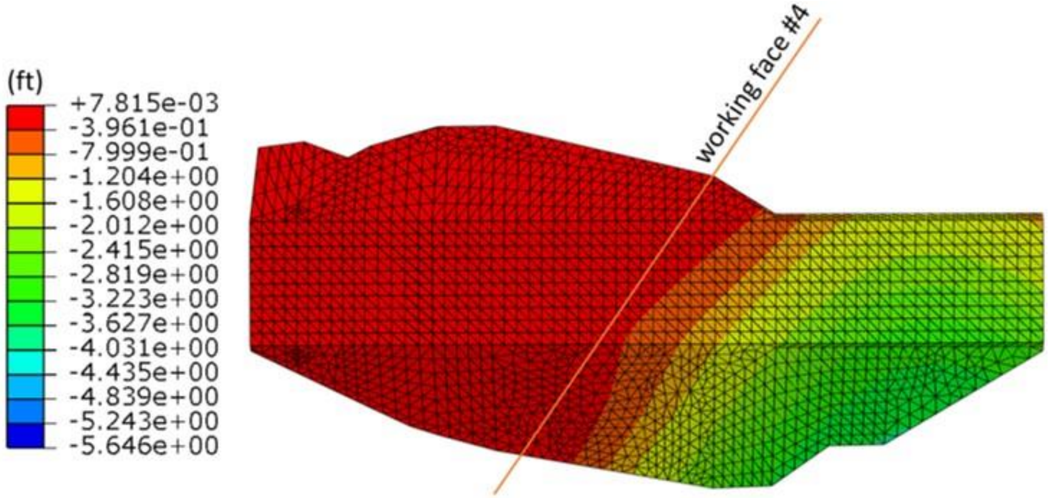

Figure IVa.6 – Embankment #1 subjected to subsidence from a developing longwall panel at the working face position #4

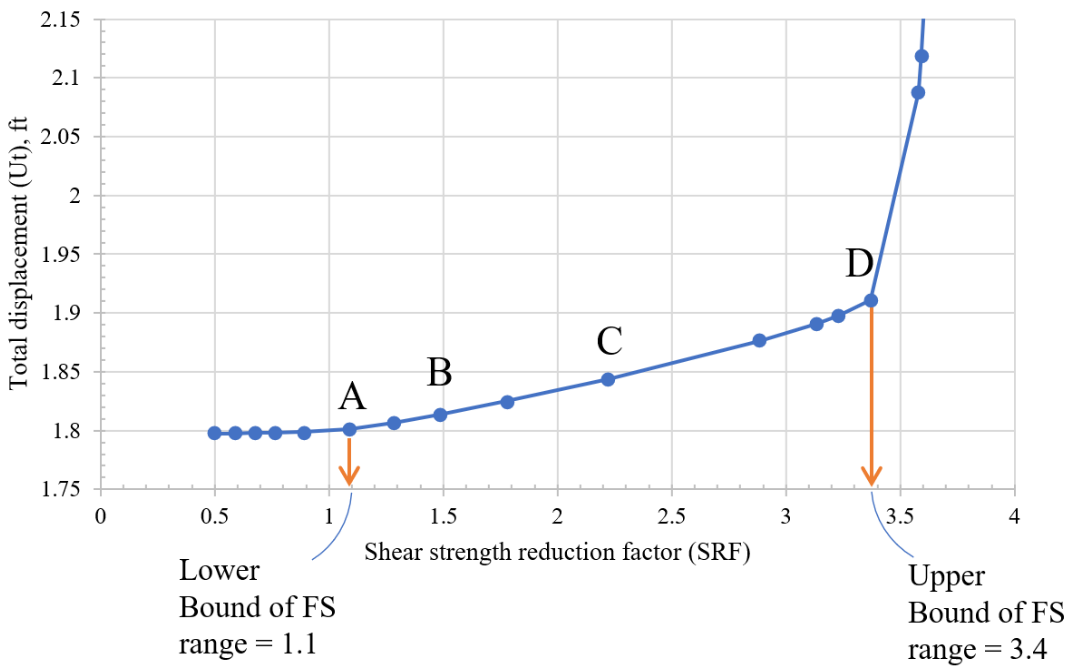

Figure IVa.7 – Total displacement at the crest of the critical cross-section versus the shear strength reduction factor for the case with working face position #4

The plastic strain as well as the horizontal displacement at four SRF points are plotted in Figure IVa.8 and IVa.9, respectively. At the lower bound factor of safety, where the plastic strain initiates, small deformation occurs at the embankment crest. Point D is the upper bond factor of safety when the shear band completely forms and the slope becomes unstable.

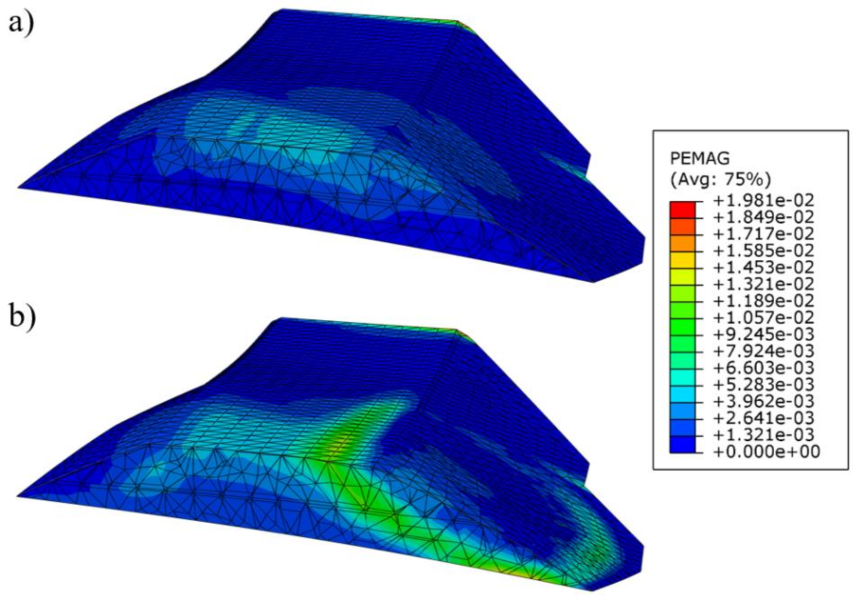

Figure IVa.8 – Rupture surface indicated by the plastic strain at the critical cross section when SRF equals to (a) 1.1 and (b) 3.4

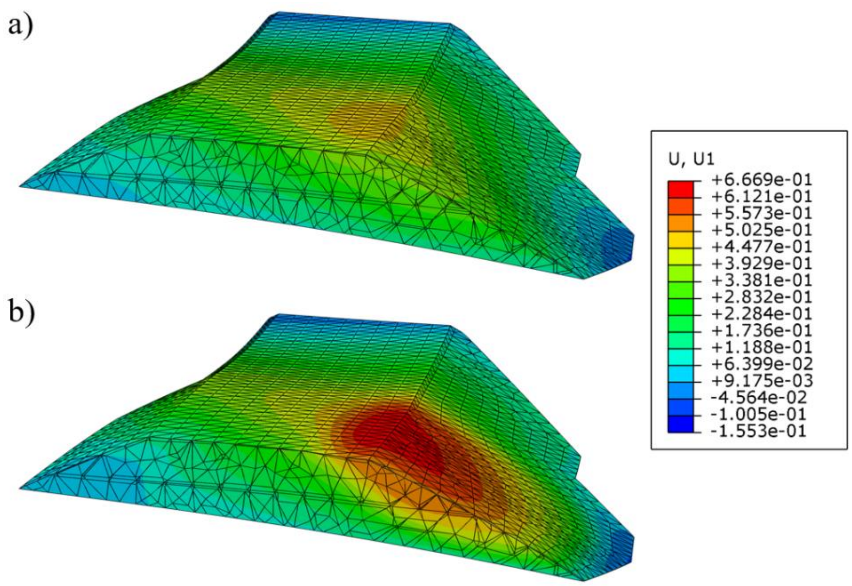

Figure IVa.9 – Horizontal displacement at the critical cross section when SRF equals to a) 1.1 and b) 3.4 (unit:ft)

Generally, the factor of safety is calculated using Eq. IVa.3.

$$FS = \frac{c + (\sigma_n - u)tan\phi}{\tau} \qquad \text{[Eq. IVa.3]}$$

Where:

c is the cohesion,

ϕ is the friction angle,

σ_n is the normal stress generated by gravity,

u is the water pressure generated by the ground water table.

However, when large deformation is experienced, like those associated with longwall mining, the calculation for factor of safety takes on a different form. According to Johnson (1970), the factor of safety of the slope under large displacement in the thick shear band is given in Eq. IVa.4.

$$FS = \frac{c + (\sigma_n - u)tan\phi + \eta(\frac{dv}{dy})}{\tau} \quad \text{[Eq. IVa.4]}$$

Where:

η = the viscosity of soil,

$\frac{dv}{dy}$ = the change of velocity with depth in the shear band, and

τ = the shear stress induced by gravity.

In Eq. IVa.4, the numerator represents the shear strength of the soil for the case of long deformations. At large deformations, the factor of safety is increased by the third term in the numerator of Eq. IVa.3. The shear strength of soil will increase once the embankment experience large deformations. For an embankment subjected to subsidence, the moving ground makes the embankment to contract in the vertical direction and expand in the horizontal direction. Such movements will translate in an increase in the shear strength of the embankment according to Eq. IVa.3. As analyzed in the last section, the horizontal displacements started at the bottom of the embankment in the form of a shear band. The large deformations of the embankment concentrated in this shear band. The increase in shear strength provided by the third term in the numerator of Eq. IVa.3 is implemented in the FEM by increasing the original shear parameters (before large movements develop) by a factor of 1.25.

The reason for increasing the shear strength parameters by a factor of 1.25 is explained as follows. In practice, it is very difficult to obtain the value of the viscosity, η , for the solid mass forming part of Embankment #1. Recently, a different approach has been developed by Vallejo et. al (2004) and Vallejo and Lobo-Guerrero (2012) to obtain the shear strength of soil-rock mixtures, S_{mix}, at large deformations. The material forming part of Embankment #1 is made of a matrix of soil and dispersed limestone rock fragments. The shear strength at large deformations of this type of mixture can be obtained from the following relationship,

$$S_{mix} = S_0(1 + 2.5C) \quad \text{[Eq. IVa.4]}$$

Where:

S_0 = the shear strength of the soil matrix in the soil-rock mixtures and
C = the volume concentration of the rock fragments in the mixtures.

The shear strength of the soil matrix, S_0, can be obtained from the following equation,

$$S_0 = c + (\sigma_n - u)\tan\varphi \qquad \text{[Eq. IVa.5]}$$

Thus, the factor of safety considering the gravel in the soil rock mixtures experiencing large deformations becomes,

$$FS = \frac{[c + (\sigma_n - u)\tan\varphi][1 + 2.5C]}{\tau} \qquad \text{[Eq. IVa.6]}$$

For the fill forming part of Embankment #1, field and laboratory investigations have indicated that it is formed of a matrix of soil in which fragments of limestone rock are dispersed. Table IVa.2 indicates the concentration of the rock fragments in terms of weight and volume.

Table IVa.2 – Percentage of rock fragments in samples

Borehole	**Depth, ft**	**USCS**	**AASHTO**	**Cw = Percent of Rock Fragments by Weight**	**C = Percent Rock Fragments by Volume***
TB-1	21.0-23.6	CL	a-6	7	2.8
TB-4	3.0-12.0	GC	a-7-6	44	23
TB-5	24.2-26.0	CL	a-7-6	33	15.7
TB-6	55.5-64.5	CL	a-7-6	25	11.2
TB-7	22.5-31.5	GC	a-2-6	41	20.8
TB-8	6.5-8.5	MH	a-7-5	5	2

*C = [C_w]/[G_s – (G_s -1)C_w], G_s = Specific gravity = 2.65

An analysis of Table IVa.2 indicates that the concentration of the rock fragments by volume, C, varies between 2-pct and 23-pct with an average of 12.5-pct. Thus, for the stability analysis a C value equal to 10% was used. If one examines the numerator of Eq. IVa.6, the shear strength of the matrix will be increased by a factor equal to 1.3.

The same procedure was conducted to determine the factor of safety range of Embankment #1 when subjected to subsidence with the working face at different locations. The variation of the factor of safety with different steps of subsidence was shown in Figure IVa.10. For this case, when the orientation is 35-deg, overburden is 675-ft, the critical factor of safety range is [1.1, 3.2].

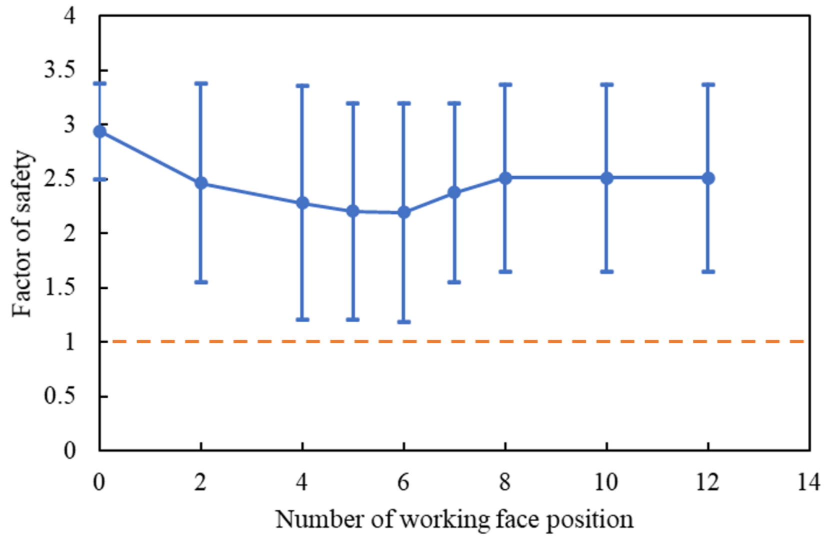

Figure IVa.10 – Plot of factor of safety versus the number of working face position when the orientation of highway is 35-deg with respect to the direction of mining and the overburden is 675-ft

2.0 Influence of Highway and Longwall Panel Orientation

Embankment #1 was assumed to be subjected to the direction of longwall mining subsidence at three angles, 0, 35, and 90-deg shown in Figure IVa.11 to analyze the influence of orientation of highway on the behavior of embankment. The deformation and the slope stability of the Embankment #1 were analyzed in these three cases. It should be noticed that the overburden for this analysis is set to be a constant value of 675-ft in this orientation analysis. The factor of safety for other cases are summarized later in this report.

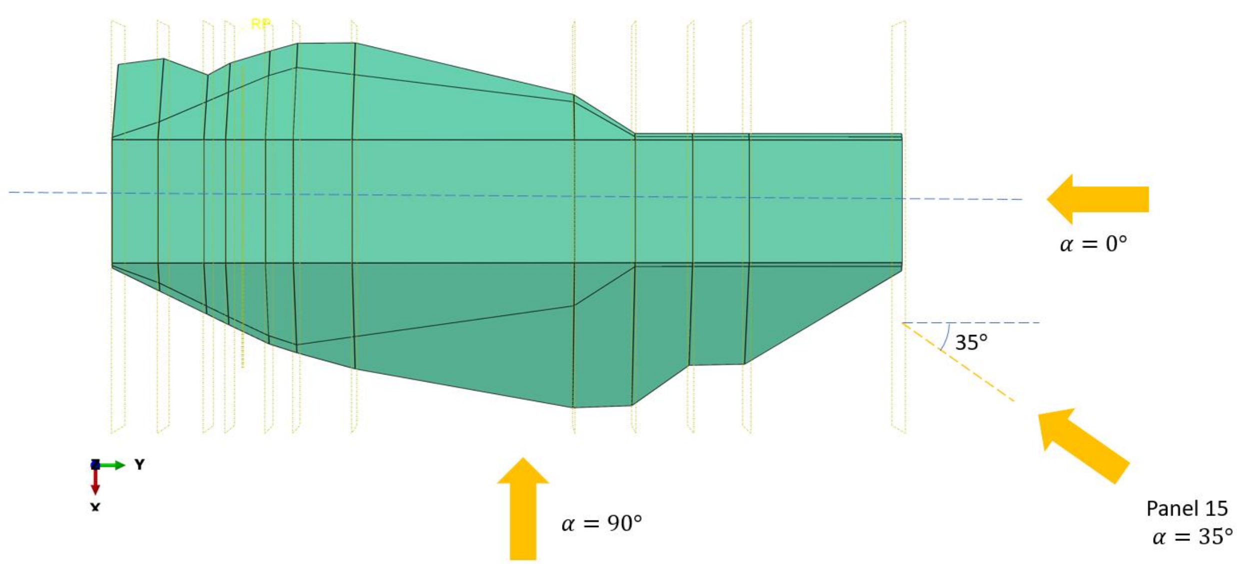

Figure IVa.11 – Three angels between the direction of highway and the direction of mining

2.1 Deformation Analysis

This section will compare the maximum vertical subsidence in the embankment when the angles between the highway and the mining are 0, 35, and 90-deg at the overburden of 675-ft. The vertical displacement contour from the finite element model was shown in Figure IVa.12. When the orientation increases from 0 to 35-deg, the maximum subsidence increases from 5.3-ft to 5.3-ft. The deformation analysis for 90-deg is not compared here for the reason that the embankment failed in the case of 90-deg and the analysis aborted. SRM was utilized to generate the deformation for the case of 90-deg to show the trend of deformation in the embankment when the direction of mining is perpendicular to the highway.

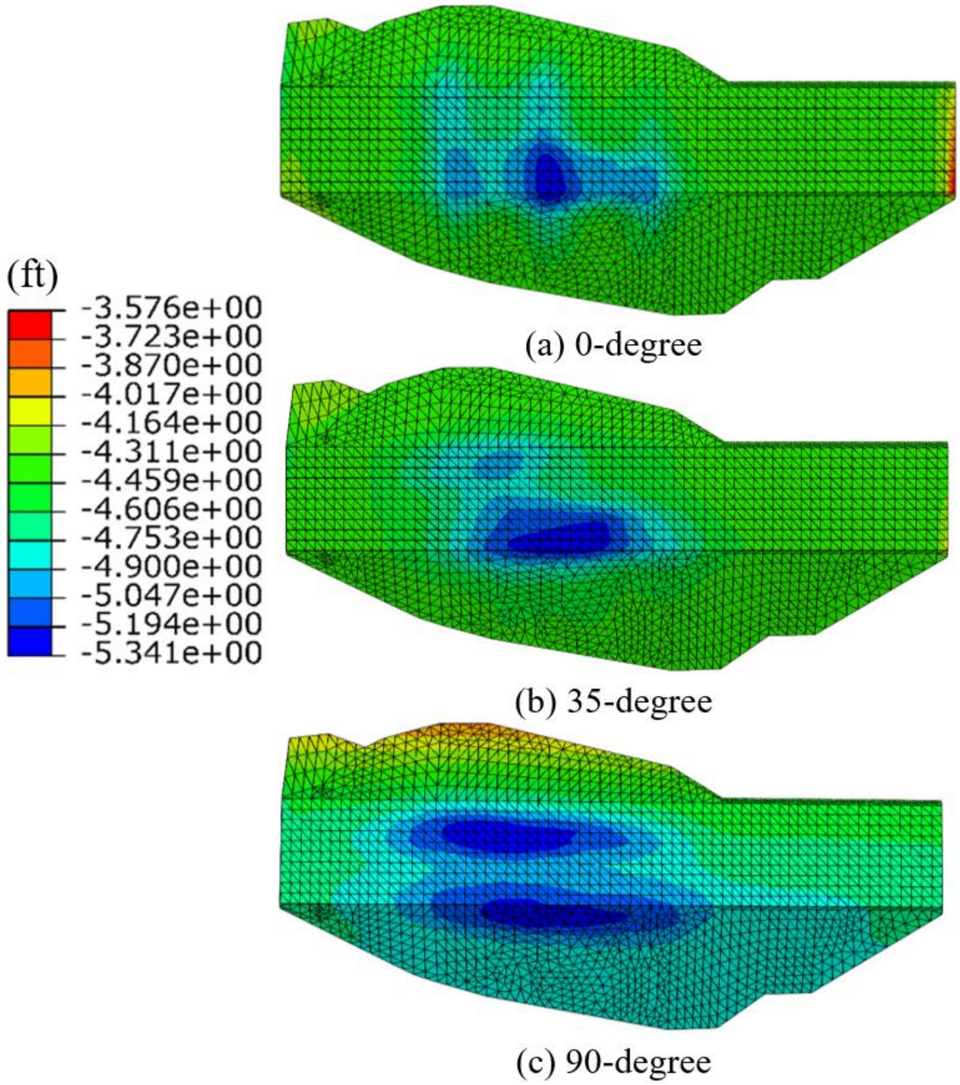

Figure IVa.12 – The vertical subsidence on Embankment #1 when the angle between the orientation of highway and mining is (a) 0-deg; (b) 35-deg and (c) 90-deg

2.2 Slope Stability Analysis

Plastic strain which represents the failure was plotted at each case of the orientations at the critical cross sections in Embankment #1 shown in Figure IVa.13. The shear strength reduction factors were set to be equal to one. Higher plastic strains develop on the top of the embankment when the direction of the longwall mining is at 0-deg with respect to the long axis of the embankment (direction of the highway). When the direction of mining is inclined at 35-deg with respect to the long axis of the embankment, large plastic strains exist on the bottom of the embankment. For the case of 90-deg direction, larger plastic strain developed inside the embankment, which contributes to the local deformations and failure in the embankment. These large strains developed in the finite element method stability of the embankment causes the model to stop its calculations. The analysis cannot be keep running in the normal way unless the SRM is applied.

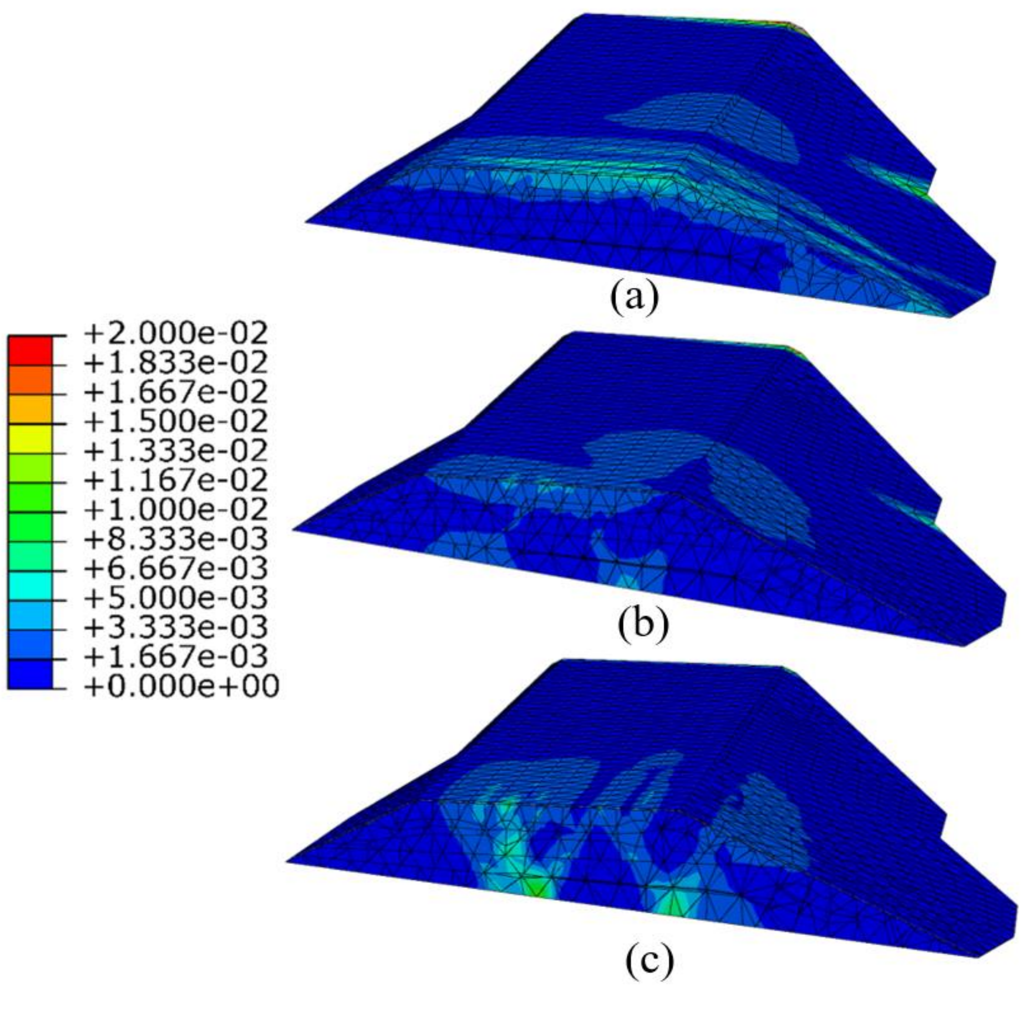

Figure IVa.13 – Plastic strain at the critical cross section of Embankment #1 when the angle between the orientation of highway and mining is (a) 0-deg; (b) 35-deg; and (c) 90-deg with SRF equals to one

The factor of safety in each case of orientation was obtained using shear strength reduction method (SRM) as illustrated in the previous sections. The ranges of the final factor of safety with respect to different orientations of longwall are shown in Figure IVa.14. The factor of safety decreases in value as the direction of mining with respect to the embankment increases in value. For the 90-deg case, the lower bound of the factor of safety was less than one, which is consistent with the large amount of plastic strain inside the embankment.

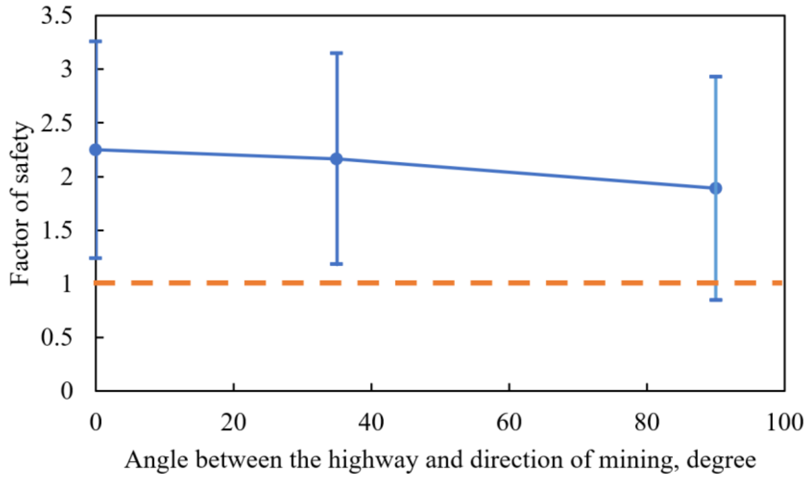

Figure IVa.14 – Factor of safety for Embankment #1 at different angles with respect to the mining direction

The failure mechanism for the 90-deg case is shown in Figure IVa.15. Shear band did not form at the SRF of equal to 1 and the embankment did not experience large deformations. However, local parts of the embankment are creeping in the center of two large zones of plastic strain, which will induce settlement of the highway embankment. Some lateral spreading was also observed on the side of the red arrows, forming a bulge on the adjacent slope.

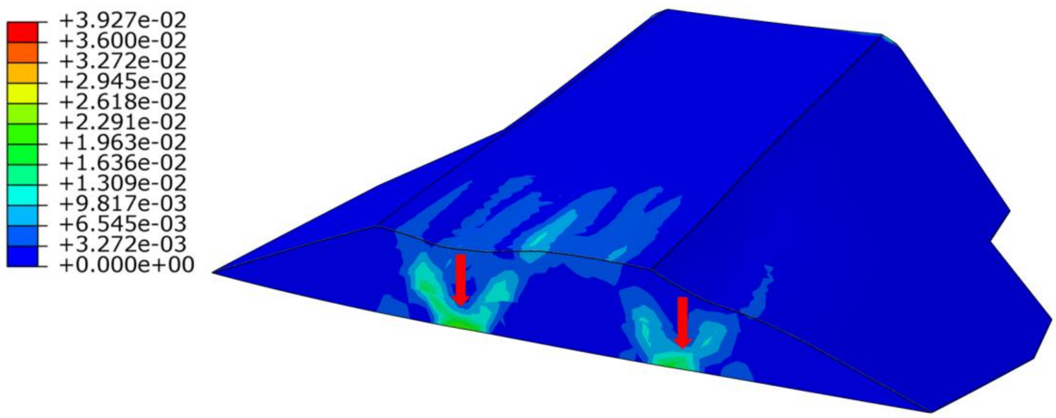

Figure IVa.15 – Plastic strain and deformations inside Embankment #1 when subjected to longwall mining at an angle of 90-deg

3.0 Influence of Overburden

Embankment #1 was subjected to longwall mining subsidence with different overburden values that included 400, 500, 600 and 675-ft. The vertical subsidence on the embankment changed depending on the overburden values. Also, the slope stability analysis was conducted and the factor of safety was calculated using SRM for each case of the overburden values.

3.1 <u>Deformation Analysis</u>

Deformation analysis was conducted based on the longwall mining orientation of 35-degrees. The vertical subsidence on the embankment is plotted in Figure IVa.16 considering different overburden values. This figure shows that the magnitude of the maximum vertical subsidence decreases as the overburden value increases.

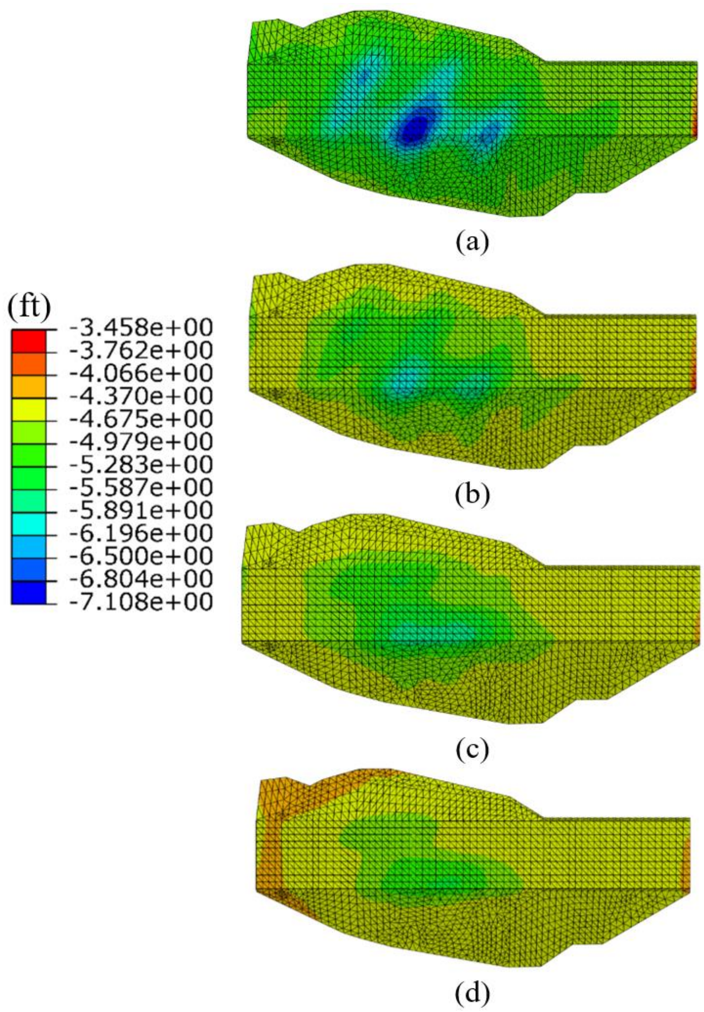

Figure IVa.16 – Final vertical subsidence on Embankment #1 subjected to longwall mining with different overburdens of a) 400-ft; b) 500-ft; c) 600-ft; and d) 675-ft

The movement on the ground below the embankment was predicted for different overburdens as shown in Figure IVa.17. The maximum subsidence increases as the overburden decreases in value. Also, the slope of the subsidence contour increases as the overburden decreases in value. The ground movement beneath the embankment, the total subsidence at the surface of the embankment, and the settlement of the embankment are summarized in Table IVa.3. The subsidence of the embankment itself was calculated by subtracting the ground subsidence from the total subsidence. The embankment subsidence, that is, the settlement in the embankment was plotted against the overburden values. This plot is shown in Figure IVa.18. It was determined that the settlement of the embankment decreases as the overburden increases.

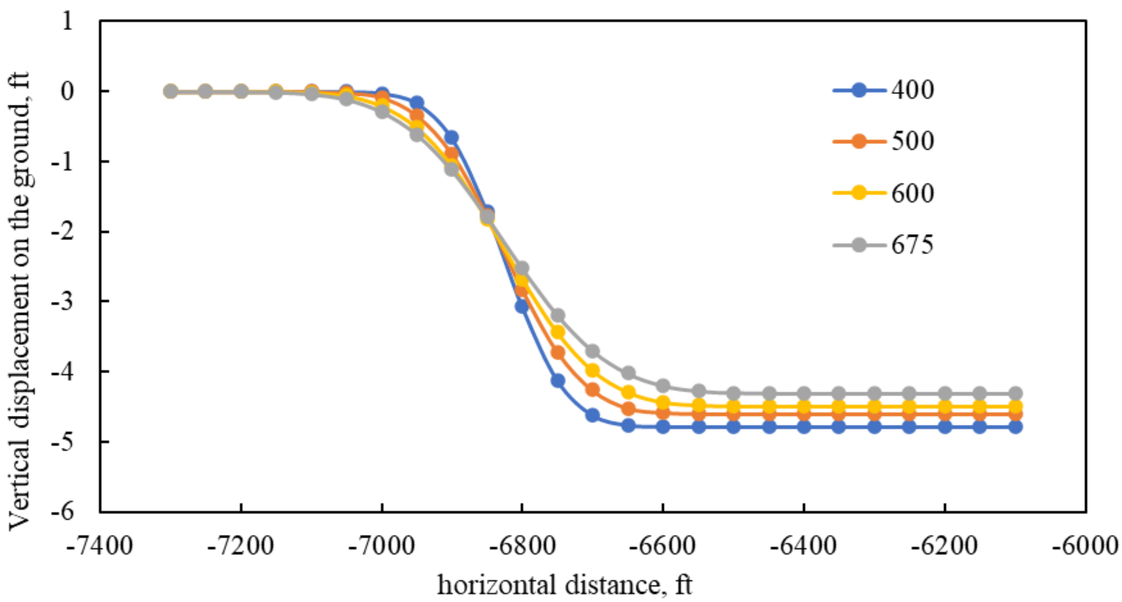

Figure IVa.17 – Influence of overburden on surface subsidence profiles

Table IVa.3 – Calculation of the settlements in the embankment with different overburdens

Overburden, ft	**Ground subsidence beneath the embankment, ft**	**Total subsidence at the surface of the embankment, ft**	**Approximately maximum embankment settlement, ft**
675	4.3	5.	1.0
600	4.5	5.8	1.3
500	4.6	6.1	1.5
400	4.8	7.1	2.3

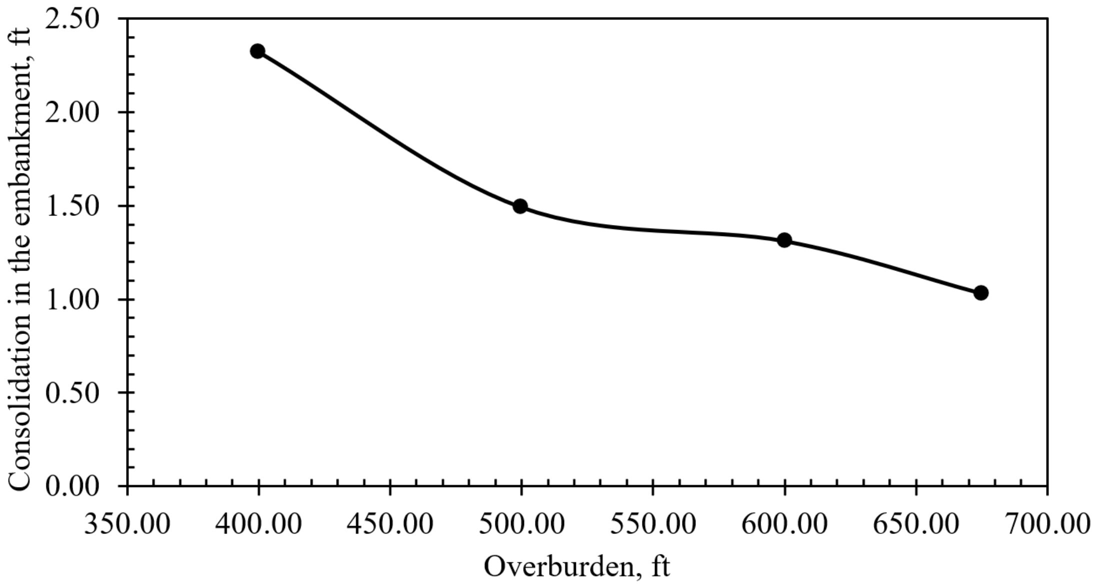

Figure IVa.18 – Variation of the settlement in the embankment with different overburdens

3.2 Slope Stability Analysis

Four overburden levels were considered to explore their influence on the slope stability of a highway embankment. The analysis was conducted when the longwall mining is at an angle of 35 and 90-deg with respect to Highway I-70 (or long axis of the embankment). A detailed analysis of the 0-deg case was not carried out. The reason being, that this orientation was considered to be non-critical for the stability of the embankment.

3.2.1 *Embankment #1 Subjected to Longwall Panel Extraction at an Orientation of 35-deg with respect to the Highway*

The slope stability analysis was conducted on Embankment #1 when it is subjected to longwall mining at an angle of 35-deg. Plastic strains inside the embankment for different overburden levels when the SRF equal to one are shown in Figure IVa.19. This figure shows that a larger overburden generates lower plastic strain inside the embankment. Also, for the case of a 400-ft of overburden, the plastic strain develops from the bottom of the embankment and continues toward its top. As a result, the parts of the embankment that develop these plastic strain zones will experience settlement as shown in the deformation analysis.

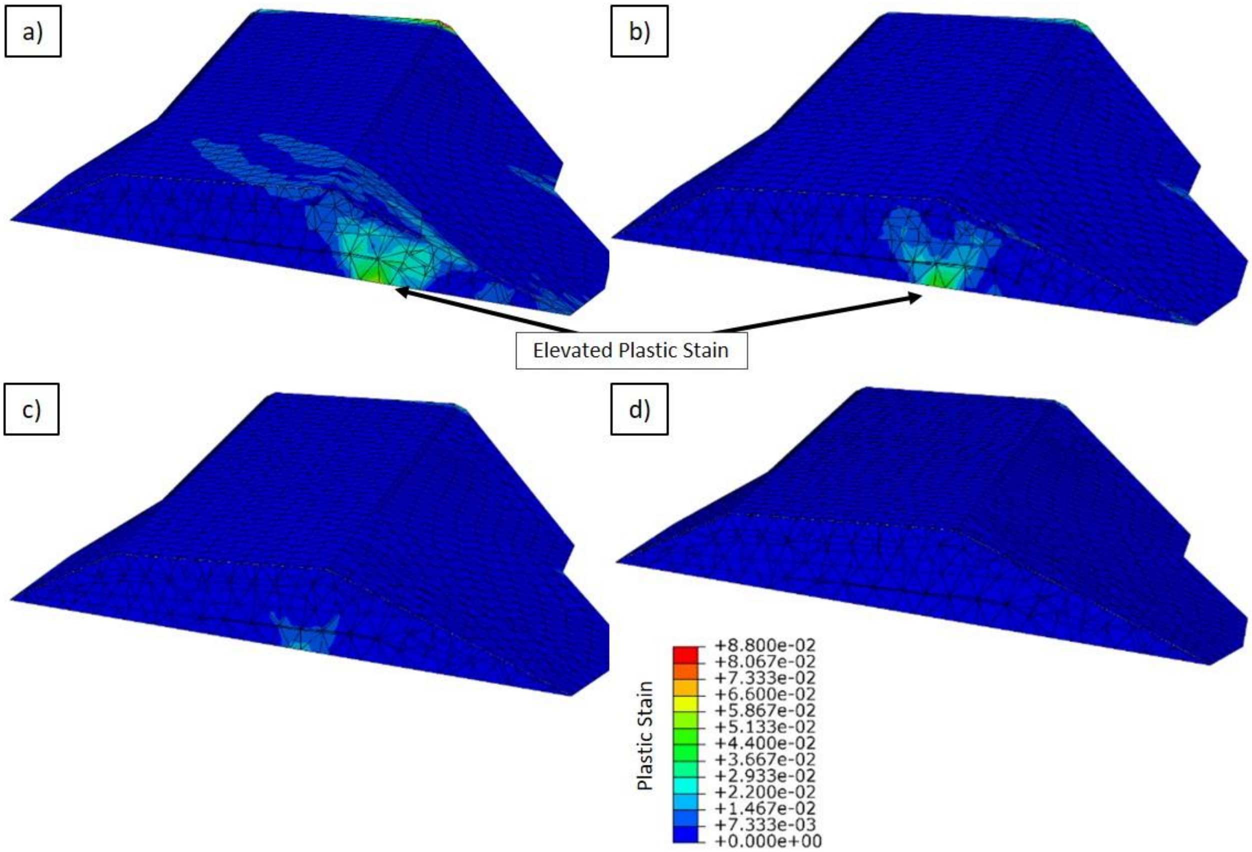

Figure IVa.19 – Plastic strain inside Embankment #1 due to longwall mining with different overburdens of a) 400-ft, b)500-ft, c)600-ft, and d)675-ft at an angle of 35-deg with respect to the highway

The resulted factor of safety range for these four cases of overburdens were plotted in Figure IVa.20. The factor of safety increases as the overburden increases in this case of 35-deg. For case of 500-ft and 400-ft, the lower bond of the factor of safety is above and below one, respectively. The plastic strain in the embankment for the case of 400-ft almost penetrates the embankment. While for the case of 500-ft, the plastic strain only exists on the bottom. The difference in the distribution of the plastic strain is consistent with the difference in the factor of safety.

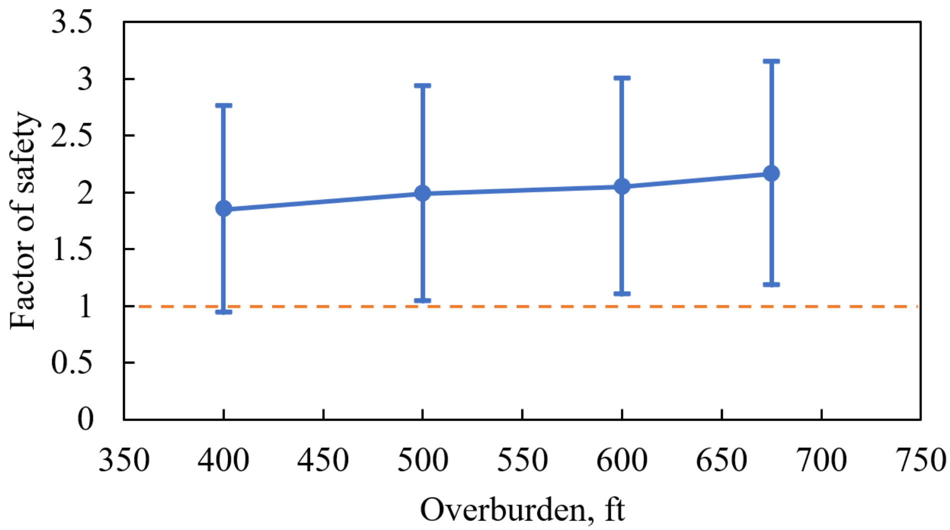

Figure IVa.20 – Influence of overburdens on the factor of safety of Embankment #1 at the orientation of 35-deg with respect to the longwall mining

3.2.2 *Embankment #1 Subjected to Longwall Panel Extraction at an Orientation of 90-Deg with Respect to the Highway*

Lastly, a slope stability analysis was conducted on Embankment #1 when it is subjected to a longwall mining at an angle of 90-deg. Plastic strain inside the embankment was plotted with different overburdens in Figure IVa.21. A larger overburden generates lower plastic strain inside the embankment. All cases present plastic strain inside the embankment.

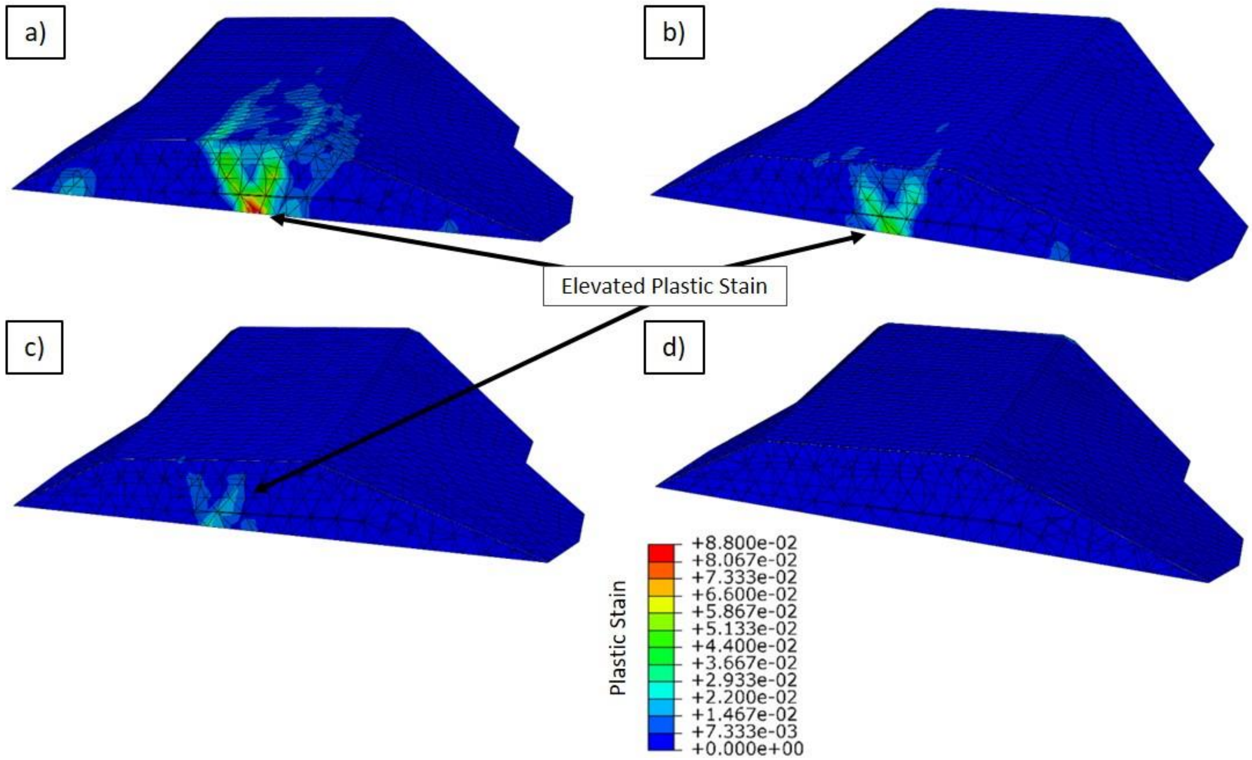

Figure IVa.21 – Plastic strain inside Embankment #1 due to longwall mining with different overburdens of a) 400-ft; b) 500-ft; c) 600-ft; d) 675-ft at an angle of 90-deg with respect to the highway

The resulting factor of safety range for these four cases of overburden levels are plotted in Figure IVa.22. This figure shows that the factor of safety increases as the overburden increases in value. For cases of 500-ft and 400-ft of overburden, the lower bound of the factor of safety is much lower than one. For cases of 600-ft and 675-ft of overburden, the lower bound of the factor of safety is a little bit lower than one. The plastic strain in the embankment for the cases of 400-ft and 500-ft of overburden almost completely covers the whole embankment (Figure IVa.21). While for the cases of 600-ft and 675-ft, of overburden the plastic strain only develops at the bottom (Figure IVa.21). The differences in the distribution of the plastic strain is consistent with the differences in the factor of safety.

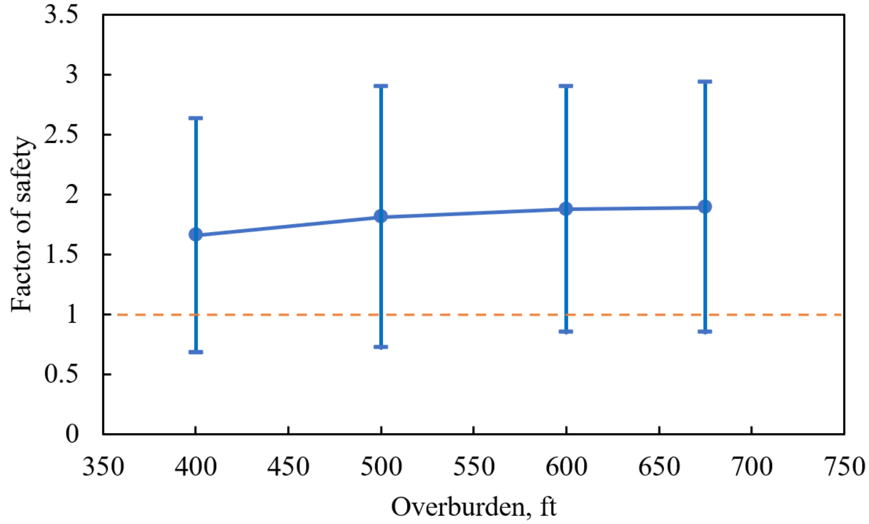

Figure IVa.22 – Influence of overburdens on the factor of safety of Embankment #1 at the orientation of 90-deg with respect to the longwall mining

4.0 Discussion (A method for estimating orientation and overburden influences on embankments)

Two parameters, direction of mining, and overburden levels were considered when constructing a chart that shows their influence on the factor of safety for the case of Embankment #1. For developing this chart, three directions of longwall mining were considered. Also, four overburden levels were considered for each case of the direction of mining. Thus, to develop these charts, a total of twelve cases were analyzed. For the mining at an orientation of 0-deg, the factor of safety results considering the four overburdens is shown in Appendix II, which is similar to the case of 35-deg discussed in the last section.

As illustrated in this study, the embankment will experience initial, limited deformations at the lower bound of the factor of safety. At large deformation levels in the embankment, when a shear band completely develops, the upper bound factor of safety is in effect. This factor of safety was equal to the traditional factor of safety obtained using the SRM. The upper bound of the factor of safety indicates if the embankment will develop large deformations. All the upper bounds of the factor of safety are much higher than lower bounds of the factor of safety. The lower bounds factor of safety indicated that plastic strains were small and of limited extent inside the embankment. However, it does not mean the embankment is stable. Some limited deformations were observed in the embankment when using the FEM and which were validated by field observations. In addition, the embankment experienced settlement at the regions experiencing high but limited plastic strain. Consequently, to be conservative, the lower bound factor of safety was utilized to identify whether the embankment is stable. The lower bound factor of safety was used when developing the chart that can be used to analyze embankment behavior under longwall mining-induced subsidence.

The lower bound (conservative) factor of safety for each of the twelve cases analyzed are depicted in Table IVa.4. The full plot relating the factor of safety versus overburden levels and directions of longwall mining is shown in Figure IVa.23. This chart shows the boundaries for the case of small, medium and large deformations in function of the lower bound factor of safety, the direction of mining, and the overburden level. The factor of safety can be calculated using this figure if the orientation and the overburden are known. It should be noticed that this model assumes that the embankment is in the center of the panel. Also, the shear parameters of the soil forming the embankment is enhanced by a factor of 1.3 considering the influence of gravel on the shear strength of the soil forming the embankment, as well as the viscosity mobilized in the embankment during subsidence. In addition, the original slope of the embankment was assumed to be equal to 1:2 (26-deg).

Table IVa.4 – Critical Factor of Safety for Embankment #1 subjected to longwall mining with different overburdens and orientations

	Highway orientation with respect to mining direction		
Overburden	**0-deg**	**35-deg**	**90-deg**
400-ft	0.98	0.94	0.68
500-ft	1.06	1.04	0.72
600-ft	1.16	1.12	0.85
675-ft	1.24	1.18	0.85

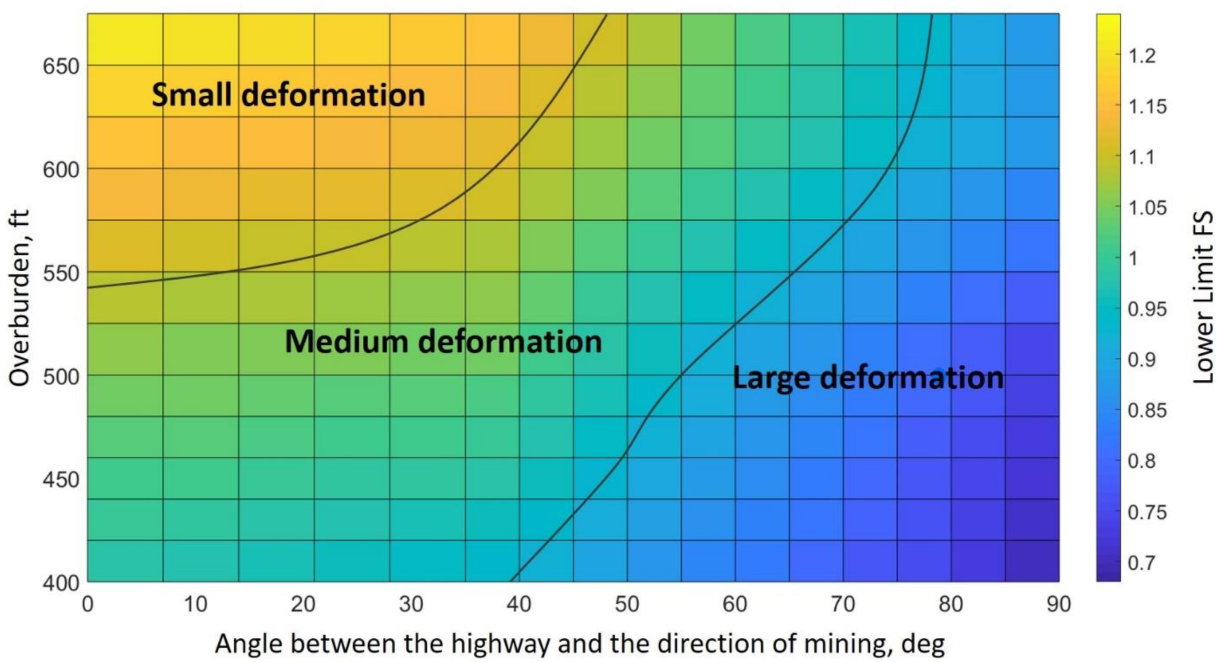

Figure IVa.23 – Chart for the behavior of the embankment located in the center of the panel using lower bound factor of safety values, overburden and direction of mining levels

Subsection IVb – Analysis of Embankment #5

As discussed in Section III, Embankment #5 is an asset within the extended study area that has the potential to be adversely impacted by undermined of I-70 in the future. Because of this potential, the University performed a detailed Finite Element Analysis (FEA) to better understand how Embankment #5 will react to undermining. This FEA draws heavily on model properties previously established for Embankment #1 (Task 2 Report, Section V – Embankment Behavior).

1.0 Embankment #5 Geology and Material Properties

As previously discussed in Section IIIa of this report, Embankment #5 is within the mid-panel area of projected Panel C (Figure IVb.1). The overburden in this area average approximately 500-ft. The orientation between the highway and the direction of future mining is 79-deg. Embankment #5 is expected to be more impacted by the formation of the subsidence basin than Embankment #1. Both embankments are similar in shape and thickness and are located mostly within the mid-panel area. However, projected Panel C is 175-ft closer to I-70 and the highway is more closely aligned with the advancing longwall face. In addition, two three-span overpasses and one significant culvert are attached to the embankment.

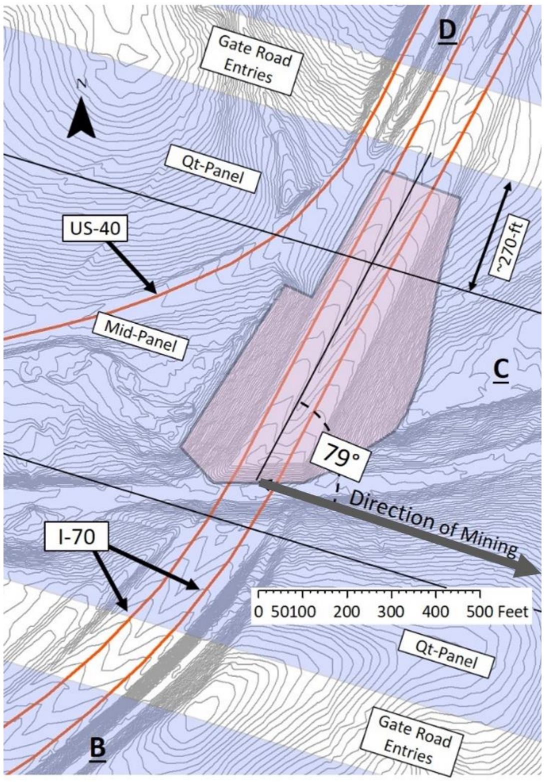

Figure IVb.1 – Location of Embankment #5 within the mid-panel area of projected Panel C

Based on the topographic surface shown in Figure IVb.1, the geometry of Embankment #5 is determined to be 428-ft wide and 770-ft long (Figure IVb.2). Borings recently drilled by PennDOT found the embankment to have a maximum thickness of 70-ft (Section IIIa). The slope on the north and south is 1:2 (26-deg), which is identical to the slopes of Embankment #1. The cross section is generalized from the three borings located within Embankment #5 shown in Figure IVb.3. The soil profiles found in Embankment #5 are similar to those in Embankment #1. It is thought that similar construction methods were used for both embankments.

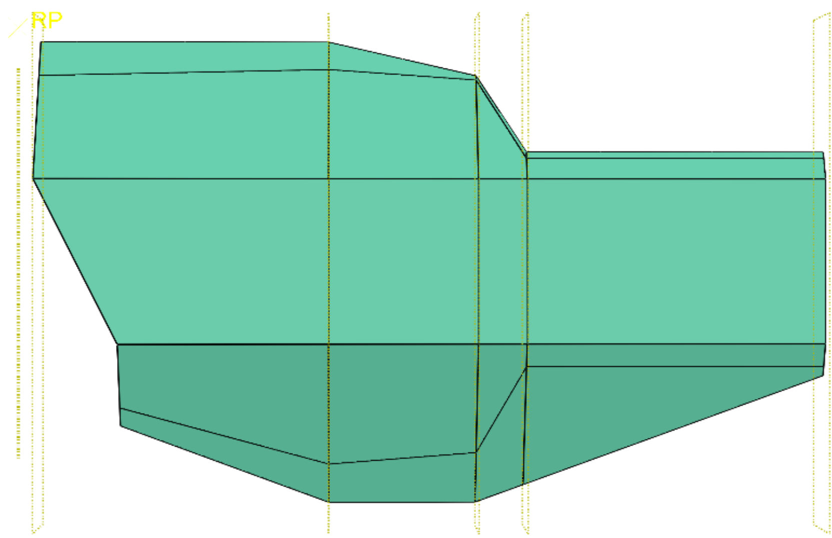

Figure IVb.2 – Overview of the three-dimensional FEA of Embankment #5

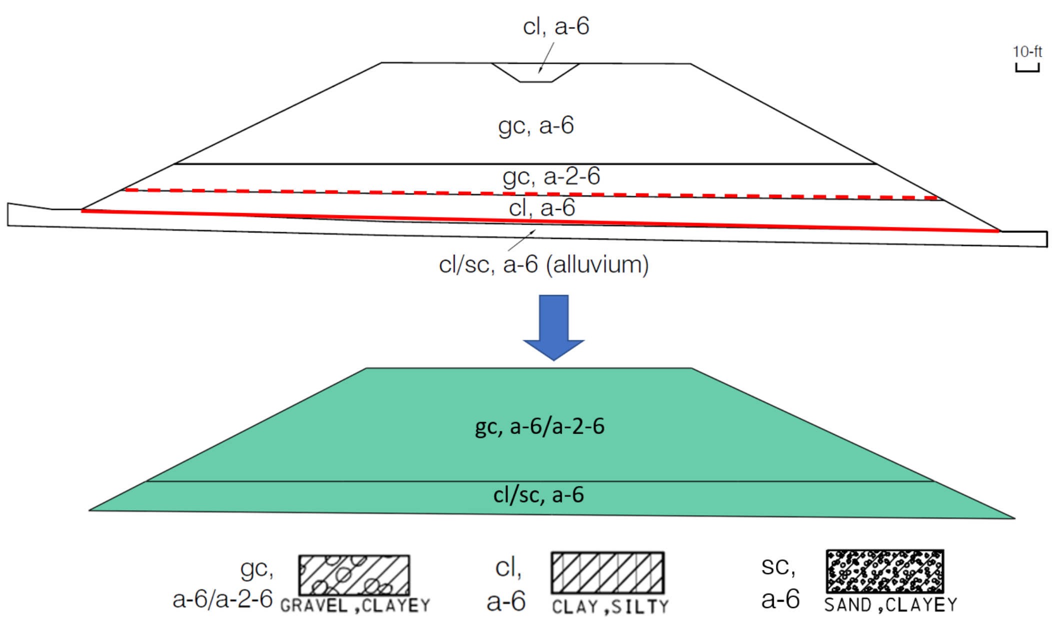

Figure IVb.3 – Configuration of the simplified layered Embankment #5 at cross section 92+25

Triaxial compression tests were conducted on the soil sample located at the depth of middle of the upper layer. It should be noticed that these tests are conducted on soil samples where the largest rock particles have been removed due to testing restriction. To compensate for this, the average material properties were adjusted based on the influence of the rock ratio on the shear strength of soil. The resulted material properties were summarized in Table IVb.1. It was found that a strength reduction factor of 0.75 produced an increase shear strength that adequately compensated for the influence of large particles found in the embankment but removed during testing. In this case, the shear strength of soil is increased by 30-pct.

Table IVb.1 – Material properties of the two layered FE model of Embankment #5 considering the influence of the rock ratio on the shear strength of the gravels

Layer	**Soil Type**	**AASHTO**	**Depth, ft**	**C, psf**	**Φ, deg**
Upper	Clayey gravel	a-2-6/a-6	0-60	785	42
Lower	Clay/Clayey sandy	a-6	60-70	775	41

Underneath Embankment #5, a regression model of the vertical subsidence basin (denoted by rectangles) fitting a Surface Deformation Prediction System (SDPS) model (denoted by blue dots) with an overburden of 500-ft was constructed using the Richard's model shown in Figure IVb.4. It was implemented into the Finite Element Model (FEM) of Embankment #5. The maximum subsidence of the ground surface is 4.6-ft which is slightly higher than 4.3-ft predicted for Embankment #1.

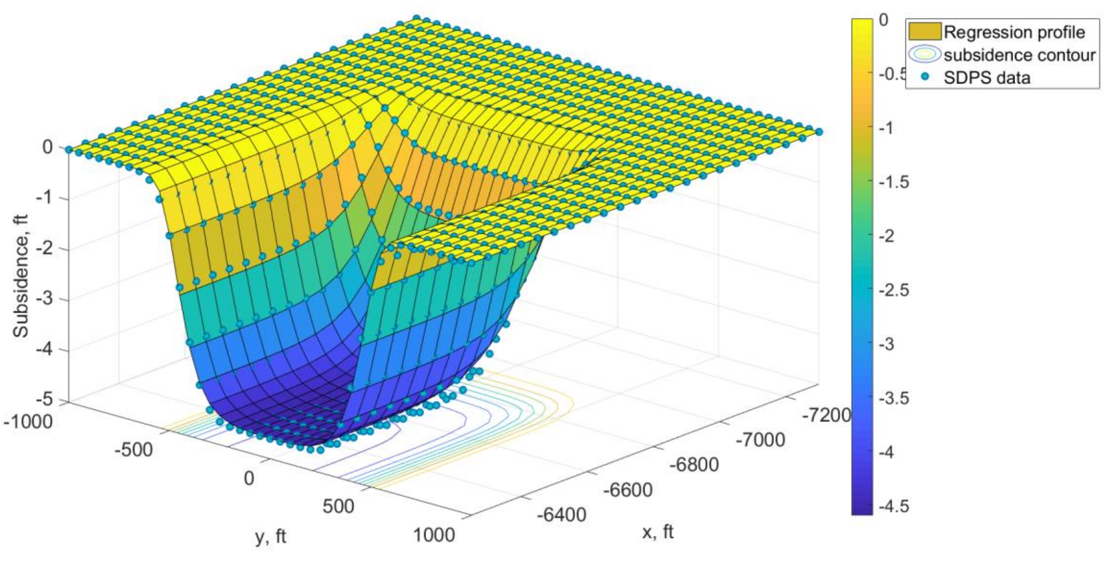

Figure IVb.4 – Regression model of the subsidence basin with an overburden of 500-ft. (The SDPS profile with topography is denoted by the blue solid circles; the numerical regression profile with topography is denoted by colored rectangles)

2.0 Deformation Analysis

The deformation analysis of Embankment #5 was conducted using the working face positions summarized in Figure IVb.5. The regression model of subsidence introduced above was applied on the bottom of the embankment in the form of displacement. The coordinate system of the embankment in the FEM and the subsidence in the regression function are correlated using the transformation equations.

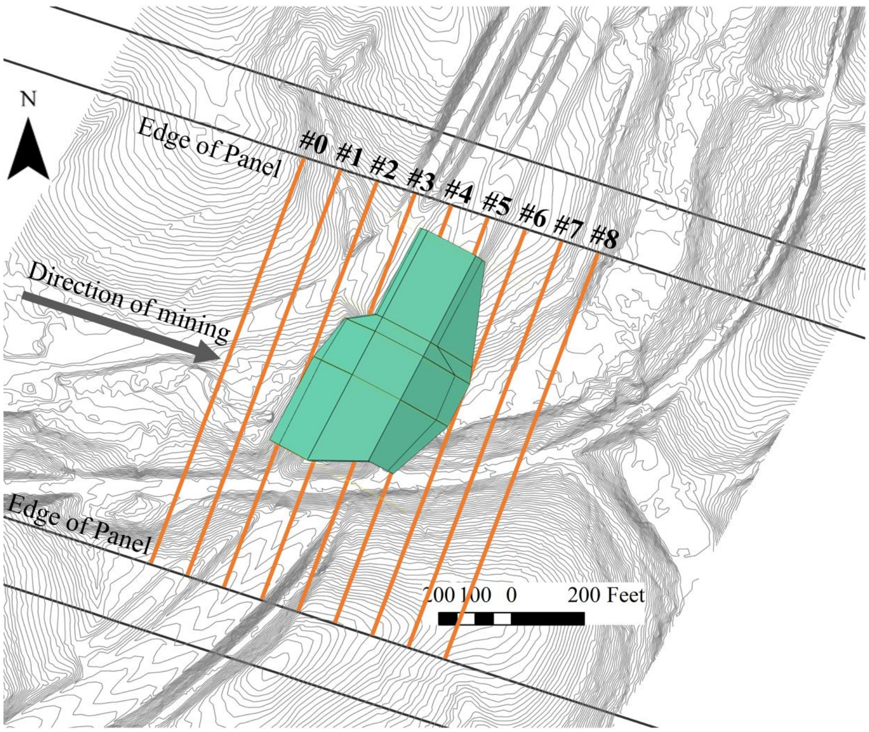

Figure IVb.5 – Working face positions under Embankment #5

The vertical displacement contours were plotted on Embankment #5 with selected working face positions shown in Figure IVb.6. The displacement is quite small at working face position #0. When the working face is at the middle of the embankment, the soil at the crest of the south slope moves apart perpendicular to the highway direction. The local depression in the form of a sinking region is shown in a light blue color. This region is located in the center of the edge of the east bound lane along the highway. When the working face passes the embankment, the top of the embankment experiences a settlement of about 7.6-ft at two different regions shown in Figure IVb.6d). Such deformations can be considered significant and can produce damage to the embankment structure.

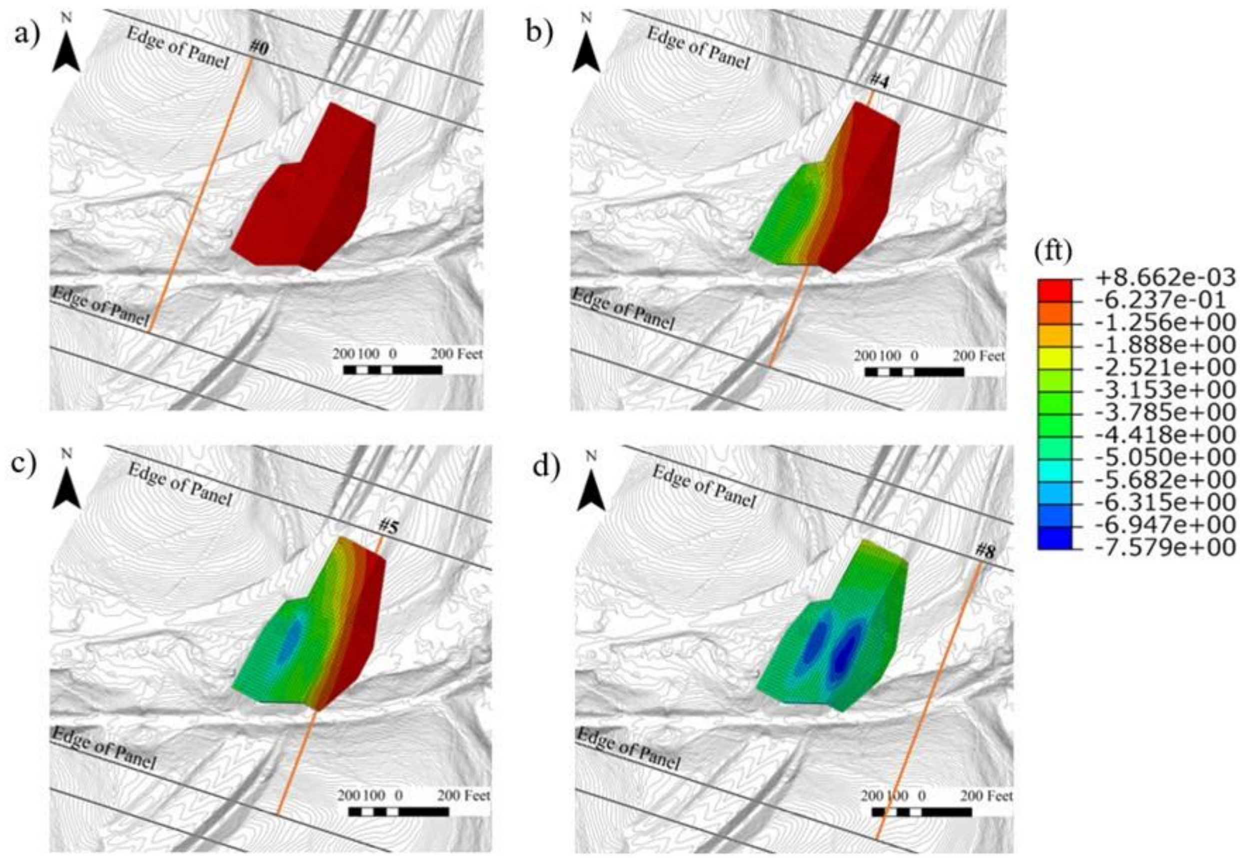

Figure IVb.6 – Vertical displacement on Embankment #5 with working face positions a) #0, b) #4, c) #5, and d) #8

Interior tensile strain was plotted in Figure IVb.7b) to explain how the subsidence influence the deformation of the embankment shown in Figure IVb.7a). After the embankment is subjected to successive stages of subsidence, tensile strains developed beneath the crest of the southern slope and the middle of the west bound lane, forming a 'V' shape tension zone. These regions with higher tensile strain correspond to the vertical deformations at the top. The region at the middle of the west bound lane and the southern crest will experience large concentrated settlements induced by longwall mining-induced subsidence.

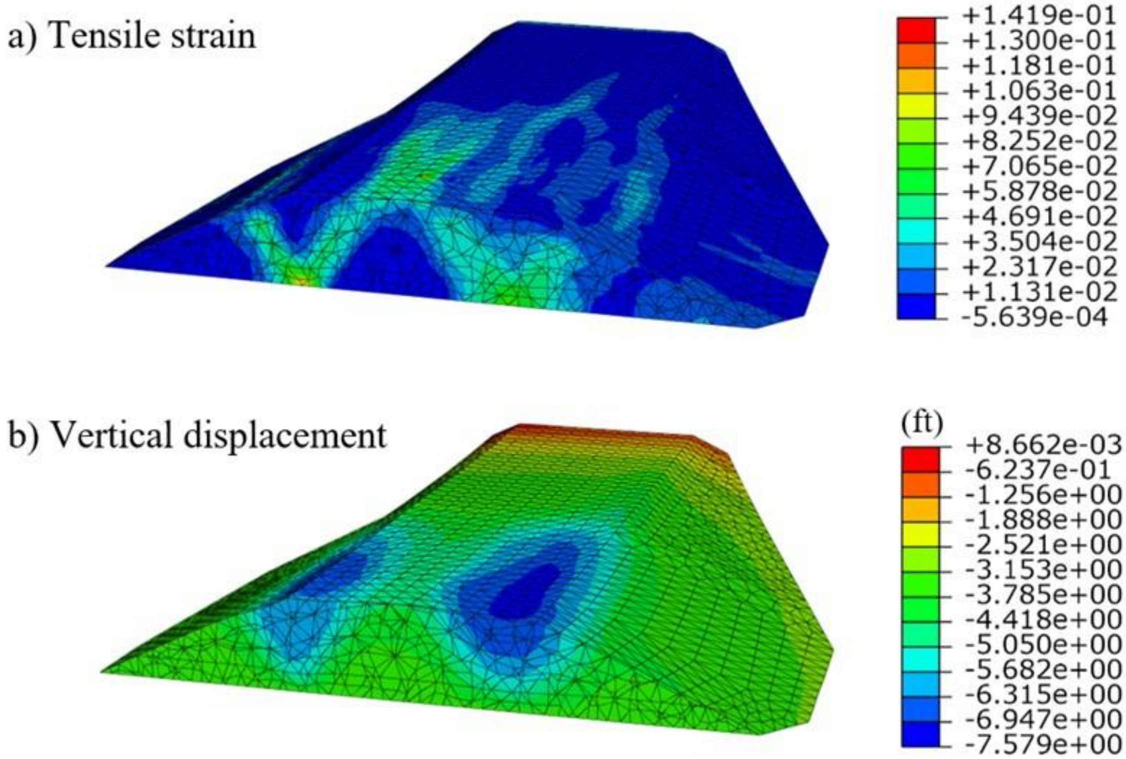

Figure IVb.7 – a) Principal tensile strain and b) Vertical displacement inside Embankment #5 after subsidence

3.0 Slope Stability Analysis

The SRM introduced in Section IVa was utilized to find the potential critical part as well as the factor of safety of Embankment #5. The results will be compared to that obtained using the orientation and overburden model obtained in Section IVa.

3.1 Potential Critical Cross-Section

Centrifuge tests have indicated that the plastic shear strain zone in unstable slopes coincides with the rupture surface (Roscoe, 1970). The university utilized SRM to make the embankment collapse and identify the critical area with the higher plastic shear strain. The critical area was utilized to conduct the factor of safety analysis in the next section. The magnitude of the plastic strain in the embankment at the final point of SRM when a complete sliding failure happened is plotted in Figure IVb.8. The contours resulted from four steps of successive subsidence. It is shown that the critical cross section was located on the north facing slope in the middle of the longitudinal length of the embankment staying at the same location during the successive subsidence.

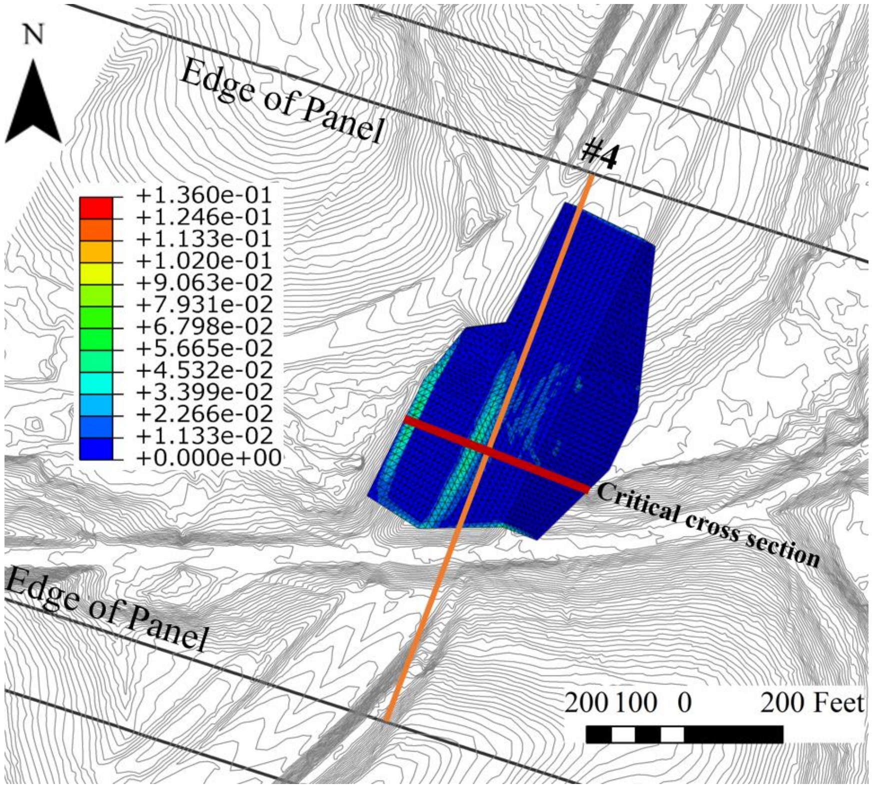

Figure IVb.8 – Critical cross section for the factor of safety analysis taking working face position #4 as an example indicated by the magnitude of plastic shear strain

3.2 Factor of Safety

As discussed in Section IVa, the factor of safety is obtained using SRM which utilizes the SRF to reduce the cohesion and $tan\phi$ until the embankment failed. Total displacement is plotted against the SRF to estimate the factor of safety. The knee point, which represents failure of the slope, is found to be equivalent to the factor of safety when using the LEM (Dawson, 1999).

Figure IVb.9 shows the determination of the factor of safety of the embankment with working face position #0 (under gravity). The plastic strain inside the embankment at the critical cross section with SRF equal to 2.8 is shown in Figure IVb.10. The shear band reaches the top of the embankment and a complete rupture surface is formed when SRF reaches the knee point.

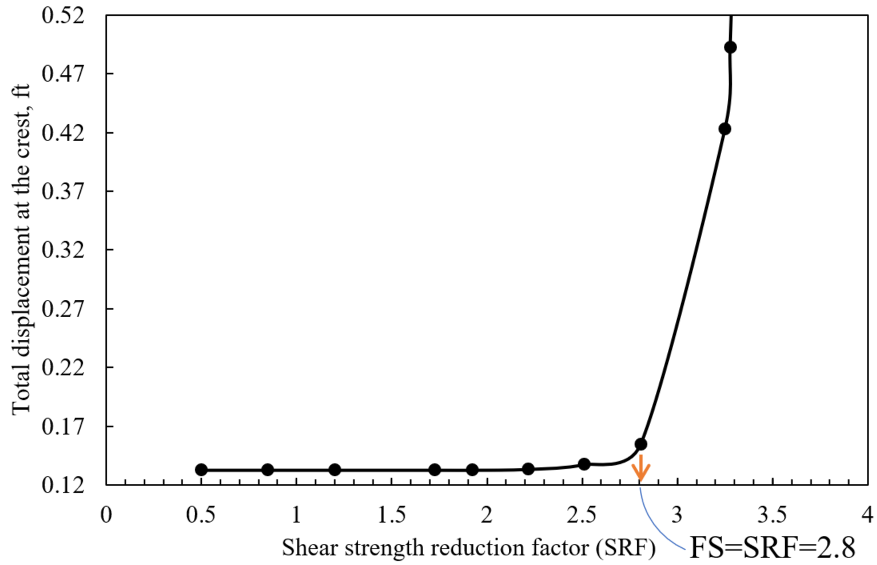

Figure IVb.9 – Determination of the factor of safety of Embankment #5 under gravity

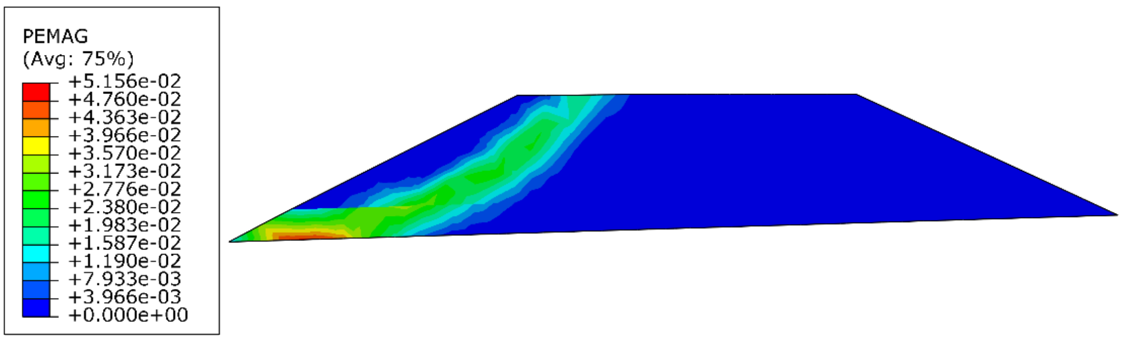

Figure IVb.10 – Potential plastic shear strain at the critical cross section in Embankment #5 using SRM with SRF equals to 2.8

Then the factor of safety of the embankment subjected to subsidence was determined in Figure IVb.12. In this case, more deformation was observed before the knee point. The same methodology introduced in Section IVa using a lower and upper bound of the factor of safety was applied to characterize the slope stability of Embankment #5.

The critical factor of safety occurred when the longwall working face was located under the middle of embankment with working face #4 shown in Figure IVb.11. Figure IVb.12 indicates that the lower bound factor of safety was found to be 0.8. Before this point, the displacement increased at a relatively low rate. After this point, the embankment presented the initial deformations. The upper bond factor of safety was found to be 2.8, where the total displacement started to increase exponentially and the complete shear band developed.

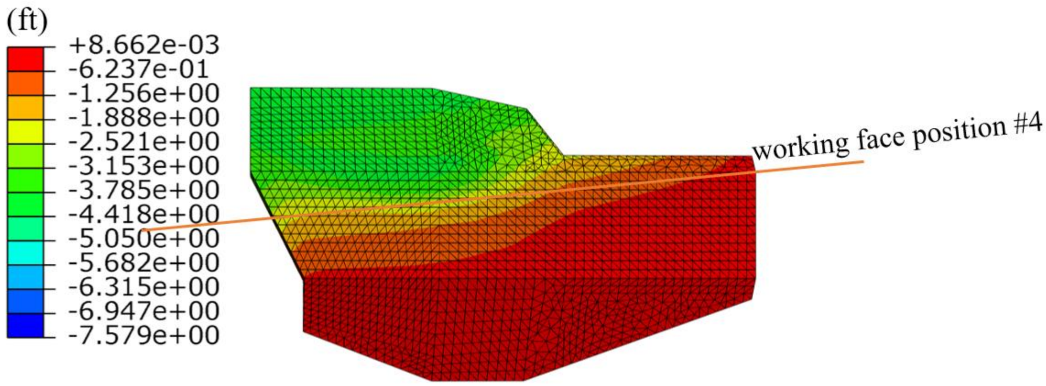

Figure IVb.11 – Embankment #5 subjected to subsidence from a developing longwall panel with working face position #4

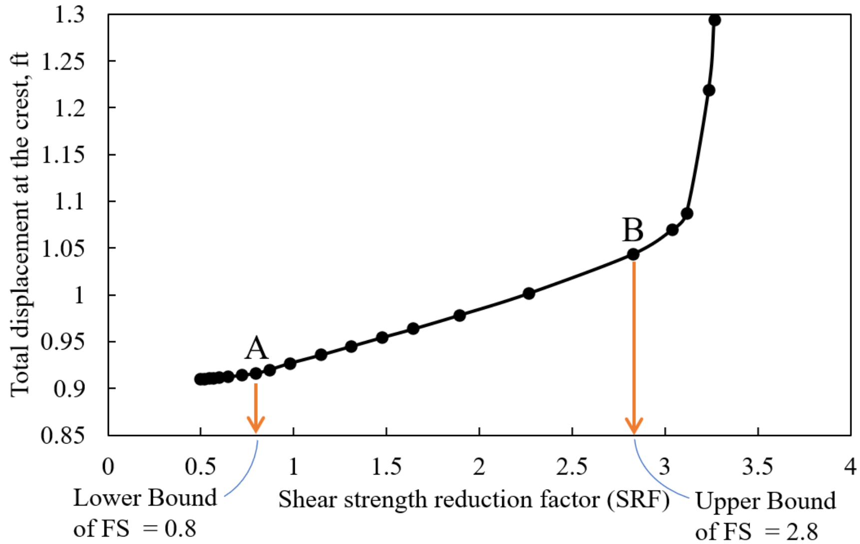

Figure IVb.12 – Total displacement at the crest of the critical cross section in Embankment #5 versus the shear strength reduction factor for the case with working face position # 4

The plastic strain as well as the horizontal displacement are plotted in Figure IVb.13 and IVb.14, respectively. At the lower bound factor of safety (critical factor of safety), where the plastic strain initiates, small deformation happens. At the upper bond factor of safety, shear band completely forms in the north-facing slope, resulting in large deformation within the embankment.

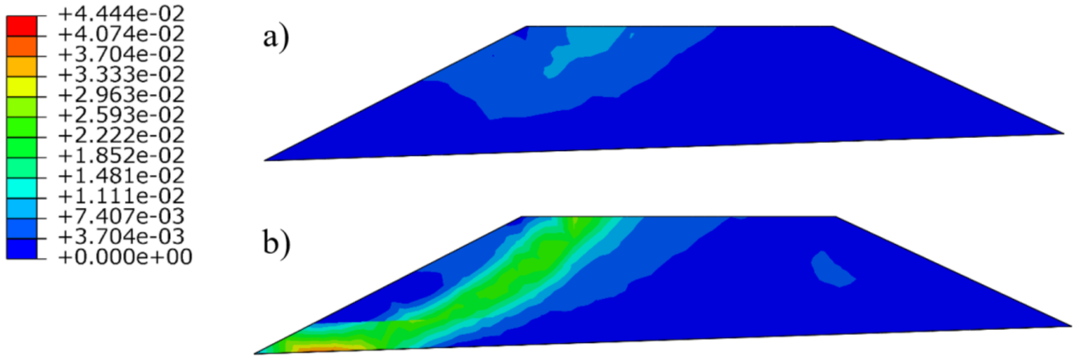

FigureIVb.13 – Plastic shear strain at the critical cross section when SRF equals to a) 0.8 and b) 2.8

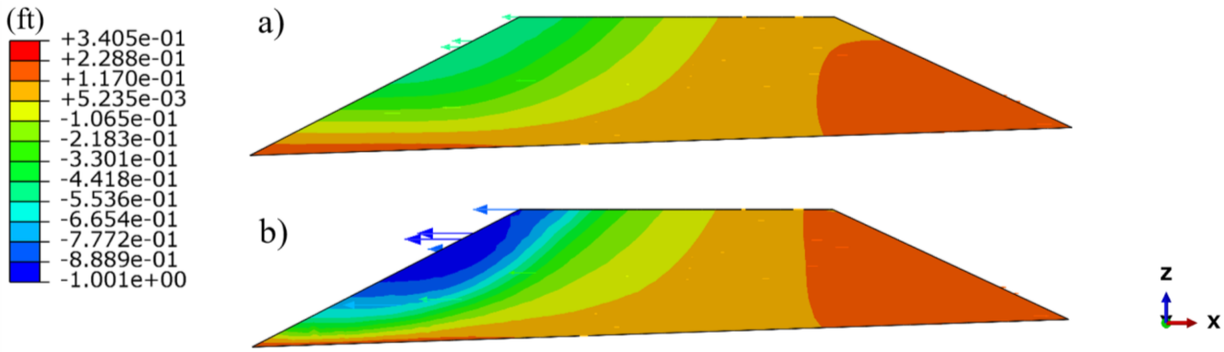

FigureIVb.14 – Horizontal displacement at the critical cross section when SRF equals to a) 0.8 and b) 2.8

Figure IVb.15 indicates the factor of safety of Embankment #5 calculated at different working face positions (see Figure IVb.5). At working face position #0, the factor of safety is much higher than one, which means it is quite safe before subsidence. In the critical stages of subsidence with working face position #3 and #4, the lower bound of factor of safety is 0.8, indicating that the embankment will experience the significant deformations. However, the plastic shear strains are of limited extent since that the upper bound of factor of safety is still higher than one.

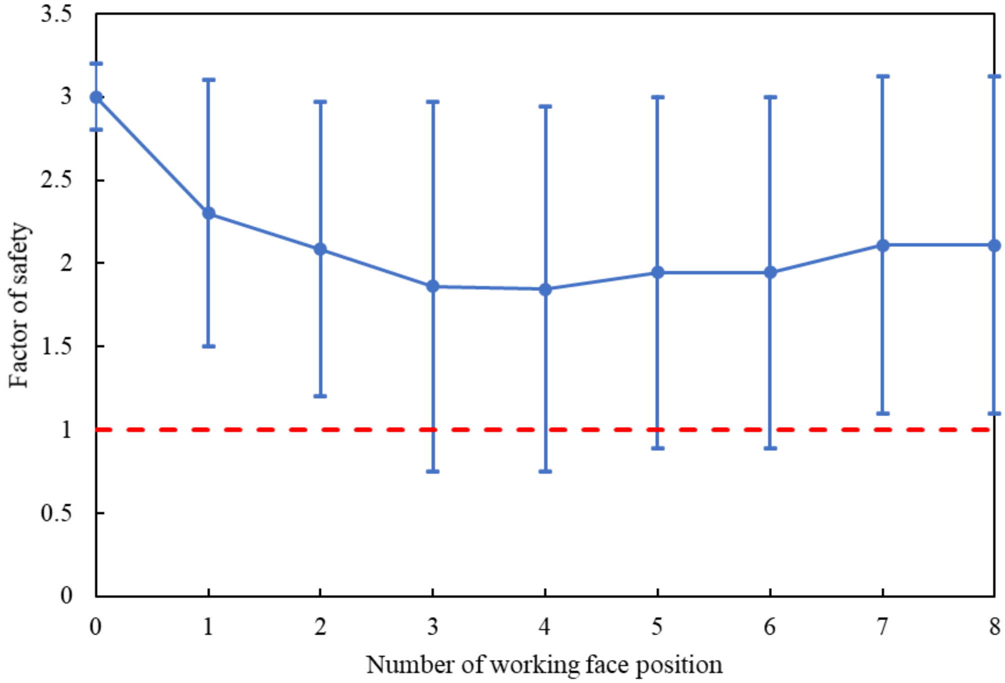

Figure IVb.15 – Factor of safety for Embankment #5 subjected to subsidence with different working face positions

Although Embankment #5 will be we relatively stable during subsidence, it will experience significant deformations affecting detrimentally the geometry of the embankment. Soil will settle in the embankment as much as 7.6-ft, forming a longitudinal sink at the crest of the southern slope and in the middle of west bound lane. A bulge was also caused on the slope by the basin at the crest. These levels of deformations can make significant changes to the geometry of the embankment, especially on the top.

3.3 <u>Sensitivity Tests of the Shear Parameters on the Slope Stability of Embankment #5</u>

Sensitivity tests were conducted for the slope stability of Embankment #5 using the jointly random shear parameters. The triaxial compression test was conducted only on one soil sample on Embankment #5. The material properties were assumed to be same as the well calibrated Embankment #1. However, there is possibility that the shear strength parameters may differ from those utilized in Embankment #1. Sensitivity tests were conducted on Embankment #5 by using different values of the cohesion (c) and tan ϕ assuming their values are jointly random variables. Random values of c and tan ϕ were generated with correlations using the Monte Carlo method introduced by Griffith (2004; 2008; 2012).

First, two independent random values were generated from the standard normal distribution $N(0,1)$ using the random number generators in spreadsheet. Then, these two independent random values from the standard normal distribution were utilized to generate the jointly random c and $\tan\phi$ using Eq. IVb.1.

$$c = \mu_c + X * \sigma_c$$
$$\tan\phi = \mu_{\tan\phi} + \left(X * \rho + Y * \sqrt{1-\rho^2}\right)\sigma_{\tan\phi} \qquad \text{[Eq. IVb.1]}$$

Where:
c = the random cohesion;
ϕ = the random friction angle;
X, Y = the two random values generated for $N(0,1)$;
μ_c, σ_c = the mean (550-psf) and the standard deviation (140-psf) of cohesion;
$\mu_{\tan\phi}, \sigma_{\tan\phi}$ = the mean (0.74) and the standard deviation (0.086) of $\tan\phi$;
ρ = correlation between the variation of c and $\tan\phi$.

The value of ρ is set to be -0.3 assuming the variation of c and $\tan\phi$ are negatively correlated. In other words, when the value of $\tan\phi$ is higher than its mean, the value of c would be lower than its mean. The correlation at each generation of c and $\tan\phi$ can be checked using Eq. IVb.2 (Griffith, 2007).

$$\rho = \frac{E\left[(\mu_c - c)\left(\mu_{\tan\phi} - \tan\phi\right)\right]}{\sigma_{\tan\phi}\sigma_c} \qquad \text{[Eq. IVb.2]}$$

Where:
E = the expectation function.

The generated shear strength parameters were plugged into the FEM to conduct the SRM procedure in order to calculate the factor of safety for each generation. Totally 10 random c and $\tan\phi$ were obtained from the Monte-Carlo generation. The resulted mean and standard deviation of the 10 generations are checked with respect to the values of mean and standard deviations that are initially set for c and $\tan\phi$. The resulting random shear parameters are summarized in Table IVb.2 and plotted in Figure IVb.16. As shown in the table, the mean and standard deviation of the shear parameters from the Monte-Carlo generation is close to the pre-defined values. Also, the generated blue points are distributed surrounding the orange point representing the defined mean values.

Table IVb.2 Generated jointly random shear parameters and the resulting factor of safety of Embankment #5

Test No.	tan ϕ	ϕ	c, psf	Factor of Safety	Critical Factor of Safety
1	0.73	36	650	2.5	0.5
2	0.72	36	523	2.6	0.6
3	0.71	35	703	2.7	0.7
4	0.75	37	350	2.4	0.4
5	0.86	41	507	2.6	0.6
6	0.87	41	628	2.7	0.7
7	0.63	32	549	2.4	0.6
8	0.76	37	541	2.8	0.7
9	0.62	32	556	2.4	0.5
10	0.73	36	657	2.5	0.5
Mean	0.74		566		
Standard deviation	0.08		100.5		

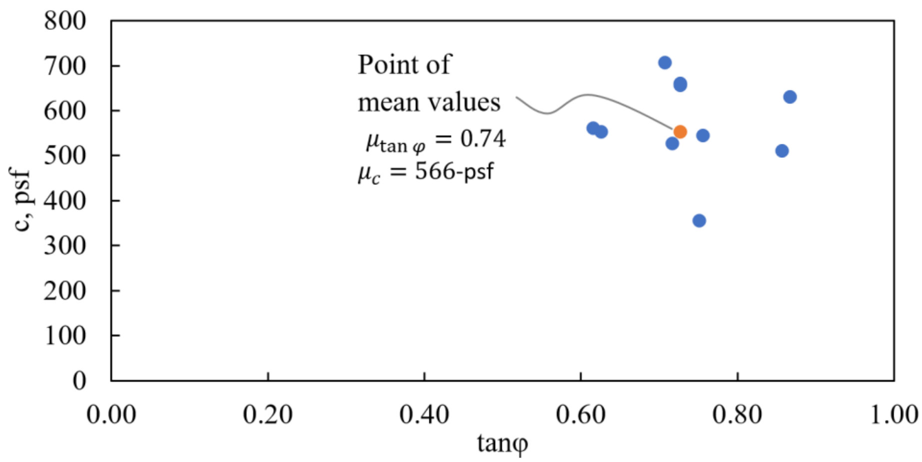

Figure IVb.16 – Distribution of the generated jointly random shear parameters for Embankment #5

The resulting factors of safety calculated using these jointly random shear parameters are plotted in Figure IVb.17. It is indicated that the upper bond factor of safety ranges from 2.4 to 2.8. The lower bond factor of safety (critical factor of safety) ranges from 0.4 to 0.8. Through doing the sensitivity tests, the possible variation of the shear parameters was taken into consideration. The resulting factor of safety range for the upper and lower bond was obtained to better predict the stability and behavior of Embankment #5.

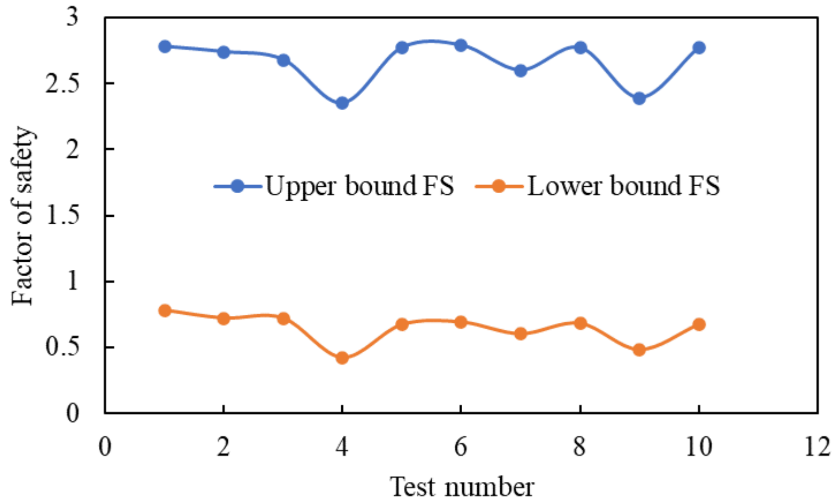

Figure IVb.17 – Resulting factor of safety calculated in FEM using the jointly random shear parameters for Embankment #5

4.0 Discussion

A University's Embankment #5 finite element model was constructed considering information from multiple borings, laboratory test results. Properties established during the evaluation of Embankment #1 by Panel 15. The material properties used in the model, the shape of the subsidence basin applied to the base of the model, and the application of the SRM to help estimate the factor of safety for the embankment during different longwall face positions.

This approach was applied to predicted conditions for Embankment #5. These efforts found that substantial deformations occur within the fill. Parametric evaluation found that a factor of safety less than one was possible under certain material properties, highway orientation, and overburden conditions. For the potential conditions outlined in this research study, significant settlement could occur on the crest of Embankment #5 with the potential to form longitudinal depressions in the highway alignment. The reasons for these potential instabilities are directly related to the lower overburden and orientation of longwall mining direction and highway direction.

A significant outcome of this research study is the development of a method for estimating orientation and overburden influences on embankments. The chart in Section IVa (Figure IVa.23) proposed how different orientation and overburden could affect the lower limit factor of safety. This chart allows for a first approximation of the risk posed by the unique orientation and overburden associated with individual embankments. For example, Embankment #5 the overburden is estimated to be 500-ft and the highway is at a 79-deg angle with the direction of longwall mining. The lower limit estimated factor of safety is ~0.8. This value is plotted on Figure IVb.18 and is in the zone of potential large deformations. Also, for Embankment #1, the overburden is estimated to be 675-ft and the highway is at a 35-deg angle with the direction of longwall mining. The lower limit estimated factor of safety is ~1.2. This value is also plotted on Figure IVb.18 and is in the zone of potential small deformations.

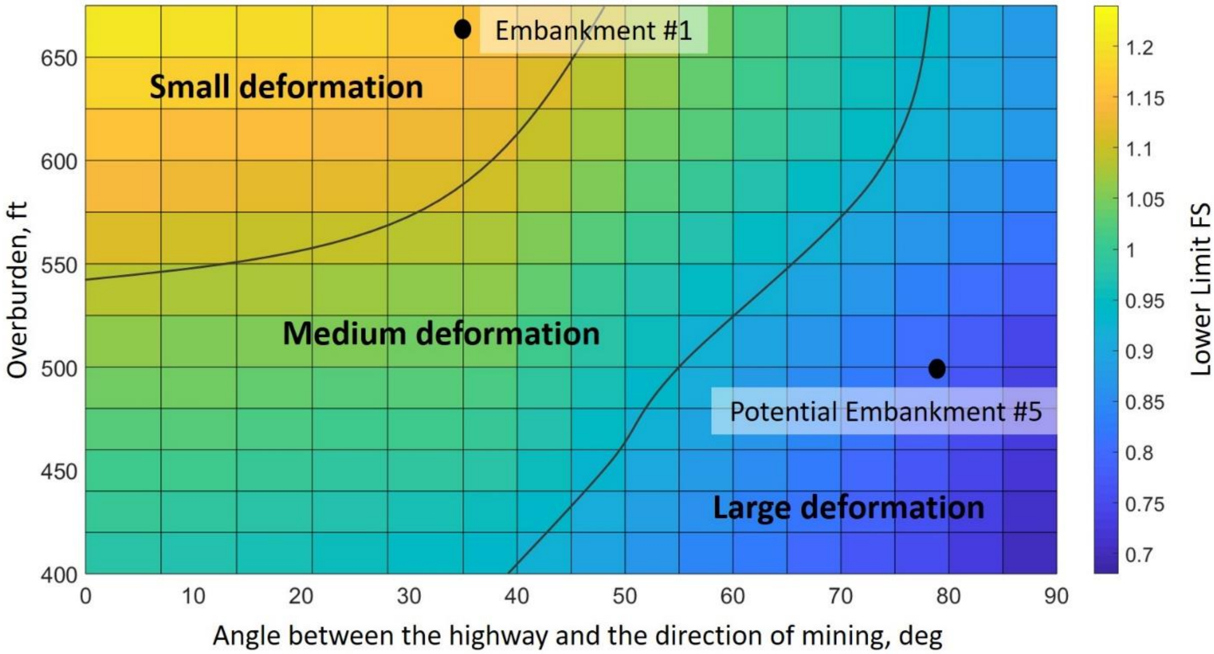

Figure IVb.18 – Chart showing the proposed method for estimating orientation and overburden influences on embankments found within the study area. All conditions apply to a fully developed subsidence basin in the mid-panel area. The lower limit factor of safety for Embankments #1 and #5 are provided

REFERENCES

Agioutantis, Z. and Karmis, M. (2013). “Recent Developments on Surface Ground Strain Calculations due to Underground Mining in Appalachia.” In: *Proceedings of the 32nd International Conference on Ground Control in Mining*. Morgantown, WV: West Virginia University, pp. 214–219.

Agioutantis, Z. and Karmis, M. (2015). “Quick Reference Guide and Working Examples,” SDPS for Windows, version 6.2B,” 330 p.

Agioutantis, Z., Karmis, M., and Jarosz, A. (1988). “Prediction of Surface Subsidence and Strain in the Appalachian Coalfields using Numerical Methods.” In: *Proceedings of the 7th International Conference on Ground Control in Mining*. Morgantown, WV: West Virginia University, pp. 95–100.

Andrew, K. (2008). “Enhancing Mine Subsidence Prediction and Control Methodologies for Long-Term Landscape Stability,” MS Thesis, Virginia Polytechnic Institute and State University, Blacksburg, VA, 154 p.

Anon (1975). Subsidence Engineers’ Handbook, National Coal Board, Mining Department, 111 p.

Anon (2004a). Buried Structures and Tunnel Liners, AASHTO LRFD Load and Resistance Factor Design, Chapter 12 on Pipes and Buried Structures, 91 p.

Anon (2004b). Buried Structures and Tunnel Liners, AASHTO LRFD Bridge Design Specifications, Section 10: Foundations, 3rd ed., p. 113.

Anon (2019). “Structures, Procedures, Design, and Plans Presentation”, PennDOT Design Manual, Part 4 (DM-4), PDT No., 15M, December 2019 ed., 1084 p.

Boone, S. (1996). “Ground-Movement-Related Building Damage,” Journal of Geotechnical Engineering, November, pp. 886-896.

Wikipedia (2020). “Stream Order,” https://en.wikipedia.org/wiki/Stream_order

Bain, D., DaCanal, T., Iannacchione, A., Kautz, A., Shirey, P., Tonsor, S. Copeland, M., Deglmann, J., Hill, M., Kandanarachchi, D., Trout, S. and Winn, R. (2019). “The Effects of Subsidence Resulting from Underground Bituminous Coal Mining in Pennsylvania, 2013-2018,” 5th Five-Year Report, Bituminous Mine Subsidence and Land Conservation Act, Act 54 Amendments, PA Department of Environmental Protection, submitted by the University of Pittsburgh, August 31, 2019, vol. 1 and vol. 2, p.

Dawson, E. M., Roth, W. H., & Drescher, A. (1999). Slope Stability Analysis by Strength Reduction. *Geotechnique, 49*(6), 835-840.

Geddes, J. and Cooper, D. (1962). “Structures in Areas of Mining Subsidence”, The Structural Engineer, pp. 79-93.

Griffiths, D. V., & Lane, P. A. (1999). Slope Stability Analysis by Finite Elements. Geotechnique, 49(3), 387-403.

Hescock, J. and Agioutantis, Z. (2017). “SDPS Update: Easy Calculation of the Edge Effect Offset for Complex Extraction Panels.” In: Proceedings of the 36th International Conference on Ground Control in Mining. Morgantown, WV: West Virginia University, pp. 353–358.

Hood, M., Ewy, R., and Riddle, L. (1981). “Empirical Methods of Subsidence Prediction – A Case Study,” Proceedings Workshop on Surface Subsidence Due to Underground Mining, S. Peng, ed., West Virginia University, Morgantown, WV, pp. 100-123.

Iannacchione, A., Tonsor, S., Witkowski, M., Benner, J., Hale, A., and Shendge, M. (2011). “The Effects of Subsidence Resulting from Underground Bituminous Coal Mining on Surface Structures and Features and on Water Resources, 2003 to 2008,” 3rd Five-Year Report, Bituminous Mine Subsidence and Land Conservation Act, Act 54 Amendments, PA Department of Environmental Protection, submitted by the University of Pittsburgh on January 10, 2011, 499 pages and 1 plate.

Iannacchione, A., Iannacchione, N., and Keener, M. (2013). “Selected Factors Affecting Longwall Mine Layouts in the Pittsburgh Coalbed of Southwestern Pennsylvania,”, SME Annual Meeting, Preprint 13-151, Denver, CO, Feb. 24-27, 2013, 7 p.

Iannacchione, A., Vallejo, L, Li, Mingzhou, Adelsohn, E., and Winn, R. (2019). “Task 1: PreMining Activities Report: Identification of Factors Controlling the Development of Subsidence Impacts Forecasting Methodology to the I-70 Alignment over Longwall Mining of the Tunnel Ridge Mine,” PennDOT Contract No. 4400011482, 2 July 2019, 129 p., available upon request to PennDOT or the University of Pittsburgh.

Iannacchione, A., Vallejo, L, Vandenbossche, J., Li, Mingzhou, Adelsohn, E., and Winn, R. (2020). “Task 2: Undermining Activities Report: Identification of Factors Controlling the Development of Subsidence Impacts Forecasting Methodology to the I-70 Alignment over Longwall Mining of the Tunnel Ridge Mine,” PennDOT Contract No. 4400011482, 3 February 2020, 185 p., available upon request to PennDOT or the University of Pittsburgh.

Karmis, M., Goodman, G., and Hasenfus, G. (1984). “Subsidence Prediction Techniques for Longwall and Room and Pillar Panels in Appalachia,” Proceedings of the 2nd International Conference on Stability in Underground Mining, University of Kentucky, Lexington, KY, August 6-8, 1984, pp. 541-553.

Karmis, M., Mastoris, J. and Agioutantis, Z. (1994), “Potential of the ’Damage Angle’ concept for assessing surface impacts of underground mining”, Transactions, Society for Mining, Metallurgy and Exploration, Inc., Vol. 296, pp. 1883-1886.

Karmis, M., Agioutantis, Z., and Andrews, K. (2008). "Enhancing Mine Subsidence Prediction and Control Methodologies," Proceedings, 27th International Conference on Ground Control in Mining, July 29-31, Morgantown, WV, pp. 131-136.

Luo, Y., Peng, S., Miller, B. (2003), "Influences of Longwall Subsidence on a Guyed Steel Tower - A Case Study", 22nd International Conference on Ground Control in Mining, Morgantown, WV, pp. 360-366.

Mark, C, and T.P. Mucho, T.P. (1994). "Longwall Mine Design for Control of Horizontal Stress," in New Technology for Longwall Ground Control: Proceedings of the USBM Technology Transfer Seminar, USBM Special Publication 94-01, pp. 53-76.

Matsui, T., & San, K. C. (1992). Finite element slope stability analysis by shear strength reduction technique. *Soils and foundations*, *32*(1), 59-70.

Newman, D., Agioutantis, Z. and Karmis, M. (2001). "SDPS for Windows: An Integrated Approach to Ground Deformation Prediction," In: Proceedings of the 20th International Conference on Ground Control in Mining. Morgantown, WV: West Virginia University, pp. 157–162.

Painter, R. (2020). Personal communication.

Peng S. and Cheng, S. (1981). "Predicting Surface Subsidence for Damage Preventions," Coal Mining and Processing, May 1981, pp. 84-95.

Peng, S. (1992). Surface Subsidence Engineering. Littleton, CO: Society for Mining Metallurgy and Exploration, Inc.

Peng, S. S., Luo, Y, and Zhang, Z. M. (1995a). "Subsidence Parameters – Their Definition and Determination," SME Transactions, vol. 300, 1995, pp. 60-65.

Peng, S. S., Luo, Y, and Zhang, Z. M. (1995b). "Development of a Subsidence Database and Determination of Subsidence Parameters," Proceedings of the 14th International Conference on Ground Control in Mining, West Virginia University, Morgantown, WV, August 1995, pp. 226-235.

Singh, M. (1992), "Mine Subsidence", SME Mining Engineering Handbook, SME Inc., Littleton, Colorado, vol. 1, pp. 938-971.

Tonsor, S., Hale, A., Iannacchione, A., Bain, D., Keener, M., Pfeil-McCullough, E., and Garmire, K. (2014). "The Effects of Subsidence Resulting from Underground Bituminous Coal Mining, 2008-2013," 4th Five-Year Report, Bituminous Mine Subsidence and Land Conservation Act, Act 54 Amendments, PA Department of Environmental Protection, submitted by the University of Pittsburgh on August 30, 2014, p.

Vallejo, L., and Lobo-Guerrero, S. (2012). "The Shear Strength of Granular Materials Containing Dispersed Oversized Particles: DEM Analysis," International Journal of Geotechnical Engineering 6.3, pp. 371-380.

Vallejo, L., Sass, R., Craig, R., Lobo-Guerrero, S. (2004). “The Shear Strength and Stability of a Soil Mass Containing Dispersed Large Particles,” Landslides: Evaluation and Stabilization, pp. 697-700.

Wardell, K. (1957). “The Minimisation of Surface Damage by Special Arrangement of Underground Workings,” In Proceedings of the European Congress on Ground Movement, pp. 13-19.

Whittaker, B.N. and Reddish, D.J. (1989). Subsidence Occurrence, Prediction, and Control, Developments in Geotechnical Engineering, Amsterdam: Elsevier.

Zheng, Y. R., Zhao, S. Y., Kong, W. X., & Deng, C. J. (2005). “Geotechnical Engineering Limit Analysis Using Finite Element Method,”*Yantu Lixue (Rock Soil Mech.), 26* (1), pp. 163-168.

Zienkiewicz, O. C., Humpheson, C., & Lewis, R. W. (1975). Associated and non-associated Visco-plasticity and Plasticity in Soil Mechanics. *Geotechnique*, *25*(4), pp. 671-689.

APPENDIX I – Strain Profiles and Deformation Features from Seven Longwall Face Positions during Undermining of Panel 15

29 January 2019 – EB and WB Strain Profiles

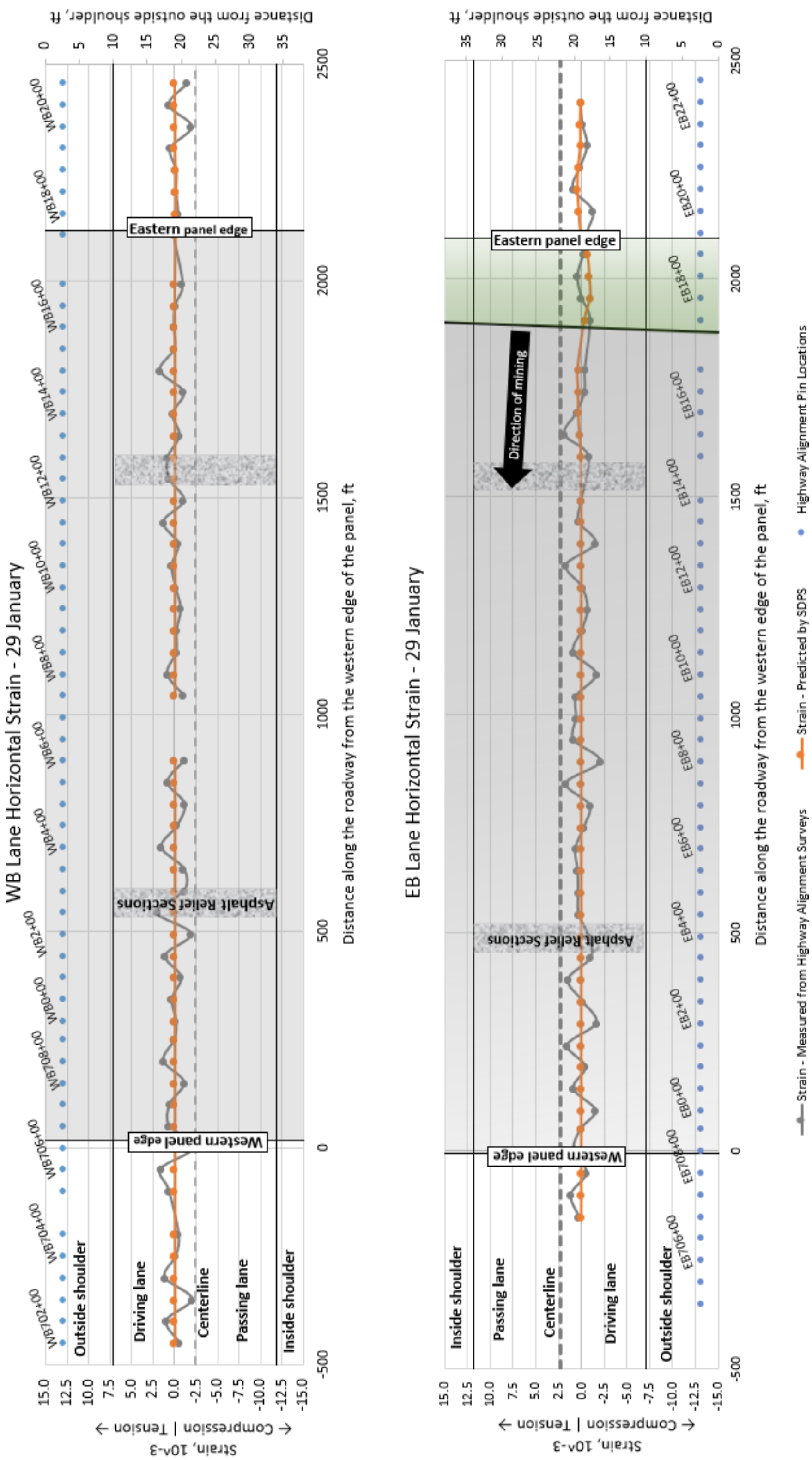

5 February 2019 – EB Lane Strain Profiles and Deformation Photos

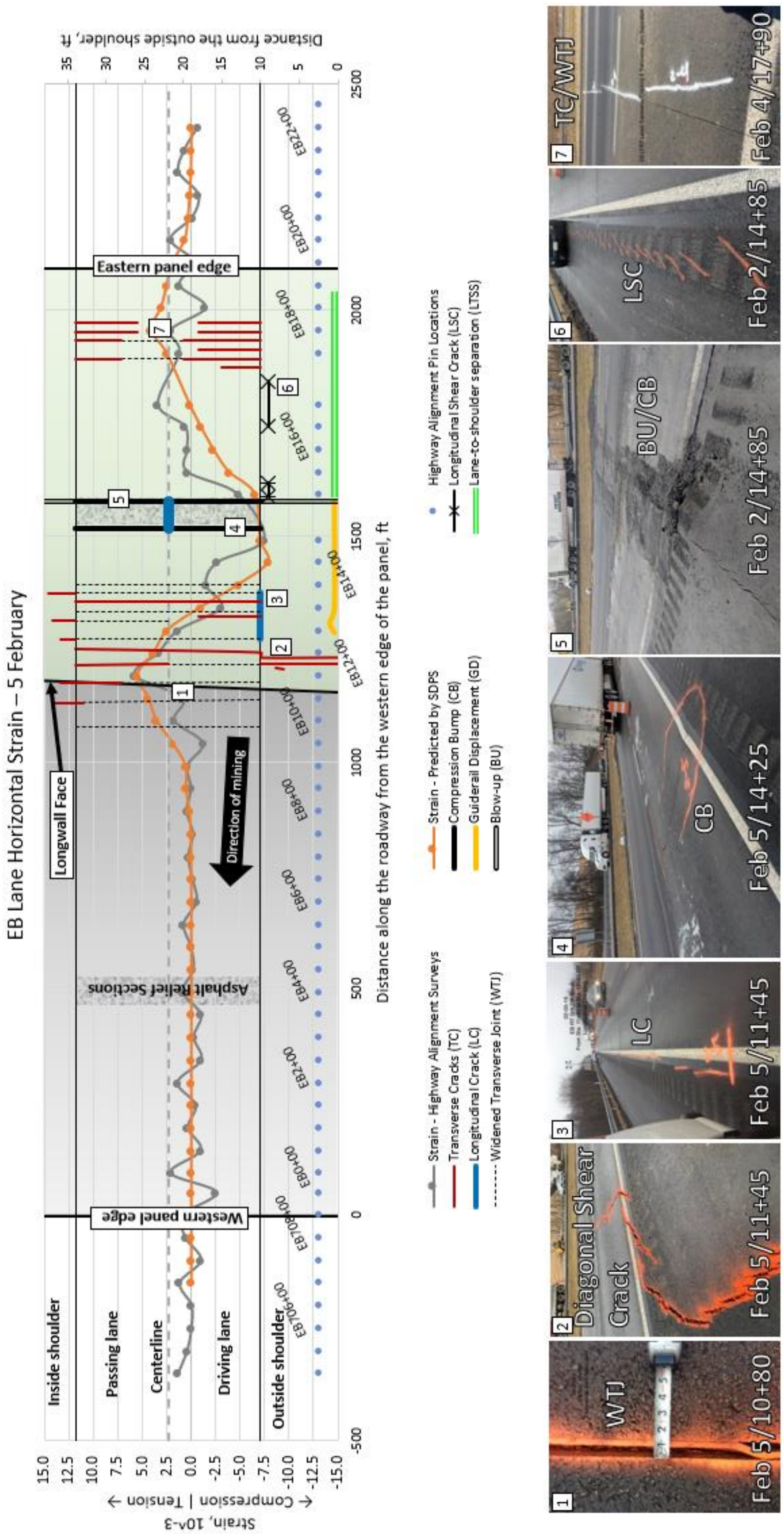

5 February 2019 – More EB Deformation Photos

5 February 2019 – WB Lane Strain Profiles and Deformation Photos

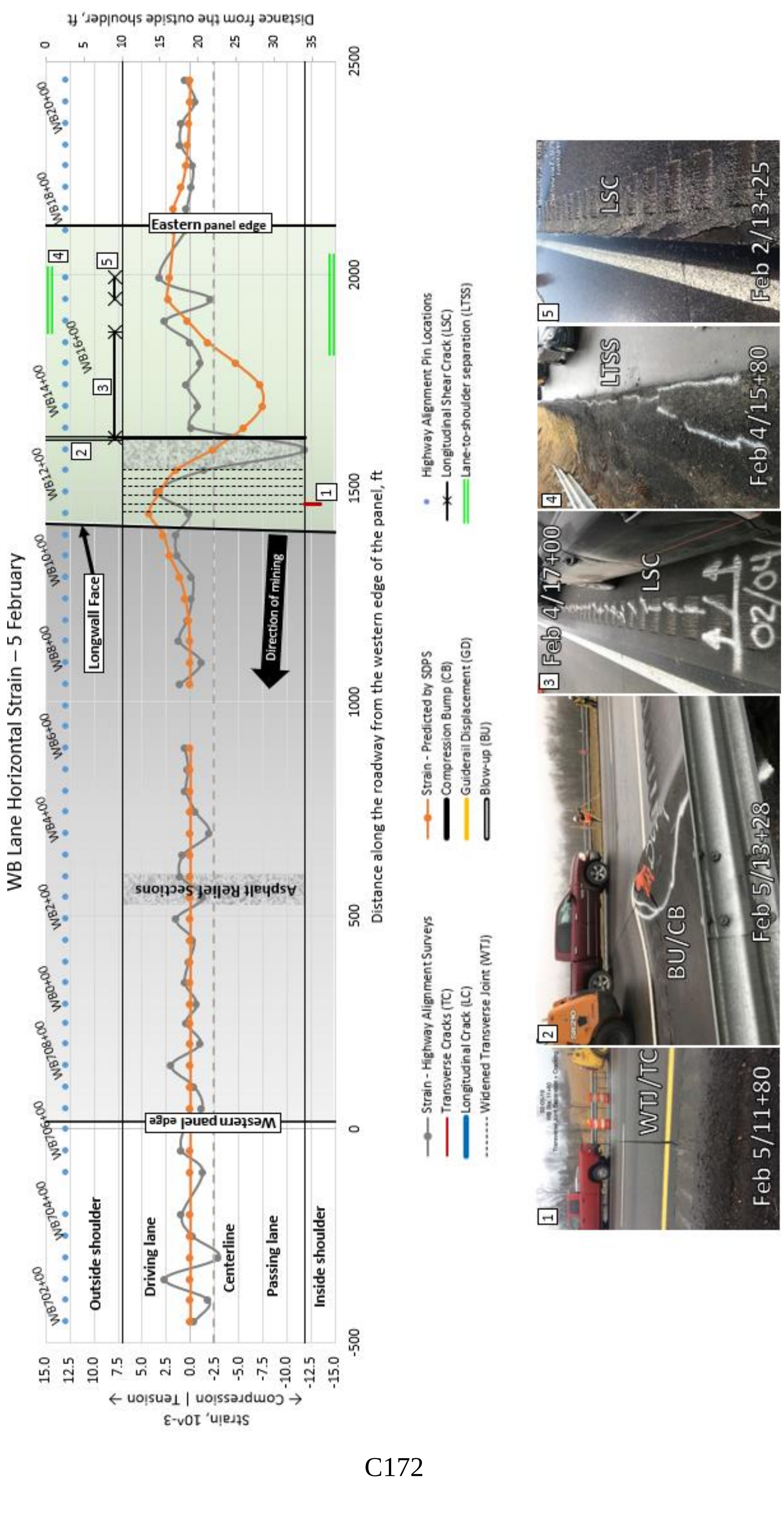

14 February 2019 – EB Lane Strain Profiles and Deformation Photos

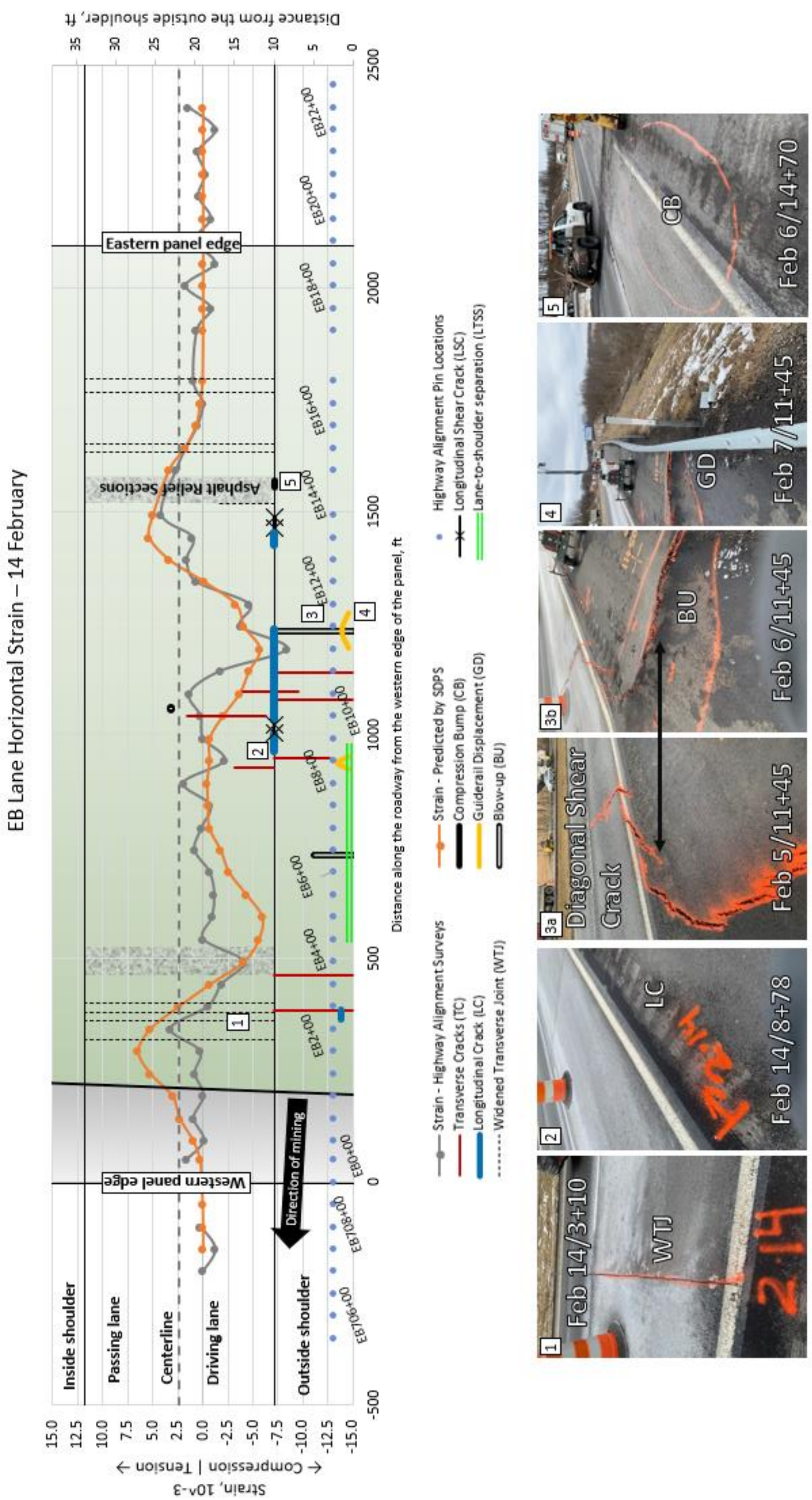

14 February 2019 – More EB Deformation Photos

14 February 2019 – WB Lane Strain Profiles and Deformation Photos

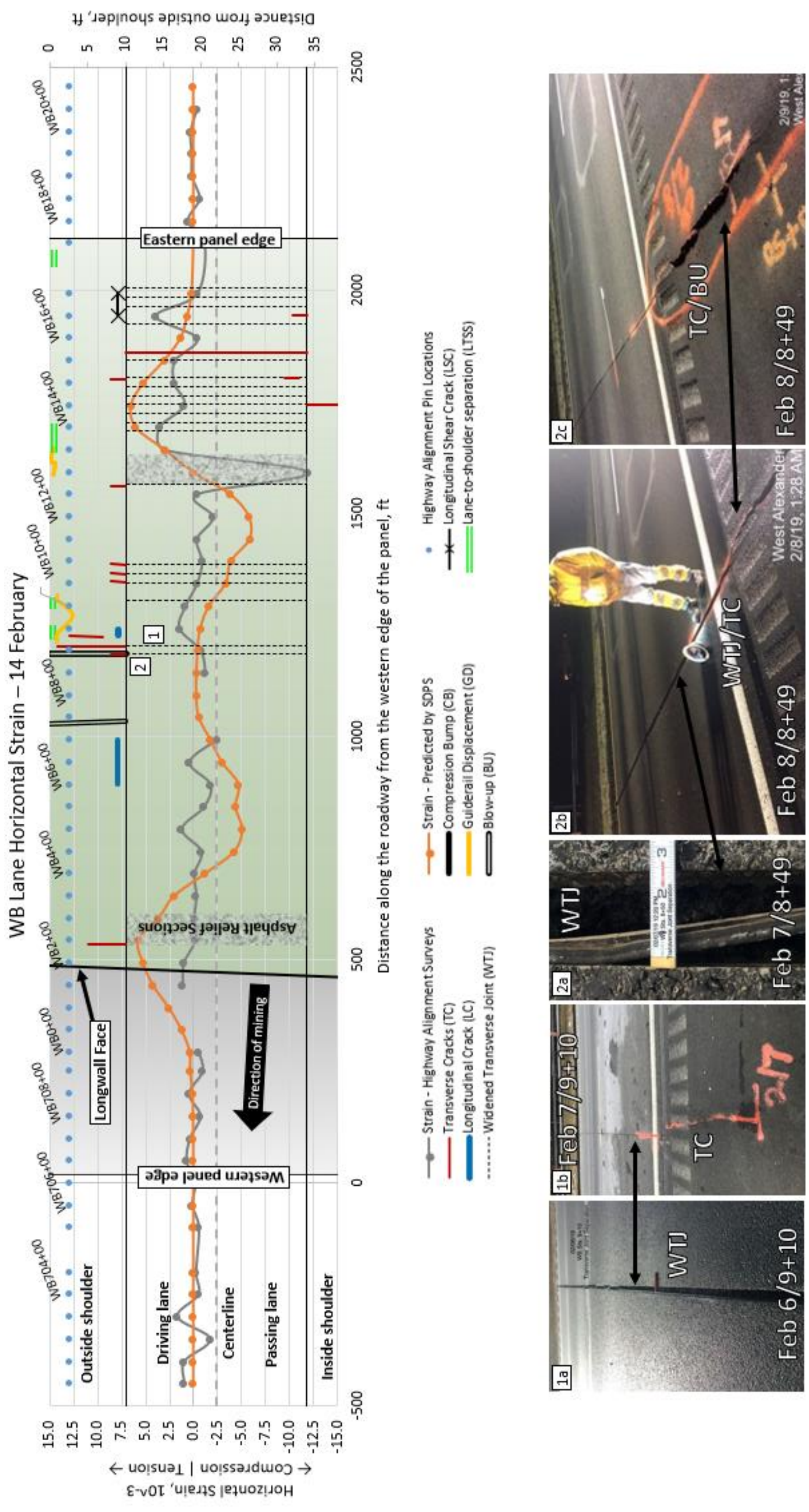

14 February 2019 – More WB Deformation Photos

19 February 2019 – EB Lane Strain Profiles and Deformation Photos

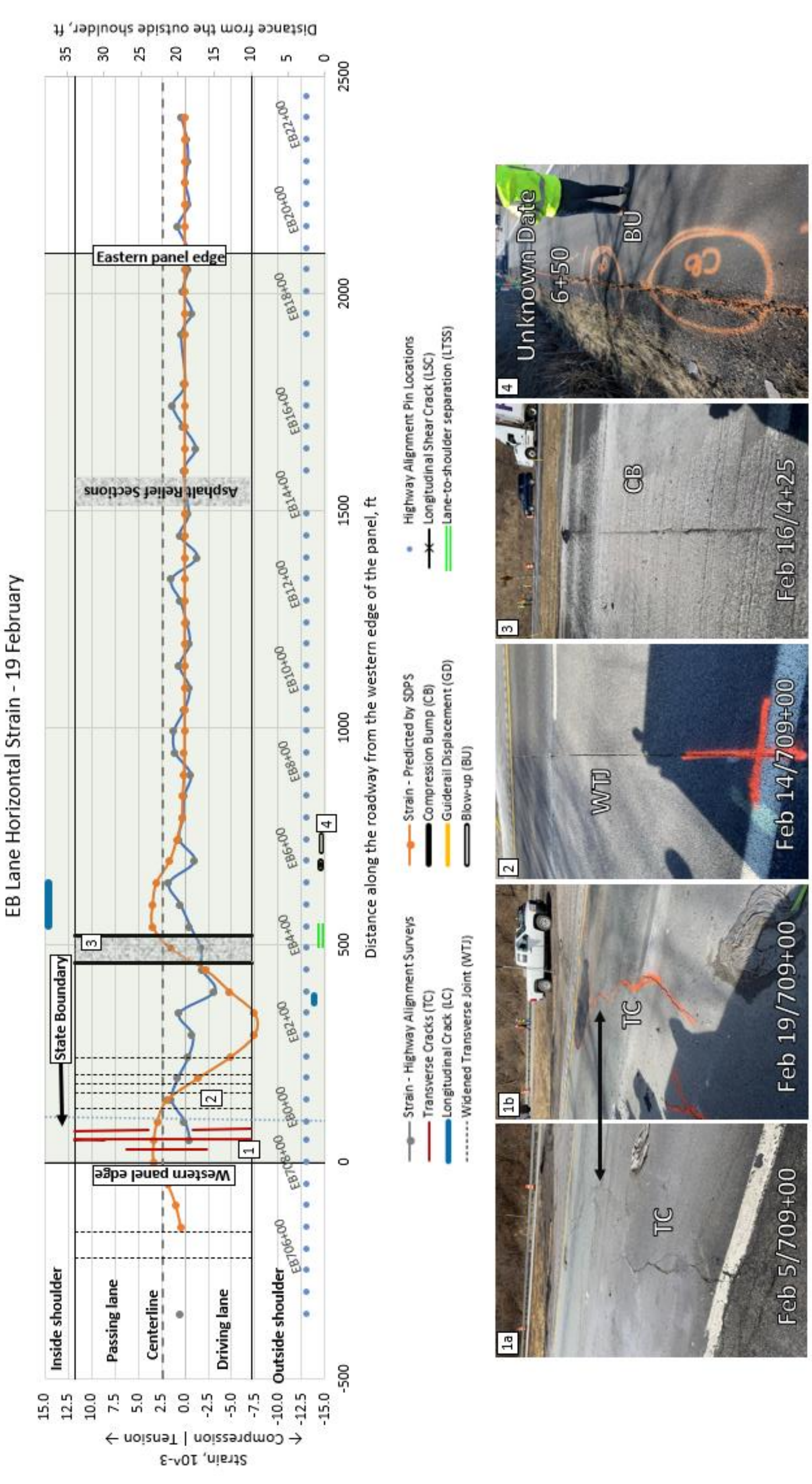

19 February 2019 – WB Lane Strain Profiles and Deformation Photos

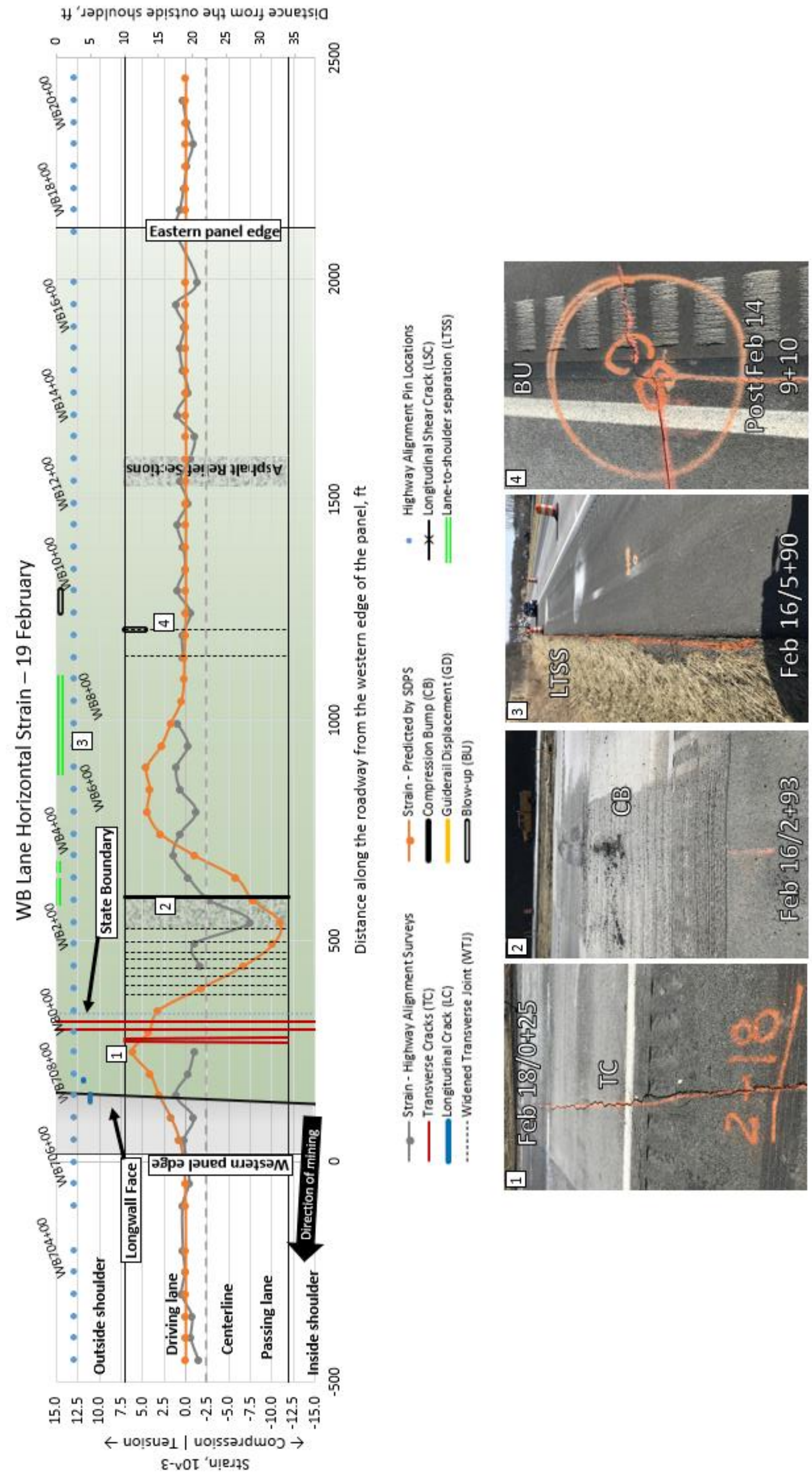

19 February 2019 – More WB Deformation Photos

7 March 2019 – EB and WB Strain Profiles

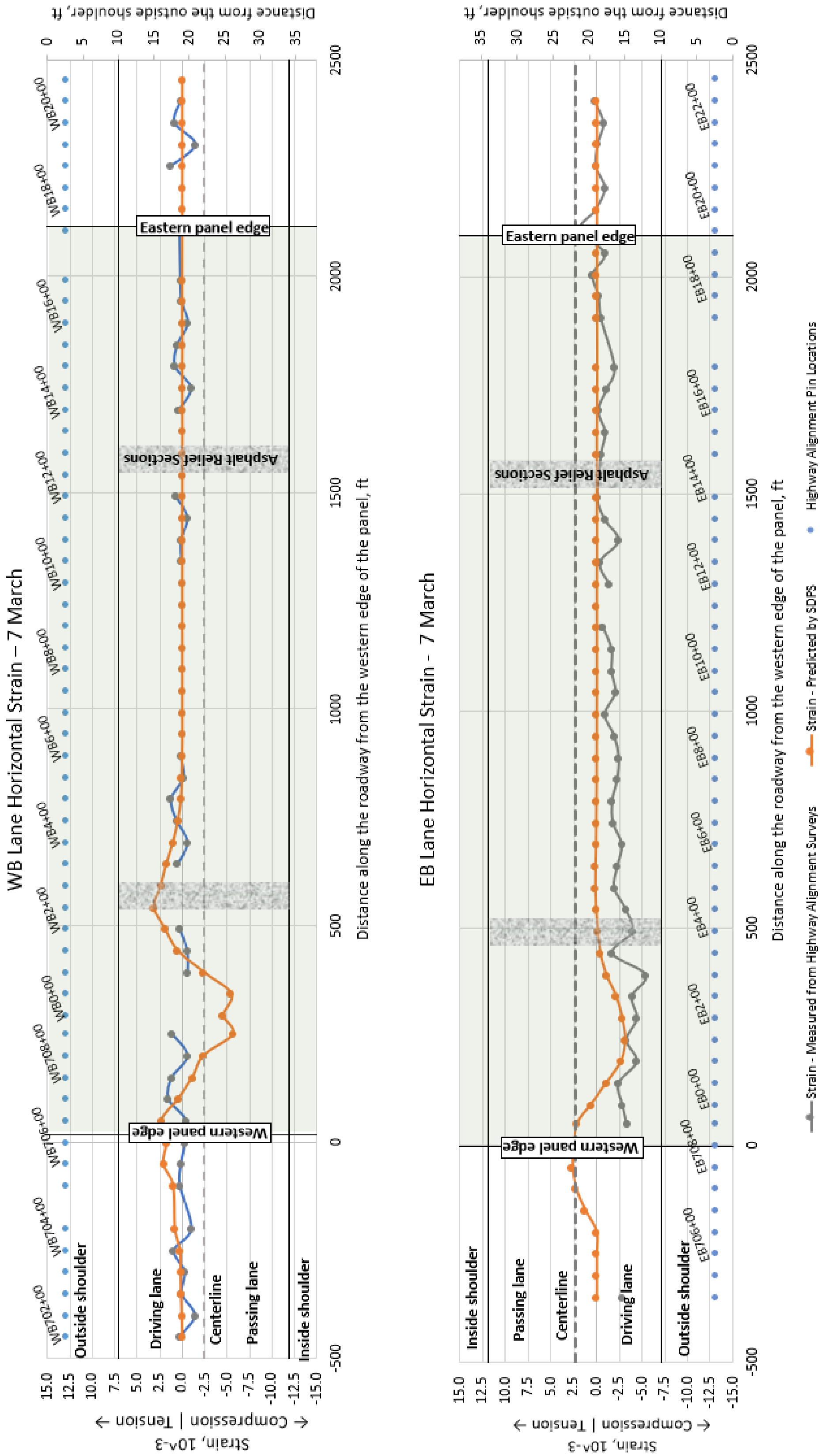

26 March 2019 – EB and WB Strain Profiles

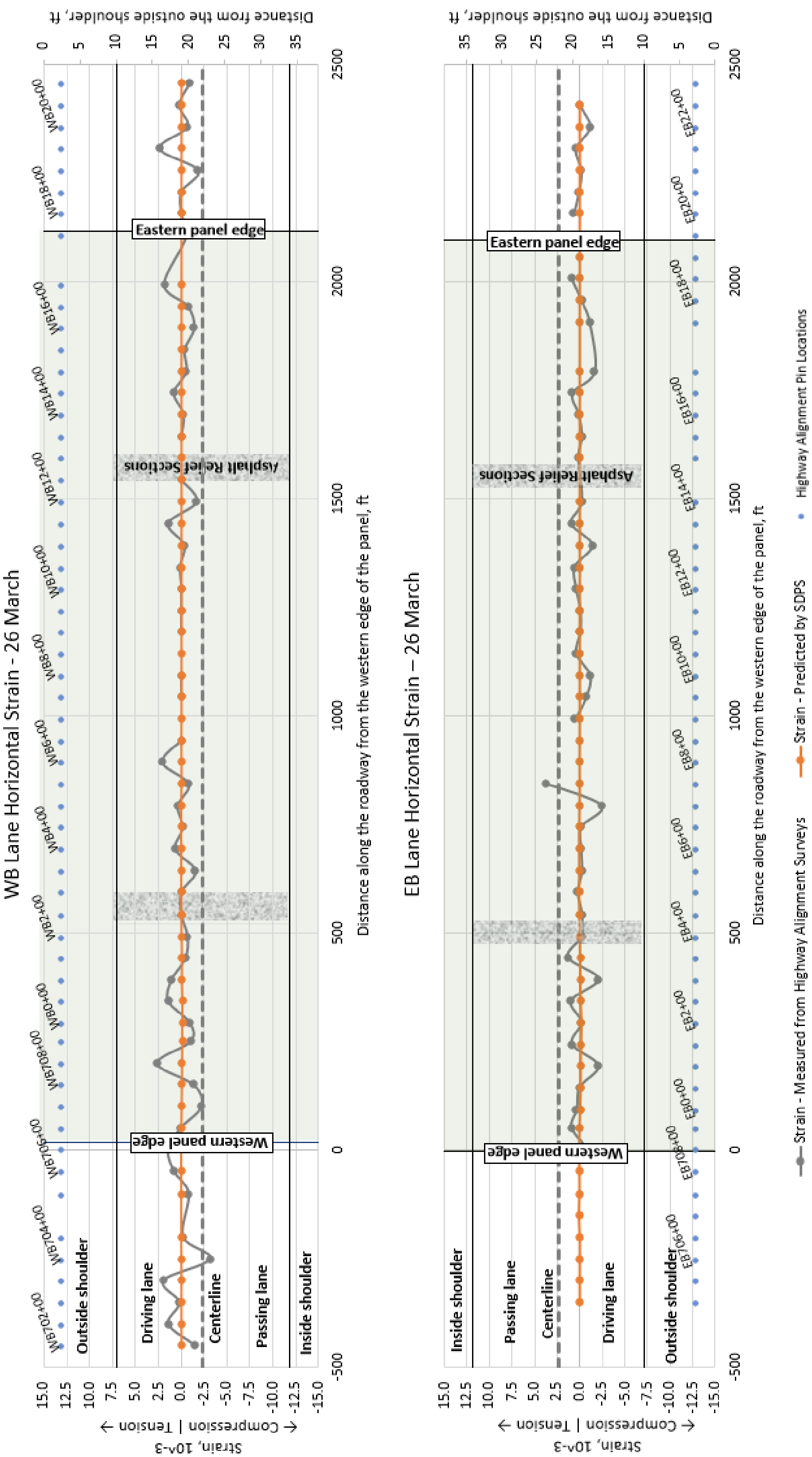

APPENDIX II – Factor of Safety for the Case of 0-Degree with Different Overburdens

Variation of the factor of safety of Embankment #1 Subjected to Subsidence with an Orientation of 0-Degree and an Overburden of 400-ft:

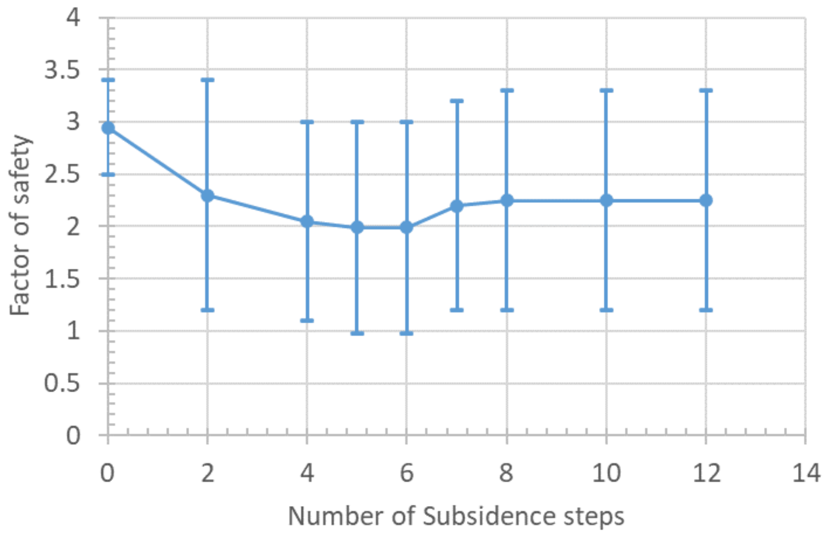

Variation of the factor of safety of Embankment #1 Subjected to Subsidence with an Orientation of 0-Degree and an Overburden of 500-ft:

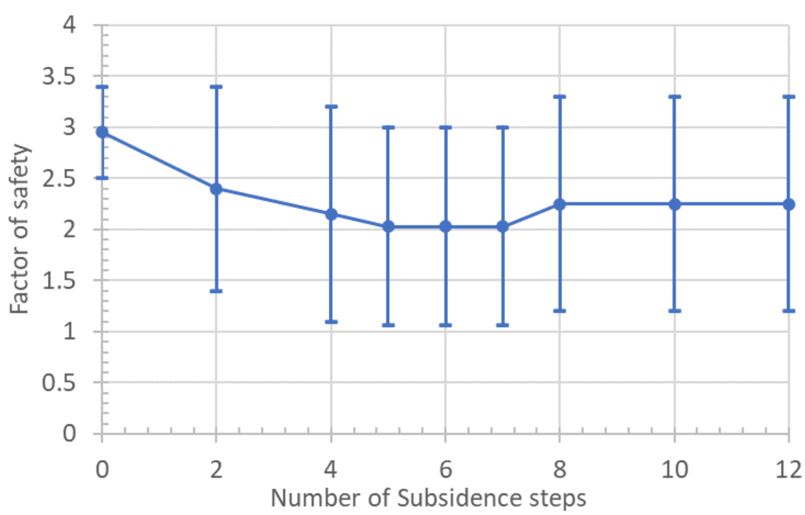

Variation of the factor of safety of Embankment #1 Subjected to Subsidence with an Orientation of 0-Degree and an Overburden of 600-ft:

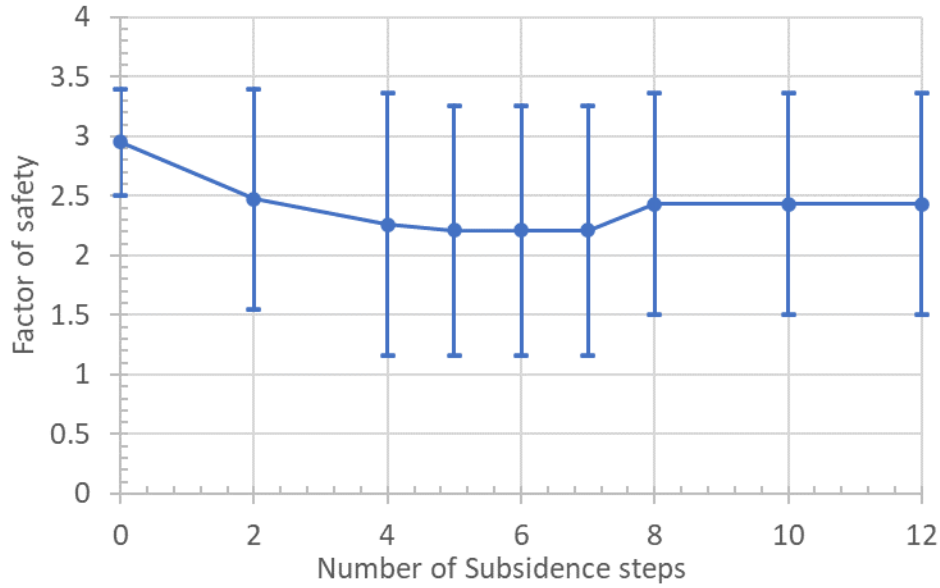

Variation of the factor of safety of Embankment #1 Subjected to Subsidence with an Orientation of 0-Degree and an Overburden of 675-ft:

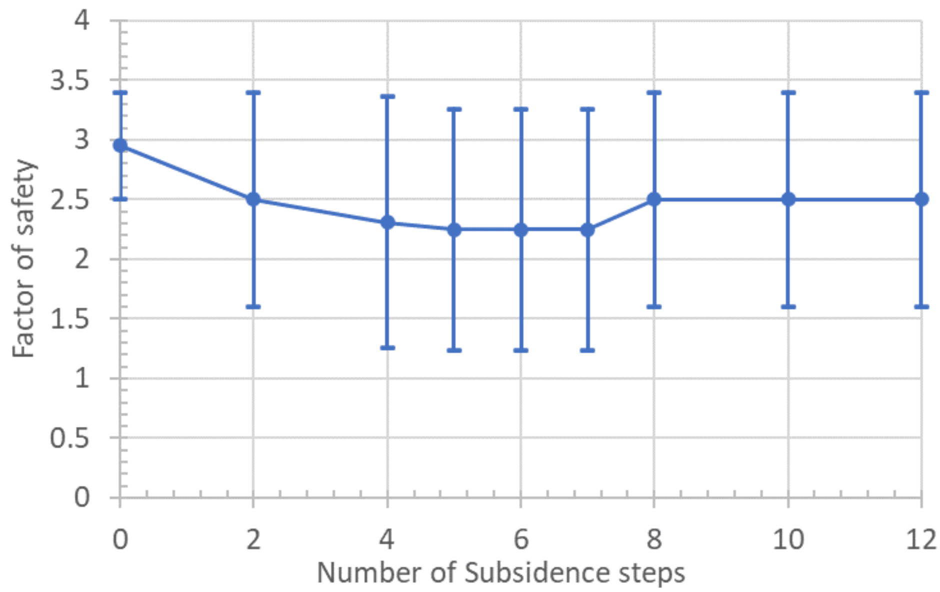

Influence of Overburden on the factor of safety of Embankment #1 when the Highway Orientation with respect to the Mining is 0-Degree:

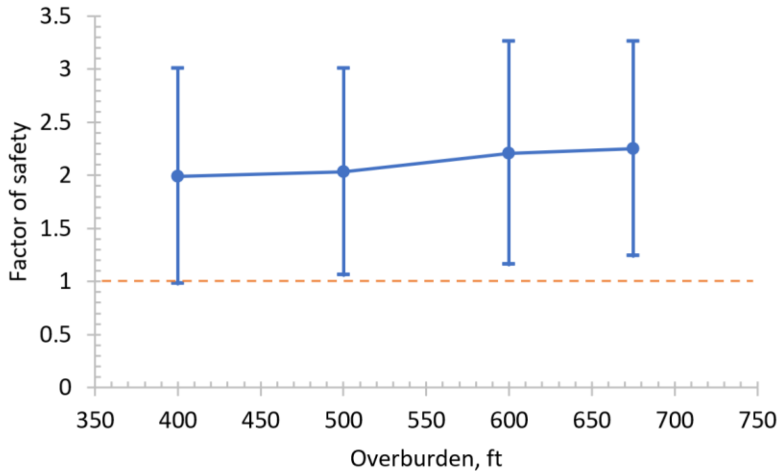

APPENDIX III – Subsidence Contour on Embankment #5 Using Finite Element Analysis

Vertical displacement on Embankment #5 with working face position #0:

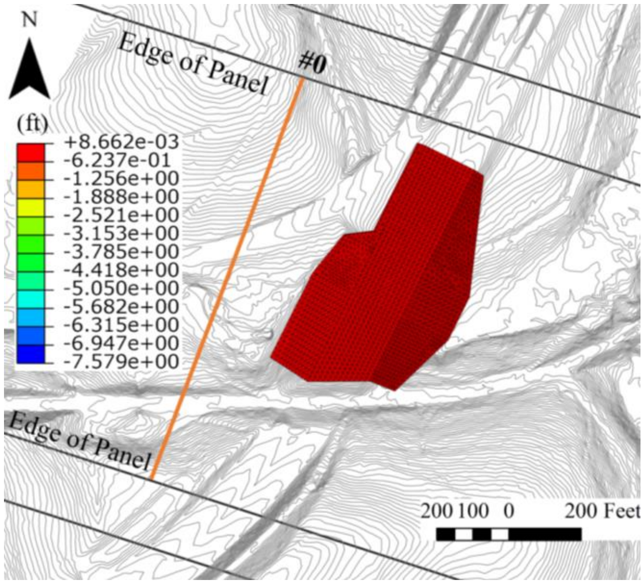

Vertical displacement on Embankment #5 with working face position #1:

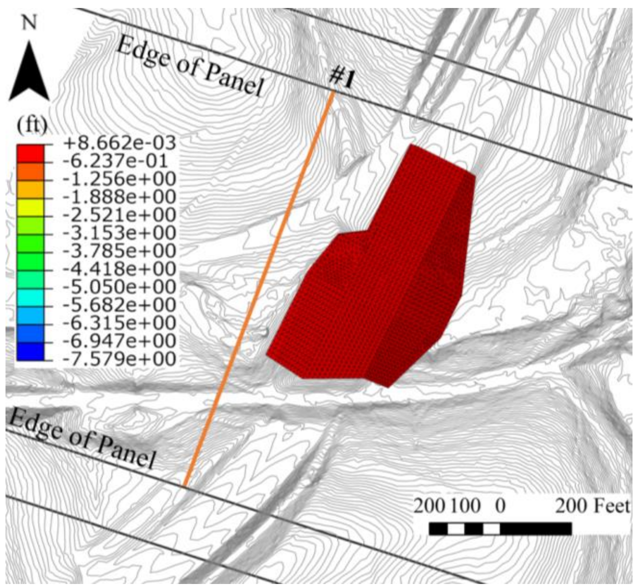

Vertical displacement on Embankment #5 with working face position #2:

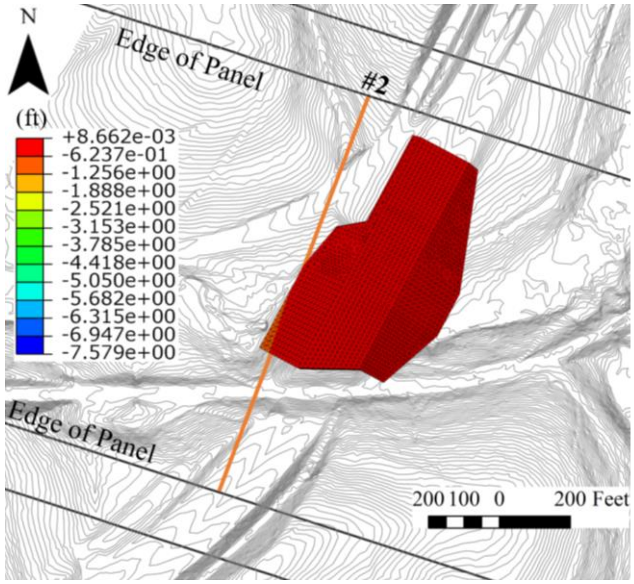

Vertical displacement on Embankment #5 with working face position #3:

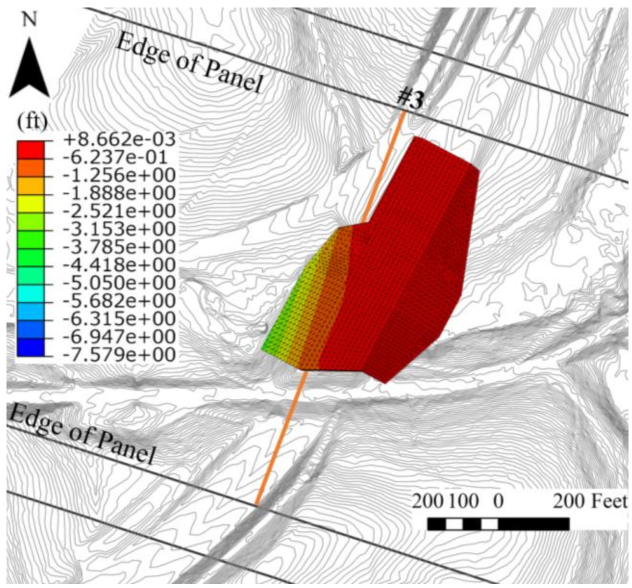

Vertical displacement on Embankment #5 with working face position #4:

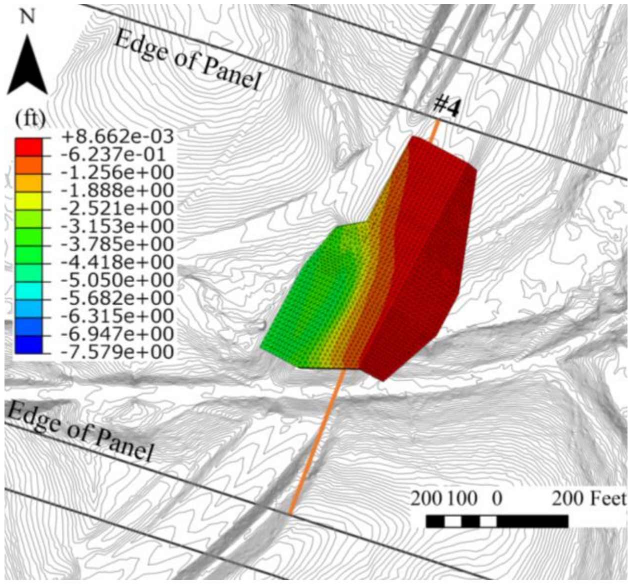

Vertical displacement on Embankment #5 with working face position #5:

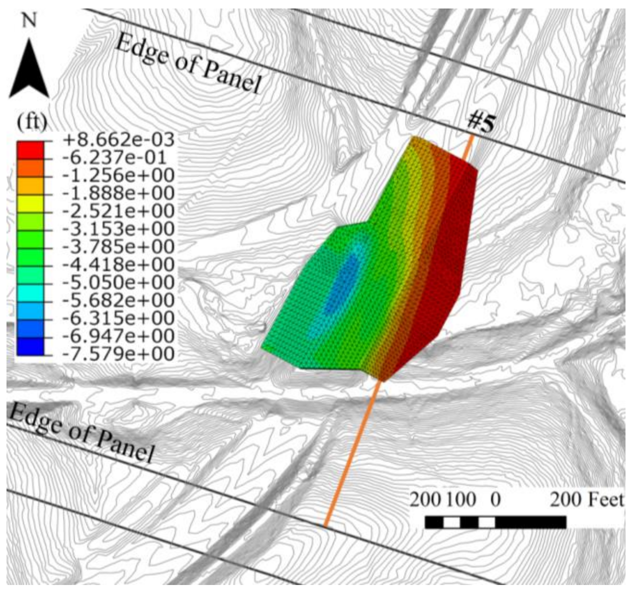

Vertical displacement on Embankment #5 with working face position #6:

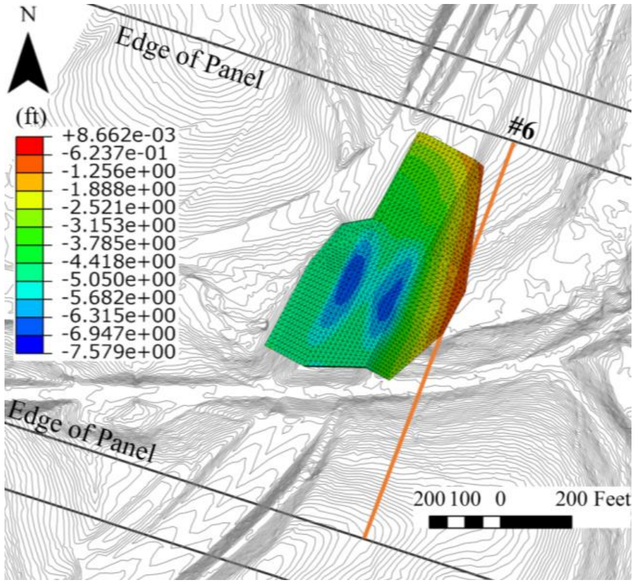

Vertical displacement on Embankment #5 with working face position #7:

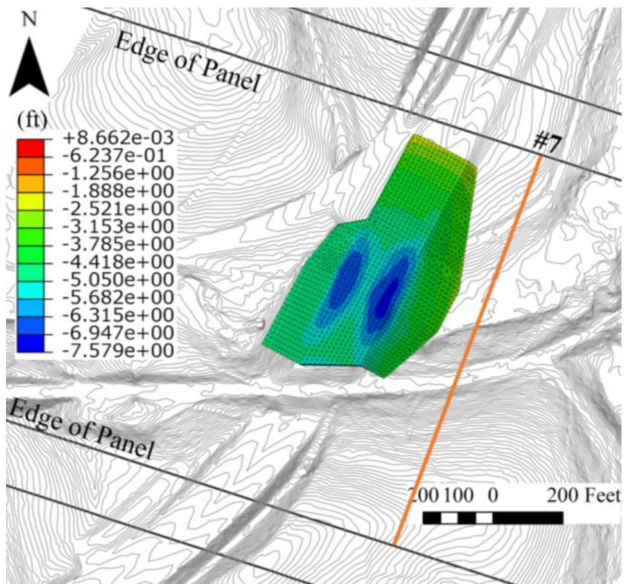

Vertical displacement on Embankment #5 with working face position #8: